The Institute of Paper Chemistry

Appleton, Wisconsin

Doctor's Dissertation

Longitudinal Dispersion, Intrafiber Diffusion, and Liquid-Phase Mass Transfer During Flow Through Fiber Beds

Gerald L. Pellett

June, 1964

LONGITUDINAL DISPERSION, INTRAFIBER DIFFUSION, AND LIQUID-PHASE MASS TRANSFER DURING FLOW THROUGH FIBER BEDS

A thesis submitted by

Gerald L. Pellett

B.Ch.E. 1958, Rensselaer Polytechnic Institute
M.S. 1960, Lawrence College

in partial fulfillment of the requirements
of The Institute of Paper Chemistry
for the degree of Doctor of Philosophy
from Lawrence College,
Appleton, Wisconsin

June, 1964

Errata Sheet for Doctoral Dissertation by Gerald L. Pellett

Page 16, line 12 should read:

$((1-\epsilon)/\epsilon)\ \partial \underline{Q}/\partial t = -\underline{k}''\underline{C}$, is given ....

Page 182, 4th entry should read:

$\underline{A}'_{\underline{C}}$ = intimate contact ....

Page 184

Third entry from bottom should be deleted

Last entry on page should be changed from $\underline{k}''$ to $\underline{k}$

Add line at bottom of page:

$\underline{k}'' = \underline{k}\ (1-\epsilon)/\epsilon$

Page 186, line 4 should read:

mg./cc. fiber

Page 197, line 3 should read:

the second term ....

Page 214, Equation (180), first line should read:

$Q = KP_o - 4KP_oL$ ....

Page 226

Equation (247) should read:

$\partial Q/\partial t = -kC$

Insert in last line after the word "constant"

(note that $\underline{k}$ must be negative).

Page 227, Equation (248) should read:

$-H_5(p)C_o$

Page 228, insert at bottom

the relation $k'' = k(1-\epsilon)/\epsilon$

TABLE OF CONTENTS

SUMMARY

The removal of a soluble material from a solution-saturated fiber bed by flowing a solvent through the bed is commonly called the washing process. The displacement of solute from the void space of the bed is associated with a physical dispersion of the washing liquid in the direction of flow. This effect is often referred to as longitudinal dispersion, and the resulting change of exit concentration with time, from the original value to an asymptotic value, as a breakthrough curve. If the fibers are porous, stagnant liquid which contains solute is present in the intrafiber voids; thus, solute must diffuse out of the fibers before it is dispersed by the flowing liquid. In the case of an adsorbable solute, its transfer from the internal and external fiber surfaces to the liquid must also be taken into account.

Mathematical models were developed to describe the washing process. These models account for (a) longitudinal dispersion of fluid, according to a one-dimensional differential equation, (b) intraparticle diffusion of a solute which is linearly adsorbed, and (c) mass transfer (in the flowing liquid) from particle surfaces, assuming a driving force equal to the surface minus bulk concentration. The simultaneous differential equations were solved for the initial conditions of bed saturation and sorption equilibrium; the inlet boundary condition for the wash fluid was a modified step-function. The most refined models, designated as Cases 2(F) and 2(S), account for all three of the above phenomena and apply to cylindrical (fiber) and spherical particle geometries, respectively; Cases 1(F) and 1(S) are the same except they assume no mass transfer resistance. The Equilibrium and No-Sorption cases account for longitudinal dispersion, but represent infinitely rapid and infinitely slow intraparticle diffusion cases.

Washing experiments, on mechanically compressed beds of 1, 4, 16, and 64-denier all-skin viscose fibers, were analyzed by trial and error fitting of

breakthrough curves. The solutes were (a) diacetyl, which diffused rapidly in viscose, is nonionic and was not appreciably adsorbed, (b) p-phenylazoaniline (PAA) which diffused at a relatively lower rate in viscose, is nonionic and was linearly adsorbed, and (c) Benzopurpurine 4B (BPP), a very slowly diffusing ionic direct dye. The range of average bed porosities was $0.7 < \epsilon < 0.9$; the Reynolds number range, in terms of the fiber diameter d and average linear pore velocity U, was 0.006 - 1.8; the Peclet number range was 10-2000.

Longitudinal dispersion coefficients, D_L, were determined by applying the Equilibrium case to the diacetyl-1 and 4-denier systems and the No-Sorption case to the BPP-16 denier system. Since D_L was found to be proportional to U, molecular diffusion effects appeared unimportant. At a constant fiber-length-to-diameter ratio, ℓ'/d, D_L/U was approximately proportional to both d and ϵ; $D_L/Ud\epsilon$ increased from 5 to 75 over the ℓ'/d range 50-400. The results suggest that the viscose beds are geometrically similar, approximately, when ℓ'/d and ϵ are constant.

The intrafiber diffusion and mass transfer properties of the PAA-1, 4, and 16-denier systems, and the diacetyl-64 denier system, were characterized by a sequential application of Cases 1(F) and 2(F). Apparent intrafiber diffusion coefficients, $(D_F)_A$, from Case 1(F), increased with U to approximately asymptotic values, D_F. Thus, the assumption of an infinite mass transfer coefficient, k_L, was unsatisfactory in the lower velocity regions of all the systems where $(D_F)_A < D_F$. Case 2(F) was applied over these regions by employing D_F at all values of U and ϵ in each system. The resulting k_L values increased as $U^{1.2}$ and ϵ^3; both of these results indicate the inherent complexity of unsteady-state mass transfer phenomena in the present systems. Since equally adequate fits of breakthrough curves were generally obtained with both Cases 1(F) and 2(F), neither model had a predictive advantage, but Case 2(F) was clearly more appropriate from a physical standpoint.

INTRODUCTION AND PRESENTATION OF THE PROBLEM

The general problems of heat and mass transfer during flow through a bed of packed solids have numerous applications in the chemical process industries. Although this work deals almost exclusively with mass transport phenomena in fiber beds, much of the theory which has been developed, and many of the considerations involved in the analysis and interpretation of results, apply to mass and heat transfer in other multiparticle systems.

The immediate objective of this work was to account for the mass transport phenomena that took place when washing experiments were performed on ideal solute-fiber systems. Typically, a viscose fiber bed was initially saturated with a dye solution until sorption equilibrium was attained; then a washing experiment was commenced at time zero by flowing water through the bed. By measuring the exit dye concentration as a function of time, it was possible to construct an exit-concentration curve or breakthrough curve. The initial stage of the analysis was designed to provide mathematical descriptions of the breakthrough curves in terms of models that were developed to represent the various mass transport phenomena. Later stages of the analysis were designed to generalize these results in a manner that would (a) define the relative importance, and (b) clarify the fundamental significance, of the various physical phenomena involved.

Longitudinal (or axial) dispersion refers to the physical dispersion of a fluid in the average direction of flow. In a porous medium it results from local axial velocity variations that inherently exist during flow through an irregular network of channels. The longitudinal dispersion effect that applies in the present systems can be observed by following the destruction of an initially sharp interface between two miscible fluids (of the same density and

viscosity), as the first, which contains a dynamically neutral solute, is displaced from the porous medium by the second.

Sherman (1) demonstrated that the longitudinal dispersion effect was important when displacement experiments were performed on beds of nonporous fibers, and was described by a commonly used one-dimensional, differential equation. The fiber boundary condition for the nonporous fiber system specified that no solute exchange took place between the fibers and the fluid. From another viewpoint, this effectively corresponded to the case of infinitely slow intrafiber diffusion. Sherman also demonstrated the application of a second fiber boundary condition for determining the longitudinal dispersion properties of certain solute-porous fiber systems. This was based on the assumption that the movement of intrafiber solute was rapid enough to approximate the Equilibrium case, or roughly the infinitely rapid intrafiber diffusion case.

When Sherman attempted to analyze breakthrough curves from the diacetyl-64 denier viscose system, it became apparent that neither the infinitely rapid nor the infinitely slow intrafiber diffusion cases applied. The present thesis arose from this finding, and was ultimately aimed at providing a general description of intermediate cases where longitudinal dispersion, solute adsorption, intrafiber diffusion, and liquid-phase mass transfer effects are important to various degrees, depending on the experimental system and conditions.

The dissertation consists broadly of four major parts. The first includes the theoretical development, which accounts for various combinations of the above-mentioned effects in terms of a number of mathematical models. Pertinent theoretical developments by other workers are discussed in light of the present models. The second part describes the various characterizations of solute-fiber

systems, the experimental details pertaining to washing runs, the technique of analysis, and a number of related considerations such as material balances, reproducibility, and the effect of nonuniform porosity distributions. The third part involves detailed descriptions of experimental exit-concentration breakthrough curves in terms of the various parameters in the mathematical models. The fourth part represents attempts to generalize and account for the various results obtained.

Introductory background information, concerning longitudinal dispersion, solute adsorption, intrafiber diffusion, and liquid-phase mass transfer, is presented in the respective discussion of results sections, and therefore is not repeated here.

THEORETICAL DEVELOPMENT

The objective of the theoretical development was to provide suitable mathematical models for describing the movement of an adsorbable solute in the intraparticle pores and interparticle channels of an unconsolidated bed of porous particles, while a fluid is flowing through the bed. For purposes of generality, granular, spherical, and cylindrical particle geometries were considered, but the latter system is of greatest interest in the present work since it applies to beds of fibers.

The models of greatest importance account for three physical rate phenomena that occur simultaneously. These phenomena are (a) longitudinal or axial dispersion of fluid, (b) intraparticle Fick's law diffusion of a solute which is linearly adsorbed by the solid phase, and (c) liquid-phase mass transfer, which accounts for the transport of solute from particle surfaces to the flowing fluid.

BASIC ASSUMPTIONS

The development of the mathematical models was based on a number of assumptions concerning the nature of a particle-solute system. The assumptions for fibrous systems were:

1. The fiber bed is composed of long circular cylinders of uniform diameter, which are randomly oriented in the x-y or horizontal plane. The fiber diameter is small in comparison to the over-all bed height, and the bed is effectively uniform in porosity.

2. The dispersion of fluid in a fiber bed can be described by the usual one-dimensional differential equation for longitudinal dispersion.

This equation is based on (a) a longitudinal dispersion coefficient that is independent of the total bed length, and (b) an average concentration that is

defined by integration over the entire cross section in the horizontal plane. Thus, any radial dispersion, and/or wall effects that occur, are absorbed by the treatment and are analyzed as a part of the longitudinal dispersion effect.

3. The adsorption equilibrium relationship, describing the intrafiber solute concentration as a function of the external solution concentration, is linear.

4. The attainment of local adsorption equilibrium at any solid-liquid interface (external or internal) is very rapid and effectively independent of time.

5. The movement of solute within the fibers can be mathematically described by a Fick's law diffusion equation for a long circular cylinder (with a cylindrically uniform boundary condition about its external surface), where the intrafiber diffusion coefficient is constant and independent of concentration. It will be subsequently shown that this mathematical description can be conceived in terms of solute molecules that diffuse only in solution (no surface diffusion) through numerous intrafiber pores, where the local concentration of dye adsorbed on the walls of the pores is always in equilibrium with the local pore concentration.

SUMMARY OF CASES CONSIDERED

Longitudinal dispersion is accounted for in all of the following six cases, but the particle geometry, and the boundary conditions that describe solute exchange at the particle surfaces, are different. These cases are summarized as follows:

A. The No-Sorption case applies to all particle shapes, and is based on the assumption that no solute is exchanged between the particles and the fluid. This is equivalent to the case of infinitely slow intraparticle diffusion.

B. The Equilibrium case applies to all particle shapes, and is based on the assumption that the intraparticle solute, at an axial distance Z, is constantly in equilibrium with the bulk solution at Z. This is equivalent to the case of infinitely rapid intraparticle diffusion with no mass transfer resistance at the fiber surfaces.

C. Case 1(F) applies to fiber beds, and is based on the assumptions that (a) intrafiber diffusion is described by Fick's law, and (b) the cylindrically uniform solution concentration at fiber surfaces, located at Z, is always equal to the bulk solution concentration at Z. Thus, no liquid-phase mass transfer resistance exists in this case.

D. Case 2(F) applies to fiber beds, and is based on the assumptions that (a) intrafiber diffusion is described by Fick's law, and (b) the rate of solute transport from external fiber surfaces, located at Z, is equal to a mass transfer coefficient times the difference in cylindrically uniform solution concentrations between the fiber surfaces, and the bulk solution, at Z. Thus, a finite liquid-phase mass transfer resistance can be accounted for in this case.

E. Case 1(S) is the same as Case 1(F), except that it applies to beds of spherical particles.

F. Case 2(S) is the same as Case 2(F), except that it applies to beds of spherical particles.

BASIC EQUATIONS

LONGITUDINAL DISPERSION

The one-dimensional diffusionlike differential equation that describes the longitudinal dispersion of a fluid containing a dynamically neutral solute is

$$D_L \frac{\partial^2 C}{\partial Z^2} - U \frac{\partial C}{\partial Z} = \frac{\partial C}{\partial t} \qquad (1),$$

where

D_L = longitudinal dispersion coefficient, sq. cm./sec.

C = solute concentration in fluid, mg./cc. fluid

Z = axial distance from top of bed, cm.

U = average linear pore velocity (superficial velocity/void fraction), cm./sec.

t = time, sec.

The use of Equation (1) is commonly accepted. Its historical development has been discussed by Sherman (1) and its theoretical significance is elaborated upon later in this paper.

If the porous medium consists of porous solids that have a capacity for solute, it is necessary to specify an accumulation term that accounts for the exchange of solute with the fluid; thus, the differential equation becomes:

$$D_L \frac{\partial^2 C}{\partial Z^2} - U \frac{\partial C}{\partial Z} = \frac{\partial C}{\partial t} + \frac{(1 - \epsilon)}{\epsilon} \frac{\partial Q}{\partial t} \qquad (2)$$

where the additional nomenclature is

ϵ = average bed porosity or void fraction

Q = average intraparticle solute concentration, mg./cc. fiber

It is desired to obtain solutions of Equation (2) for the desorption washing process, using the initial condition

$$C = C_o \qquad Z \geq 0 \qquad t = 0 \tag{3}$$

and the inlet boundary condition at $\underline{Z} = 0$, $\underline{t} > 0$,

$$C(0,t) = C_o(k_o + k_1't + k_2't^2 + k_3't^3 + \ldots) \exp(-\gamma' t) \tag{4}.$$

Equation (4) is the same modified step-function that Sherman used to describe experimentally observed input concentration histories (1). As he pointed out, it is especially important to account for the actual inputs in studies on fibrous systems, since it is impractical to form sufficiently thick beds so that deviations from a perfect step change (which are unavoidable) can be safely neglected in the analysis.

In order to achieve solutions of Equation (2) it is first necessary to define expressions for $\partial \underline{Q}/\partial \underline{t}$, the rate of solute exchange between the particles and the fluid. For the No-Sorption case, $\partial \underline{Q}/\partial \underline{t}$ is simply zero. For the Equilibrium case, where the linear adsorption isotherm is described in terms of the partition coefficient $\underline{K}$ as $\underline{Q} = \underline{KC}$, it follows that

$$\partial Q/\partial t = K\, \partial C/\partial t \tag{5}.$$

Analytical solutions of the No-Sorption case and the Equilibrium case were obtained by Sherman in a slightly different form than employed by this writer. It will be seen later that numerical comparisons of the respective solutions provided an important check on this writer's solution and method of calculation.

INTRAPARTICLE DIFFUSION

The intraparticle diffusion cases are much more complex since $\partial Q/\partial t$ must be obtained from solutions of the appropriate diffusion equations and boundary conditions. One Fick's law diffusion equation that describes the radial movement of solute in an infinitely long circular fiber is[1]

$$D_F \left[\frac{\partial^2 A}{\partial r^2} + \frac{1}{r} \frac{\partial A}{\partial r} \right] = \frac{\partial A}{\partial t} \qquad (6),$$

where

D_F = intrafiber diffusion coefficient, sq. cm./sec.

A = local intrafiber solute concentration, mg./cc. fiber[2]

r = radial distance, cm.

t = time, sec.

It is noted here that the definition of A makes no distinction between solute that is (a) adsorbed on solid surfaces within a fiber, and (b) contained by solution within intrafiber pores.

Although the concept of an intrafiber pore-network in a swollen solid is an oversimplification in many respects, it serves an important function in the present diffusion considerations; i.e., if the very likely assumption is made that true surface diffusion effects are negligible, the transport of solute within a fiber should be effectively described by diffusion in the solution phase only. In accordance with this concept, Equation (6) can be modified to describe the

---

[1] Assuming a uniform external solution concentration.

[2] cc. fiber always refers to volume bounded by the exterior surface of fiber.

intrapore diffusion of solute in a swollen fiber, thus permitting a more meaningful comparison of intrafiber diffusion phenomena in different solute systems.

Suppose that the following definitions for local solute concentrations apply to a swollen fiber at any given radial distance, $\underline{r}$.

$\underline{A}$ = intrafiber solute concentration, mg./cc. fiber

$\underline{P}$ = intrapore solute concentration, mg./cc. solution

$\underline{S}'$ = adsorbed solute concentration, mg./cc. fiber

If it is assumed that the driving force for diffusion is the intrapore concentration gradient, the alternate differential equation for intrafiber diffusion can be written as

$$D_F' \left[\frac{\partial^2 P}{\partial r^2} + \frac{1}{r} \frac{\partial P}{\partial r} \right] = \frac{\partial P}{\partial t} + \frac{1}{\epsilon'} \frac{\partial S'}{\partial t} \qquad (7),$$

where $\underline{D_F'}$ is the intrapore diffusion coefficient, $\partial \underline{S}'/\partial \underline{t}$ represents the exchange of solute between local adsorption sites and adjacent solution in the pores of the fiber, and ϵ' is the internal porosity of a swollen fiber (cc. solution/cc. fiber). It follows from the nomenclature that $\underline{A} = \epsilon' \underline{P} + \underline{S}'$. If it is assumed that local equilibrium always prevails in the individual intrafiber pores, it follows from the linear adsorption equilibrium that $\underline{A} = \underline{KP}$, and therefore $\underline{S}' = (\underline{K} - \epsilon')\underline{P}$. Differentiating,

$$\frac{\partial S'}{\partial t} = (K - \epsilon') \frac{\partial P}{\partial t} \qquad (8).$$

Substituting into Equation (7), the following differential equation for intrafiber diffusion is obtained:

$$D_F' \left[\frac{\partial^2 P}{\partial r^2} + \frac{1}{r} \frac{\partial P}{\partial r} \right] = \frac{K}{\epsilon'} \frac{\partial P}{\partial t} \qquad (9).$$

It can be seen in this case that when $\underline{A}/\underline{K}$ is substituted for $\underline{P}$, Equation (9) becomes identical with Equation (6) when

$$D_F = D'_F \epsilon'/K \qquad (10).$$

SUMMARY OF INTRAPARTICLE DIFFUSION EQUATIONS, INITIAL CONDITIONS, AND BOUNDARY CONDITIONS

For intrafiber diffusion, the differential equation is

$$D_F \left[\frac{\partial^2 P}{\partial r^2} + \frac{1}{r} \frac{\partial P}{\partial r} \right] = \frac{\partial P}{\partial t} \qquad (11).$$

The initial condition is

$$P = C_o \qquad 0 \leq r \leq a \qquad t = 0 \qquad (12).$$

The boundary condition for Case 1(F) at $\underline{r} = \underline{a}$ is

$$P = C(Z,t) \qquad t > 0 \qquad (13).$$

The boundary condition for Case 2(F) at $\underline{r} = \underline{a}$ is

$$-D'_F \frac{\partial P}{\partial r} = k_L(P - C(Z,t)) \qquad t > 0 \qquad (14),$$

where $\underline{k_L}$ is the mass transfer coefficient, cm./sec.

For intrasphere diffusion, the differential equation is

$$D_F \left[\frac{\partial^2 P}{\partial r^2} + \frac{2}{r} \frac{\partial P}{\partial r} \right] = \frac{\partial P}{\partial t} \qquad (15).$$

The initial condition, and the boundary conditions for Cases 1(S) and 2(S), are the same as the corresponding intrafiber diffusion cases.

FINAL SOLUTIONS

The mathematical details involved, in obtaining analytical solutions of the two simultaneous, linear, second order, partial differential equations, are given in Appendix I for the various indicated initial and boundary conditions.

For purposes of generality, the input boundary condition given by Equation (4) for $\underline{Z} = 0$, $\underline{t} > 0$, was expressed in terms of dimensionless variables as

$$\frac{C(0,R)}{C_o} = \left[k_o + \sum_{n=1}^{f} k_n R^n \right] \exp(-\gamma R) \qquad (16),$$

where $\underline{R}$ $(= \underline{Ut}/\underline{Z_e})$ is the number of pore volumes of fluid displaced from a bed of length $\underline{Z_e}$, and $\underline{k_o}$, $\underline{k_1} = \underline{k_1'}(\underline{Z_e}/\underline{U})$, $\underline{k_2} = \underline{k_2'}(\underline{Z_e}/\underline{U})^2$, ... $\underline{k_f} = \underline{k_f'}\ (\underline{Z_e}/\underline{U})^{\underline{f}}$, and $\gamma = \gamma'(\underline{Z_e}/\underline{U})$ are experimentally determined input constants.

All six of the previously mentioned cases were found to be described by a single desorption washing equation that can be expressed in terms of dimensionless variables as follows:

$$\frac{C}{C_o} = 1 - \frac{1}{\pi} \int_{o}^{\omega=R} \left[1 - \left(k_o + \sum_{n=1}^{f} k_n (R-\omega)^n\right) \exp(-\gamma(R-\omega))\right]$$

$$\int_{o}^{\eta=\infty} \exp\left[\frac{1}{2S} - \left(\frac{\psi}{2S}\left(1 + M/\psi\right)\right)^{1/2}\right]$$

$$\cos\left[\omega\eta - \left(\frac{\psi}{2S}\left(1 - M/\psi\right)\right)^{1/2}\right] \, d\eta \, d\omega \qquad (17).$$

Here, $\underline{R} = \underline{Ut}/\underline{Z_e}$, $\underline{S} = \underline{D_L}/\underline{UZ_e}$, η and ω are dimensionless variables of integration,

$$\psi = (M^2 + N^2)^{1/2} \qquad (18)$$

and $\underline{M}$ and $\underline{N}$ represent characteristic expressions for the various cases.

The six solutions, differing only in the definitions used for the dimensionless quantities $\underline{M}$ and $\underline{N}$, are summarized as follows, using the additional nomenclature $\underline{F} = \underline{D_F}/\underline{a}^2$ and $\underline{K}' = \underline{K}(1 - \epsilon)/\epsilon$:

1. For the No-Sorption case, $\underline{M} = 1/4\underline{S}$ and $\underline{N} = \eta$.

2. For the Equilibrium case, $\underline{M} = 1/4\underline{S}$ and $\underline{N} = \eta(1 + \underline{K}')$. The characteristic expressions for $\underline{M}$ and $\underline{N}$, that apply to intraparticle diffusion Cases 1(F), 2(F), 1(S), and 2(S), can be conveniently written as follows, where $\underline{A_n}$ depends on the particular case.

$$M = 1/4S + 4FK' \sum_{n=1}^{\infty} \frac{\eta^2 (U/Z_e) A_n}{(\eta U/Z_e)^2 + F^2 \beta_n^4} \tag{19}$$

$$N = \eta + 4F^2K' \sum_{n=1}^{\infty} \frac{\eta \beta_n^2 A_n}{(\eta U/Z_e)^2 + F^2 \beta_n^4} \tag{20}$$

3. For the intrafiber diffusion Case 1(F), where no liquid-phase mass transfer resistance exists, $\underline{A_n} = 1$, and the β_n's are positive roots of the zero-order Bessel function

$$J_o(\beta_n) = 0 \tag{21}$$

4. For the intrafiber diffusion Case 2(F), where a finite mass transfer resistance exists in the fluid,

$$A_n = L^2/(L^2 + \beta_n^2) \tag{22}$$

Here, $\underline{L} = \underline{ak_L}/\underline{D_F'}$, and the β_n's are positive roots of the transcendental equation (involving zero and first-order Bessel functions)

$$\beta_n J_1(\beta_n) = L J_o(\beta_n) \tag{23}$$

5. For the intrasphere diffusion Case 1(S), where no mass transfer resistance exists in the fluid, $\underline{A}_n = 6/4$, and the $\beta_{\underline{n}}$'s are real roots of

$$\beta_n \cot(\beta_n) = -\infty \qquad (24).$$

6. For the intrasphere diffusion Case 2(S), where a finite mass transfer resistance exists in the fluid,

$$A_n = 6L^2/4(L^2 - L + \beta_n^2) \qquad (25).$$

Here $\underline{L}$ is defined as before and the $\beta_{\underline{n}}$'s are real roots of the transcendental equation

$$\beta_n \cot(\beta_n) + L = 1 \qquad (26).$$

Finally, the solution to a first-order chemical reaction case, where intrafiber diffusion is described by the Equilibrium case and the rate of reaction is $\frac{(1-\epsilon)}{\epsilon} \partial\underline{Q}/\partial\underline{t} = -\underline{k}''\underline{C}$, is given by $\underline{M} = 1/4\underline{S}$ and $\underline{N} = \eta$ when the exponential of the inner integral of Equation (17) is redefined as

$$\exp\left[\frac{1}{2S} + \frac{k''Z_e\omega}{U} - \left(\frac{\psi}{2S}(1 + M/\psi)\right)^{1/2}\right] \qquad (27).$$

SOLUTIONS FOR SORPTION WASHING

It is noted that Equation (17) describes the desorption washing process. It follows that the various solutions can also be used to describe the sorption washing process, according to the simple relation

$$(C/C_\infty)_{sorption} = 1 - (C/C_o)_{desorption} \qquad (28).$$

In this case $\underline{C}_\infty$ is the equilibrium solute concentration (at long times), the initial condition is

$$C = 0 \qquad Z \geq 0 \qquad t = 0 \qquad (29),$$

and the inlet boundary condition for $Z = 0.$, $t > 0.$, is expressed as

$$\frac{C(0,R)}{C_\infty} = 1 - \left[k_o + \sum_{n=1}^{f} k_n R^n\right] \exp(-\gamma R) \qquad (30).$$

The various equations describing the No-Sorption case, Equilibrium case, Case 1(F) and Case 2(F) were programmed for calculation on an IBM 1620 computer. The details of the programs, and verification of calculated results, are given in Appendix II. Cases 1(S) and 2(S) can also be evaluated by these programs if the appropriate β_n values are supplied.

RELATED THEORETICAL DEVELOPMENTS BY OTHER WORKERS

PREVIOUS DERIVATIONS

Sherman (1) has indicated some solutions of Equation (2) that have been obtained by other workers for linear equilibrium cases where $\partial Q/\partial t$ is proportional to $\partial C/\partial t$. Generally, one of three different inlet boundary conditions have been employed; these are the (a) sinusoidal or harmonic input, (b) pulse input, and (c) instantaneous step-function input.

Kasten, Lapidus, and Amundson (2), and Rosen (3) presented analytical solutions for the equivalent of Cases 1(S) and 2(S) when longitudinal dispersion is neglected, a step-function input is used, and a linear adsorption isotherm is assumed. Rosen (4) illustrated some numerical solutions for these cases.

SIMULTANEOUS SOLUTIONS OF DISPERSION AND DIFFUSION EQUATIONS

An important theoretical development was recently made by Turner (5, 6), who obtained a solution to Equation (2) that (a) utilized the sinusoidal inlet boundary

condition, (b) accounted for longitudinal dispersion, and (c) accounted for molecular diffusion from stagnant pockets of fluid within a packed bed. The stagnant pockets were assumed to be uniformly distributed along each flow channel. His Model 1 assumed uniform sized pockets and his Model 2 assumed pockets of different radii and length. The solutions he obtained could be used in trial and error fitting of frequency response data under certain experimental conditions. His intended application, of determining the physical flow structure of a bed, is limited to the extent that a distribution of pocket radii and lengths must be assumed before the volume distribution of deadwater spaces can be evaluated.

In connection with the present work, it is apparent that Turner's models might be applied to certain systems where intraparticle diffusion is involved. For example, his Model 1 was based on many of the same considerations as Cases 1(F) and 1(S), except for the facts that he used (a) a sinusoidal input, and (b) a prismatic "particle" geometry, which considerably simplified the mathematical treatment.

Aris (7) further generalized Turner's Model 1 in terms of a continuous distribution of pocket sizes, which removed some of the arbitrariness in the choice of pocket length. Aris made a further contribution by demonstrating an important alternative solution to Turner's models. In this case he substituted the Laplace transform of $\partial Q/\partial t$ into the transformed differential equation for longitudinal dispersion. The equivalent step for cylindrical and spherical particle geometries is seen in Appendix I of this paper. His solution differed at this point, however, in that the inverse transform was not evaluated. Instead he applied a previously demonstrated method of moments (8) to the transformed equation, and illustrated how the longitudinal dispersion and diffusion parameters of Turner's models can be obtained directly from the first and second moments of breakthrough curves,

when a pulse input boundary condition is employed. One result of his derivation, for a slightly modified version of Model 1 (where the pocket length follows a continuous distribution and the cross section is constant), was that the mean square length of the pockets is the determining geometric factor that affects diffusion in this case. Aris also applied this technique to Model 2, where the cross sections of the pockets are distributed; the results for this case were more complicated than those for Model 1, however.

The application of the method of moments deserves brief mention, since it is very useful in characterizing certain types of response functions in unsteady state analysis. It can be illustrated as follows in terms of the exit concentration $\underline{C}(\underline{Z},\underline{t})$. The $\underline{n}$'th moment with respect to the origin is defined as

$$M_n = \int_0^\infty t^n \, C(Z,t) \, dt \qquad (31)$$

If $\underline{M_n}$ is finite, then it can also be defined in terms of the Laplace transform of $\underline{C}$ (with respect to $\underline{t}$), $\overline{\underline{C}} = \underline{f}(\underline{p})$, as

$$M_n = (-1)^n \lim_{p \to 0} \frac{d^n}{dp^n} f(p) \qquad (32)$$

Thus, the parameters of a given model must appear in the various moment expressions, and can therefore be evaluated from experimental moment values.

The important advantages of the method of moments are that (a) it is unnecessary to perform the laborious inverse transformation and the subsequent additional integrations, and (b) trial and error calculations on individual breakthrough curves are avoided. Butt (9) has discussed a number of applications and limitations of the method. In general, its usefulness is limited by the facts that (a) it is very difficult to obtain sufficiently accurate experimental

data so that moments higher than second order can be accurately evaluated, and (b) the mathematical expressions for higher moments are often quite similar in different models. Thus, one soon approaches a point of diminishing returns in devising and applying elaborate mathematical models.

Finally, Glaser and Litt (10) have indicated some recent studies on mixed phase flow through fixed beds of porous particles (sometimes called trickle beds), and have applied Aris' method of moments treatment (7) (on Turner's Model 1) to this problem. Instead of employing an average dispersion coefficient, Glaser and Litt defined an expression for longitudinal dispersion in terms of the molecular diffusivity and three geometric bed parameters. The physical significance of these factors was attributed to (a) liquid dispersion due to mixing of streams from various channels of different residence times, (b) dispersion from axial diffusion in the void channels, and (c) dispersion from stagnant-pocket diffusion.

INTRAFIBER DIFFUSION AS APPLIED TO RATE OF SORPTION IN A WELL-STIRRED FINITE DYEBATH

A convenient means of determining D_F/a^2 independently, in some solute-fiber systems, involves rate of sorption measurements in a well-stirred finite dyebath. Well-stirred in this case refers to the assumption that no mass transfer resistance exists in the fluid. That a finite dyebath is used indicates that the concentration of solute in solution changes with time until an equilibrium value is obtained.

The previously described differential equation for Fick's law diffusion in a long circular cylinder was assumed to apply; i.e., Equation (11). The initial condition, in terms of the initial solution concentration C_o, is

$$P = C_o \qquad 0 \leq r \leq a \qquad t = 0 \qquad (33).$$

It is assumed that the fiber slurry is sufficiently well stirred so that the boundary condition at the fiber surface becomes

$$P = C \qquad r = a \qquad t > 0 \tag{34}$$

where C is the uniform solution concentration which changes with time. The solution to these conditions has been previously worked out (11).

$$\frac{Q_t}{Q_\infty} = Q_F = 1 - \sum_{n=1}^{\infty} \frac{4\lambda'(1+\lambda')}{4(1+\lambda') + \lambda'^2\beta_n^2} \exp(-\beta_n^2 D_F t/a^2) \tag{35}$$

λ' = $V_s/K\pi a^2 W_F V$, ratio of fluid volume to effective fiber volume, dimensionless

Q_t = solute sorbed at time t, mg./cc. fiber

Q_∞ = solute sorbed at equilibrium, mg./cc. fiber

Q_F = fractional sorption

β_n = nonzero positive roots of the transcendental equation

$$2J_1(\beta_n) + \lambda' \beta_n J_o(\beta_n) = 0 \tag{36}$$

J_o, J_1 = Bessel functions of zero and first order

V_s = solution volume, cc.

K = partition coefficient

W_F = fiber mass, g., o.d.

V = swollen specific volume of fibers, wet cc./g., o.d.

The fractional uptake was calculated from the above equation and verified against previously published results (12) over the time range of 2-30 sec. for values of D_F/a^2 varying between 0.005 and 0.03. The first six roots (β_1, β_2,... β_6) were found to yield adequate convergence of the series when the values of λ'

were varied between 2 and 3 (this corresponded to the prevailing conditions in the sorption rate experiments).

EXPERIMENTAL

CHARACTERIZATION OF ALL-SKIN VISCOSE

GENERAL CHARACTERISTICS

The all-skin viscose yarns used in this study were supplied on special order by The American Viscose Co., Inc. The 1, 4, 16, and 64-denier yarns came from the same skeins that were used by Sherman (1). Cross-section photomicrographs of dry-mounted fibers at 800X are shown in Fig. 1 and 2.

It was important to characterize certain properties of the viscose yarns which could affect the intrafiber diffusion process. The degree of circularity is often a good indication of whether or not the usual skin-core structure prevails in a viscose rayon, since differential shrinkage during coagulation generally results in the appearance of serrated edges. The physical properties of the fibers (to be discussed later) indicate that the 1-denier viscose was stretched to the greatest degree after coagulation, and the 64-denier to the least. If all four viscoses were coagulated and regenerated in the same baths (which is assumed, but cannot be established) the observed differences in properties should be primarily due to differences in stretching. Although the manufacturing conditions were not given, it can be speculated from other results that the coagulating bath contained ammonium sulfate (not other metallic sulfates), and the subsequent regenerating bath a dilute solution of sulfuric acid; in this manner an all-skin viscose with a highly uniform cross section can be formed (13, 14).

There are several means of demonstrating the presence of a skin-core structure. One technique, outlined by Hermans (15), is well suited for viscose that has an especially thin skin. This method was applied to samples of 1, 4, and

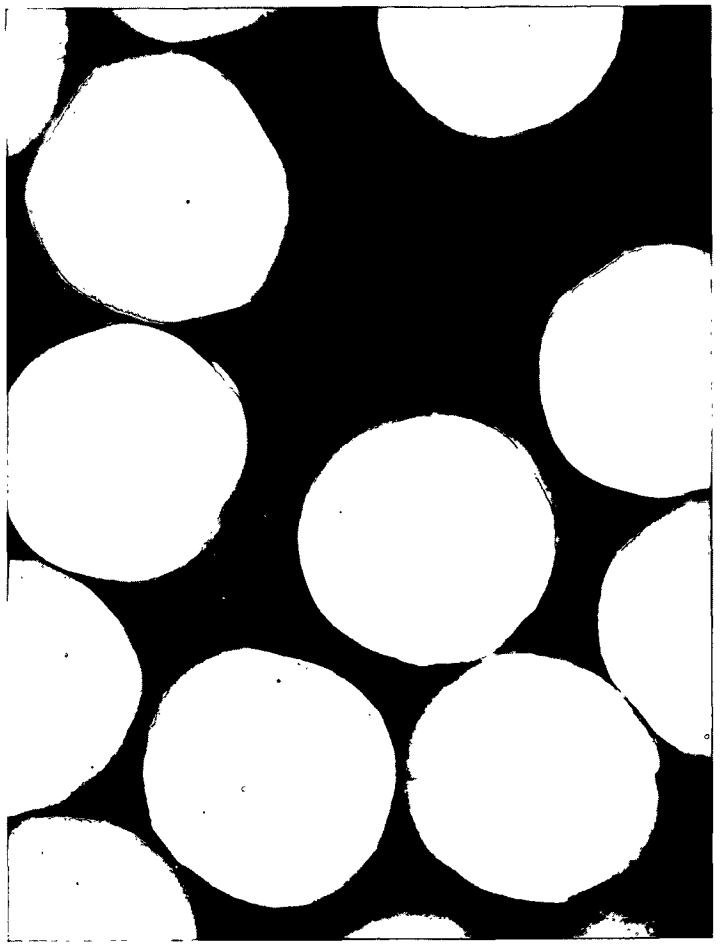

16-Denier Viscose, 800X

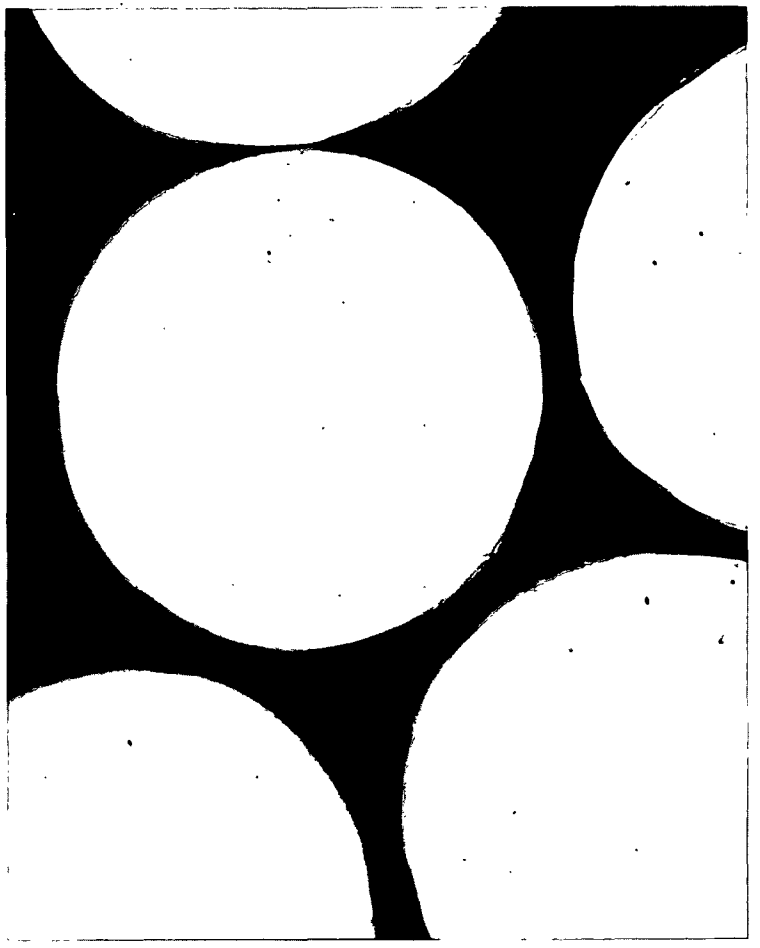

64-Denier Viscose, 800X

Figure 1. Cross-Section Photomicrographs of Dry-Mounted Fibers

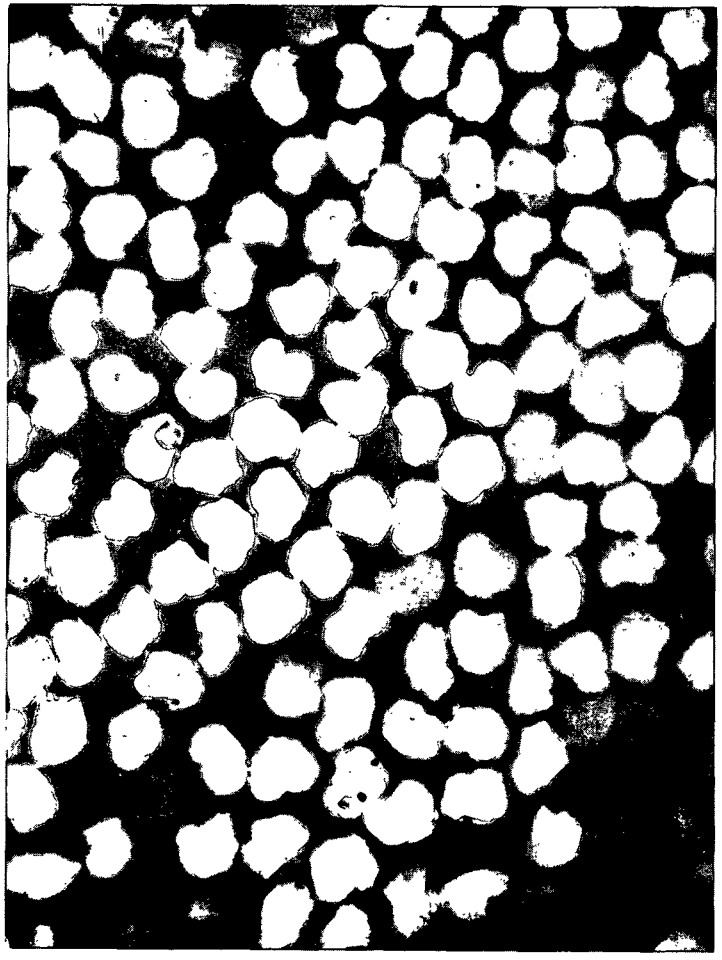

1-Denier Viscose, 800X

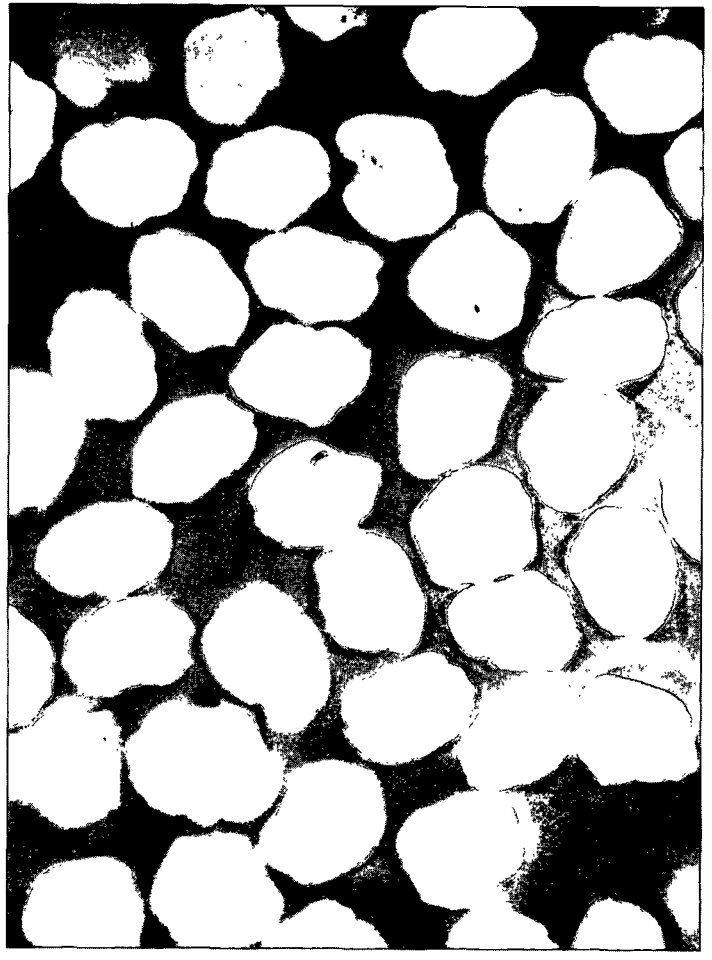

4-Denier Viscose, 800X

Figure 2. Cross-Section Photomicrographs of Dry-Mounted Fibers

16-denier fibers. It essentially consisted of (a) staining mounted cross sections with Victoria Blue B (CI 729) for a minimum of one hour, (b) rinsing and washing the mounted sections with 89% alcohol (5-10 minutes for the 1 and 4-denier viscose, and one hour or more for the 16-denier viscose), (c) clearing the mounts with xylene, and (d) mounting the sections in Canada Balsam for examination. Figure 3 illustrates photomicrographs of the most revealing sections that were obtained. In each case a thin peripheral skin is seen, but its relative size is generally much smaller than found in normal viscoses.

PHYSICAL MEASUREMENTS

The airdry and water-swollen fiber diameters were measured microscopically with a calibrated eyepiece (magnification of 278X).

The longitudinal swelling was determined by first mounting a number of long, airdry fibers between glass slides. The fiber images, in conjunction with calibration marks, were projected at a relatively high magnification (about 20X) on a flat surface. The individual fiber projections were traced over and measured with a planimeter. The fibers were then wetted and similar length measurements were made. The longitudinal swelling was expressed as a percentage of the airdry length.

The water-swollen specific volume (wet cc./g., o.d.) was determined by cutting a length of yarn (from 5 to 30 cm.) and subdividing it into a strand having a manageable number of filaments. A thin cross section of the strand was cut with scissors and the resulting bundle of short fibers was carefully transferred to the glass plate of a low-power, large field, binocular microscope. The fibers were counted one-by-one with the aid of a dissecting needle. The strand of fibers was then weighed on a semimicro balance. The moisture content

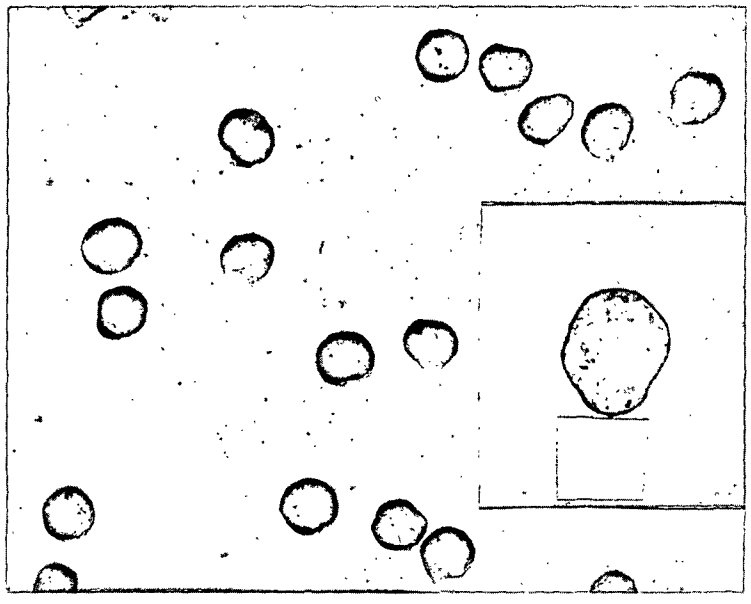

16-Denier, 150X
(insert, 325X)

4-Denier Viscose, 540X

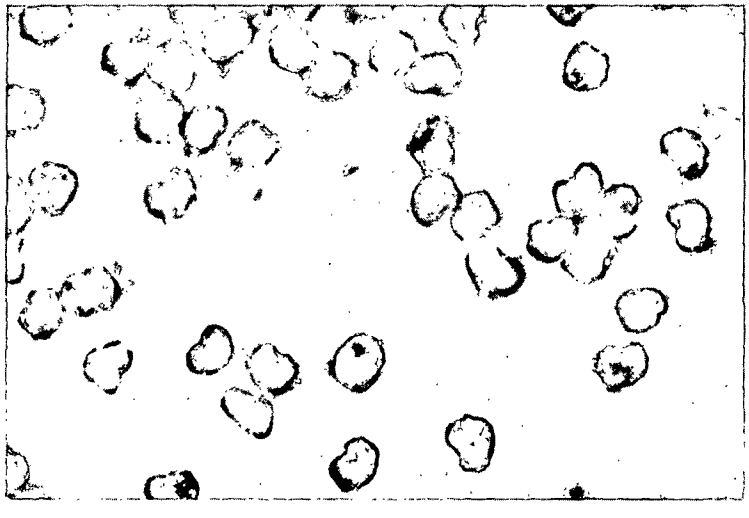

1-Denier, 540X

Figure 3. Cross-Section Photomicrographs of Viscose Fibers Stained with Victoria Blue

of a separate sample of fibers was determined after drying at 105°C. The water-swollen specific volume was calculated from the water-swollen fiber diameter, the airdry length of the filaments in the strand, the longitudinal swelling, and the ovendry weight of the fibers.

The pycnometric specific volume, defined as the volume of fiber denied to water per gram of ovendry fiber, was determined in the following manner. About four grams of yarn were immersed in boiling water and were deaerated in a vacuum desiccator by applying a partial vacuum for about 10 min. When the slurry had cooled to 30°C. the yarn was transferred underwater to a 25-ml. wide mouth pycnometer, and the pycnometer was sealed and weighed. The weight of the pycnometer containing water only was recorded. The yarn was dried at 105°C. and weighed. The pycnometric specific volume was calculated from the expression

$$V_p = [1 - (\overline{PWF} - \overline{PW})/W_F]/\rho \qquad (37),$$

where

ρ = density of water, g./cc.

$\underline{W_F}$ = mass of fiber, g., o.d.

$\underline{\overline{PW}}$ = mass of pycnometer plus water, g.

$\underline{\overline{PWF}}$ = mass of pycnometer plus water plus fiber, g.

The porosity of the swollen fibers was calculated from the expression

$$\epsilon' = (V - V_p)/V \qquad (38),$$

where $\underline{V}$ is the water-swollen specific volume of the fibers.

The results of the all-skin viscose fiber characterization are shown in Table I. The data in parentheses were obtained by this author; the remainder of the data was obtained by Sherman (1) on the same viscose yarn.

TABLE I

ALL-SKIN VISCOSE CHARACTERISTICS

	Denier			
	1	4	16	64
Av. fiber diameter				
Airdry, μ	11.07 ±2.8%[a]	--	40.82 ±2.2%	84.56 ±1.8%
Water-swollen, μ	15.91 ±3.3%	29.89 ±2.3%	60.35 ±2.3%	122.1 ±1.2%
Swelling (diameter), %	43.7	--	46.8 ±13%	44.5 ±13%
Swelling (length), %	(3.1)	(2.9)	6.4	--
Water-swollen sp. vol., cc./g., o.d.	(1.925)	(1.694)	1.622 ±6.9%	1.612
Pycnometric sp. vol., cc./g., o.d.	(0.598)	(0.613)	0.6207 ±0.3%	--
Fiber porosity	(0.690)	(0.638)	0.618	--

[a] ± Limits are 2σ limits (measure of precision).

The x-ray diffraction of small straightly-oriented bundles of 1, 4, and 16-denier fibers was investigated to look for differences in crystallite orientation. The focused x-ray beam was passed perpendicular to the fiber axis and the film plane was perpendicular to the incident beam. Details of the equipment and techniques used are given elsewhere (16). Figure 4 illustrates the x-ray diffraction patterns that were obtained. It appeared that the crystallite orientation of the 16-denier viscose was considerably less than that in the 1 and 4-denier viscoses. The ranking of the latter two was uncertain without the benefit of quantitative measurements.

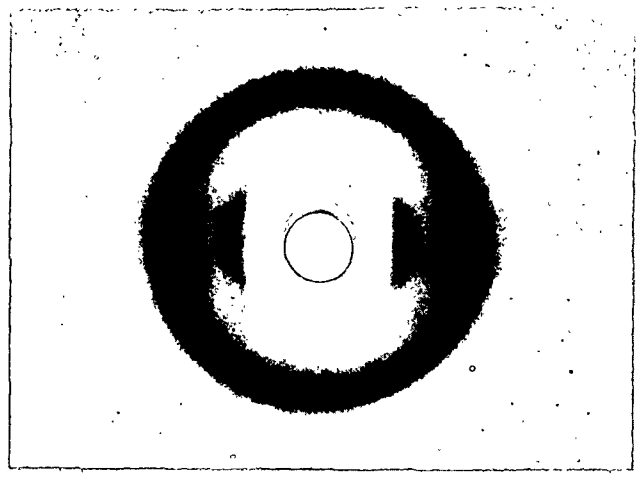

16-Denier Viscose

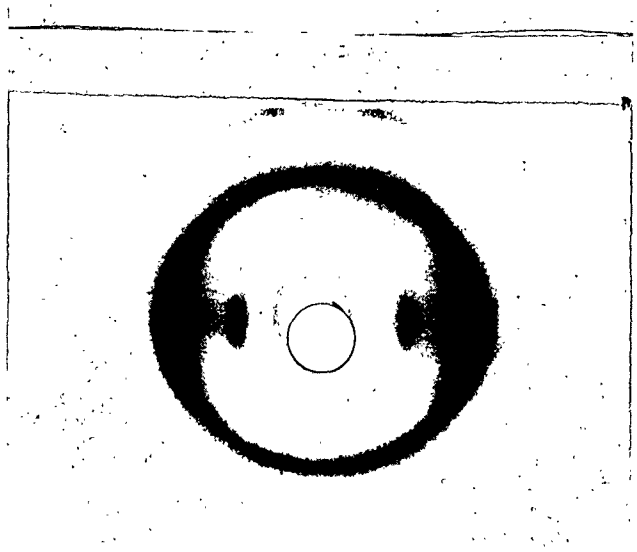

4-Denier Viscose

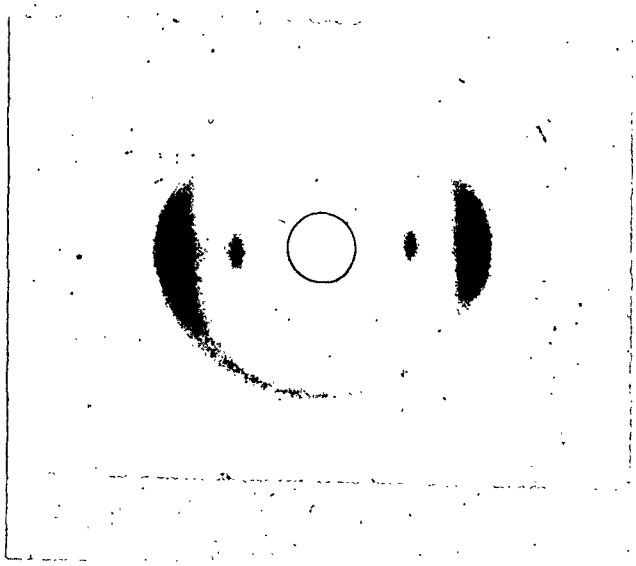

1-Denier Viscose

Figure 4. X-ray Diffraction Patterns from Viscose Fibers

FIBER PREPARATION

Viscose yarn was cut into various uniform fiber lengths with a razor blade jig. The jig consisted of several single edge razor blades pinned together with three bolts, and uniformly spaced with small washers. The jig was used in conjunction with an air-operated press to cut straight lengths of yarn into fibers.

Random samples of the resulting fibers were examined by projecting their magnified images (20X) on a sheet of paper in conjunction with suitable calibration marks. The fiber images were traced over in pencil and their lengths were determined with a planimeter. For each fiber size, three samples of 30-40 fibers were measured. Table II illustrates the results obtained.

TABLE II

FIBER LENGTH DETERMINATIONS

	Denier			
	1	4	16	64
Sample A, length, mm.	1.900	2.73	5.34	6.18
Sample B, length, mm.	1.830	2.83	5.32	6.21
Sample C, length, mm.	1.880	2.74	5.25	6.08
Av. length, airdry, mm.	1.871	2.77	5.30	6.16
Av. length, water-swollen, mm.	1.93	2.85	5.64	6.55
Length-to-diameter ratio, water-swollen	121.3	95.3	93.5	53.6

CHARACTERIZATION OF SOLUTES

CHOICE OF SOLUTE

The measurement of solute concentration by means of light transmission, in a continuously changing aqueous medium, is considerably simplified when (a) the

solute in solution absorbs light in the visible region, (b) the absorption obeys Beer's law, and (c) the refractive index of a sufficiently concentrated solution is nearly the same as that of water, so that a negligible amount of light is scattered when the solution concentration is suddenly changed.

DIACETYL

Diacetyl was chosen as a solute because it satisfies the above requirements and has three additional important characteristics (1). First, it is nonionic; thus, long range electrical effects in solute-solute interactions and in solute-substrate interactions are rendered negligible. Secondly, it is not adsorbed on viscose to an appreciable extent. Thirdly, it is a small molecule and it diffuses quite rapidly in swollen viscose. Diacetyl was obtained in a relatively pure form from Distillation Products, a division of Eastman Kodak Co.

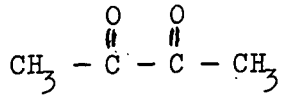

Diacetyl

PARA-PHENYLAZOANILINE

Para-phenylazoaniline, hereafter referred to as PAA, was chosen as a second solute.

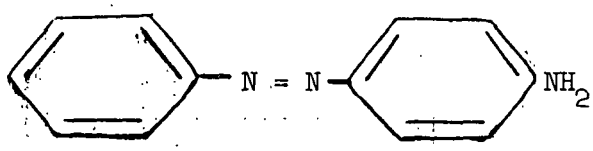

p-Phenylazoaniline

It has the following properties.

1. Water solubility is 141 mg./l. at 60°C. (17) and is considerably lower at 25°C.

2. Solutions are colored yellow-green and they obey Beer's law (to be shown later).
3. Refractive index of a 3 mg./l. solution (average initial concentration used in washing runs) differs very little from that of water at the same temperature.
4. PAA is nonionic at neutral pH values; a color change occurs in solution between pH 2.2 and 3.3.
5. PAA is adsorbed to a considerable extent on viscose and its isotherm is linear (17).

PAA was obtained in a relatively pure form from Distillation Products. The melting point of the raw material was 121-123°C. A sufficiently large quantity of this product was dissolved in 95% ethanol, precipitated in a large volume of distilled water, filtered, and air dried. The melting point of the precipitated material was 122-123°C. An accepted melting point of PAA is 123°C. (18).

BENZOPURPURINE 4B

Benzopurpurine 4B, C.I. 448, referred to as BPP, was chosen as a third solute. It is an ionic direct dye and has the following molecular structure.

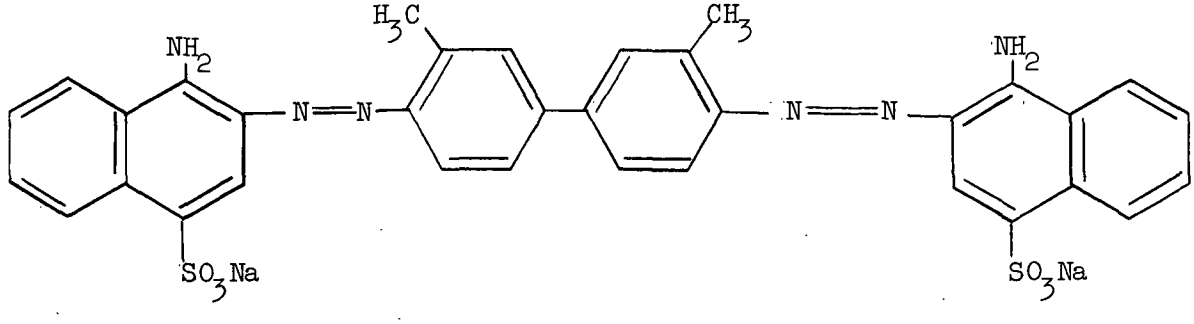

The BPP used in this study was obtained from the American Cyanamid Company, Calco Chemical Division. The application of Beer's law, to dilute solutions,

was checked in the washing apparatus and found to be valid (the technique of measurement is described in greater detail, later).

APPLICABILITY OF BEER'S LAW IN THE PAA-WATER SYSTEM

The data presented in Table III show that Beer's law was obeyed by PAA in aqueous solution. The optical densities were determined on a Beckman DU Spectrophotometer at 372 mμ.

TABLE III

APPLICABILITY OF BEER'S LAW IN PAA-WATER SYSTEM

Concentration[a]	Optical Density[b]	$\frac{k}{b}$[c]
0.387	0.041	9.44
0.970	0.104	9.33
1.45	0.157	9.24
1.93	0.206	9.37
2.41	0.259	9.30
2.90	0.309	9.39
3.87	0.411	9.42
4.84	0.509	9.50

[a] Concentration, mg. PAA/l. solution.

[b] Log_{10} (1/transmission) determined at 372 mμ.

[c] $\frac{k}{b}$ = concentration/optical density.

ADSORPTION ISOTHERM DETERMINATION

The adsorption isotherms of PAA on 1, 4, and 16-denier viscose were determined experimentally in aqueous media. The technique and method of analysis is described in Appendix III. The results of the determinations are shown in Fig. 5,

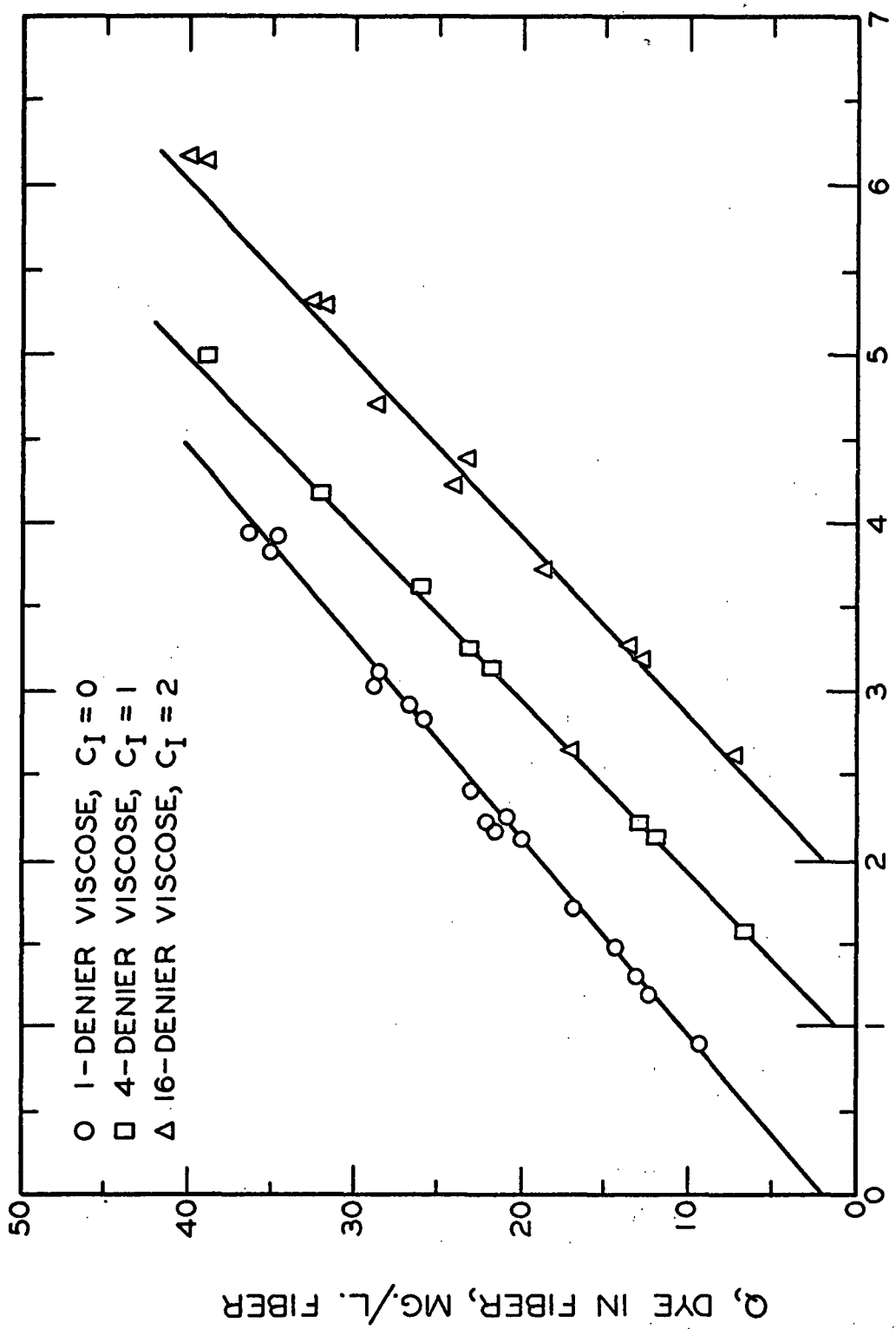

Figure 5. Adsorption Isotherms of PAA on Viscose

where the intrafiber dye concentration, Q, is plotted against the solution dye concentration, C. The isotherms are seen to be linear with a small positive intercept at zero solution concentration. The partition coefficients K_I were obtained by evaluating the slopes of the isotherms, and are listed in Table IV.

TABLE IV

PARTITION COEFFICIENTS OF PAA ON VISCOSE

Denier	V, wet cc./g., o.d.	T, °C.	K_I[a]	$K''=K_IV$
1	1.925	26.5	8.58	16.5
4	1.694	26.4	9.80	16.6
16	1.622	26.3	9.50	15.4

[a] K_I = (mg. dye/wet cc.)/(mg. dye/cc. solution)

PREVIOUS ADSORPTION RESULTS

The PAA-viscose system has a number of important characteristic properties. The following is a summary of results obtained by Aspland and Bird (17), who investigated the adsorption of several nonionic dyes on viscose rayon, at temperatures between 40 and 80°C. Among the 13 dyes studied, PAA and eight derivatives of PAA were included. For the PAA-viscose system (and the 12 other dye systems), they observed the following results.

1. The adsorption isotherms were linear up to a fiber saturation point, corresponding to saturation of the aqueous phase.

2. A small positive intercept existed at zero solution concentration in each case. These intercepts were attributed to the presence of viscose particles in their dye extracts, which could not be removed by filtration or centrifugation, and which absorbed visible and ultraviolet radiation.

3. The equilibrium was found to be truly reversible in one case, and was assumed to be in the remaining cases.

4. The partition coefficients were observed to decrease with increasing temperature in the usual manner when physical adsorption is involved.

5. The fiber saturation values increased with increasing temperature (as did the aqueous solubilities). The highest fiber saturation values (as well as the lowest partition coefficients) were obtained with the compounds having the highest aqueous solubility.

6. No evidence of aggregation in aqueous solution was detected from spectrophotometric measurements.

7. The affinity (a measure of the degree of adsorption in the swollen cellulose phase; to be defined later) of one dye was nearly the same on viscose rayon and cotton. This suggested that the adsorption was not affected by (a) the type of cellulose, or (b) the presence of carboxyl groups in viscose.

8. The affinity of PAA for viscose was only slightly changed (from 1.91 to 1.97 kcal./mol.) by dyeing in the presence of 0.05 mole/liter sodium chloride.

THERMODYNAMICS OF ADSORPTION

Aspland and Bird investigated the thermodynamics of nonionic dye adsorption, on viscose, by obtaining isotherms at three different temperatures (40, 60, 80°C.) for seven related dyes. The affinity of a dye for viscose was defined as the change in standard chemical potential, $-\Delta\mu^{\circ}$, given by

$$-\Delta\mu^{\circ} = RT \ln (K''/V_{\phi}) \qquad (39).$$

In this case, $\underline{K}''$ was defined as the partition coefficient, and it had the units of (mg. dye/g. fiber)/(mg. dye/cc. solution); the volume term, $\underline{V}_{\phi}$, was defined as the effective volume of the cellulose phase, and it had the units of cc./g. fiber to make $\underline{K}''/\underline{V}_{\phi}$ dimensionless. The purpose of introducing the effective volume of the cellulose phase was to standardize the affinity for different cellulose substrates; thus, by using an appropriate value of the volume term for a given cellulose substrate, one would obtain the same numerical results for the affinity. For viscose, Aspland and Bird chose a value of $\underline{V}_{\phi}$ = 0.45 cc./g. fiber. This figure was based on results obtained by Marshall and Peters (19), where it was found that consistent affinities were obtained for a limited number of adsorption isotherms on four different cellulose substrates. Attempts to relate $\underline{V}_{\phi}$ to the physical properties of the various celluloses yielded unaccounted-for discrepancies in the results, however.

Table V summarizes the experimental values of the partition coefficient, and the calculated affinities, that were obtained by Aspland and Bird. The results in parentheses represent values that were extrapolated by this writer.

TABLE V

TEMPERATURE DEPENDENCE OF PAA ADSORPTION

$\underline{T}$, °C.	$-\Delta\mu^{o}$, cal./mol.[a]	$\underline{K}''/\underline{V}_{\phi}$ [a]	$\underline{K}''$[b]
25	--	(42.9)	(19.30)
28	--	(39.7)	(17.87)
40	2120	30.2	13.60
60	1910	18.0	8.10
80	1800	13.0	5.85

[a] Using $\underline{V}_{\phi}$ = 0.45 cc./g., o.d., from Marshall and Peters (19).

[b] $\underline{K}''$ = (mg. PAA/g., o.d.)/(mg. PAA/cc. solution).

Aspland and Bird calculated heats of dyeing from the slopes of linear plots, $(\Delta\mu^{\circ}/T)$ vs. $(1/T)$; a value of -4.7 kcal./mol. (exothermic) was obtained for the PAA-viscose system. The heat of solution of PAA in water was given elsewhere (20) as +10.3 kcal./mol. By comparing the seven related nonionic dye systems, they observed a statistically significant inverse correlation between the heats of dyeing and the aqueous solubilities. They concluded that this finding suggests that the combination between nonionic dyes and cellulose takes place through non-polar van der Waals forces.

SORPTION RATE DETERMINATION IN A WELL-STIRRED FINITE DYEBATH

A method was developed for measuring the rate of sorption of PAA by viscose fibers in a well-stirred dilute slurry. These rate data corresponded to the diffusion case given by Equation (35) for sorption in a well-mixed dyebath of finite size. An analysis of these data was used to provide an independent determination of the intrafiber diffusion parameter, D_F/a^2.

The experimental details and method of analysis are given in Appendix IV. It should be noted that the use of a finite dyebath has an important advantage; i.e., the fractional uptake of dye, by the fiber, can be calculated accurately from a knowledge of how the dye solution concentration changes with time.

A total of 17 sorption rate experiments were performed on the PAA-16 denier system. Thirteen of these represent Series 1, where one batch of viscose was used. Four additional experiments, representing Series 2, were conducted on a second batch of viscose at lower consistencies, lower initial concentrations, and higher final concentrations. The stirring action appeared to be slightly better in Series 2.

Eleven sorption rate experiments were performed on the PAA-4 denier system. The stirring action was noticeably less effective with these fibers. It will be evident that the experimental technique was not well suited for application to the PAA-4 (and also 1) denier system.

The experimentally determined fractional sorptions, Q_F, were plotted as functions of elapsed time, t, in Fig. 6. The corresponding numerical values, along with C_o and C_∞, the initial and final solution concentrations, and the partition ratios, $\Delta Q/\Delta C$, are given in Appendix IV.

Predicted Q_F vs. t relationships from Equation (35) are also shown in Fig. 6. It is apparent that the PAA-16 denier rate data were quite well described by $D_F/a^2 = 0.010$. The PAA-4 denier rate data were considerably scattered, less conclusive, and only approximately described by $D_F/a^2 = 0.030$.

Approximate evaluations of the partition coefficients, K_S, from each series of sorption rate experiments, are shown in Table VI. The 4-denier result was in fairly good agreement with the adsorption isotherm value (9.56 vs. 9.80, respectively), but the 16-denier result was in somewhat lesser agreement (9.91 vs. 9.50). Difficulties related to the positive isotherm intercept, at zero solution concentration, were apparently responsible for a small degree of uncertainty in the partition coefficient results.

EXPERIMENTAL EQUIPMENT FOR WASHING RUNS

WASHING APPARATUS

The central piece of experimental equipment, the washing apparatus, was designed and built by Sherman (1). In this apparatus, fiber beds were formed, compressed to a known porosity, and subjected to a number of washing experiments.

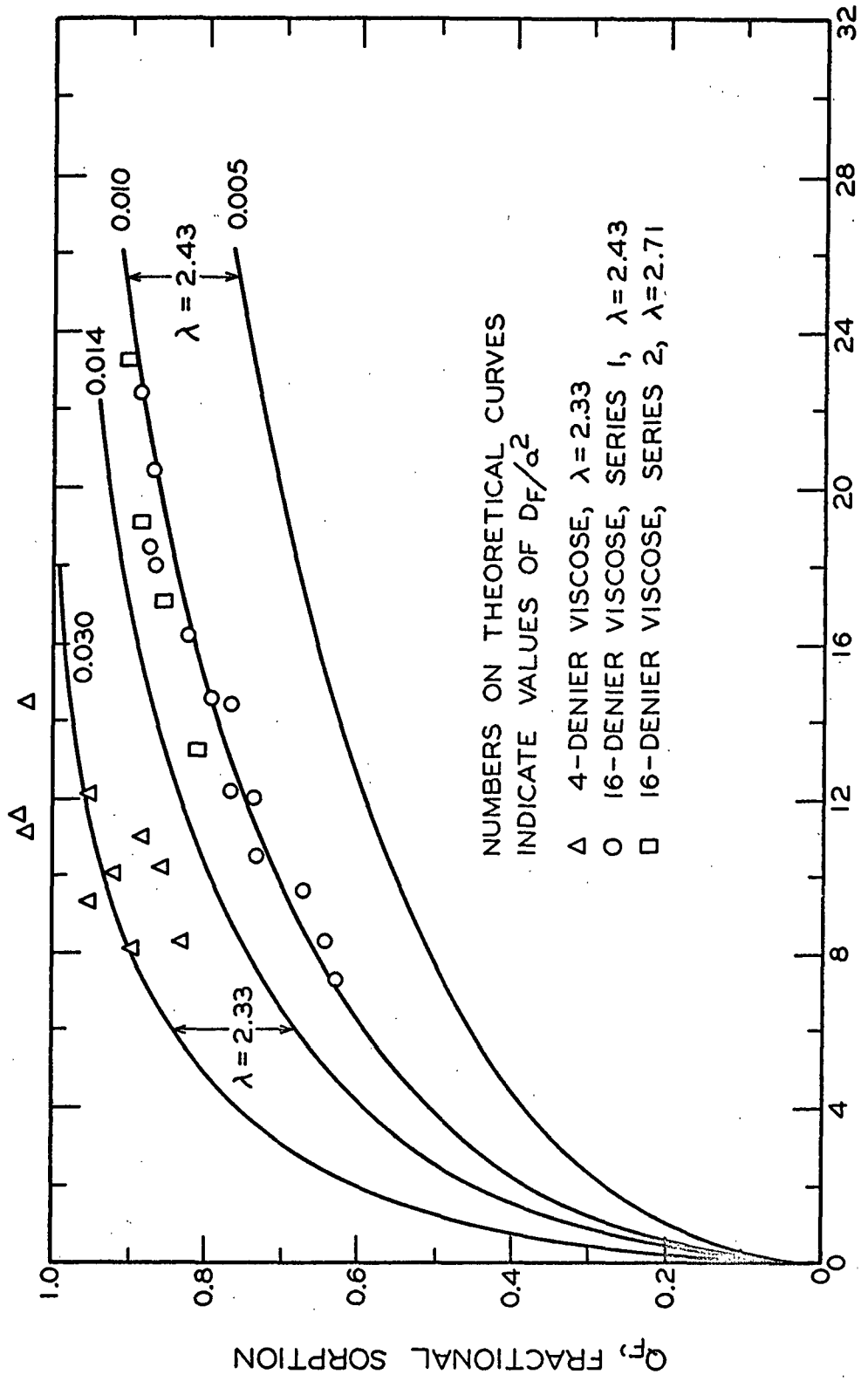

Figure 6. Sorption of PAA by Viscose in a Well-Stirred Finite Dyebath

TABLE VI

PARTITION COEFFICIENT DATA FROM SORPTION RATE EXPERIMENTS

Designation	Number of Experiments	Q_I[a]	Averaged Quantities C_o mg./l.	C_∞ mg./l.	$\Delta Q/\Delta C$[b]	K_S[c]	T, °C.
PAA-16 denier	13	1.8	0.34	2.26	10.80	9.86	25.9
PAA-16 denier	4	1.8	0.04	3.47	10.64	10.11 9.91	27.1 26.2
PAA- 4 denier	11	1.5	0.34	2.31	10.32	9.56	26.3

[a] Q_I is Q intercept at zero concentration on adsorption isotherm, mg. PAA/l. fiber.

[b] $\Delta Q/\Delta C = (Q_\infty - Q_o)/(C_\infty - C_o)$.

[c] $K_S = (\Delta Q - Q_I)/\Delta C$.

The principal features of the apparatus were a septum tube, a permeable piston actuated by a hydraulic jack, and a sliding valve assembly. The details of the washing apparatus are shown in Fig. 7; the sliding valve assembly is shown in Fig. 8.

FLOW SYSTEMS

A schematic of the flow systems is shown in Fig. 9. Portions of this equipment were utilized in the bed-forming operation, and additional parts were used in performing the various washing experiments. The essential features of the equipment needed for the bed-forming operations were:

A. the washing apparatus with the sliding valve assembly and top screen removed,

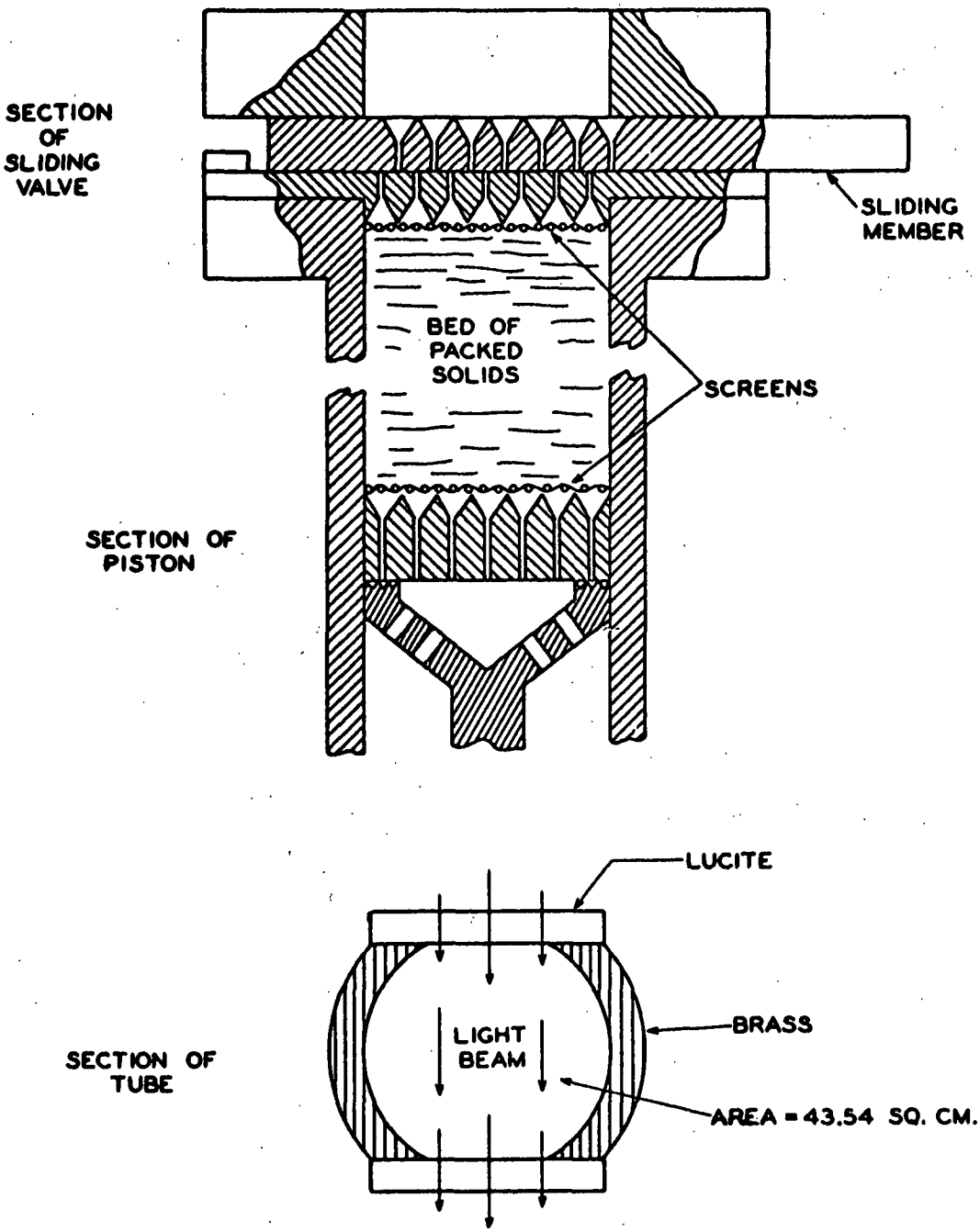

Figure 7. The Washing Apparatus

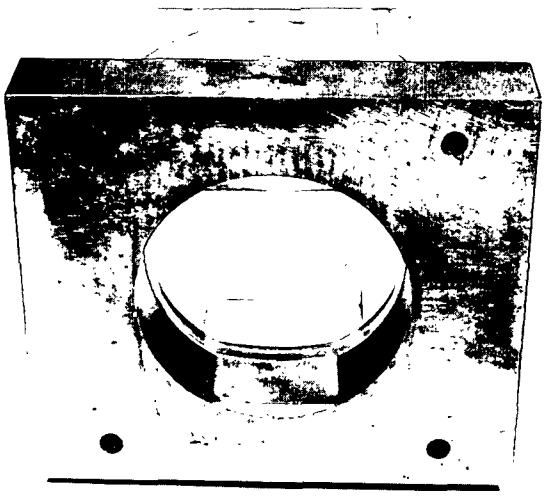

Upper Tube and Flange

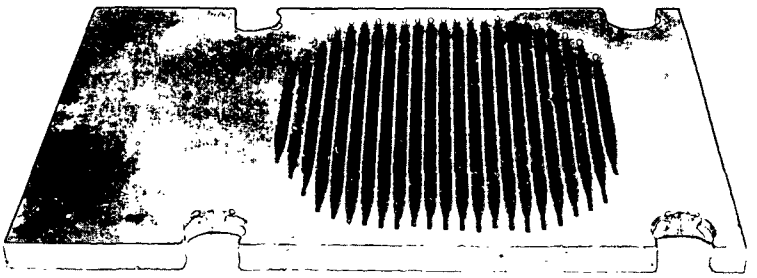

Top of Sliding Member

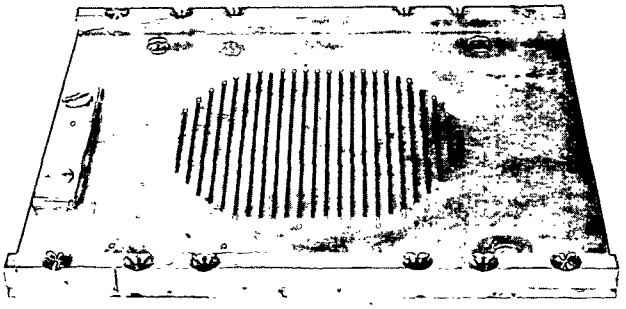

Top of Fixed Member

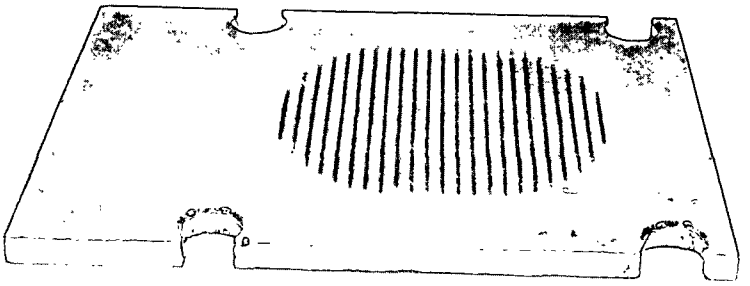

Bottom of Sliding Member

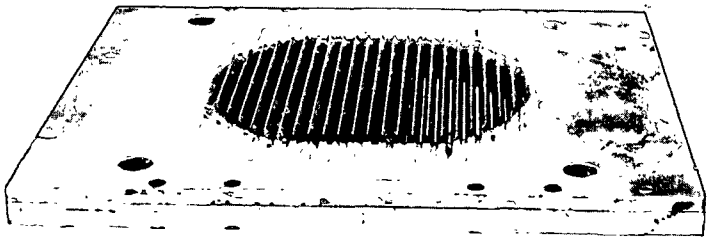

Bottom of Fixed Member

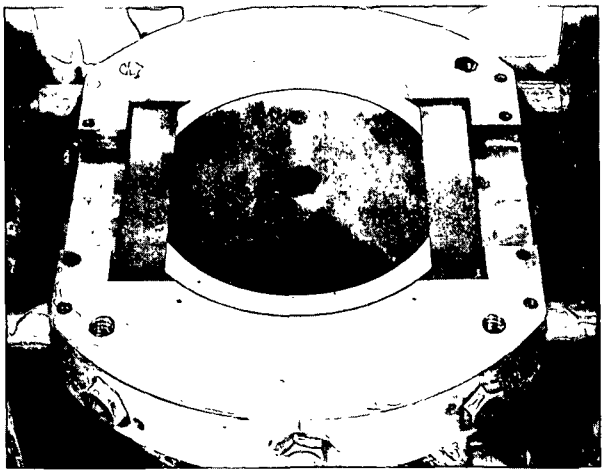

Lower Tube and Flange

Figure 8. Details of Sliding Valve Assembly

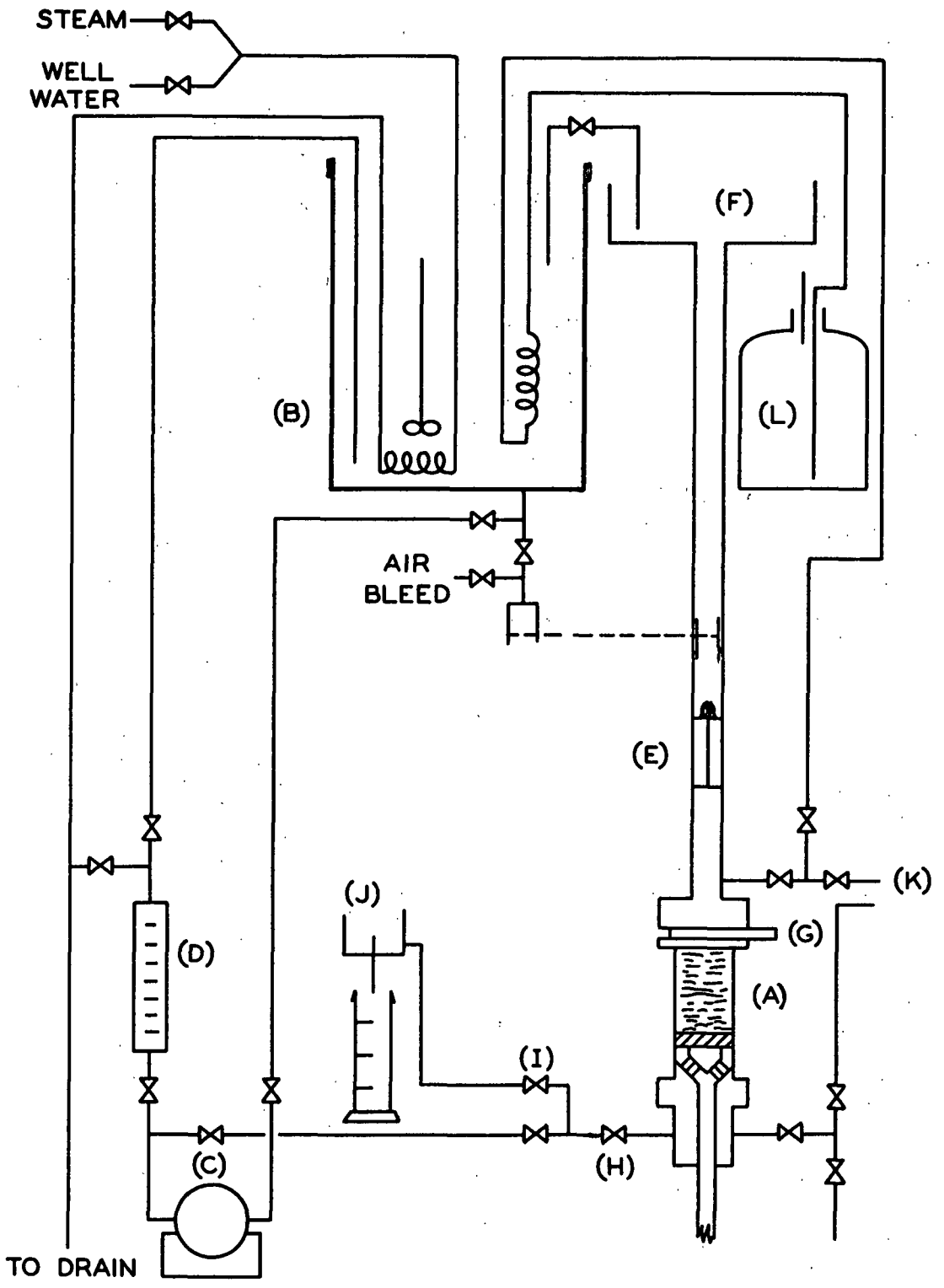

Figure 9. Schematic of Flow System

B. a movable 55-gal. stainless steel tank (SS tank) with a coil for heating or cooling, and a stirrer, all of which could be positioned over the washing apparatus,

C. a recirculation system with a positive displacement centrifugal pump,

D. a rotometer to measure the flow rate in the recirculation system,

E. a plexiglass flow tube (positioned between the SS tank outlet and the washing apparatus) which contained a blunt nosecone to create mild turbulence (10 tube diameters above the septum) and was followed by four radial tube dividers (3 tube diameters long) to dampen any large eddies or circular motions which might persist in the fiber slurry.

The additional features of the flow system that were employed during the washing runs were:

F. a shallow tank of large area (connected by siphon to the SS tank) to serve as a temporary constant head reservoir for wash water,

G. a removable sliding valve at the top of the washing apparatus to maintain an interface between the solution saturating the bed, and the wash fluid,

H. a solenoid valve to start and stop flow through the washing apparatus,

I. a needle valve to control the flow rate of wash fluid,

J. a constant level drain,

K. pressure taps connected to a differential manometer for measuring the over-all fluid pressure drop across the fiber bed,

L. a 20-liter glass vessel (for dye solution) and a gravity supply system, including a 12-ft. copper heat exchange coil in the SS tank.

PHOTOMETRIC SYSTEM

A photometric system consisting of optical, recording, and timing devices (not shown in Fig. 9) was used to monitor the transmission of two light beams, passing just above and just below the fiber bed. Changes in light transmission were used to measure concentration changes of solute in the fluid passing through these beams. A schematic of the optical system is shown in Fig. 10. The spectral characteristics of the optical system are shown in Fig. 11.

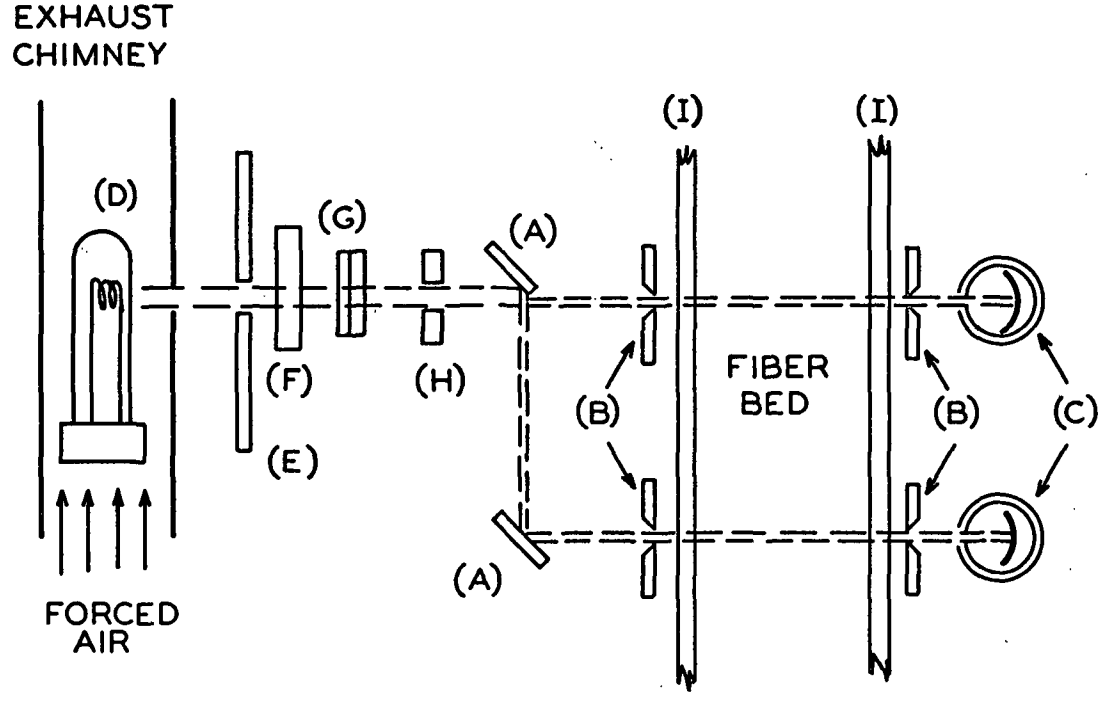

A SURFACE-SILVERED MIRRORS
B LIGHT DEFINING SLITS (ABOUT 1 X 30 MM.)
C VACUUM PHOTOTUBES, CE 61-R
D 500-WATT PROJECTION LAMP
E OPAQUE SHIELD
F GLASS INFRARED HEAT FILTER
G TWO BLUE GLASS FILTERS
H OPAQUE SHIELD
I FLAT SECTIONS OF TRANSPARENT PLEXIGLASS WHICH ARE A PART OF THE SEPTUM

Figure 10. Details of the Optical System

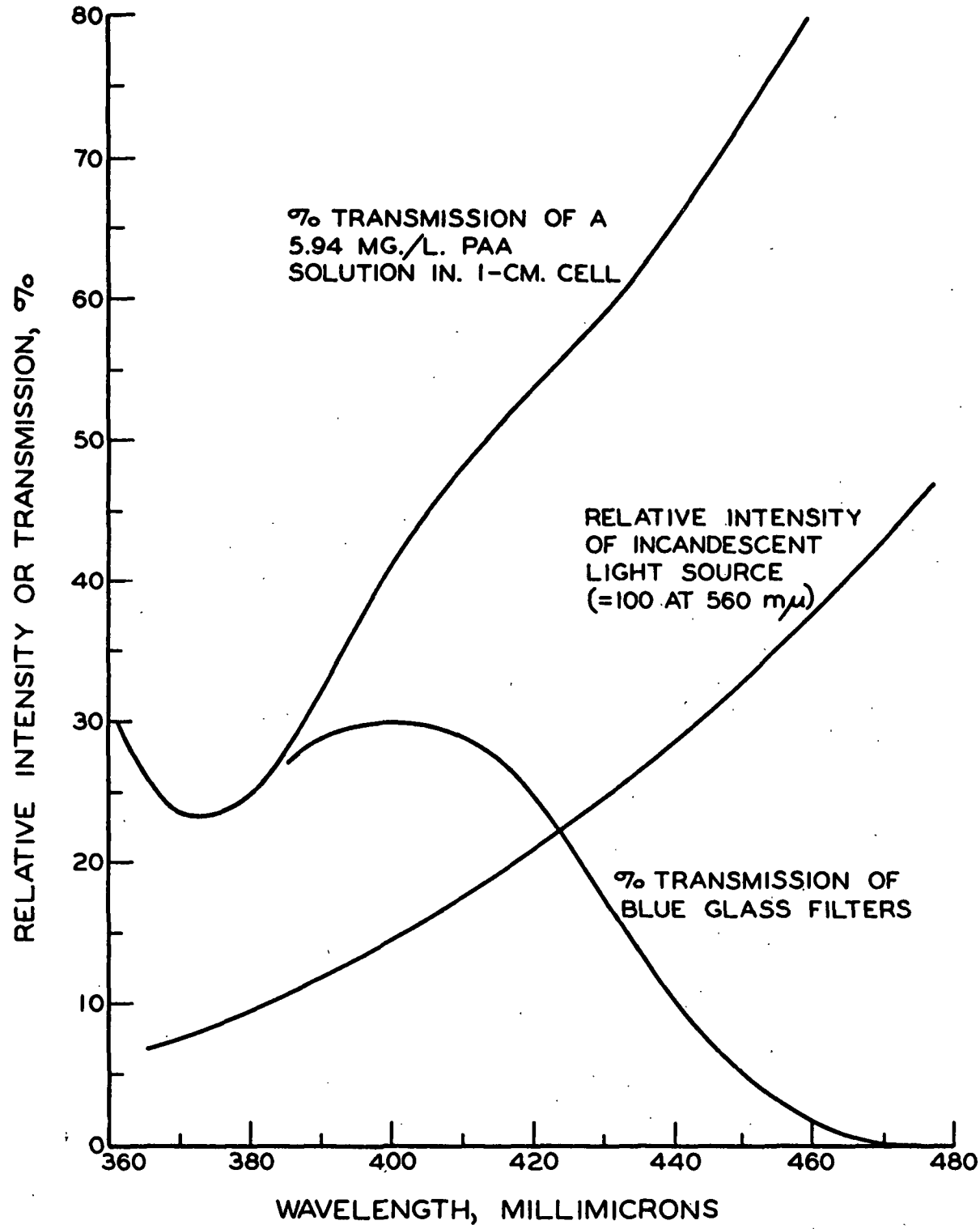

Figure 11. Characteristics of Optical System

The recording and timing devices consisted of the following components:

A. a Dynograph Type RS oscillograph to record voltage signals from either the inlet or exit phototube circuit,

B. a timer clock, reading to 0.01 second,

C. a microswitch and the appropriate circuitry to simultaneously open the solenoid valve, trip the timer clock, and record a timing trace on the oscillograph.

The details of the phototube-oscillograph circuit, and the timer clock-solenoid valve-oscillograph circuit, are shown in Fig. 12. In the phototube-oscillograph circuit, it was necessary to place a capacitor across the input terminals of the oscillograph preamplifier. This largely eliminated the effects of noise originating in the high impedance source circuits. The recorder was then capable of achieving 95% full-scale deflection in about 0.02 second. Sensitivities of 5 or 2 mv. per cm. (depending on the degree of bed compaction) were found to be adequate during normal operation to achieve the optimum full-scale deflection of 4 cm. (8 mv. was the usual signal strength). The dark current voltage was generally about 0.1 mv. Sixty-cycle hum was always found to be present to the extent of about 0.01 mv.

The linearity of the relation between light transmission, and deflection on the oscillograph, was checked each time the equipment was set up for a series of washing runs. The check was accomplished by intercepting the filtered light beam with a series of three transmission screens which had been calibrated on a General Electric recording spectrophotometer. The results shown in Table VII indicate that a linear response was achieved.

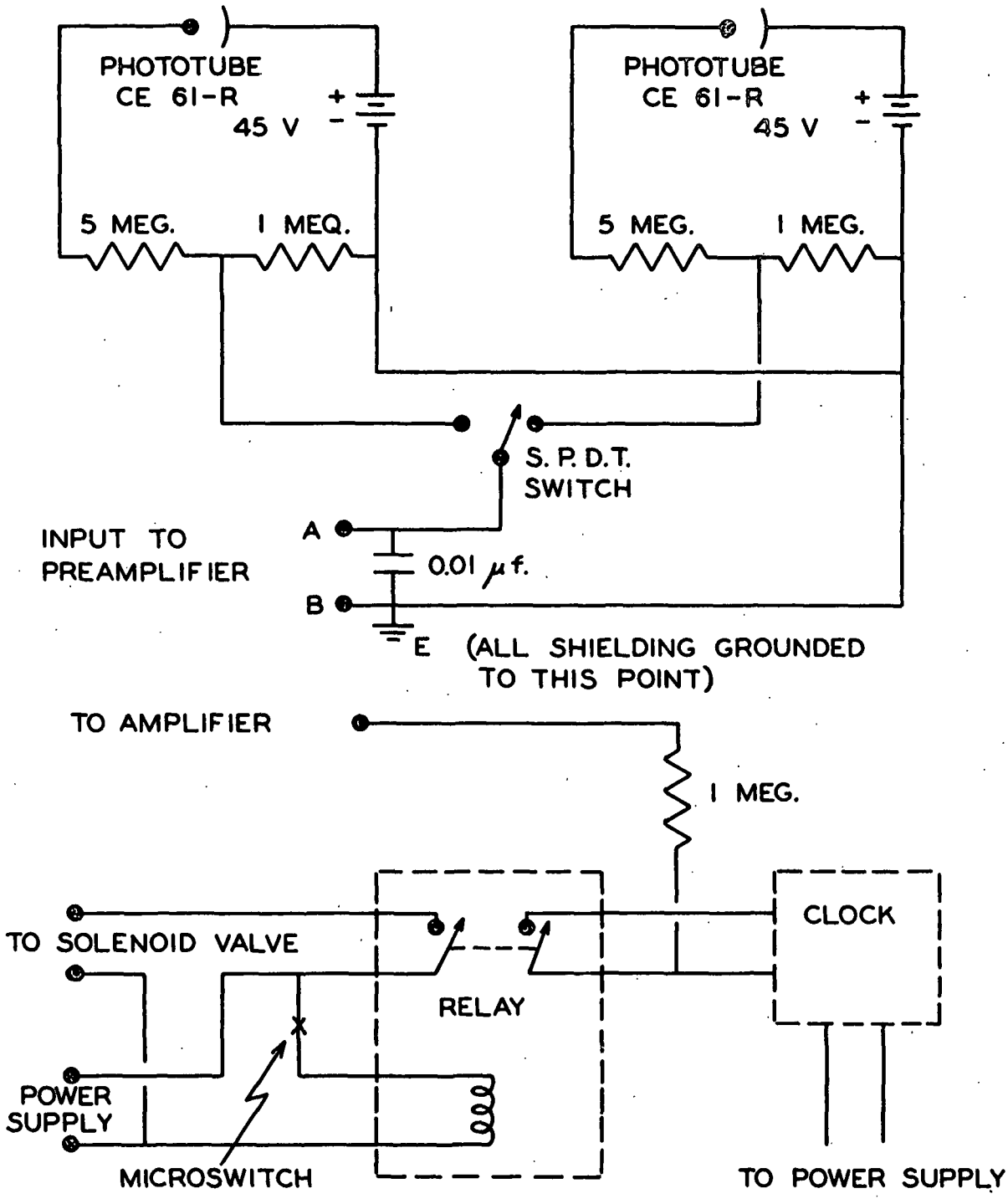

Figure 12. Details of Phototube – Oscillograph Circuit and Timer Clock – Solenoid Valve – Oscillograph Circuit

TABLE VII

CHECK ON TRANSMISSION LINEARITY

	Transmission, %		
Screen calibrated on GERS (± 0.5%)	19.4	47.4	60.8
Inlet circuit[a]	19.9	47.2	61.0
Exit circuit[a]	19.6	46.6	60.3

[a]Average of three or more values taken at various times during the experimental work.

FIBER BED FORMATION

INITIAL PREPARATION

Approximately 32 g. of airdry viscose fibers were sequentially washed with distilled water, 95% ethanol, and distilled water. The fiber batch was divided into 18 equal portions, and these were subsequently deaerated by immersing in boiling water and evacuating for ten minutes in a vacuum desiccator. Prior to use, each fiber charge was thoroughly dispersed in about two liters of deaerated water.

The 55-gal. SS tank was positioned over the washing apparatus and filled with distilled water. Steam was passed through the heating coil and the water was boiled for several minutes. Cooling water was then passed through the coil and the deaerated water was brought to room temperature.

The washing apparatus was filled via the recirculation system so as to avoid trapping air in any part of the system. The constant level drain was filled, the solenoid valve was operated intermittently, and several liters of water were allowed to flow through the system until no more air bubbles were

observed. Bubbles trapped in the holes of the permeable piston were teased out with a piece of piano wire. The bottom septum screen was scrubbed with cleanser (until it held a continuous film of water) and was positioned underwater on the permeable piston. The flow tube was mounted in position, mated with the SS tank coupling, and filled with water from below. The valve at the bottom of the SS tank was then opened to clear the system. The recirculation pump was started and all the valve seals were tightened until no air bubbles were observed at the recirculation outlet.

BED FORMATION

To commence the bed-forming process, the recirculation rate was set between 1.7 and 1.9 gal. per min., corresponding to a superficial velocity in the flow tube between 2.5 and 2.8 cm./sec. The first fiber charge (previously dispersed) was then introduced into the continuously stirred contents of the SS tank; thereafter approximately one charge every 20 min. was introduced until all 18 charges were used. Using this formation procedure, the average fiber concentration was always kept below 0.003% by weight, where very little fiber-fiber interaction was observed in the flow tube.

When the SS tank was finally drained to complete the formation process, the flow tube was removed, keeping the bed underwater at all times. The top screen was cleaned and placed on the bed surface, and the sliding valve assembly (lubricated with silicone grease to prevent water leakage) was fastened in place. The flow tube was then fixed in place on the sliding valve and the constant head tank was positioned overhead and connected. The water level was raised above the sliding valve and the bed was compacted to a precalculated porosity level by raising the permeable piston.

CHARACTERIZATION OF FIBER BEDS

PERMEABILITY MEASUREMENTS

Each fiber bed was characterized with respect to its permeability, at one or more porosity levels, by performing a series of pressure drop vs. flow-rate measurements. The equipment was readied by filling the flow tube with water, and connecting a siphon from the SS tank to the constant head tank. The needle valve was then opened to a preselected position and the solenoid valve and time clock were tripped. The pressure drop was measured with a differential manometer containing a manometer fluid of density 1.484 g./cc. at 26°C. The volume of fluid displaced was measured in a graduated cylinder and the flow rate was calculated from the elapsed time.

PERMEABILITY DECAY AND TRANSIENT FLOW EFFECTS

The possible presence of a systematic decay in the permeability was checked on the first (chronologically) 16-denier bed, 1-16. The permeability was found to be unchanged after performing 12 washing runs (which required a period of two days. The possible presence of transient flow effects was checked on Bed 2-16. The following conditions prevailed in the system: $\epsilon = 0.7443$; $q' = 58.5$ cc./sec.; $U = 1.805$ cm./sec.; $\Delta P = 18.15$ cm. water; $P_s = 110$ cm. water. A negligible change in the average flow rate (with time) was observed in this case.

PREDICTION OF PERMEABILITY FROM A MODIFIED HYDRAULIC RADIUS THEORY

The primary reason for obtaining permeability data was to provide a check on the reproducibility of the fiber beds. This check was accomplished by comparing experimental results with predicted results from an empirical equation

developed by Ingmanson and Andrews (21). Their modified hydraulic radius theory included inertial flow effects and was based on a Kozeny factor that is a function of bed porosity. The permeability equation for a uniform bed was shown to be

$$\Delta P/(W_F/A_c) = [\bar{k}(1 - \epsilon)/\epsilon^3]\mu V S_v^2 U_s + [0.1\bar{k}^{1/2}/\epsilon^3]\, V S_v U_s^2 \qquad (40)$$

with

$$\bar{k} = [3.5\, \epsilon^3 (1 - \epsilon)^{-1/2}][1 + 57(1 - \epsilon)^3] \qquad (41),$$

where

ΔP = over-all pressure drop, dyne/sq. cm.

W_F = mass of fiber, g., o.d.

A_c = 43.54 sq. cm., cross-section area

$\bar{k}$ = Kozeny factor, dimensionless

ϵ = porosity of bed, dimensionless

μ = viscosity, poise

V = swollen specific volume of fibers, wet cc./g., o.d.

S_v = specific surface, $cm.^{-1}$, (calculated from 4/fiber diameter)

U_s = superficial velocity based on A_c, cm./sec.

The expression for the Kozeny factor was empirically established by Ingmanson, Andrews, and Johnson (22) from data on beds of glass and nylon fibers, over the porosity range of 0.68-0.96. In applying Equations (40) and (41) to the present viscose fiber beds, the bed porosity was assumed to be uniform. This condition was satisfied by operating in the lower velocity regions where ΔP was small in comparison to the static compacting pressure. (The problem of nonuniform porosity distributions, at higher velocities, is taken up at a later point.)

According to Ingmanson (23), Equation (40) has been found to yield reliable predictions within 15%, when applied to carefully formed beds of glass, nylon,

and dacron fibers, and when the specific volumes and specific surfaces are accurately known from independent measurements. Its applicability has not been checked on the highly swollen viscose beds used here, however. It is likely that the viscose fibers are deformed and deswollen to some extent at the fiber-fiber contacts, due to the influence of compacting forces. This possibility was quite evident when the deformation of a swollen 64-denier fiber (between two glass slides) was observed under a microscope.

PREDICTED VS. EXPERIMENTAL PERMEABILITY

Bed Reproducibility

Experimental and predicted pressure drop vs. flow rate relationships are shown in Fig. 13 for the two 16-denier beds. The relative agreement obtained indicates that they possessed reproducible permeability characteristics. It will be shown later that these beds also exhibited nearly identical longitudinal dispersion properties. From these findings it was assumed that the bed-forming technique was sufficiently refined to yield beds having reproducible characteristics.

Inertial Effects

A convenient measure of the inertial effect is the ratio of the inertial pressure drop contribution to the total fluid pressure drop. Table VIII shows the calculated value of this ratio, at a linear pore velocity of 1 cm./sec., for all four viscose beds. It is evident that inertial flow effects were essentially negligible at pore velocities less than 1 cm./sec. With the exception of six washing runs (performed on Bed 1-16, at pore velocities up to 2 cm./sec.) all others in the study fall within this arbitrary limiting condition.

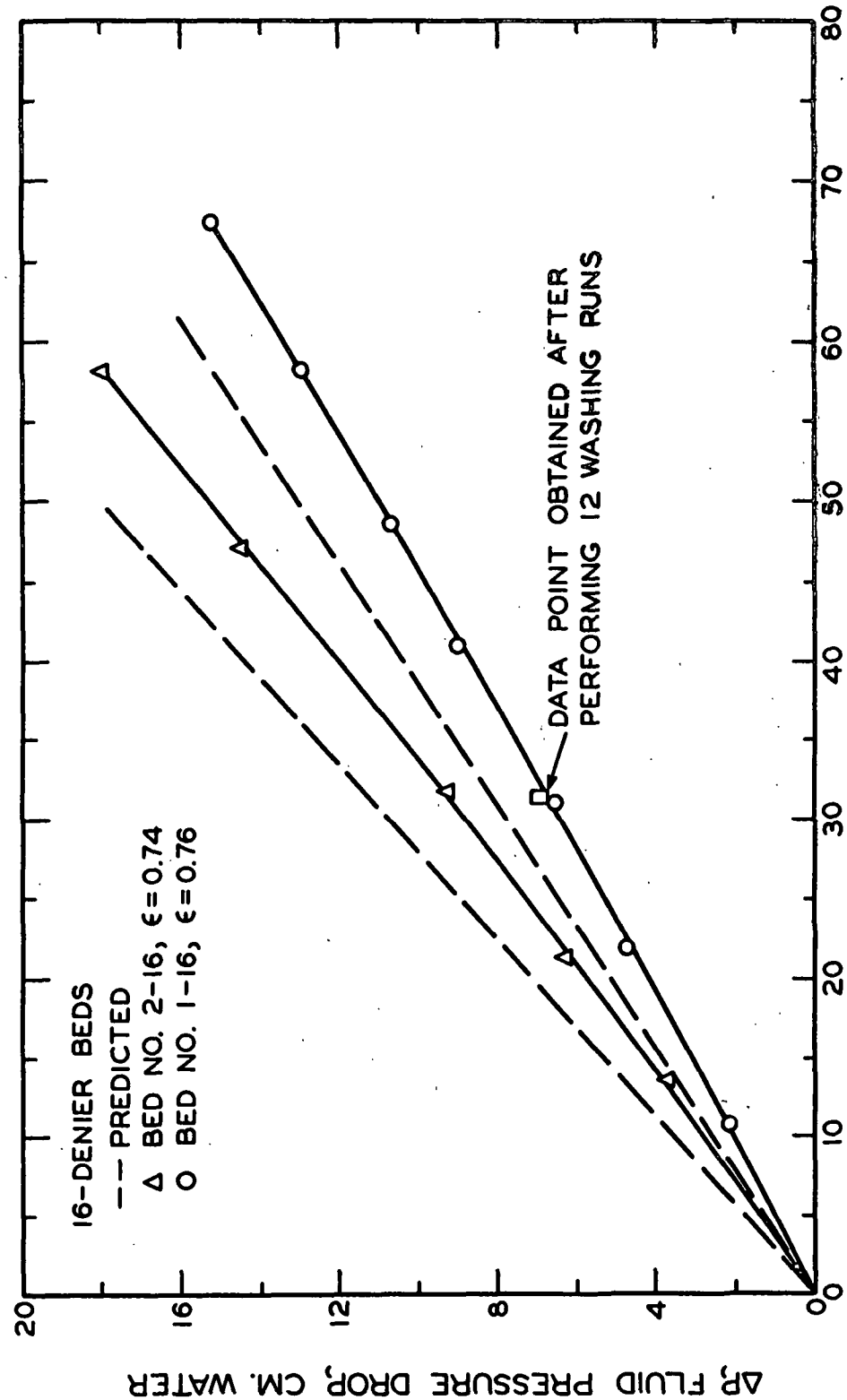

Figure 13. Permeability of 16-Denier Beds

TABLE VIII

RELATIVE IMPORTANCE OF INERTIAL FLOW EFFECTS

Bed[b]	ϵ	Contribution of[a] Inertial Effect, %
1-16	0.7636	2.34
2-16	0.7443	2.16
4- 4	0.8598	1.90
4- 4	0.8059	1.42
4- 4	0.7460	1.03
3- 1	0.7158	0.46

[a]Calculated from Equation (40) as (100) $(\Delta P_{\text{inertial}})/(\Delta P_{\text{viscous plus inertial}})$ at a linear pore velocity of 1 cm./sec.

[b]Bed 1-16 refers to the first bed (chronologically) and the 16-denier system.

Effect of Fiber Deswelling

Comparisons between the experimental and predicted pressure drop vs. flow-rate relationships exhibited a consistent discrepancy in all four viscose beds. Figure 14 is plotted to show that the discrepancy increased regularly with compacting pressure for the 4-denier viscose bed no. 4-4. Although a number of factors were undoubtedly responsible for this effect, the discrepancy can be accounted for by assuming that a small amount of fiber deswelling takes place when the bed is compacted. Since the fibers are highly swollen in water (the four-denier fibers swell approximately 45% in diameter, based on the airdry fiber diameter, and contain about 64% water by volume), it seems reasonable to expect that water contained by the largest intrafiber pores would be expressed quite easily, in the regions of fiber-fiber contacts, as the compressive forces

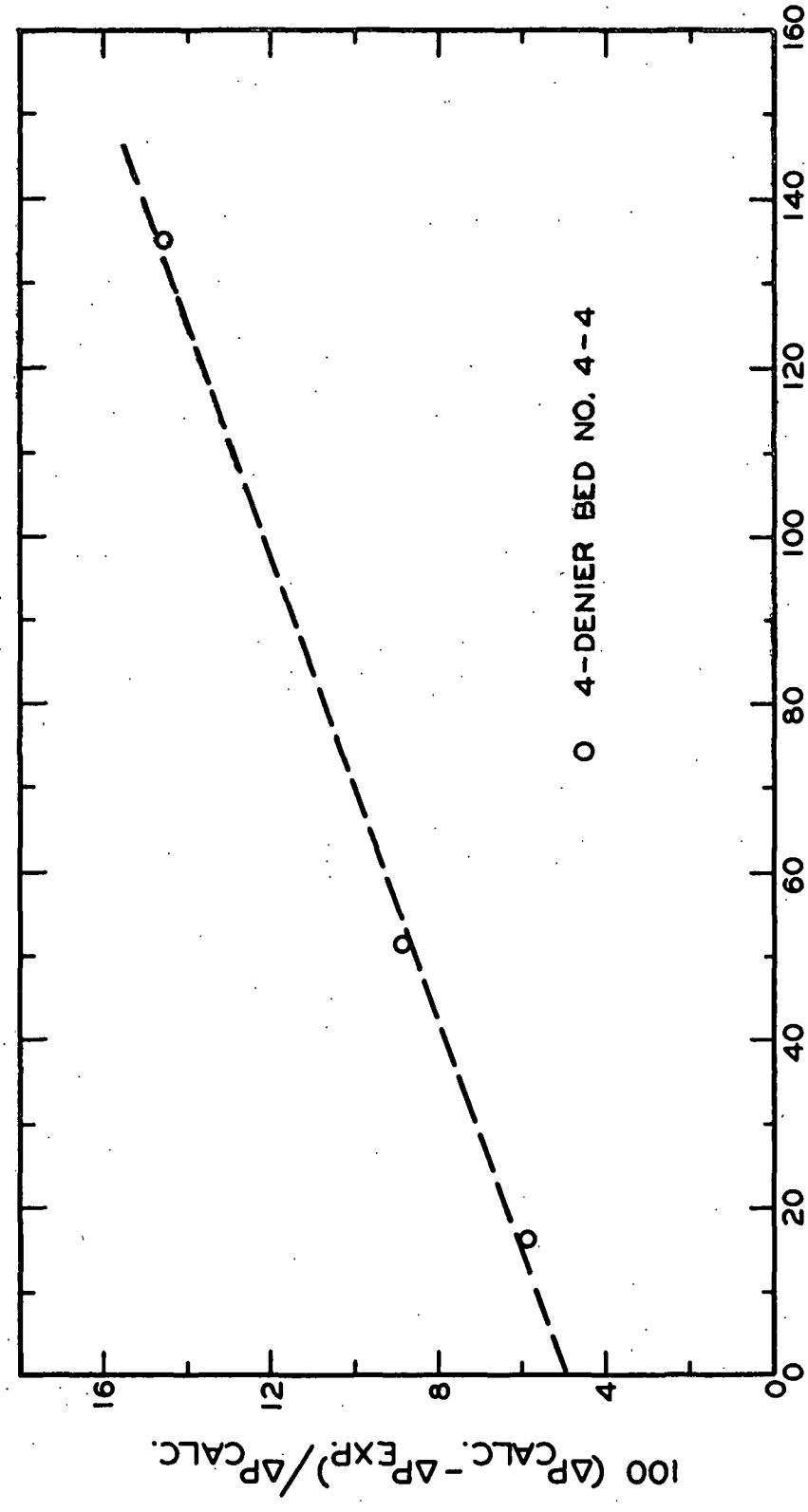

Figure 14. Predicted – Experimental Fluid Pressure Drop vs. Compacting Pressure

between fibers are increased. In this case the average fiber diameter would effectively decrease with increasing compacting pressure.

A series of calculations were made on the 4-denier viscose bed, at the lowest porosity level ($\epsilon = 0.746$), to determine the postulated extent of deswelling that would bring the experimental and predicted pressure drop *vs.* flow rate relationships into agreement. Table IX illustrates the effect of a 3% decrease in fiber diameter on the various calculated parameters that depend on an independent fiber diameter measurement.

TABLE IX

EFFECT OF DESWELLING ON CALCULATED PARAMETERS

Parameter	Original Value	Assumed Value	Per Cent Difference[a]
$\underline{d}$, μ	29.89	29.00	-2.98
$\underline{V}$, wet cc./g., o.d.	1.694	1.594	-5.90
$\epsilon_{\underline{E}}$	0.7614	0.7755	--
ϵ	0.7460	0.7610	--
$\Delta\underline{P}$, cm. water[b]	19.70	17.56	-10.87
$\underline{M}_{\underline{w}}$[c]	4.164	4.088	-1.82
$\underline{K}_{\underline{w}}$[d]	10.10	10.67	+5.64

[a] Based on original value.

[b] At a flow rate of 13.06 cc./sec.

[c] $$\underline{M}_{\underline{w}} = \int_0^{\infty} \left[\left(\frac{\underline{C}}{\underline{C}_o} \right)_{\text{Exit}} - \left(\frac{\underline{C}}{\underline{C}_o} \right)_{\text{Inlet}} \right] \underline{dR}.$$

[d] $$\underline{K}_{\underline{w}} = (\underline{M}-1)\epsilon_{\underline{E}}/(1-\epsilon_{\underline{E}}).$$

It should be noted that the estimated solute ratio, $\underline{M}_w$, (from Run 4-67-4) was calculated under the assumption that the partition coefficient remained unchanged. If the swollen specific volume is effectively reduced by the expression of water, it seems probable that the partition coefficient would become somewhat larger, since the ratio of adsorbed PAA (in the cellulose phase) to PAA in solution (in the intrafiber void space) is about 15. This would make the change in $\underline{M}_w$ considerably smaller than 1.82%, and the change in $\underline{K}_w$ proportionally smaller. The over-all result, with a 3% decrease in fiber diameter, would thus be a large decrease in the experimental pressure drop (-10.87%) and a very small change in the calculated value of $\underline{K}_w$ (probably less than 2%). This is one explanation for the observed fact that $\underline{K}_w$ did not change significantly with porosity in the washing runs (to be shown later).

STATIC COMPRESSIBILITY MEASUREMENTS

The static compressibility of 1, 4, and 16-denier fiber beds was measured with an apparatus built for this purpose (24). The basic technique involved forming a fiber bed (about 10 g.) in the septum of the apparatus from 1500 ml. of deaerated slurry. A freely moving permeable piston, positioned on top of the bed, was then successively loaded with weights of increasing size. The corresponding pad thicknesses were measured each time with a traveling micrometer, after allowing about 10 min. for the pad to deform. The static loading pressure, $\underline{P}_s$, and mat consistency, $\underline{C}'$, were calculated for each load. A straight line was obtained by plotting log ($\underline{C}'$) vs. log ($\underline{P}_s$). By evaluating the intercept (at $\underline{P}_s = 1$) and slope of this line, the constants $\overline{\underline{N}}$ and $\overline{\underline{M}}$, satisfying the empirical compressibility function $\underline{C}' = \overline{\underline{M}}(\underline{P}_s)^{\overline{N}}$ were obtained as shown in Table X.

TABLE X

COMPRESSIBILITY CONSTANTS

Denier	Length/Diameter	$\overline{M}^a$	$\overline{N}^a$
1	121.3	0.0415	0.278
4	95.3	0.0380	0.280
16	93.5	0.0295	0.357

[a]For $\underline{P}_s$ = cm. water and $\underline{C}'$ = g., o.d. fiber/cc. bed.

THE WALL EFFECT

The presence of a wall effect was observed to various extents during the bed formation process. It was evident at this time from the concave "dishlike" contour of the bed's upper surface. The curvature appeared to be greatest near the wall, and the profile tended to become flat a few mm. from the wall. Subsequent detailed examination of the beds revealed what one might call a "brush pile" near the wall. Here the fibers were observed to have a definite orientation in the axial or $\underline{Z}$ direction; this orientation was found to disappear at distances greater than about one fiber length from the wall. Further observation of the wall effect indicated that it was an additive phenomena, as the apparent degree of surface curvature near the wall, and the characteristic radial dimension of the "brush pile," increased with the total amount of fiber deposited.

As the fluid pressure drop was increased, the bed surface became more concave. In retrospect it was felt that the flow rate should have been maintained at a lower level during the bed formation process with the smaller diameter fibers (one-denier especially). This may have (a) helped to minimize the wall effect, and (b) made conditions less favorable for the development of basis weight variations due to preferential deposition of fibers toward the bed axis.

When the highly compacted fiber beds were finally removed from the apparatus, they were delaminated into layers quite easily. Examination of various layers from the upper half of the bed, indicated the existence of a definite zone of crimping which had a zig-zag orientation in the region of about one fiber length from the wall. Sequential layers taken from the lower half of the bed showed less and less crimp as the bottom was approached. It thus appeared that the crimping effect resulted from (a) the "brush piling" of fibers near the wall, creating a zone of bed structure that responded differently to deformation (in comparison to the remainder of the bed) when the bed was compacted, and (b) the "dishlike" curvature of the orientation planes, during the formation stage, which apparently became planes of shear when the bed was compacted.

When the bed layers were viewed with transmitted light, no basis weight variations were noted from the zones of crimping to the pad centers. When the zones of crimping were subjected to radial compression (needed to return the pad to its original dimensions in the restrained condition), the crimped regions easily yielded by folding in. The resulting regions appeared to be of approximately the same basis weight as the central regions.

WASHING EXPERIMENTS

PREPARATION OF DYE SOLUTIONS

After a large supply of distilled water was deaerated in the SS tank, the various dye solutions were prepared. Diacetyl solution was made by dissolving 50 g. of diacetyl in 16 liters of deaerated water. The PAA solution was made by dissolving 50 mg. of PAA in 10 ml. of 95% ethanol; this solution was then poured into 18 liters of deaerated water. The purpose of predissolving in ethanol was to eliminate the possibility of having undissolved particles of PAA

suspended in the aqueous solution (PAA dissolves slowly in water, and it is often difficult to determine when complete solution has taken place).

OPTICAL SYSTEM ALIGNMENT

The components of the optical system were fixed in place and a number of fine adjustments were made on the movable mirrors and light-defining slits. The objectives here were (a) to adjust the total amount of light reaching the phototubes so that nearly full-scale deflection was recorded when no solute was present, and (b) to anchor and adjust the components in such a manner that the recorded deflection was constant and relatively insensitive to mechanical vibrations in the system.

BED SATURATION

In preparation for a washing run, a fiber bed was first saturated with dye solution to bring the bed to concentration and temperature equilibrium. This was accomplished by flowing 12-15 liters of dye solution through the bed at the rate of about one liter per min. Prior to entering the bed, the dye solution was passed through a heat exchange coil to equilibrate it with the subsequent wash water. The incoming dye at the top of the bed was allowed to seek a sufficiently high level so that no air was introduced into the solution, or the bed. The solution leaving the bed exit was collected in a glass vessel (without introducing air) for use in the next washing run.

After the fiber bed was saturated, the sliding valve was closed by pulling the sliding member out 1/16 of an inch and tightening down on the assembly bolts. The light transmissions through the inlet and exit slits were then recorded. The flow tube was filled with wash water (using gravity feed from the SS tank) through

a radial inlet located a few cm. above the sliding valve assembly. When the water level reached the constant head tank, a direct siphon was opened from the SS tank and the gravity feed at the base of the flow tube was disconnected.

WASHING RUN PROCEDURES

1. The recorder and light source were turned on and the 4 by 8 by 6-ft. enclosure (surrounding the equipment) was darkened to outside light.

2. The needle valve was opened to a preselected position, and the solenoid valve and time clock were activated.

3. The inlet and exit traces, and the respective dark currents (obtained by blocking-off the filtered light beam), were recorded.

4. The recorder was set to a preselected chart speed and the three-way switch (open circuit, inlet circuit, and exit circuit) was thrown to record the inlet.

5. The sliding valve was pushed open, and the microswitch was quickly released to open the solenoid valve, start the time clock, and commence the timing trace on the recorder.

6. As soon as the inlet trace was sufficiently defined, the three-way switch was thrown to record the exit trace. At intermittent intervals, while the exit was being recorded, the light was briefly intercepted to give a dark current reading, thus affirming the base line. The inlet was also recorded intermittently to check the constancy of the optical system and/or the wash water.

When the bed was considered to be effectively washed, the microswitch was depressed and the solenoid valve and timer circuits were deactivated. The time

clock was read and the volume of fluid displaced was measured in a graduated cylinder. At the end of a complete series of washing experiments the bed was carefully removed and dried at 105°C. to determine the total fiber mass.

RAW DATA

The essential features of a chart record, for a typical washing run, are illustrated in Fig. 15.

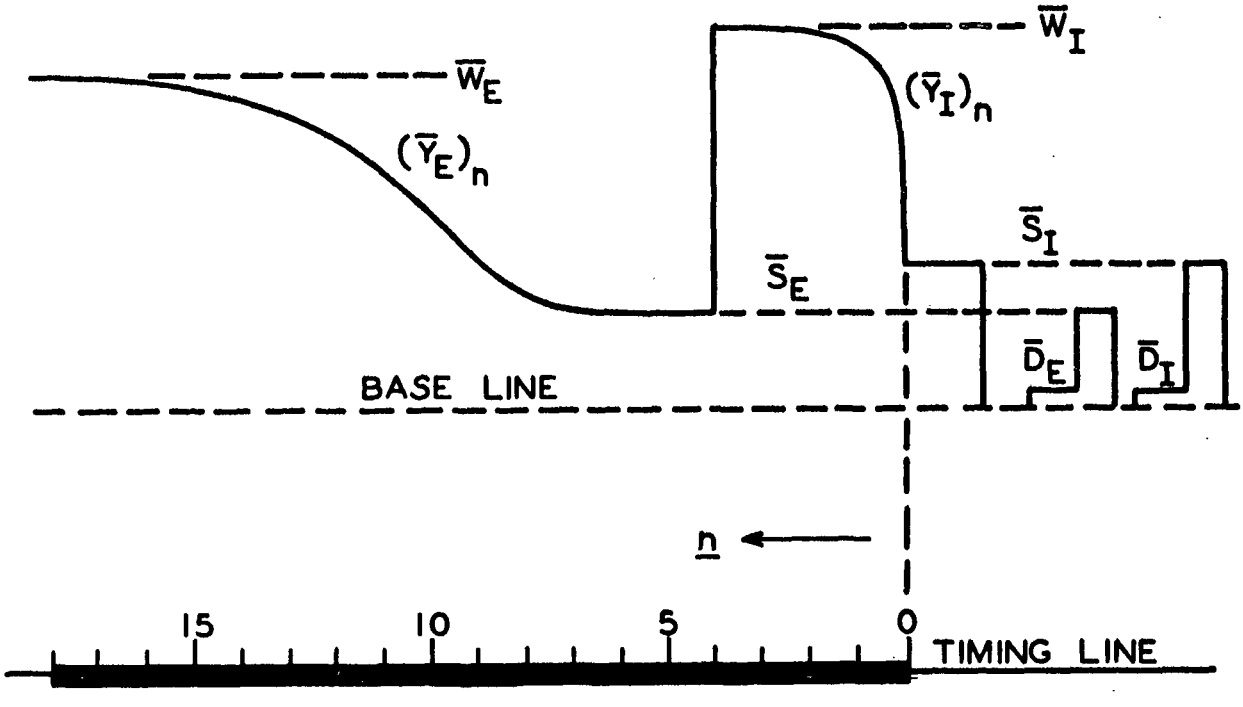

Figure 15. Illustration of a Chart Record for a Washing Run

The subscripts I and E refer to the bed inlet and exit, respectively, and the various deflection values are measured in mm. from the base line. The thick portion of the timing line (a 60-cycle trace) represents the duration of the washing experiment. The following nomenclature applies to the chart record.

$\bar{D}$ = dark current (light blocked off) value

$\bar{S}$ = initial solute value (generally about 20-30% of $\bar{W}$)

$\overline{W}$ = water value

$(\overline{Y})_n$ = solution value as a function of n

n = number of 5-mm. increments from time zero

The following additional data were recorded for each run.

Q_w = total volume of wash, cc.

t = elapsed time, sec.

$\overline{CS}$ = chart speed, mm./sec.

L' = total length of timing trace, mm.

T = temperature of wash water, °C.

The bed parameters that were known are:

W_F = mass of fibers in bed, g., o.d.

A_c = 43.54 sq. cm. (cross-section area of bed)

V = swollen specific volume of fibers, wet cc./g., o.d.

Cathetometer readings (in cm.) of the bed dimensions at each porosity level were recorded as follows, proceeding from the top of the bed to the bottom.

$\hat{A}$ = slit upper edge (inlet)

$\hat{B}$ = slit lower edge

$\hat{C}$ = screen upper edge

$\hat{D}$ = screen lower edge (top of fiber bed)

$\hat{E}$ = screen upper edge (bottom of fiber bed)

$\hat{F}$ = screen lower edge

$\hat{G}$ = slit upper edge (exit)

$\hat{H}$ = slit lower edge

The first step in checking the raw data was to verify the chart speed by calculating the run time from $\underline{t} = \underline{L'}/\overline{CS}$ and comparing the result to the clock reading. Generally, these were found to agree within 0.4%. The next step was to check the chart for any irregularities and record a suitable number of deflection values at equally spaced intervals.

RAW DATA PROCESSING

A data processing program was then used to calculate the following quantities:

Flow rate, cc./sec.

$$q' = Q_w/t \tag{42}$$

Void volume of fiber bed, cc.

$$V_B = 43.54\ (\hat{D} - \hat{E}) - VW_F \tag{43}$$

Void volume of valve, screens, and piston, cc. (1)

$$V_{VSP} = 43.54\ \left[\frac{0.330\ \overline{AA} - 0.4142\ \overline{AA}^2}{0.330}\right] + 30.5\ (\hat{C} - \hat{D} + \hat{E} - \hat{F}) + 43.54\ \left[\frac{0.330\ \overline{BB} - 0.4142\ \overline{BB}^2}{0.330}\right] \tag{44}$$

where

$$\overline{AA} = (\hat{A} + \hat{B})/2 - \hat{C} \tag{45}$$

$$\overline{BB} = -(\hat{G} + \hat{H})/2 + \hat{F} \tag{46}$$

Effective bed height, cm.

$$Z_E = (\hat{A} + \hat{B} - \hat{G} - \hat{H})/2 \tag{47}$$

Porosity of fiber bed.

$$\epsilon = V_B/(43.54(\hat{D} - \hat{E})) \tag{48}$$

Total void volume of bed, cc.

$$V_T = V_B + V_{VSP} \tag{49}$$

Effective porosity of bed system.

$$\epsilon_E = V_T/(V_T + VW_F) \tag{50}$$

Average linear pore velocity.

$$U = q'/43.54\epsilon \tag{51}$$

The number of pore volumes of fluid displaced from the bed system, as a function of evenly spaced $\underline{n}$ values, was calculated from the expression $(\underline{R})_{\underline{n}} = 5\underline{n}\underline{q}'/\underline{V_T}(\overline{\underline{CS}})$. The corresponding relative concentrations were calculated from Equation (52), which is based on the system's linear response to light transmission, and the application of Beer's law.

$$(C/C_o)_n = \log\left[\frac{(\overline{Y})_n - \overline{D}}{\overline{W} - \overline{D}}\right] \Big/ \log\left[\frac{\overline{S} - \overline{D}}{\overline{W} - \overline{D}}\right] \tag{52}$$

The areas under the inlet and exit concentration curves were evaluated numerically, using the Newton-Cotes seven point integration formula for evenly spaced values. The integrals are expressed as

$$I = \int_o^{R_F} (C/C_o)_I \, dR \quad , \qquad E = \int_o^{R_F} (C/C_o)_E \, dR \tag{53, 54}$$

The upper integration limits were chosen to represent the termination of the washing experiment (generally the point at which the exit concentration history became asymptotic to the apparent water value).

APPLICATION OF BEER'S LAW IN THE WASHING APPARATUS

Equation (52) results from the application of Beer's law; this can be illustrated more clearly when the expression for $\underline{C}$ is written as

$$(C)_n = -(1/k_b) \log [((\bar{Y})_n - \bar{D})/(\bar{W} - \bar{D})] \qquad (55)$$

The constant $\underline{k_b}$ is proportional to (a) the extinction coefficient of the solute in water, and (b) the length of the light path through the solution. Although Equation (55) is a correct mathematical expression for Beer's law, it is actually used in the sense of an integrated result, representing the entire spectrum of wavelengths that are transmitted and sensed in the system. This is readily apparent when we remember that the extinction coefficient, and the characteristics of the optical system, are both functions of wavelength. The important criteria which determine the validity of applying Beer's law, over a finite range of wavelengths, are that (a) the extinction coefficient is independent of concentration at any given wavelength (solute-solute interaction effects are negligible), and (b) there are no wavelength interaction effects such as the production of fluorescence at one wavelength resulting from stimulation at another wavelength.

In view of these possible complications, the use of Equation (52) was verified in the washing apparatus. This was accomplished by successively filling the empty septum with various solutions of known relative concentration. The light transmission of each solution was recorded as usual and the apparent

relative concentrations were calculated from Equation (52). Although the experiments were somewhat crude (the transmission response was not continuously monitored between solution changes and there was a small amount of contamination between successive solutions in some cases), the results in Table XI indicate that the application of Beer's law, through Equation (52), was valid in the system when PAA was used. Similar results were obtained with BPP solutions, and the application to diacetyl solutions was checked by Sherman in essentially the same manner (1).

TABLE XI

MEASUREMENT OF PAA CONCENTRATION IN WASHING APPARATUS

C/C_o Actual	Deflection, $\bar{Y}$	$\frac{\log(\bar{Y}/41.4)}{\log(4.65/41.4)}$
0.000	41.4	0.000
0.333	19.6	0.341
0.333	18.9	0.358
0.500	13.9	0.499
0.500	13.5	0.513
0.667	10.0	0.650
0.667	9.8	0.659
1.000	4.65[a]	1.000

[a] This value was somewhat small for an accurate determination; and $\bar{S}$ value of 10 would have been considerably better.

PRESENTATION OF PRELIMINARY RESULTS

WASHING RUN DATA

The washing data in this study were expressed in the generally useful form of dimensionless exit concentration curves, or breakthrough curves; here, $\underline{C}/\underline{C}_o$, the relative concentration at the bed exit, was expressed as a function of $\underline{R} = \underline{Ut}/\underline{Z}_E$, the number of pore volumes of fluid displaced from the bed system.

INPUT CONSIDERATIONS

Each washing experiment had a characteristic input that was expressed in terms of the same dimensionless co-ordinate $\underline{R}$. To account for these inputs in the analysis of exit-concentration data, it was necessary to describe the input curves with the exponentially damped polynomial that was previously given in general form by Equation (16),

$$\frac{C(0,R)}{C_o} = (k_o + k_1 R + k_2 R^2 + k_3 R^3 + k_4 R^4) \exp(-\gamma R) \qquad (56)$$

To facilitate determination of the constants, for this equation, a transformed set of variables was defined as

$$\underline{Y} = (\underline{C}(0,R)/\underline{C}_o) \exp(\gamma \underline{R})$$

$$\underline{X}_1 = \underline{R},\ \underline{X}_2 = \underline{R}^2,\ \underline{X}_3 = \underline{R}^3,\ \underline{X}_4 = \underline{R}^4.$$

A linear multiple regression of the form

$$Y = k_o + k_1 X_1 + k_2 X_2 + k_3 X_3 + k_4 X_4 \qquad (57)$$

with the prescribed constant term $\underline{k}_o$, was then performed on several sets of input data, using a digital computer. It was necessary to adjust the exponential constant

γ by trial and error until the variance of the regression was reduced to a minimum. The functional relationship was then calculated from the regression coefficients and compared with the input data, over the range $0 < \underline{R} < 8$, to be sure that the polynomial was a good approximation to the actual input history. Figure 16 illustrates a few examples of the experimental and fitted input curves.

In some cases, experimental difficulty was experienced in producing input curves that satisfied the required boundary condition

$$\underline{C}/\underline{C}_o = 1, \qquad \underline{Z} = 0, \qquad \underline{t} = 0.$$

This was generally due to incomplete closing of the sliding valve, caused by human error and the valve construction itself. Thus, conditions were favorable for diffusional and convective (no bulk flow) loss of solute from the input portion of the system. The effect was evidenced by a slow increase of the inlet solute transmission during the 10 min. of elapsed time between bed saturation and commencement of a run. (For calculation purposes, the inlet solute value was always recorded after the sliding valve was closed and before the flow tube was filled with water.) Careful examination of the exit concentration profiles from these runs often disclosed a small dip, or an early breakthrough, as the relative concentration decreased from 1 to about 0.95. The effect was most evident in the diacetyl runs. Thus, in the subsequent analysis, it was necessary to remember that the earliest portions of the breakthrough curves were least reliable.

A second, and probably related difficulty, was that the asymptotic approach to an inlet water value was generally gradual below a relative concentration of about 0.03. This was apparently the result of (a) solute contained by stagnant pockets in the sliding valve mechanism, and (b) solute that had escaped upward

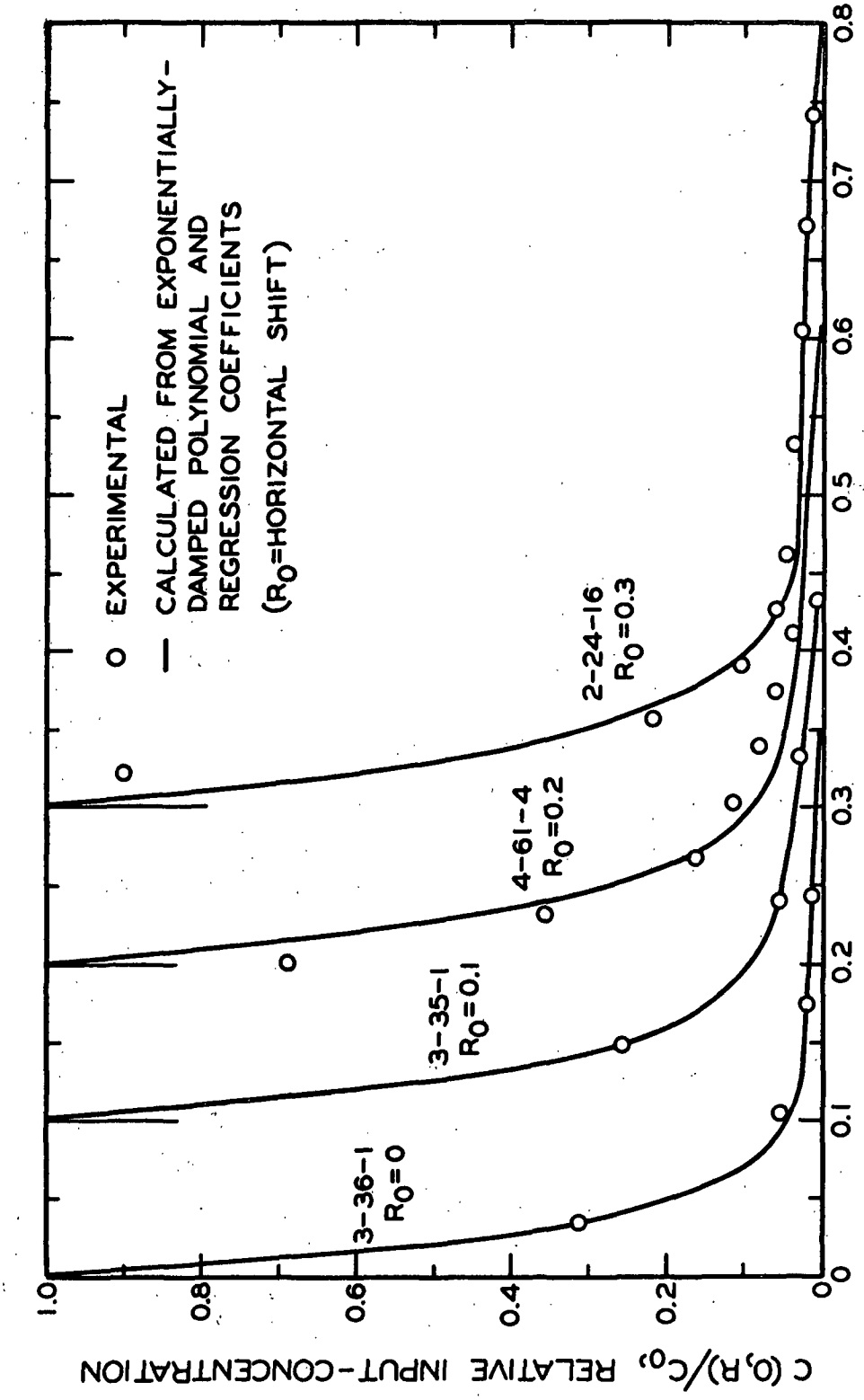

Figure 16. Examples of Input Curves

into the wash water from the input section, just prior to performing a run. The fact that some inputs were not perfectly defined, contributed in a small but significant way to errors in the material balance determinations and subsequent analyses.

A third difficulty with the input was experienced in the higher velocity runs, especially in the 16-denier system. Here the areas under the input curves were observed to increase with pore velocity, above 1 cm./sec. It became obvious that this phenomenon resulted from changes in the geometry of the inlet light path. This was caused by changes in the deformation of the upper screen, in response to flow through the bed. It was evidenced by the facts that (a) the areas under the input curves became larger than the geometry of the inlet section (above the light path) would indicate, and (b) the inlet water values were noted to decrease after terminating flow. To remedy this situation, Runs 1-2, 5, 9, 3, and 7-16, were analyzed by arbitrarily using the input constants for Run 1-8-16 as a substitute.

MATERIAL BALANCE DETERMINATION

As an internal check on the experimental data, it was important to establish the fact that material balances were achieved in the washing runs. The method of testing the processed raw data involved comparing the solute washed from a bed with the solute initially contained by the bed. To illustrate the technique, consider a fiber-solute system at equilibrium, with a linear adsorption isotherm having a partition coefficient $\underline{K_I}$. The effective porosity of the system $\epsilon_{\underline{E}}$ is defined as the ratio of total void space to total volume. At equilibrium, the ratio of solute in the system to solute in the voids, is then defined as the solute ratio,

$$M_o = 1 + (1 - \epsilon_E) K_I/\epsilon_E \qquad (58)$$

Next, assume that the bed is washed with solvent. The relative concentrations (on a volumetric basis) at the inlet, $(\underline{C}/\underline{C}_o)_{\underline{I}}$, and the exit, $(\underline{C}/\underline{C}_o)_{\underline{E}}$, are measured as functions of the number of pore volumes displaced (based on $\epsilon_{\underline{E}}$). After both relative concentrations reach zero, an appropriate estimate of the solute ratio can be calculated from the breakthrough curves as

$$M_w = \int_o^\infty [(C/C_o)_E - (C/C_o)_I] \, dR \qquad (59).$$

The two relations for the solute ratio can be equated to define an apparent partition coefficient

$$K_w = (M_w - 1) \epsilon_E/(1 - \epsilon_E) \qquad (60),$$

which specifically characterizes the removal of solute from the system during a washing run. The effectiveness of achieving a material balance can be measured by comparing $\underline{K}_{\underline{w}}$ with $\underline{K}_{\underline{I}}$, since the difference between these two should be zero (on the average) and independent of the effective bed porosity and pore velocity. Any significant trends in $\underline{K}_{\underline{w}} - \underline{K}_{\underline{I}}$ with these or other parameters, would indicate the presence of an uncontrolled variable in the system.

A reliable calculation of $\underline{M}_{\underline{w}}$ requires an accurate determination of several experimental parameters. Among these, the water value $\overline{\underline{W}}_{\underline{E}}$ was found to be one of the more difficult to estimate. The major reason was due to the fact that the photometric system exhibited a certain amount of random fluctuation. These fluctuations were generally found to be between $\pm$ 0.5 and $\pm$ 2% of the mean recorded value, and they appeared to be independent of flow. Thus, in recording the raw data it was necessary to examine the "tail" of a breakthrough curve over a relatively wide range to be certain that an accurate water value was established.

Tables XII and XIII summarize the important experimental conditions and associated material balance data that characterize the washing runs on the 1 and 4-denier viscose systems. The run number, e.g., 3-27-1, designates the third bed (chronologically), the 27th washing run (chronologically), on the 1-denier system. The description "D, PAA" refers to a desorption run, using PAA; similarly, "S, PAA" refers to a sorption run, where the initial condition is reversed. The values of bed length $\underline{Z}_e$ and average bed porosity ϵ, without the parentheses, refer to the fiber bed only. The values in parentheses refer to the effective bed length $\underline{Z}_E$, and effective porosity ϵ_E; these were used to account for the fact that the inlet and exit concentrations were measured just above and just below the bed boundaries. Thus, $\underline{Z}_E$ represents the mean distance between the planes of the light paths, and ϵ_E represents the effective porosity of the system (as previously discussed). The symbol $\underline{I}$ refers to the area under the inlet relative concentration curve.

The average values of $\underline{K}_w$ for the PAA-1 and 4-denier systems were $\overline{\underline{K}}_w = 8.16$ and 10.24, respectively. These compared reasonably well with the respective $\underline{K}_I$ values of 8.58 and 9.80 from the adsorption isotherms. It was especially encouraging that the $\underline{K}_w$ values were essentially independent of both ϵ and $\underline{U}$. The starred $\underline{K}_w$ values for Runs 4-63, 64, 65, and 69-4, were recognized as special cases, being somewhat large due to unusually low temperatures of the dye solution and water; they were not included in the above average. Further discussion on these runs is given later. It is concluded from the above results that material balance considerations were adequately satisfied in the 1 and 4-denier systems.

The determination of material balances in the PAA-16 denier viscose system proved to be more difficult because of further complications related to estimation of the water value. The determinations were most difficult in the higher pore

TABLE XII

WASHING RUN CONDITIONS AND MATERIAL BALANCE DATA

Run	Description	Z_e, (Z_E), cm.	ϵ, (ϵ_E)	U, cm./sec.	I	M_w	K_w	T, °C.
3-27-1[a]	D, PAA	8.08 (8.66)	0.8358 (0.8436)	0.0622	0.024	2.57	8.50	26.8
3-29-1	"	"	"	0.181	0.034	2.46	7.87	27.2
3-28-1	"	"	"	0.327	0.054	2.51	8.14	26.8
3-30-1	"	6.08 (6.605)	0.7817 (0.7947)	0.0499	0.027	3.06	7.97	27.4
3-32-1	"	"	"	0.183	0.019	3.17	8.40	27.4
3-31-1	"	"	"	0.355	0.015	3.15	8.43	27.4
3-33-1	"	4.67 (5.15)	0.7158 (0.7346)	0.0428	0.042	3.87	7.94	27.8
3-36-1	"	"	"	0.144	0.037	3.90	8.03	27.6
3-34-1	"	"	"	0.306	0.113	3.88	7.97	28.0
3-35-1	"	"	"	0.480	0.031	3.84	7.85	27.4
3-38-1	S, PAA	4.67 (5.15)	0.7158 (0.7346)	0.0706	0.033	4.01	8.33	28.0
3-37-1	"	"	"	0.168	0.055	3.94	8.14	28.0
3-39-1	D, Diacetyl	"	"	0.0675	0.042	1.218	0.604	--
3-40-1	"	"	"	0.159	0.014	1.206	0.570	--
3-41-1	"	"	"	0.380	0.013	1.211	0.584	--
3-42-1	D, PAA	"	"	0.215	0.077	4.04	8.42	27.1
3-43-1	"	"	"	0.885	0.043	4.00	8.31	27.1
3-44-1	D, BPP	"	"	0.213	0.015	1.775	--	--
3-46-1	"	"	"	0.165	0.041	2.018	--	--
3-47-1	S, BPP	"	"	0.117	0.015	2.093	3.015	--

[a] 3-27-1 refers to the third bed (chronologically), 27th run (chronologically), on the 1-denier system.

TABLE XIII

WASHING RUN CONDITIONS AND MATERIAL BALANCE DATA

Run	Description	Z_e,(Z_E), cm.	ϵ,(ϵ_E)	U, cm./sec.	I	M_w	K_w	T, °C.
4-48-4	D, PAA	8.29 (8.855)	0.8598 (0.8654)	0.0265	0.013	2.64	10.55	26.3
4-51-4	"	"	"	0.0709	0.026	2.56	10.03	25.8
4-49-4	"	"	"	0.219	0.006	2.57	10.10	26.0
4-50-4	"	"	"	0.405	0.023	2.58	10.16	25.9
4-52-4	D, Diacetyl	"	"	0.0757	0.012	1.131	0.850	25.8
4-53-4	"	"	"	0.156	0.011	1.146	0.945	25.0
4-56-4	D, PAA	6.06 (6.455)	0.8059 (0.8153)	0.0349	0.027	3.31	10.20	24.0
4-54-4	"	"	"	0.156	0.014	3.42	10.70	24.2
4-55-4	"	"	"	0.403	0.018	3.31	10.20	25.8
4-57-4	D, Diacetyl	"	"	0.0496	0.024	1.141	0.618	24.0
4-58-4	"	"	"	0.154	0.016	1.161	0.712	23.8
4-59-4	"	"	"	0.483	0.025	1.172	0.760	26.0
4-60-4	"	4.63 (5.015)	0.7460 (0.7614)	0.0638	0.021	1.188	0.585	26.3
4-61-4	"	"	"	0.181	0.041	1.214	0.665	26.3
4-62-4	"	"	"	0.523	0.039	1.206	0.640	26.3
4-65-4	D, PAA	"	"	0.0169	0.039	4.50	11.17[a]	--
4-63-4	"	"	"	0.0756	0.035	4.42	10.90[a]	--
4-64-4	"	"	"	0.229	0.036	4.50	11.17[a]	--
4-66-4	"	"	"	0.539	0.044	4.15	10.05	26.4
4-68-4	"	"	"	0.870	0.052	4.22	10.27	25.4
4-69-4	S, PAA	"	"	0.187	0.067	4.39	10.81[a]	--
4-67-4	"	"	"	0.206	0.051	4.16	10.09	25.9

[a]Somewhat large due to unusually low temperatures in the range of 22-24°C.

velocity runs, where asymptotic approaches to water values were quite gradual. Under these conditions, complete washing required a large number of pore volumes of fluid. As a consequence, the accuracy of calculating $\underline{M}_{\underline{W}}$ was found to be quite dependent on the accuracy of $\underline{\overline{W}}_{\underline{E}}$. For example, $\underline{M}_{\underline{W}}$ was calculated as a function of $\underline{\overline{W}}_{\underline{E}}$ for the velocity run 1-7-16 ($\underline{U}$ = 2.04 cm./sec.). The numerical integration was performed over the experimental pore volume range $0 < \underline{R} < 25$. The results indicated a 4.9% change in $\underline{M}_{\underline{W}}$ when $\underline{\overline{W}}_{\underline{E}}$ was changed by 1%. Under conditions where complete washing was accomplished with fewer pore volumes of water, $\underline{M}_{\underline{W}}$ was found to be less sensitive to changes in $\underline{\overline{W}}_{\underline{E}}$. For example, in the lower velocity run 4-23-16 ($\underline{U}$ = 0.0846 cm./sec.), a 2.8% change in $\underline{M}_{\underline{W}}$ was observed with a 1% change in the water value.

The estimation of material balances in the higher velocity runs was further complicated by the fact that many were terminated before true water values were definitely established, although the asymptotic approaches appeared to be close. In order to estimate reliable water values and determine material balances in these runs, it was necessary to develop a method of approximation.

Six of the lowest velocity runs in the PAA-16 denier system appeared to be effectively complete. Material balances were calculated for these runs as previously discussed for the 1 and 4-denier systems. Table XIV illustrates the results of these calculations. The average value of 9.45 for $\underline{K}_{\underline{W}}$ compared favorably with the independently determined partition coefficient, $\underline{K}_{\underline{I}}$ = 9.50. Thus, material balances appeared to be adequately satisfied with these runs at all five porosity levels. From this it was assumed that the remaining runs on the two 16-denier beds would also satisfy material balance considerations, provided that appropriate water values were estimated.

TABLE XIV

MATERIAL BALANCE DETERMINATIONS ON THE LOW VELOCITY RUNS OF THE PAA-16-DENIER SYSTEM

Run	ϵ_E	K_w	T, °C.
1- 8-16	0.7753	9.55	26.0
1- 4-16	0.7753	9.45	26.0
2-16-16	0.8949	9.53	25.4
2-18-16	0.8576	9.45	25.3
2-20-16	0.8067	9.30	28.0
2-23-16	0.7639	9.44	27.5
	Averages	9.45	26.4

The details of determining material balances in the PAA-16 denier systems, including the summary of washing run conditions and material balance data, are given in Appendix V. It was demonstrated in these cases that the breakthrough curves adequately satisfied material balance considerations.

ANALYSIS OF WASHING RUNS

TECHNIQUE OF ANALYSIS

The fluid dispersion properties were characterized by the longitudinal dispersion coefficient D_L, or more generally, by the mixing parameter, D_L/U. This parameter was determined at various porosity levels, in the 1, 4, and 16-denier systems, over a range of pore velocities in the laminar regime. The mass transfer phenomena were characterized (under approximately the same conditions) first by the apparent intrafiber diffusion parameter $(D_F/a^2)_A$, and secondly by the intrafiber diffusion parameter D_F/a^2 and the mass transfer parameter $L = ak_L/D'_F$.

It was originally felt that both the dispersion and mass transport effects could be separated reliably by single washing experiments in the PAA systems, provided that mass transport occurred sufficiently far from the equilibrium condition. This, in fact, was found to be true in certain instances, but it became apparent that this was not the general case. In fact, under some limiting conditions it was quite misleading, and sometimes impossible, to separate the parameters in a single washing experiment. Thus, it was evident that it would be necessary to examine several washing runs over a reasonably wide range of experimental conditions. In addition, it was found advantageous to employ diacetyl and BPP in order to determine the dispersion properties independently.

Determination of the Mixing Parameter

The experimental method of determining D_L/U, in the 1 and 4-denier systems, was based on results obtained by Sherman (1). His breakthrough curves from the diacetyl – 17 μ dacron (nonporous) system were essentially the same for each bed at various pore velocities between about 0.02 and 0.6 cm./sec. Thus, trial and error applications of the No-Sorption case yielded a linear relation between D_L and U for each of three dacron beds. Sherman then applied the Equilibrium case to the diacetyl-1 denier viscose system and observed essentially the same behavior over the pore velocity range 0.08-0.520 cm./sec., in two beds of different length (3.05 and 5.41 cm.). It was concluded at this point that (a) bed end effects were unimportant, (b) the mechanism of longitudinal dispersion was the same in both systems, and (c) intrafiber diffusion (and/or liquid-phase mass transfer at the fiber-fluid boundaries) was sufficiently rapid to approximate the Equilibrium case in the diacetyl-1 denier viscose system. Using these results as a basis, D_L/U was determined in the present 1 and 4-denier beds by employing diacetyl and applying the Equilibrium case [Case 1(F) was also applied to the latter system as a check].

Due to the presence of intrafiber diffusion effects, diacetyl was not considered a suitable solute for determining D_L/U in the 16-denier system. Instead, BPP was employed, since a previous estimate of the diffusion coefficient of BPP in cellophane (25) indicated that the dye would diffuse at a sufficiently low rate to approximate the No-Sorption case (over a large portion of a breakthrough curve), if the experimental pore velocity was 1 cm./sec. or greater.

Determination of the Apparent Intrafiber Diffusion Parameter

Once the D_L/U values were obtained in the 1, 4, and 16-denier systems as described above, it was appropriate to determine the apparent intrafiber diffusion parameter, $(D_F/a^2)_A$, in the PAA systems by applying Case 1(F). Again, this was largely a trial and error process of bracketing the curves on each side with successively refined estimates.

In analyzing the various washing runs on the PAA-1 and 4-denier viscose systems, it was readily apparent that $(D_F/a^2)_A$ was not constant; instead it increased to apparently asymptotic values as U increased; also, ϵ was found to affect the results. At this point it was necessary to make a decision concerning the over-all approach to be taken in the analysis; two possibilities were apparent, and those were:

1. Evaluate each run independently and attempt to find the best fitting value of $(D_F/a^2)_A$, without regard to the results of other runs at different pore velocities and porosities.

2. Assume that a smooth and continuous relationship exists between $(D_F/a^2)_A$ and U, and attempt to define the relationship which best describes a complete series of runs at a given porosity level.

After considering these two alternatives, the latter was chosen. By analyzing an entire set of runs in a consistent manner, it was somewhat easier to separate random deviations, in individual runs, from consistent discrepancies. The fact that several runs were performed at different velocities, at each porosity level, increased the confidence in the determinations.

Since $(\underline{D}_F/\underline{a}^2)_A$ appeared to become asymptotic as $\underline{U}$ increased in the PAA-1, 4, and 16-denier systems, the respective asymptotic values were arbitrarily used to represent the real intrafiber diffusion parameters, $\underline{D}_F/\underline{a}^2$, of the fiber-solute systems. The region of pore velocities where $(\underline{D}_F/\underline{a}^2)_A$ was found to be essentially constant was designated as the regime where intrafiber diffusion effects were controlling. The region of pore velocities below this was designated as the regime where both intrafiber diffusion and liquid-phase mass transfer effects were important; it was in this region that Case 2(F) was applied in the analysis.

Determination of the Mass Transfer Parameter

The breakthrough curves were analyzed for the conditions of Case 2(F) by employing the appropriately fixed value of $\underline{D}_F/\underline{a}^2$ at all pore velocities, and at all the porosity levels studied in each fiber system. The mass transfer parameter, $\underline{L} = \underline{a}\underline{k}_L/\underline{D}'_F$, was then determined by trial and error fitting of the breakthrough curves as before.

SUMMARY OF WASHING PARAMETERS

Tables XV-XVII summarize the run conditions, and the washing parameters that were determined in the analysis of washing runs on the 1, 4, and 16-denier systems. All dimensional quantities are in cm., g., sec. units. The effective porosity (in brackets) and the last five columns comprise the actual calculation parameters that were employed, excluding the six constants belonging to the exponentially damped polynomial for the input curves.

TABLE XV

SUMMARY OF WASHING PARAMETERS

Run	Description	$\epsilon, (\epsilon_E)$	U	D_L/U	$k_L \times 10^4$	$D_L/UZ_E \times 10^3$	K	$U/Z_E \times 10^2$	$(D_F/a^2)_A$	ak_L/D'_F [a]
3-27-1	D, PAA	0.8358 (0.8436)	0.0622	0.0309	7.07	3.57	8.15	0.718	0.013	3.5
3-29-1	"	"	0.181	"	28.3	"	"	2.095	0.023	14.0
3-28-1	"	"	0.327	"	101.0	"	"	3.78	0.0295	50.0
3-30-1	"	0.7817 (0.7947)	0.0499	"	5.05	4.68	"	0.755	0.010	2.5
3-32-1	"	"	0.183	"	20.2	"	"	2.765	0.021	10.0
3-31-1	"	"	0.355	"	80.8	"	"	5.38	0.029	40.0
3-33-1	"	0.7158 (0.7346)	0.0428	"	3.03	6.00	"	0.832	0.0080	1.5
3-36-1	"	"	0.144	"	10.1	"	"	2.79	0.017	5.0
3-34-1	"	"	0.306	"	40.4	"	"	5.94	0.026	20.0
3-35-1	"	"	0.480	"	121.0	"	"	9.33	0.030	60.0
3-38-1	S, PAA	0.7158 (0.7346)	0.0706	0.0309	5.05	6.0	8.15	1.37	0.011	2.5
3-37-1	"	"	0.168	"	13.1	"	"	3.26	0.019	6.5
3-39-1	D, Diacetyl	"	0.0675	"	--	"	0.618	1.31	--	--
3-40-1	"	"	0.159	"	--	"	"	3.09	--	--
3-41-1	"	"	0.380	"	--	"	"	7.37	--	--
3-42-1	D, PAA	"	0.215	"	20.2	"	8.15	4.175	0.022	10.0
3-43-1	"	"	0.885	"	∞	"	"	17.2	0.030	∞
3-47-1	S, BPP	"	0.117	"	--	"	3.025	2.282	0.008	--

[a] $L = ak_L/D'_F$, based on $D_F/a^2 = 0.030$ in PAA-1 denier system.

TABLE XVI

SUMMARY OF WASHING PARAMETERS

Run	Description	ϵ, (ϵ_E)	U	D_L/U	$k_L \times 10^4$	$D_L/UZ_E \times 10^3$	K	$U/Z_E \times 10^2$	$(D_F/a^2)_A$	ak_L/D_F'[a]
4-48-4	D, PAA	0.8598 (0.8654)	0.0265	0.0443	4.47	5.0	10.32	0.299	0.0050	2.0
4-51-4	"	"	0.0709	"	12.3	"	"	0.800	0.0085	5.5
4-49-4	"	"	0.219	"	67.1	"	"	2.47	0.0130	30.0
4-50-4	"	"	0.405	"	∞	"	"	4.58	0.014	∞
4-52-4	D,Diacetyl	"	0.0757	"	--	"	0.618	0.854	--	--
4-53-4	"	"	0.156	"	--	"	"	1.758	--	--
4-56-4	D, PAA	0.8059 (0.8153)	0.0349	0.0388	4.47	6.0	10.32	0.540	0.0050	2.0
4-54-4	"	"	0.156	"	24.6	"	"	2.42	0.0100	11.0
4-55-4	"	"	0.403	"	134.0	"	"	6.24	0.0135	60.0
4-57-4	D,Diacetyl	"	0.0496	"	--	"	0.618	0.768	0.35	--
4-58-4	"	"	0.154	"	--	"	"	2.38	"	--
4-59-4	"	"	0.483	"	--	"	"	7.48	"	--
4-60-4	"	0.7460 (0.7614)	0.0638	0.0351	--	7.0	0.618	1.27	0.35	--
4-61-4	"	"	0.181	"	--	"	"	3.61	"	--
4-62-4	"	"	0.523	"	--	"	"	10.42	"	--
4-65-4	D, PAA	"	0.0169	"	2.23	"	10.80	0.338	0.0030	1.0
4-63-4	"	"	0.0756	"	6.70	"	"	1.508	0.0060	3.0
4-64-4	"	"	0.229	"	31.3	"	"	4.56	0.0100	14.0
4-66-4	"	"	0.539	"	134.0	"	10.32	10.73	0.0130	60.0
4-68-4	"	"	0.870	"	∞	"	"	17.35	0.0140	∞
4-69-4	S, PAA	"	0.187	"	22.3	"	10.80	3.725	0.0090	10.0
4-67-4	"	"	0.206	"	24.6	"	10.32	4.12	0.0095	11.0

[a] Based on $D_F/a^2 = 0.014$ in PAA-4 denier system.

TABLE XVII

SUMMARY OF WASHING PARAMETERS

Run	Description	$\epsilon, (\epsilon_E)$	U	D_L/U	$k_L \times 10^4$	$D_L/UZ_E \times 10^3$	K	$U/Z_E \times 10^2$	$(D_F/a^2)_A$	ak_L/D_F[a]
1-18-16	D, PAA	0.7636 (0.7753)	0.0391	0.080	8.03	18.5	9.30	0.905	0.0029	5.5
1-14-16	"	"	0.206	"	43.8	"	"	4.78	0.0044	30.0
1-16-16	"	"	0.397	"	∞	"	"	9.18	0.0050	∞
1-10-16	"	"	0.662	"	"	"	"	15.32	"	"
1-12-16	"	"	0.950	"	"	"	"	22.0	"	"
1-15-16	"	"	1.237	"	"	"	"	28.6	"	"
1-19-16	"	"	1.473	"	"	"	"	34.1	"	"
1-13-16	"	"	1.793	"	"	"	"	41.5	"	"
1-17-16	"	"	2.039	"	"	"	"	47.2	"	"
1-11-16	S, PAA	"	0.654	"	"	"	"	15.15	"	"
1-12-16	"	"	0.917	"	"	"	"	21.25	"	"
1-14-16	D, BPP	"	0.933	"	--	"	3.025	21.6	0.0005	--
1-15-16	"	"	1.247	"	--	"	"	28.85	"	--
1-13-16	"	0.7636 (0.7753)	1.740	0.080	--	"	"	40.3	"	--
2-16-16	D, PAA	0.8920 (0.8949)	0.0642	"	26.3	7.11	9.30	0.571	0.0042	18.0
2-17-16	"	"	0.299	"	∞	"	"	2.66	0.0050	∞

[a] D_F/a^2 = 0.0050 in PAA-16 denier system.

TABLE XVII (Continued)

SUMMARY OF WASHING PARAMETERS

Run	Description	ϵ, (ϵ_E)	U	D_L/U	$k_L \times 10^4$	$D_L/UZ_E \times 10^3$	K	$U/Z_E \times 10^2$	$(D_F/a^2)_A$	ak_L/D_F [a]
2-18-16	D,PAA	0.8515 (0.8576)	0.0760	0.080	21.9	9.59	9.30	0.911	0.0040	15.0
2-19-16	"	"	0.334	"	∞	"	"	4.01	0.0050	∞
2-20-16	"	0.7934 (0.8067)	0.0778	"	19.0	12.83	"	1.25	0.0037	13.0
2-21-16	"	"	0.341	"	∞	"	"	5.47	0.0050	∞
2-23-16	"	0.7443 (0.7639)	0.0846	"	14.6	15.68	"	1.66	0.0035	10.0
2-22-16	"	"	0.209	"	43.8	"	"	4.10	0.0045	30.0
2-24-16	"	"	0.358	"	∞	"	"	7.02	0.0050	∞
2-26-16	"	"	0.955	"	"	"	"	18.72	"	"
2-25-16	S, PAA	"	0.307	"	"	"	"	6.00	"	"

[a] D_F/a^2 = 0.0050 in PAA-16 denier system.

It should be emphasized that bed end effects were taken into account in the analysis by employing (a) ϵ_E and U/Z_E as calculation parameters, since the experimental values of R were based on U, ϵ_E and Z_E, and (b) Z_E to calculate D_L/U from $S = D_L/UZ_E$.

Temperature Variations and Partition Coefficients

With one exception, the effects of run-to-run temperature variations were not accounted for in the analysis. Temperature corrections might have been applied to the partition coefficients, but these would have been of questionable value since the temperature ranges were small, and the random errors in K_W were of the same order of magnitude as the appropriate temperature corrections in K.

A degree of difficulty was experienced in controlling the temperature in Runs 4-63-4 through 4-69-4, however. Here the ambient temperature was quite low (about 18°C.) and the dye solution and wash water quickly cooled below the normal operating temperature range, without the benefit of reheating at sufficiently regular intervals (the wash water was heated just prior to Runs 4-62-4 and 4-66-4). The effect was evidenced by the relatively high values of K_W in Runs 4-63, 64, 65, and 69-4, resulting from increased adsorption of PAA at lower temperatures. To compensate for this experimental oversight, the partition coefficient was changed from 10.32 to 10.80 in the analyses of these runs.

A close examination of the K values that were used in the calculations, indicates that they were not the same as the K_I values from the respective adsorption isotherms. Instead it appeared that the analyses would be more meaningful if the $\bar{K}_W$ (average) values were employed. The analyses were originally performed with these $\bar{K}_W$ values, but a few minor errors in determining the individual K_W values were later discovered and corrected; thus, the K, K_I, and $\bar{K}_W$

values were slightly different for each system. The respective values are summarized in Table XVIII.

TABLE XVIII

SUMMARY OF PARTITION COEFFICIENTS

Denier	Adsorption Isotherms		Washing Runs		Analysis
	K_I	T, °C.	K_W	T, °C.	K
1	8.58	26.5	8.16	27.4	8.15
4	9.80	26.4	10.24	25.6	10.32
16	9.50	26.3	9.45	26.4	9.30

REPRODUCIBILITY OF WASHING DATA

Two 16-denier beds were employed for demonstrating the reproducibility of the experimental data. Since no two washing runs were performed under exactly the same conditions, it was necessary to compare predicted vs. experimental results in closely related runs on the two beds; Fig. 17 illustrates such a comparison. Further comparisons of other runs, over a wide range of pore velocities on these two beds, indicated that the agreement was generally within 2%.

It was concluded from these results, together with the previously discussed permeability and material balance results, that the experimental techniques and methods of analysis involved in (a) forming the beds, (b) performing the washing runs, (c) obtaining the raw data, and (d) reducing the raw data, were yielding reproducible and reliable breakthrough curves. It therefore appeared unnecessary to use more than one bed in each of the 1 and 4-denier systems, as long as the proper precautions were exercised, and the data were obtained over a sufficiently inclusive range.

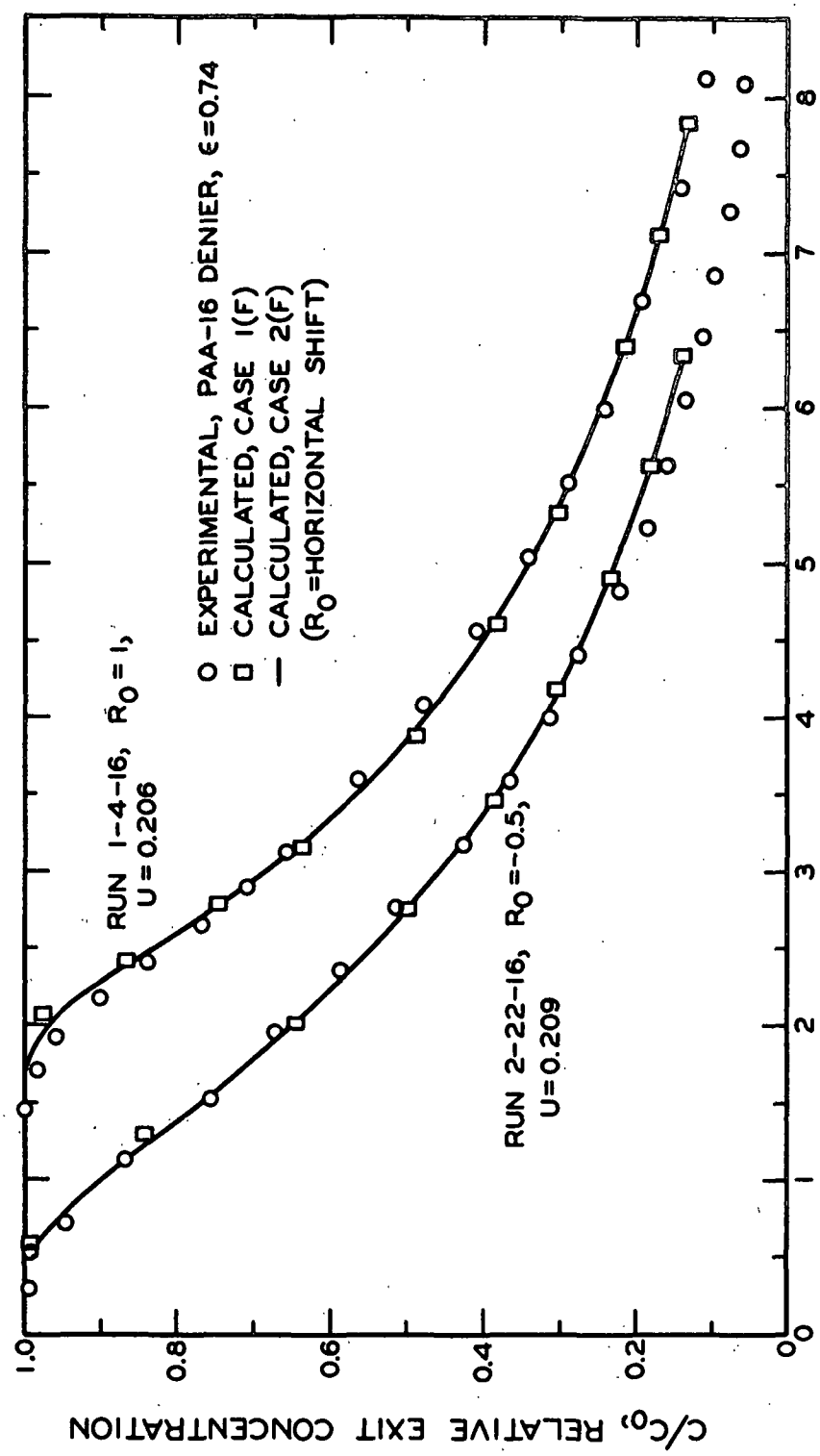

Figure 17. Reproducibility of Breakthrough Curves

EFFECT OF NONUNIFORM POROSITY DISTRIBUTION ON WASHING BEHAVIOR

When a fluid flows through a compressible fiber bed, which initially has been compacted to a fixed length and a uniform porosity, the bed assumes a nonuniform porosity distribution that satisfies a balance between the local compacting forces and the cumulative fluid drag forces. In this study, a number of washing runs were performed at relatively high flow rates, where the resulting nonuniformity was significant. Since the breakthrough curve calculations were based on average bed properties, it was important to evaluate the effect of nonuniform porosity distributions on the washing behavior.

It was beyond the scope of this work to derive a washing equation which rigorously accounted for a nonuniform porosity distribution. As an alternative means, it was decided to subdivide a nonuniform test bed into sections (that more nearly approximated uniform beds) and analyze the sections separately. These results could then be combined in a suitable manner and subsequently compared with a calculation for the over-all bed.

The porosity distribution that prevailed during Run 3-35-1 (approximately) was calculated by empirical means; the details of determining this and other porosity distributions are given in Appendix VI. It was demonstrated here that the porosity distribution was nearly linear; Table XIX illustrates the linear approximation of this porosity distribution which was arbitrarily chosen as the test case for evaluating the effect on washing behavior.

The test bed was first divided in half so that the average properties of sections one and two were defined at relative distances of 0.25 and 0.75, respectively. The relative exit concentration from the first section was then calculated from the washing equation as a function of $\underline{R}$. This result was fitted by a

statistical regression for an exponentially damped polynomial, and thus it became the input for calculating a breakthrough curve from section two. The result of this calculation was compared with the calculated breakthrough curve for the overall bed, in terms of the average bed properties defined at a fractional distance of 0.50.

TABLE XIX

POROSITY AND PORE VELOCITY DISTRIBUTIONS REPRESENTING NONUNIFORM TEST BED IN WASHING CALCULATIONS

$Z/4.67$	ϵ_z	U, cm./sec.
0.00	0.7680	0.4525
0.25	0.7460	0.4655
0.50	0.7242	0.4800
0.75	0.7023	0.4950
1.00	0.6805	0.5105

The exponentially damped polynomial, used in fitting the C/C_o vs. R curve from section one, differed slightly from the normally used input expression given by Equation (16) in that the regression was started at a finite value of R, namely R_o. The complete form of the polynomial, in terms of $R_1 = R - R_o$, was

$$\frac{C}{C_o} = (1 + k_1 R_1 + k_2 R_1^2 + k_3 R_1^3 + k_4 R_1^4) \exp (-\gamma R_1) \qquad (61).$$

The need for the initial starting point became evident after a number of trial fits were attempted with $R_o = 0.0$. In this case, the regressions were decidedly inadequate (as measured by the variance) for fitting the curve. Obviously, the polynomial lacked the desirable characteristics for fitting a curve of this shape. A suitable value of R_o was finally determined by trial and error to be 0.90; the value of C/C_o, at $R_1 = 0$, was set at unity, and 33 pairs of input data were used

in the regression over the range $0 < \underline{R}_1 < 7$. A variance of 3.74×10^{-4} resulted.

Before utilizing the polynomial as an input for section two, it was necessary to transform the independent variable to account for the change in average porosity between the two sections. Thus, the variable $\underline{R}_1$ was related to $\underline{R}_2$, for section two, by

$$R_2 = R_1 \, (\bar{\epsilon}_1/\bar{\epsilon}_2) = 1.064 \, R_1 \qquad (62)$$

where $\bar{\epsilon}_1$ and $\bar{\epsilon}_2$ were the respective average porosities of sections one and two. By substituting $\underline{R}_1 = \underline{R}_2/1.064$ in the polynomial, the various coefficients belonging to $\underline{R}_1$ were appropriately modified for use in section two.

After the exit concentration was calculated for section two, in terms of $\underline{R}_2$, it was necessary to perform a second transformation to define an $\underline{R}'$ coordinate for the over-all bed. This was expressed in terms of the average bed porosity ϵ, and $\underline{R}_2$, as

$$R' = (R_2 + R_o) \, (\bar{\epsilon}_2/2\epsilon) = 0.4855(R_2 + 0.957) \qquad (63).$$

In this manner, corresponding values of $\underline{R}'$ were calculated from $\underline{R}_2$ to represent the entire bed as a combination of individual results from the two halves.

It was originally intended to use the washing parameters from the analysis of Run 3-35-1. It became apparent, however, that practical difficulties in the numerical calculations were considerably lessened if (a) the areas under the exit concentration curves were not too large, and (b) the tails in the exit concentration curves were not excessively long. Table XX shows the washing

parameters finally chosen for this purpose. The only differences between the parameters for Run 3-35-1 and these were that (a) the value of the partition coefficient was decreased from 8.15 to 2.00, (b) $(\underline{D}_F/\underline{a}^2)_A$ was increased from 0.03 to 0.06, and (c) the effective porosity was taken as the average porosity of the test bed. The same value of the effective bed height, $\underline{Z}_E$ = 5.15 cm., was taken as usual rather than the actual bed height $\underline{Z}$ = 4.67 cm.

TABLE XX

WASHING PARAMETERS FOR 1-DENIER BED WITH A LINEAR POROSITY DISTRIBUTION

Parameter	Calculation A	B	C	D
$\underline{D}_L/\underline{UZ}_E$	0.012	0.012	0.006	0.012
$\underline{K}$	2.00	2.00	2.00	2.00
$\epsilon_{\underline{E}}$	0.7460	0.7023	0.7242	0.7023
$\underline{k}_o$	1.0	1.0	1.0	1.0
$\underline{k}_1$	-13.12	-0.7096	-13.12	-13.12
$\underline{k}_2$	83.93	0.1991	83.93	83.93
$\underline{k}_3$	-139.5	-0.02514	-139.5	-139.5
$\underline{k}_4$	0.0	0.001175	0.0	0.0
γ	14.0	0.3766	14.0	14.0
$\underline{U}/\underline{Z}_E$	0.1810	0.1923	0.0932	0.1923
$(\underline{D}_F/\underline{a}^2)_A$	0.060	0.060	0.060	0.060
$\underline{L}$	1000.0	1000.0	1000.0	1000.0
CALC	3.	3.	3.	3.

Figure 18 shows the resulting exit concentration profiles for the following designated conditions:

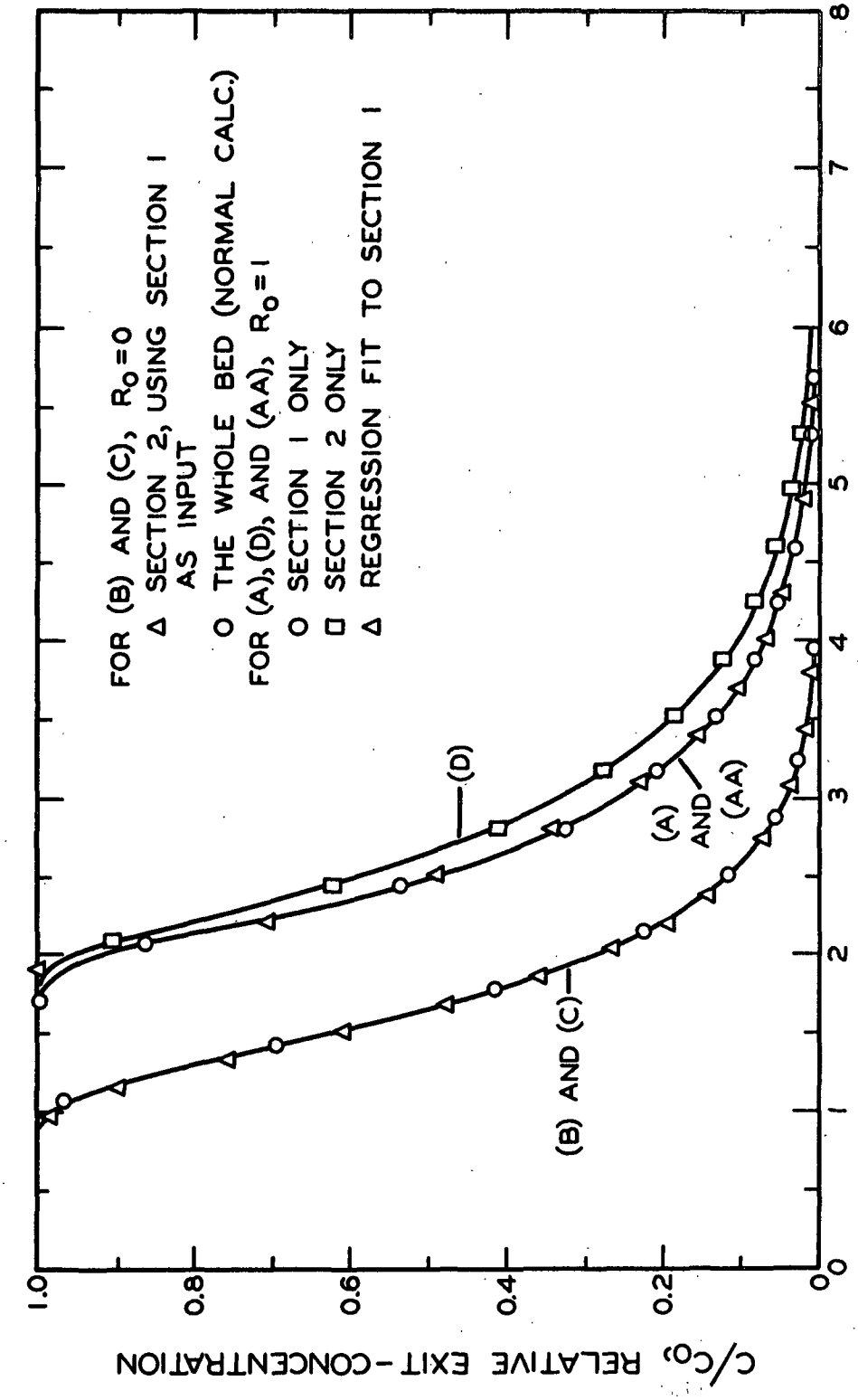

Figure 18. Effect of Nonuniform Porosity Distribution on Breakthrough Curves

A. section one, using the input constants of Run 3-35-1,

AA. section one, as fitted by the statistical regression,

B. section two, using the exit concentration from section one as its input,

C. the whole bed, using the input constants of Run 3-35-1,

D. section two, using the input constants of Run 3-35-1.

It is seen that the sequentially combined result, from the two halves, differs very little from the breakthrough curve for the over-all bed. The agreement would have been even better if a more accurate regression fit had been attained. From this finding it appears likely that an integrated result, representing a continuous account of the porosity variation, would probably differ little from the breakthrough curves that were obtained. For the purpose of this study, it was therefore assumed that applications of the washing equation, to moderately nonuniform beds, would yield approximately correct results when the average porosity and pore velocity were employed as calculated parameters.

DESORPTION VS. SORPTION WASHING RUNS

It was previously shown that both desorption and sorption washing runs could be analyzed by essentially the same equations. The equivalence was

$$(C/C_\infty)_{\text{sorption}} = 1 - (C/C_o)_{\text{desorption}} \qquad (28),$$

provided that the proper input definitions were used in each case. The sorption data were therefore plotted as $1 - C/C_\infty$ vs. R in order to simplify comparisons between the two types of runs.

Figures 19 and 20 show calculated vs. experimental comparisons between desorption and sorption runs, in the PAA-16 denier system, under closely matched velocity and porosity conditions. Intrafiber diffusion effects were controlling

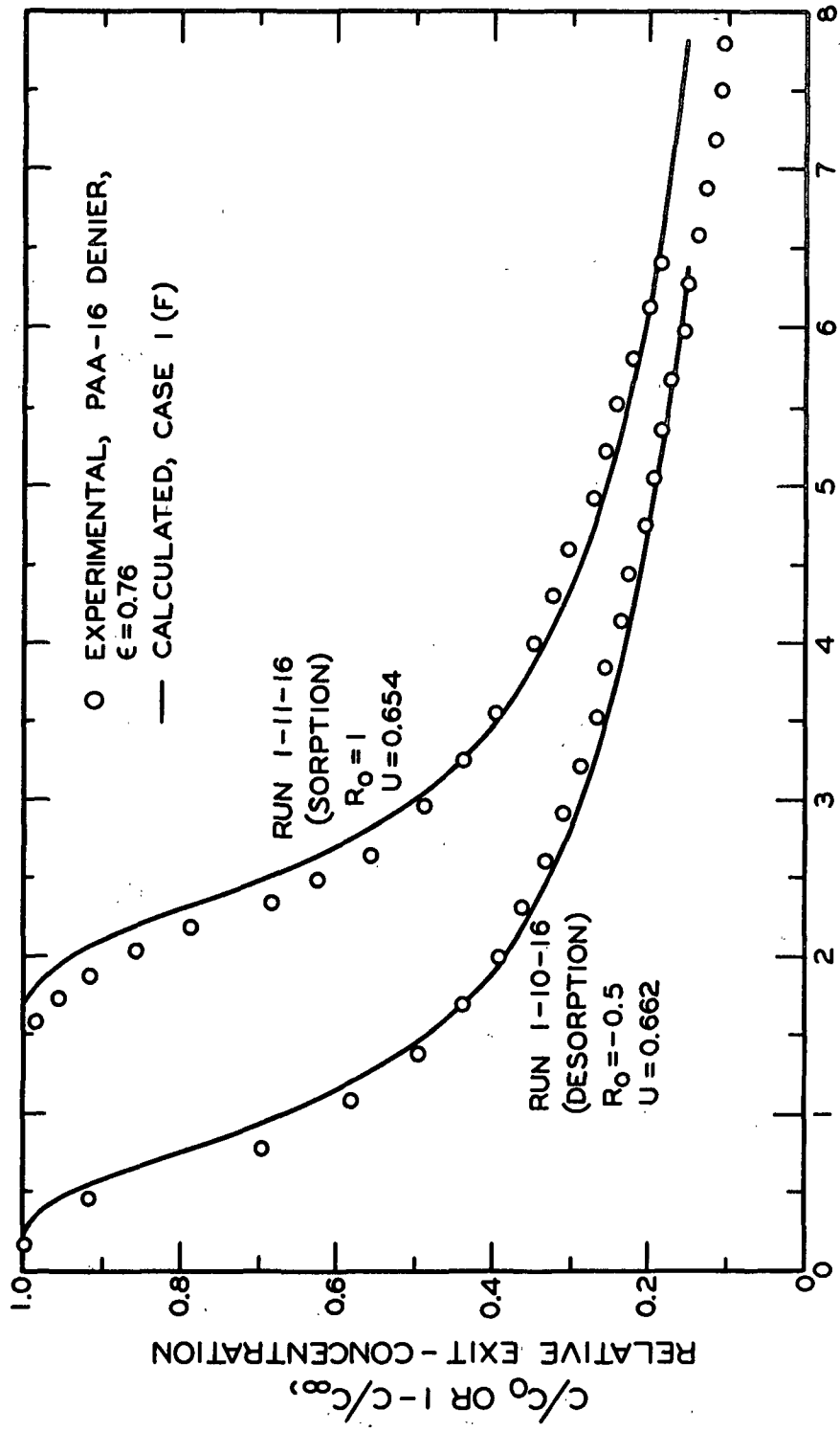

Figure 19. Breakthrough Curves for Desorption and Sorption Runs

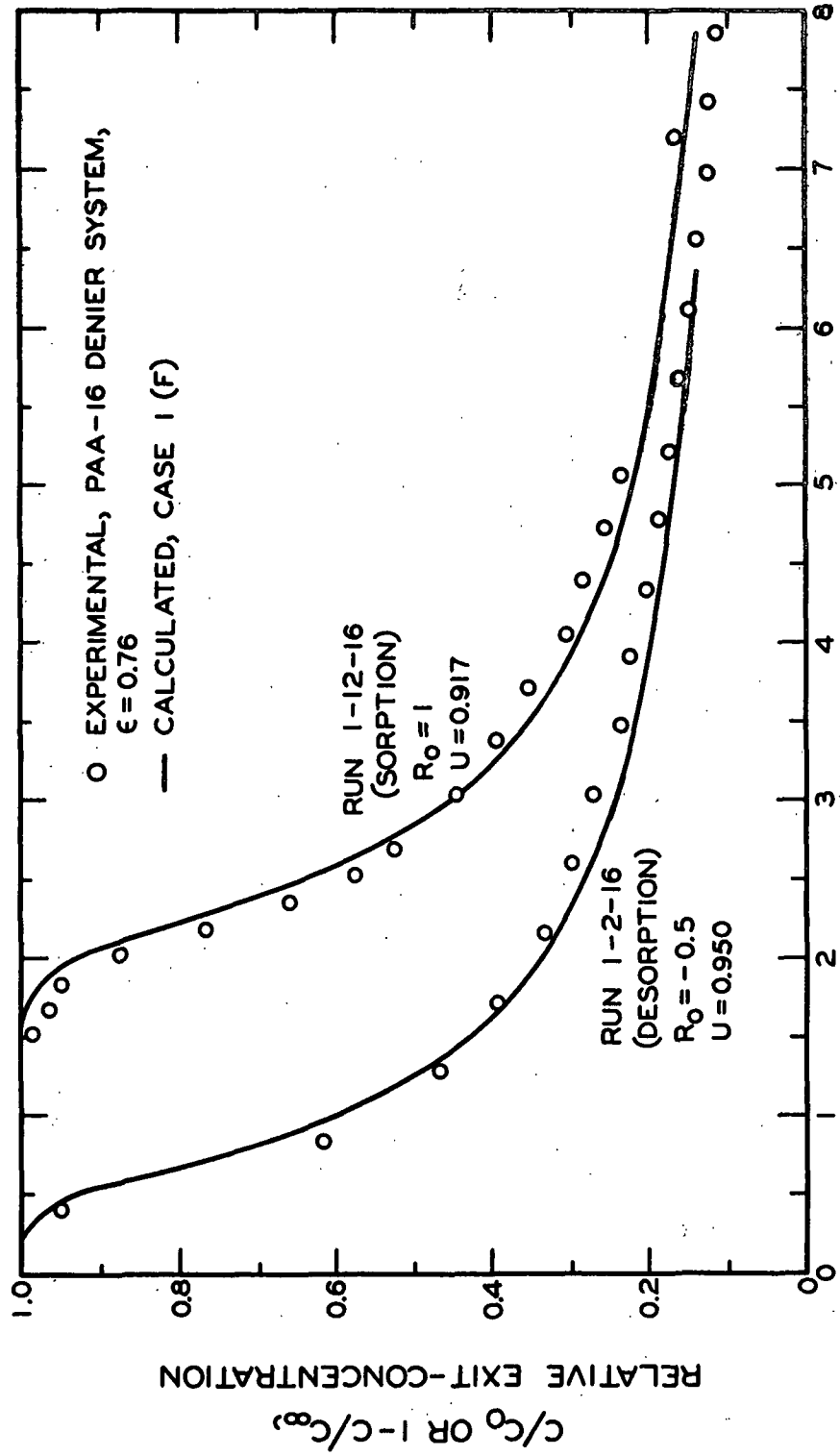

Figure 20. Breakthrough Curves for Desorption and Sorption Runs

in both sets of runs. The breakthrough curves compared favorably enough to conclude that no significant differences existed in the mechanism of mass transport under these conditions.

Crank (12) has shown in a number of examples that when Fick's law is not obeyed (when the diffusion coefficient is concentration dependent), the rates of sorption and desorption can be considerably different. Thus, the identity of results from the desorption and sorption experiments suggests that intrafiber diffusion of PAA in the 16-denier viscose system obeyed Fick's law to a good approximation.

Figure 21 shows comparisons between desorption and sorption washing runs, in the PAA-1 denier system, which demonstrate an apparent equivalence of the mass transport mechanisms when both intrafiber diffusion and liquid-phase mass transfer are important. Similar results were obtained in the PAA-4 denier system. Both of these findings suggest that Fick's law was obeyed to a good approximation.

WASHING RUNS ON 1-DENIER SYSTEMS

Figure 22 illustrates the three diacetyl runs that were performed at the lowest porosity level only. All three appear to exhibit essentially the same profiles despite the fact that the inputs for Runs 3-40-1 and 3-41-1 were not especially well defined. These results substantiate Sherman's finding that $\underline{D_L}/\underline{U}$ was independent of $\underline{U}$ in the diacetyl-1 denier system.

Figure 23 illustrates the lowest and highest pore velocity runs in the PAA-1 denier system, at the lowest porosity level. These represent the two extreme mass transport conditions that were observed in this system. The lowest velocity run was still quite far removed from the equilibrium condition. The

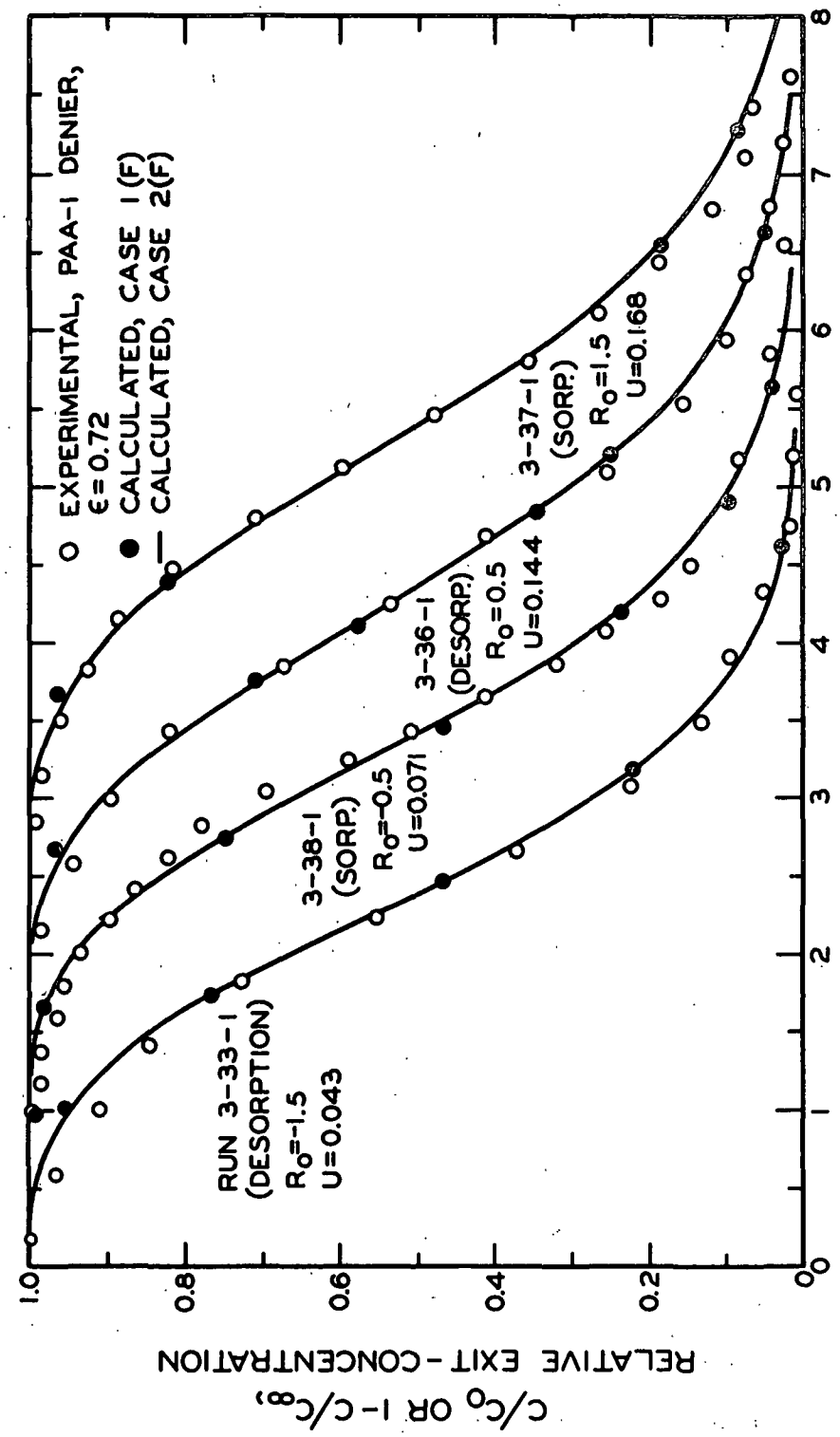

Figure 21. Breakthrough Curves for Desorption and Sorption Runs

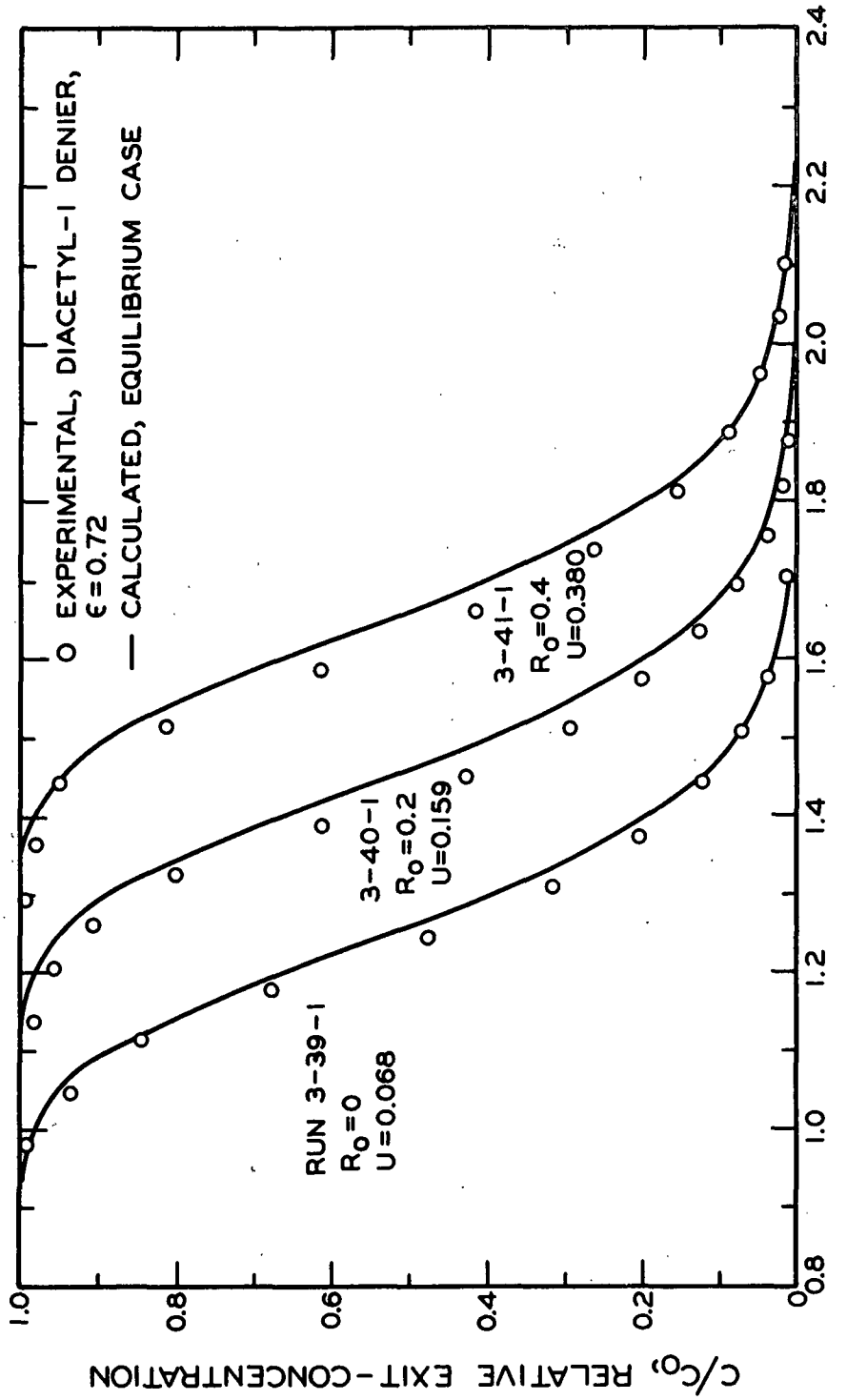

Figure 22. Breakthrough Curves for Determination of Mixing Parameter

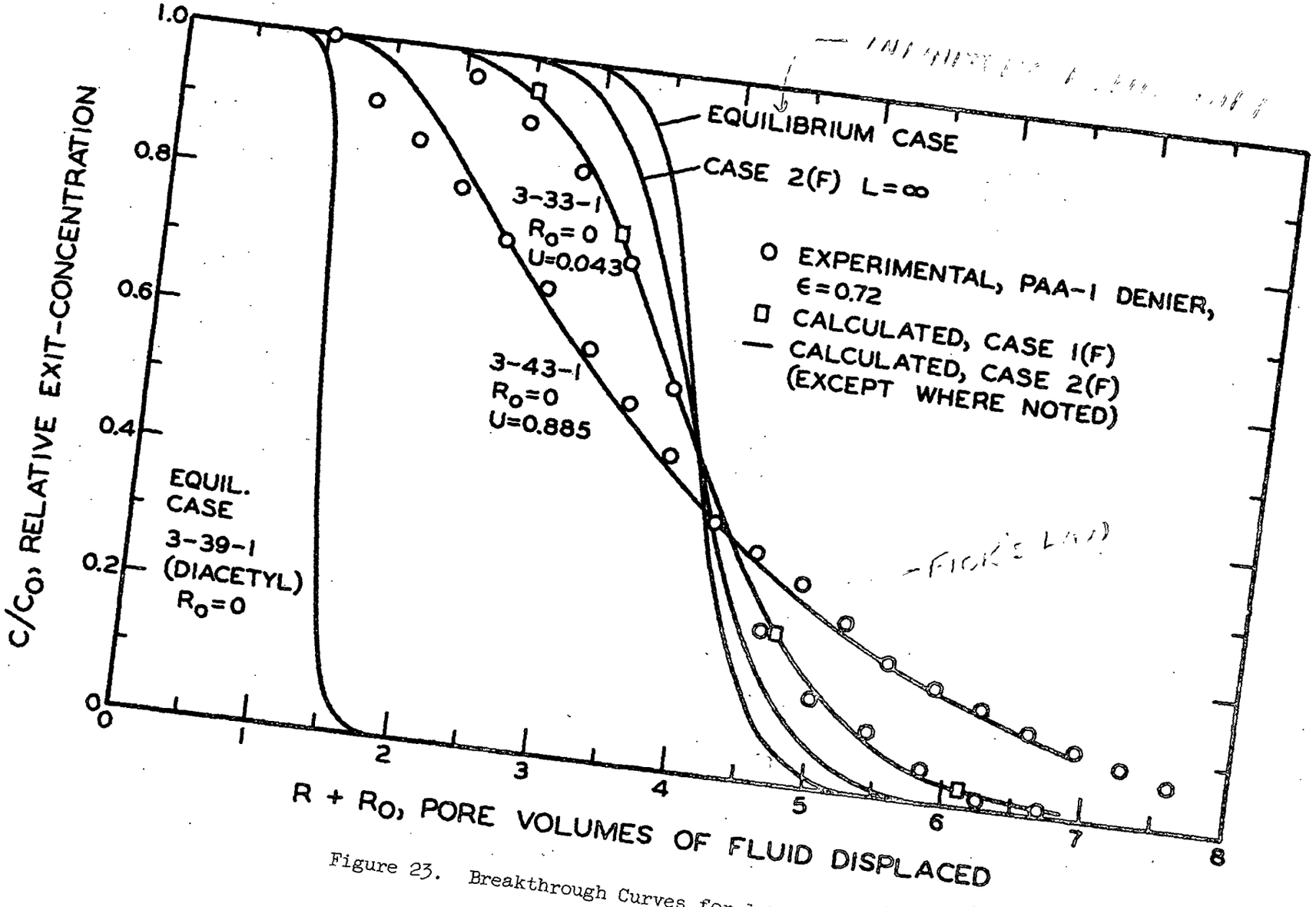

Figure 23. Breakthrough Curves for 1-Denier System

resistance to mass transfer in this case can be attributed to the presence of appreciable intrachannel concentration gradients, which effectively lower the driving force for intrafiber diffusion. The relative importance of this phenomena is illustrated in Run 3-33-1 where the difference between $\underline{L} = 1.5$ and $\underline{L} = \infty$ accounts for much of the displacement from the equilibrium case.

The various runs of the PAA-1 denier system seen in Fig. 24-26 demonstrate that a limited observation of the breakthrough curves can be quite misleading, since they appear to change very little with increasing pore velocity. This effect results from the strong velocity dependence of liquid-phase mass transfer in this system.

The reader will observe that the dual applications of Case 1(F), involving $(\underline{D_F}/\underline{a}^2)_A$, and Case 2(F), involving $\underline{D_F}/\underline{a}^2$ and $\underline{L}$, yielded essentially identical breakthrough curves. Thus, neither case had a predictive advantage.

The reader will further note that the illustrated breakthrough curves represent the results of this study in their most basic form. Alternative hypotheses of interparameter relationships, and more sophisticated mathematical models, should be tested first against these experimental *vs.* calculated breakthrough curves.

WASHING RUNS ON 4-DENIER SYSTEMS

Diacetyl was used to estimate $\underline{D_L}/\underline{U}$ at all three porosity levels in the 4-denier system; these runs are shown in Fig. 27-29. It is seen that the curves broadened slightly as $\underline{U}$ increased, suggesting that mass transport phenomena were beginning to become important. The application of Case 1(F) provided an important check on the magnitude of this effect in the determinations.

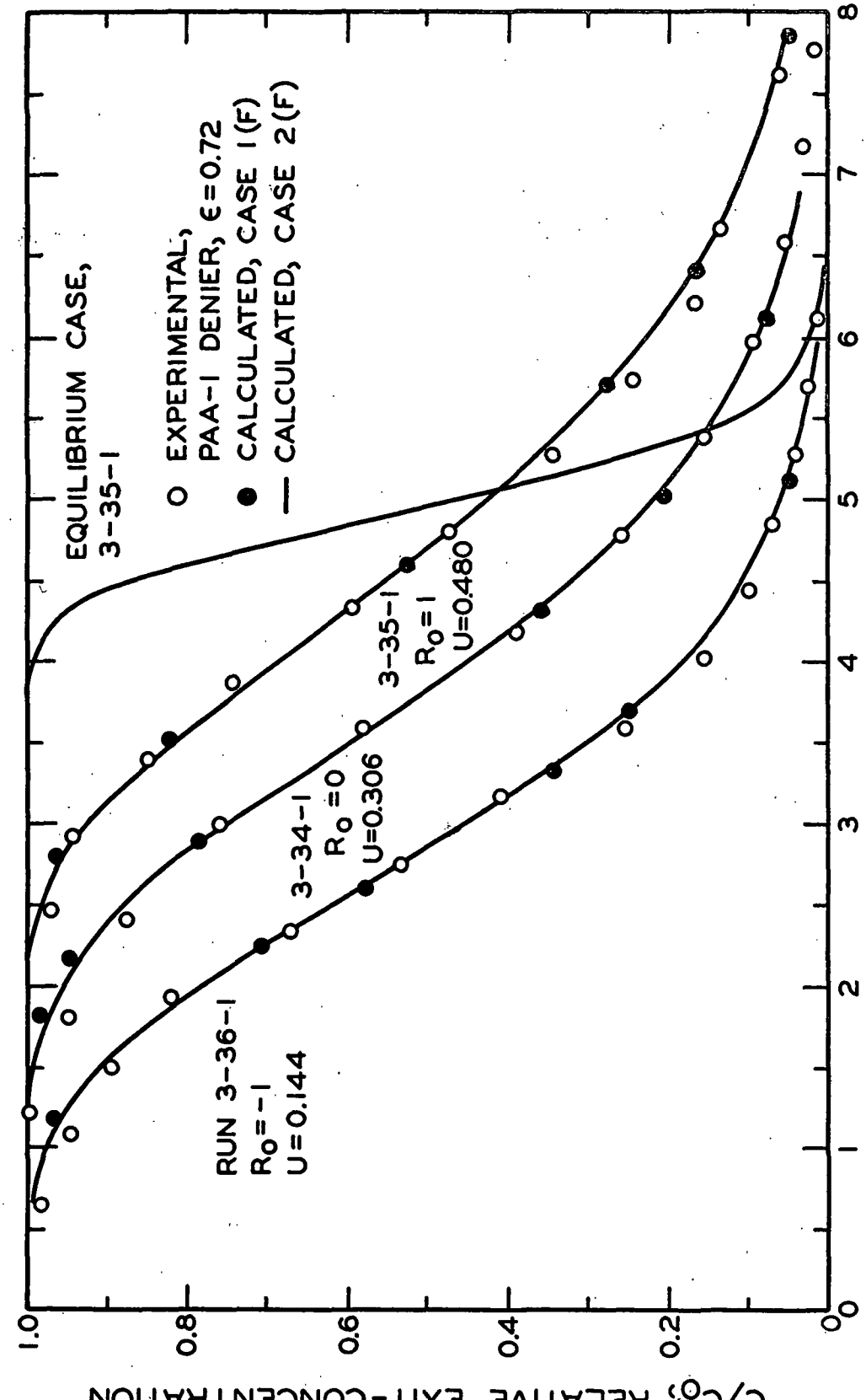

Figure 24. Breakthrough Curves for 1-Denier System

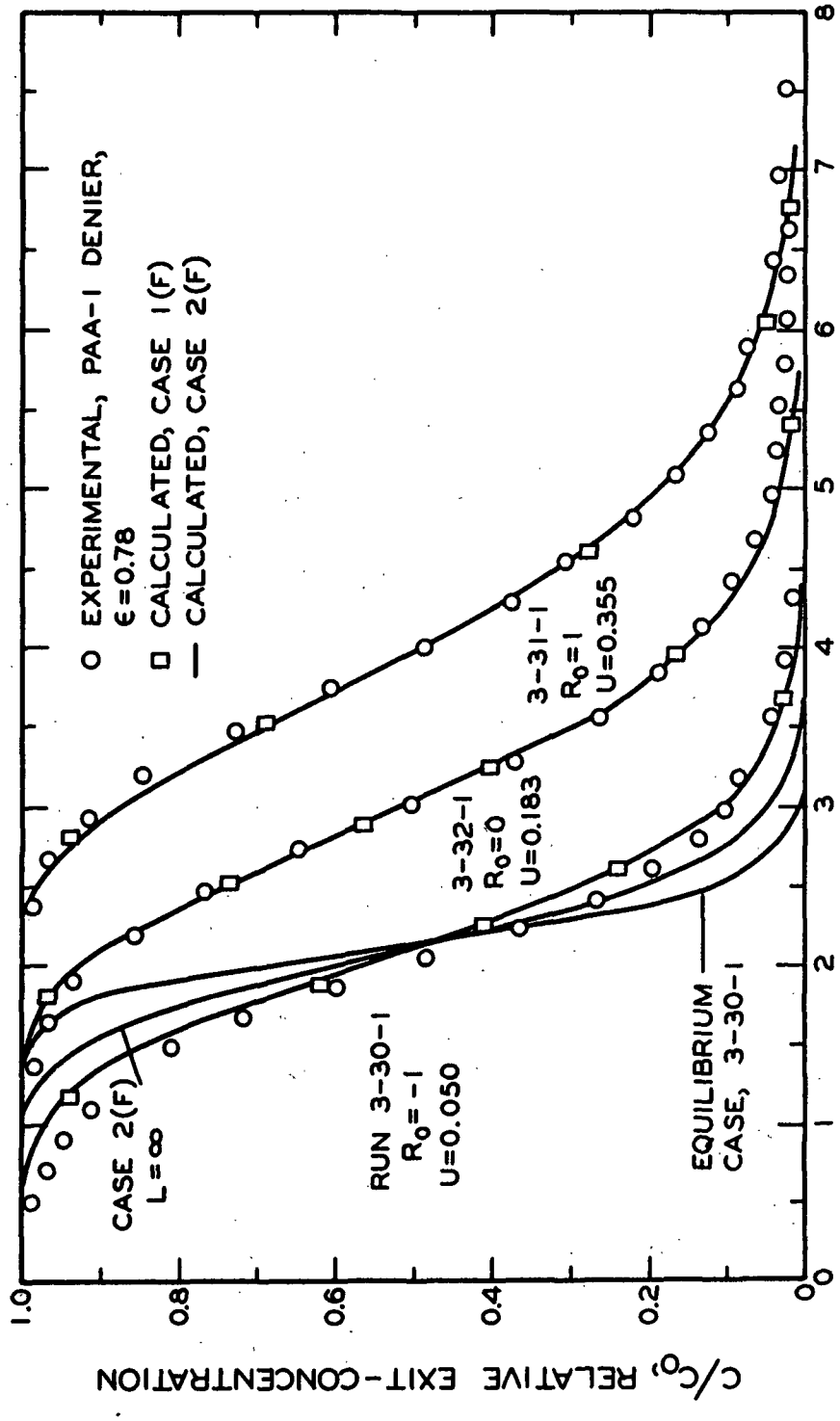

Figure 25. Breakthrough Curves for 1-Denier System

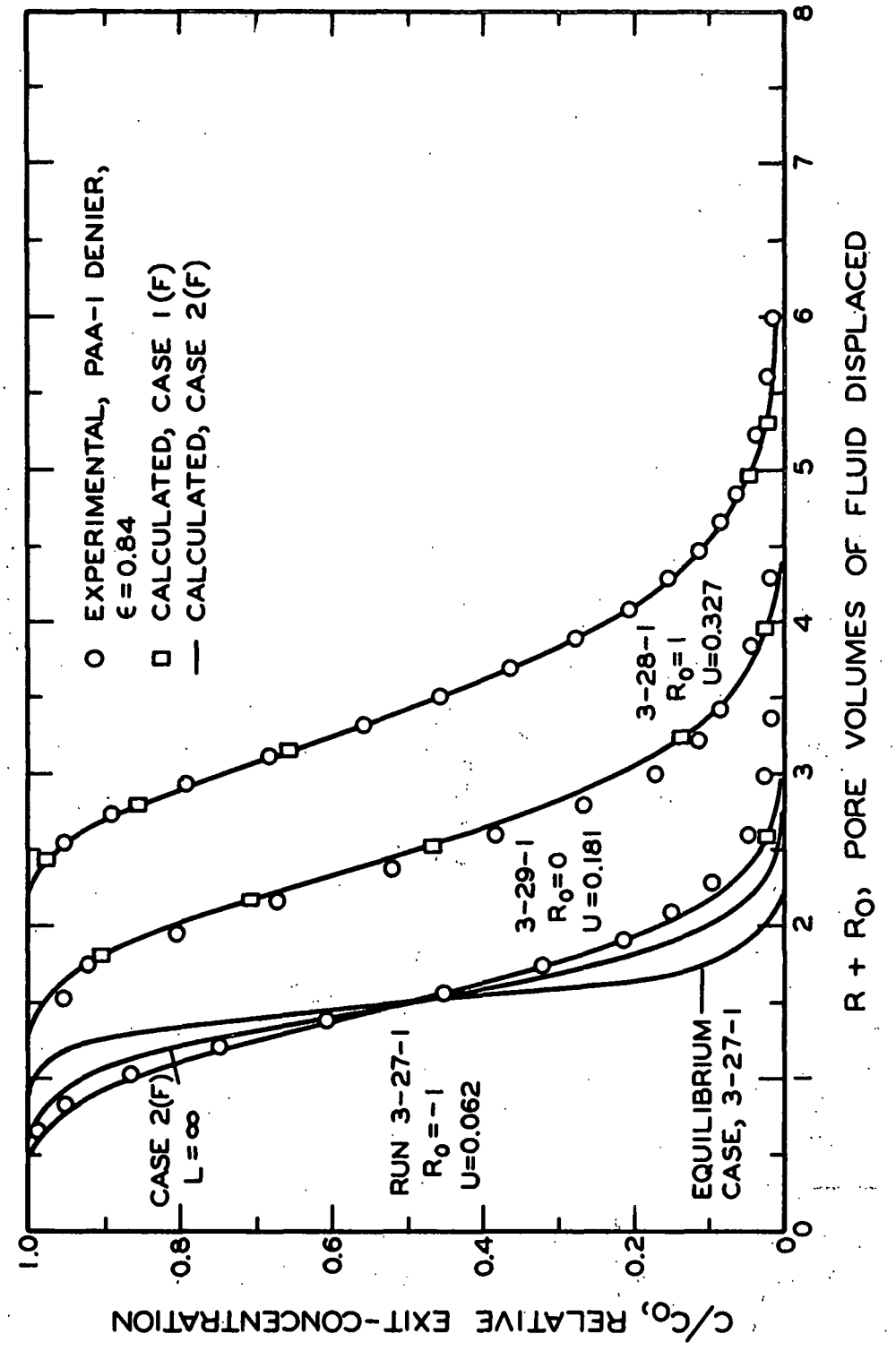

Figure 26. Breakthrough Curves for 1-Denier System

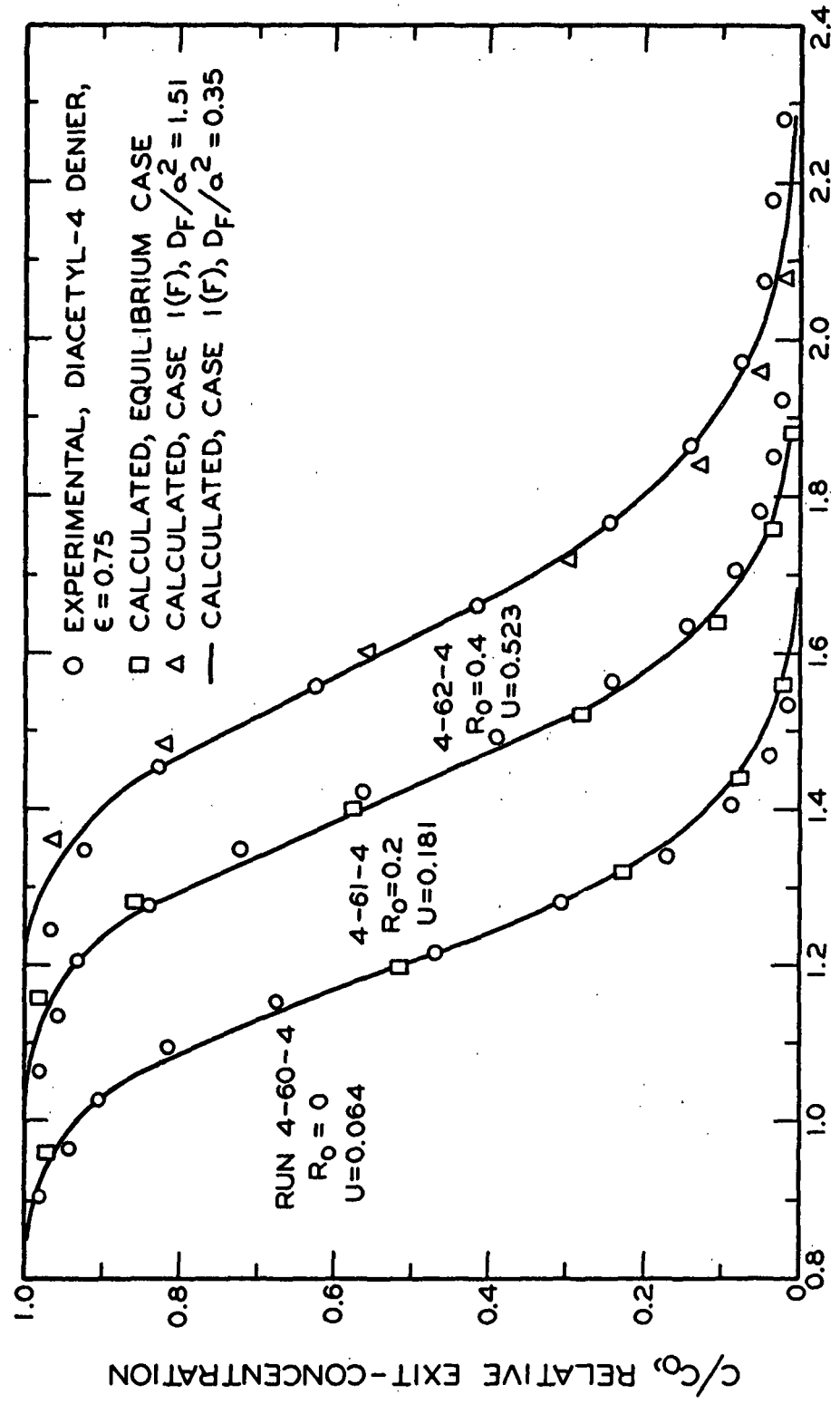

Figure 27. Breakthrough Curves for Determination of Mixing Parameter

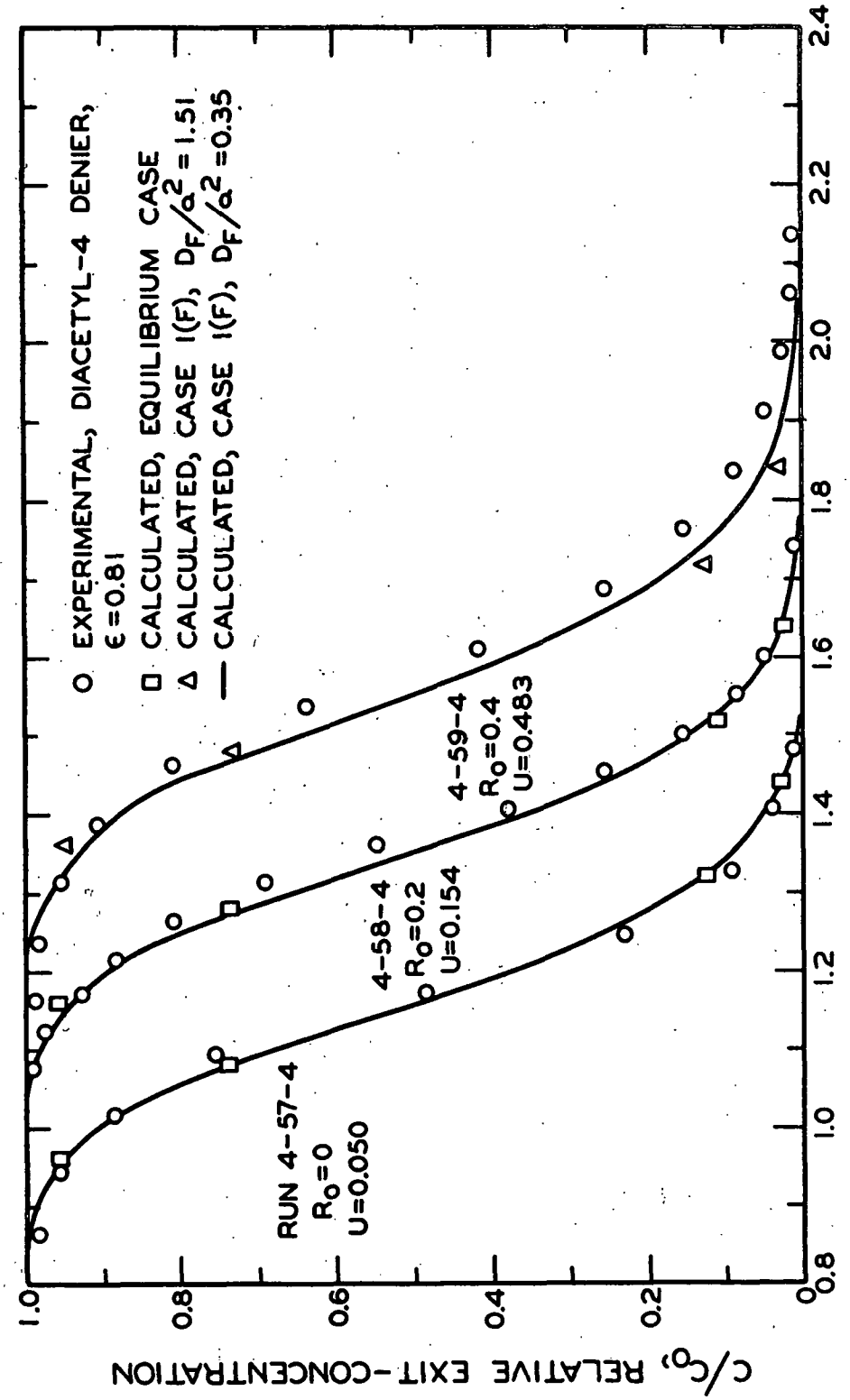

Figure 28. Breakthrough Curves for Determination of Mixing Parameter

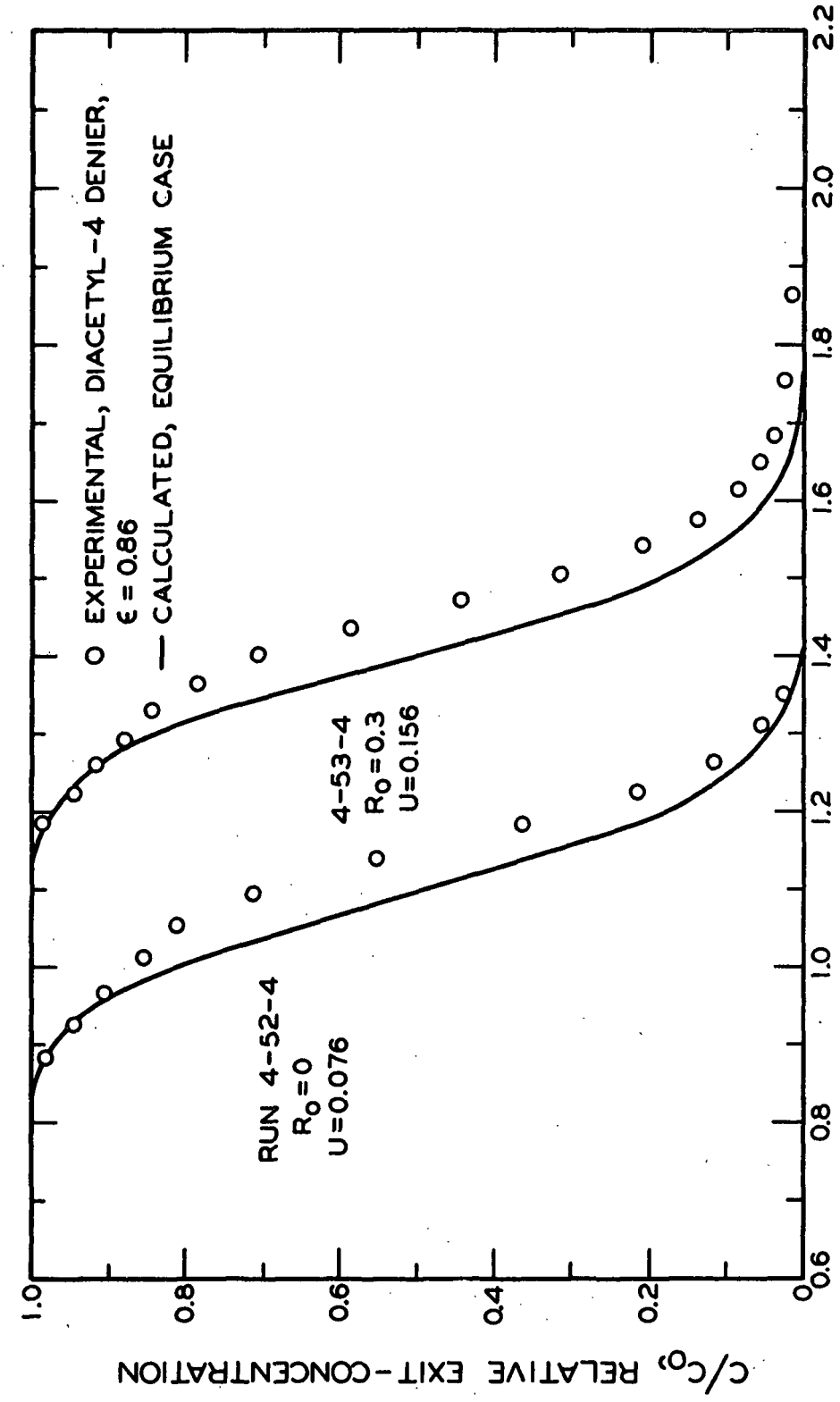

Figure 29. Breakthrough Curves for Determination of Mixing Parameter

Figure 30 illustrates the lowest and highest velocity runs in the PAA-4 denier system, at the lowest porosity level. These represent the extreme mass transport conditions that were observed in this system. Figures 31-34 exhibit many of the same types of comparisons that were made in the 1-denier system.

WASHING RUNS ON 16-DENIER SYSTEMS

Figure 35 illustrates the three BPP-16 denier viscose runs that were used to evaluate $\underline{D_L}/\underline{U}$ at $\epsilon = 0.76$. The latter portions of the breakthrough curves are seen to exhibit the effects of solute exchange from the fibers. Thus, only about the first two thirds of the curves were considered in determining $\underline{D_L}/\underline{U}$. The value obtained should be equal to, or greater than, a hypothetical value on an equivalent system of nonporous fibers.

Figure 36 illustrates the extreme mass transfer conditions that were observed in the PAA-16 denier system, on Bed 1-16. Figure 37 illustrates runs at intermediate pore velocities. It is apparent that the discrepancies between experimental and predicted breakthrough curves follow a consistent pattern, which has no obvious explanation at this point.

Figures 38-40 illustrate the washing runs that were performed in the PAA-16 denier system, on Bed 2-16, at four porosity levels. The mixing parameter was assumed to be independent of ϵ, and was assigned the previously determined value from Bed 1-16. It will be demonstrated later that the assumption of $\underline{D_L}/\underline{U}$ being constant with changes in ϵ may not have been an especially good one in the 16-denier system, but it is functional in the respect that it serves as a base line.

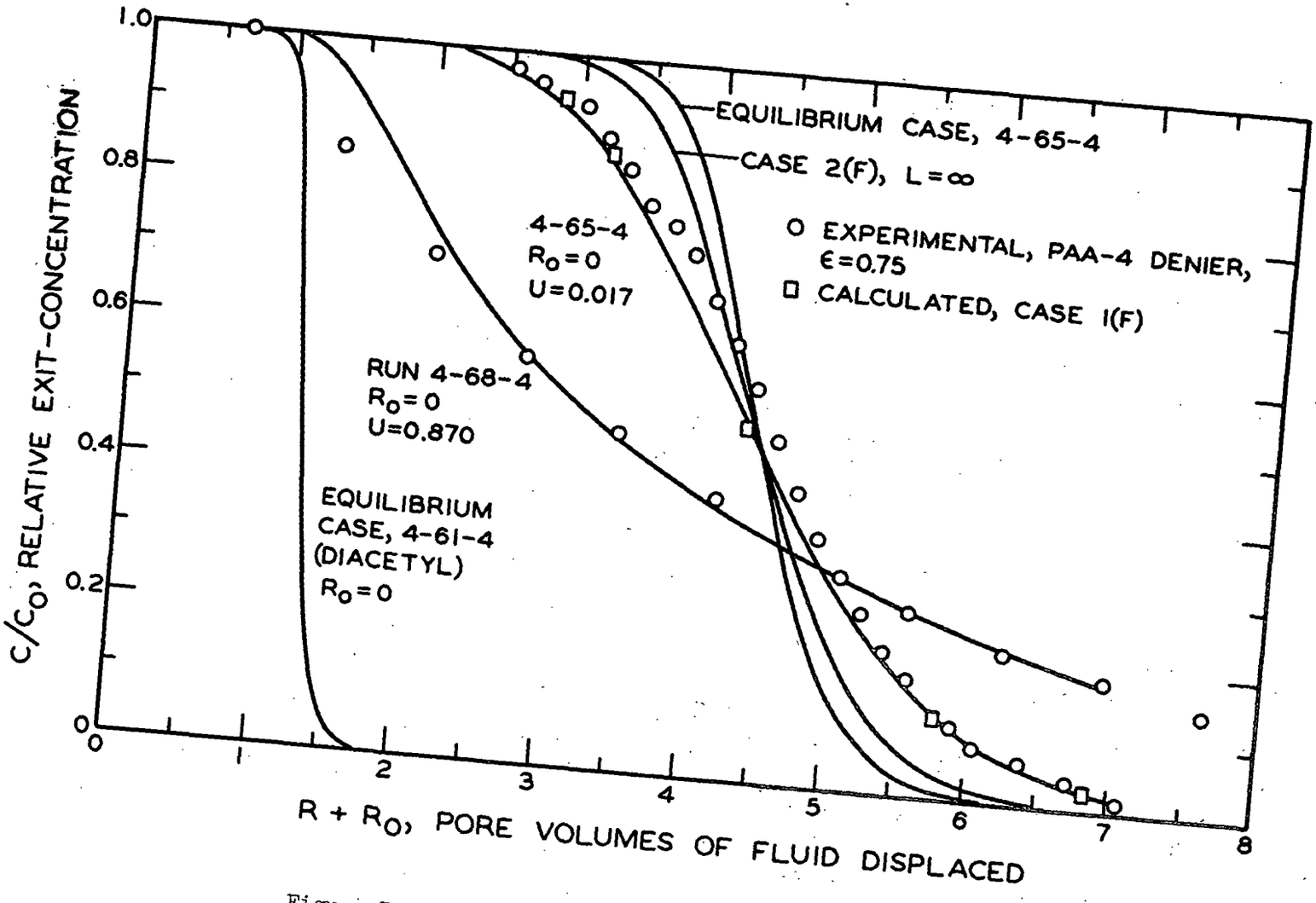

Figure 30. Breakthrough Curves for PAA-4 Denier System

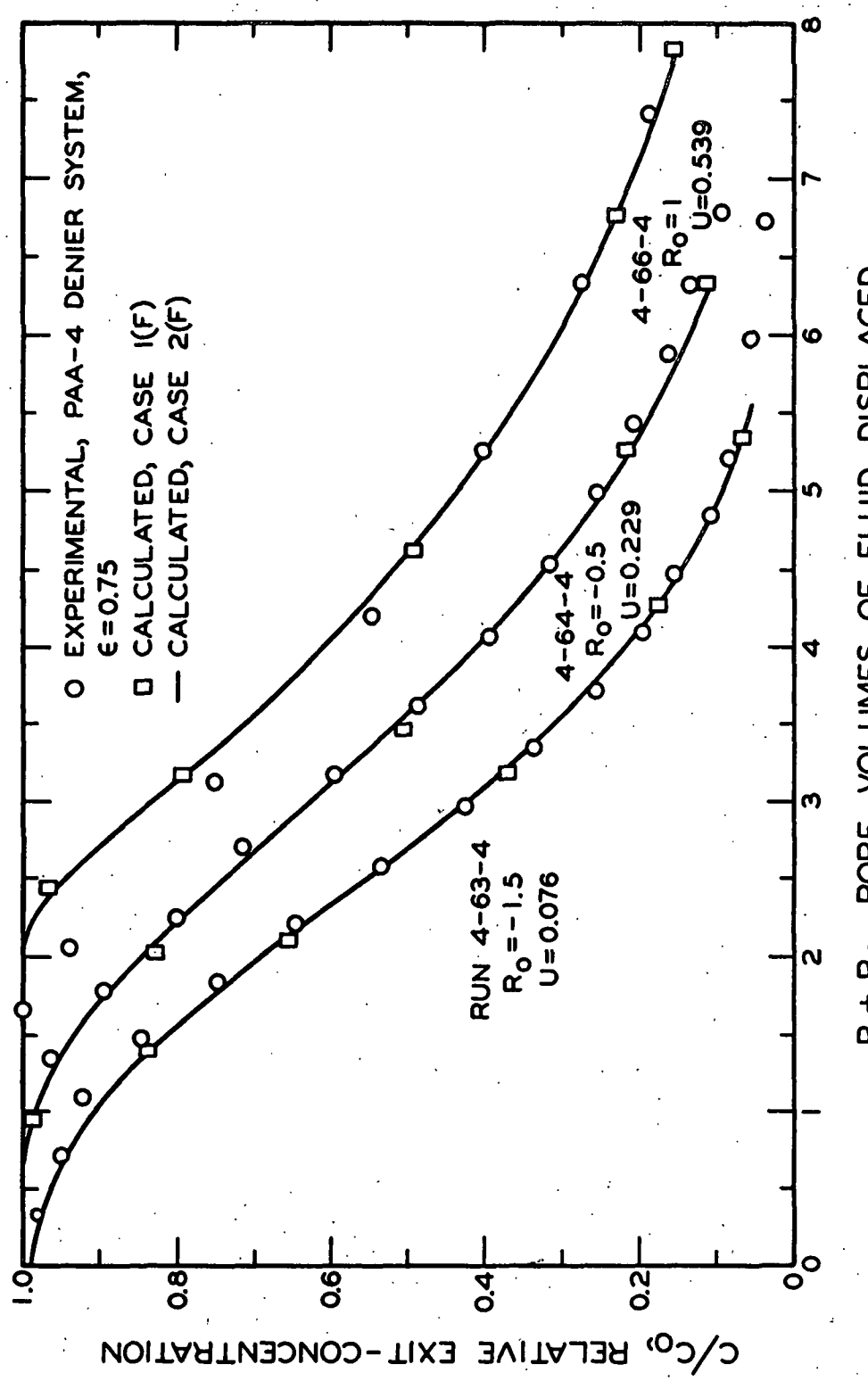

Figure 31. Breakthrough Curves for PAA-4 Denier System

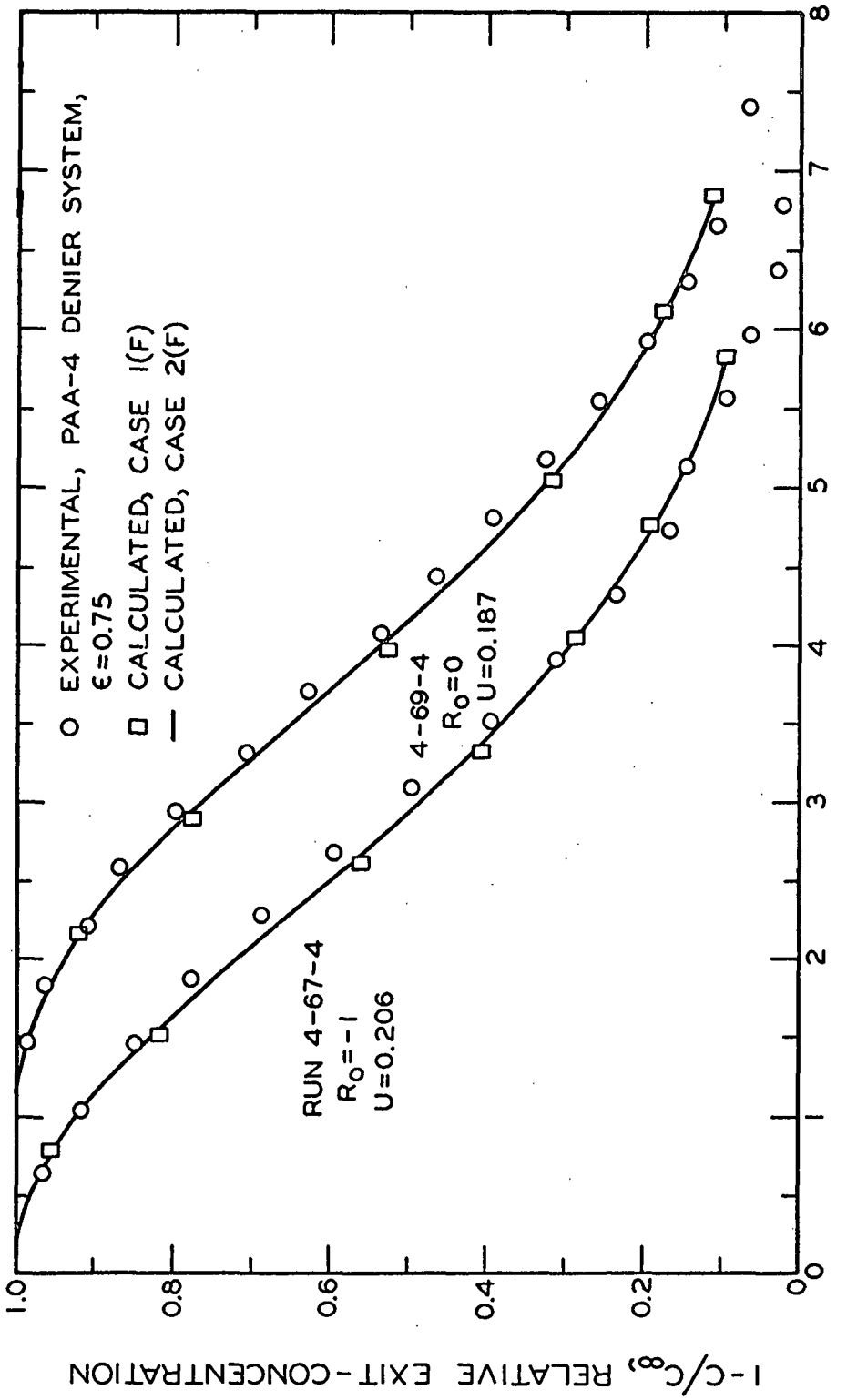

Figure 32. Breakthrough Curves for Sorption Washing Runs on PAA-4 Denier System

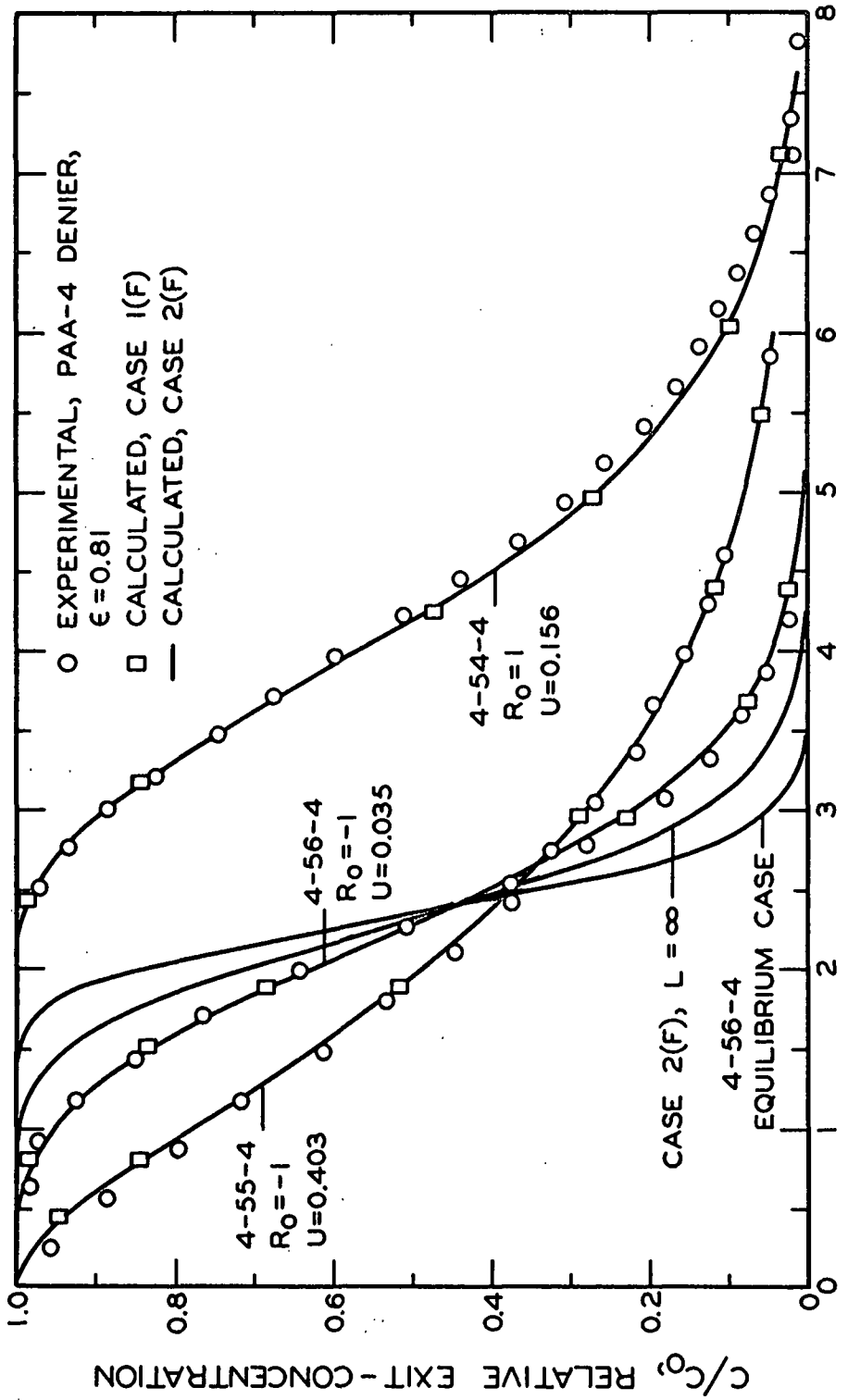

Figure 33. Breakthrough Curves for PAA-4 Denier System

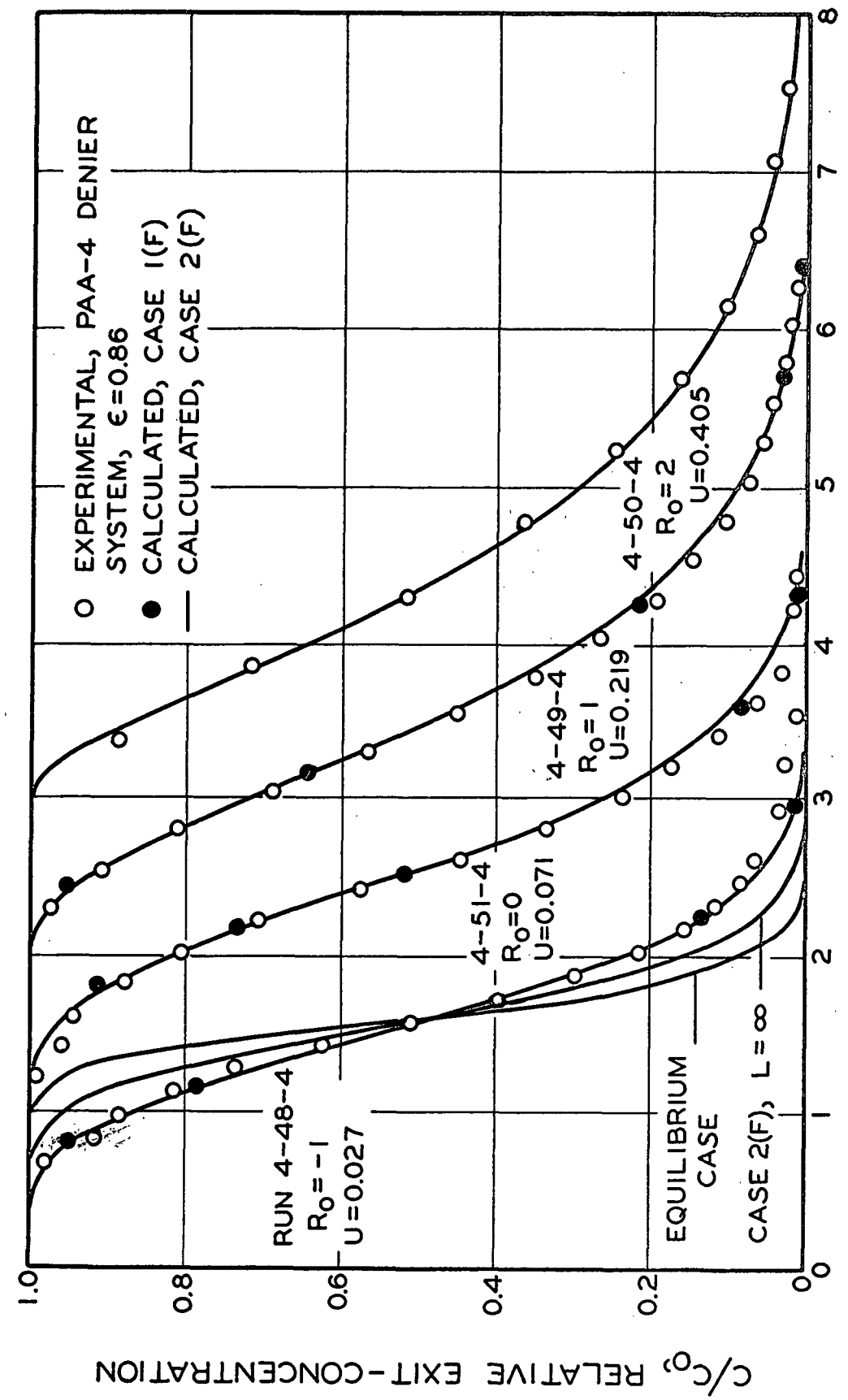

Figure 34. Breakthrough Curves for PAA-4 Denier System

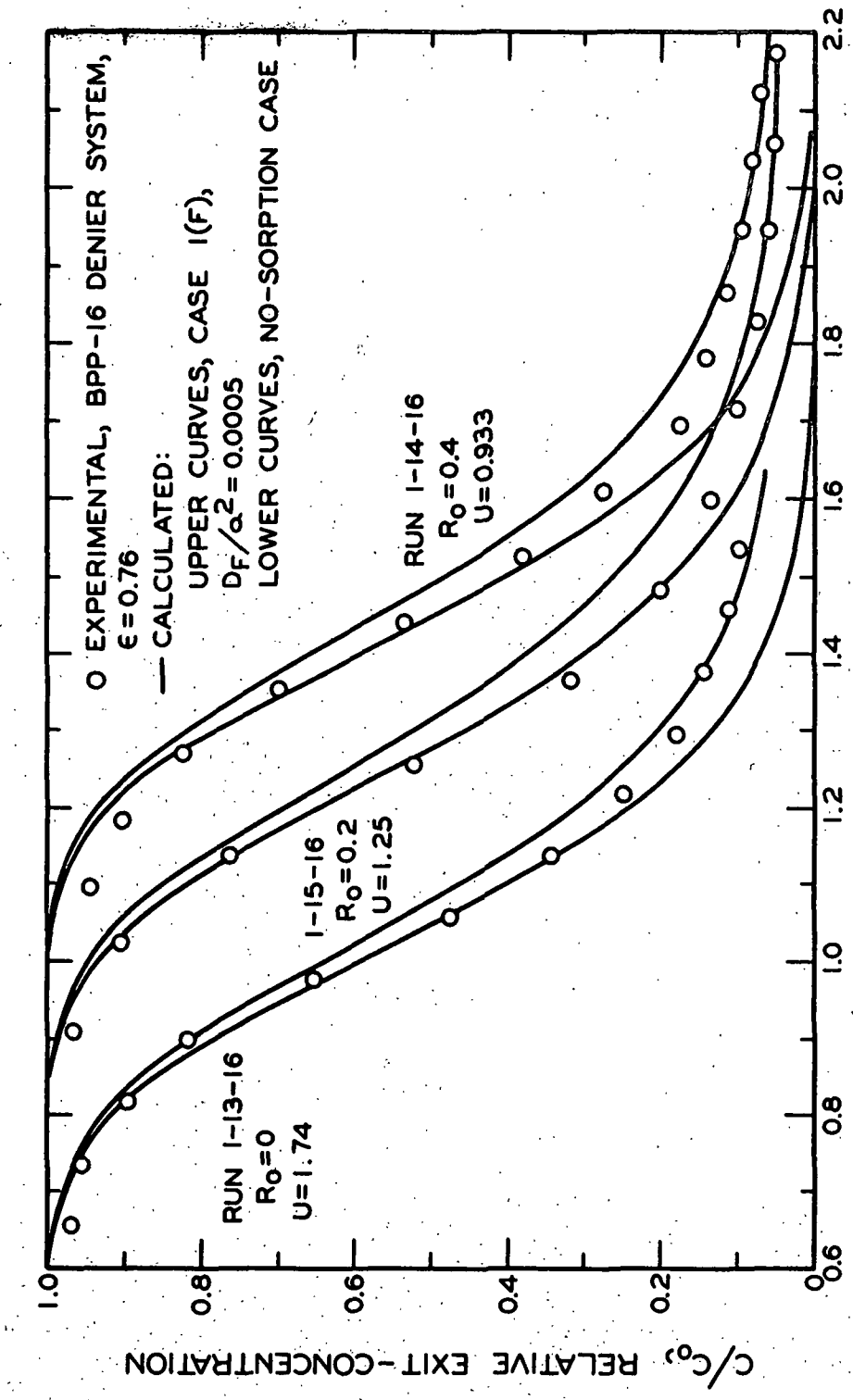

Figure 35. Breakthrough Curves for Determination of Mixing Parameter in 16-Denier System

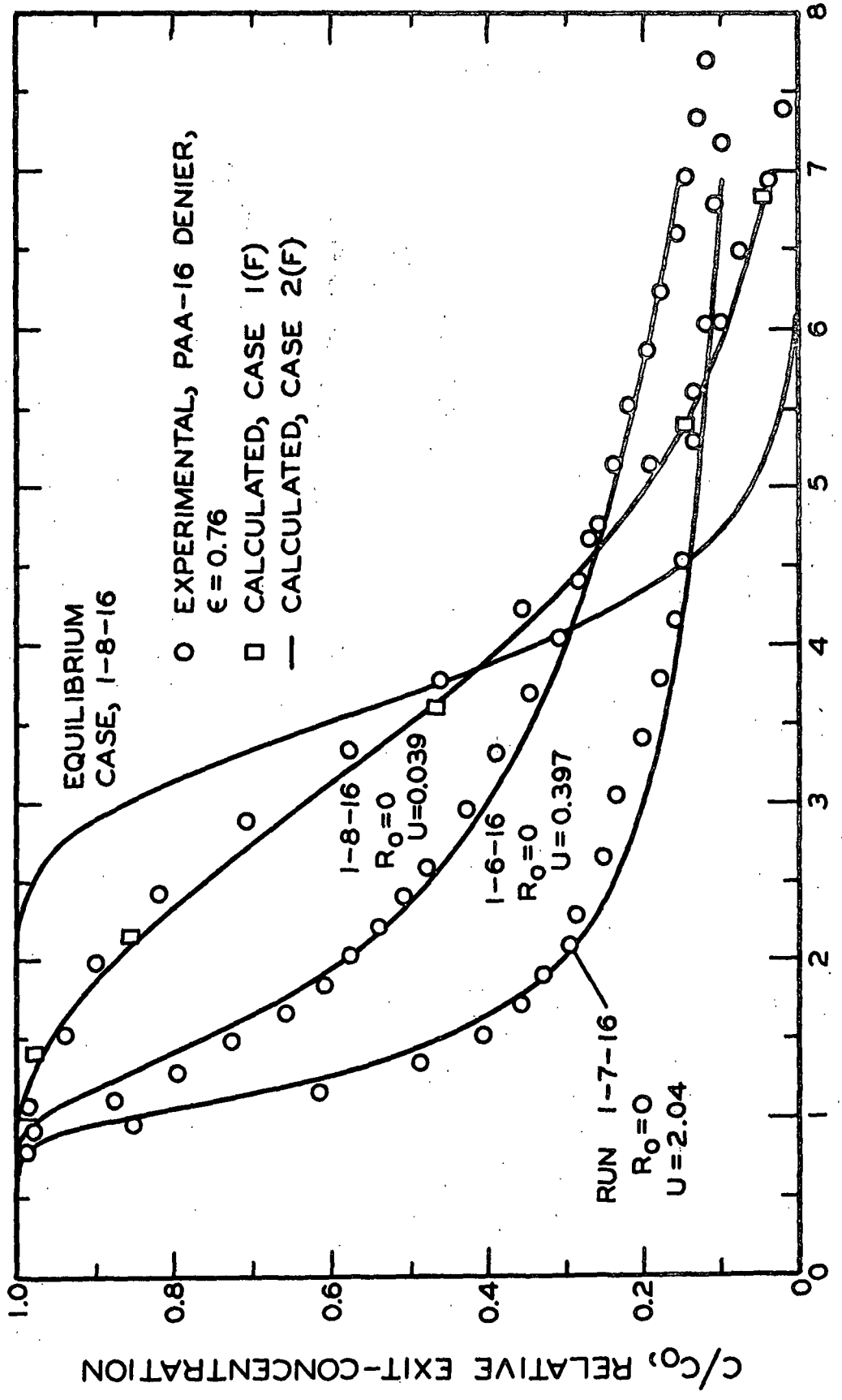

Figure 36. Breakthrough Curves for PAA-16 Denier System

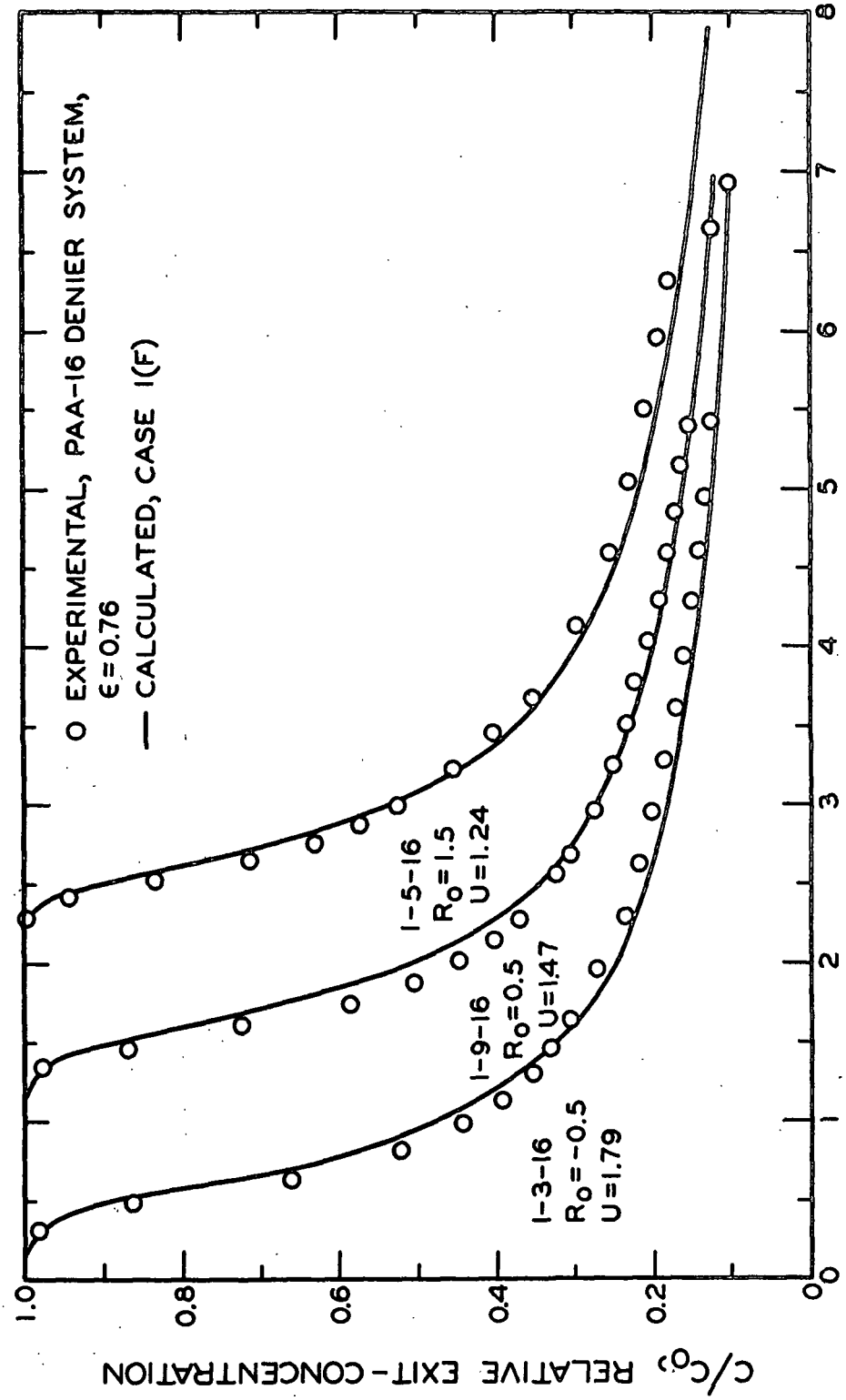

Figure 37. Breakthrough Curves for PAA-16 Denier System

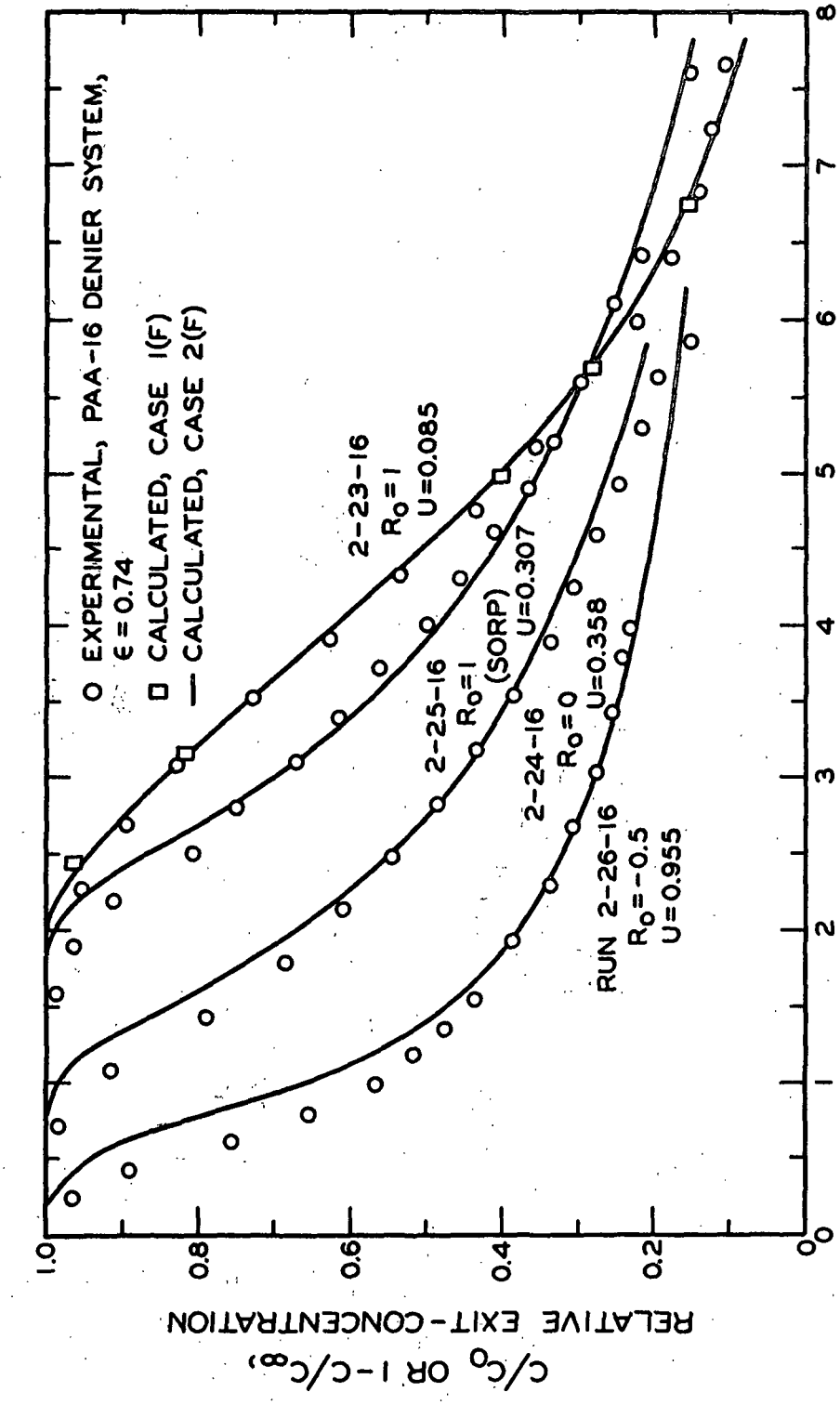

Figure 38. Breakthrough Curves for PAA-16 Denier System

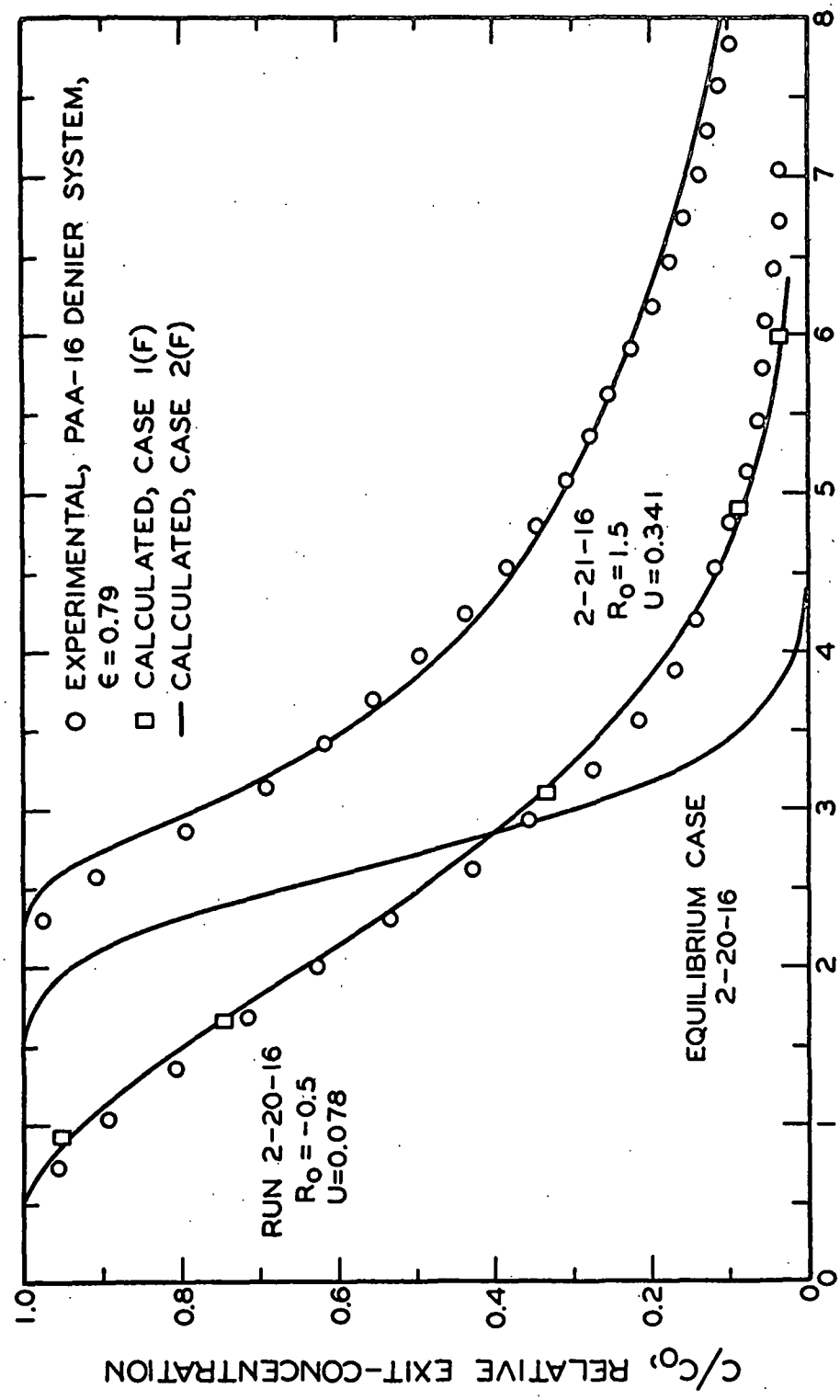

Figure 39. Breakthrough Curves for PAA-16 Denier System

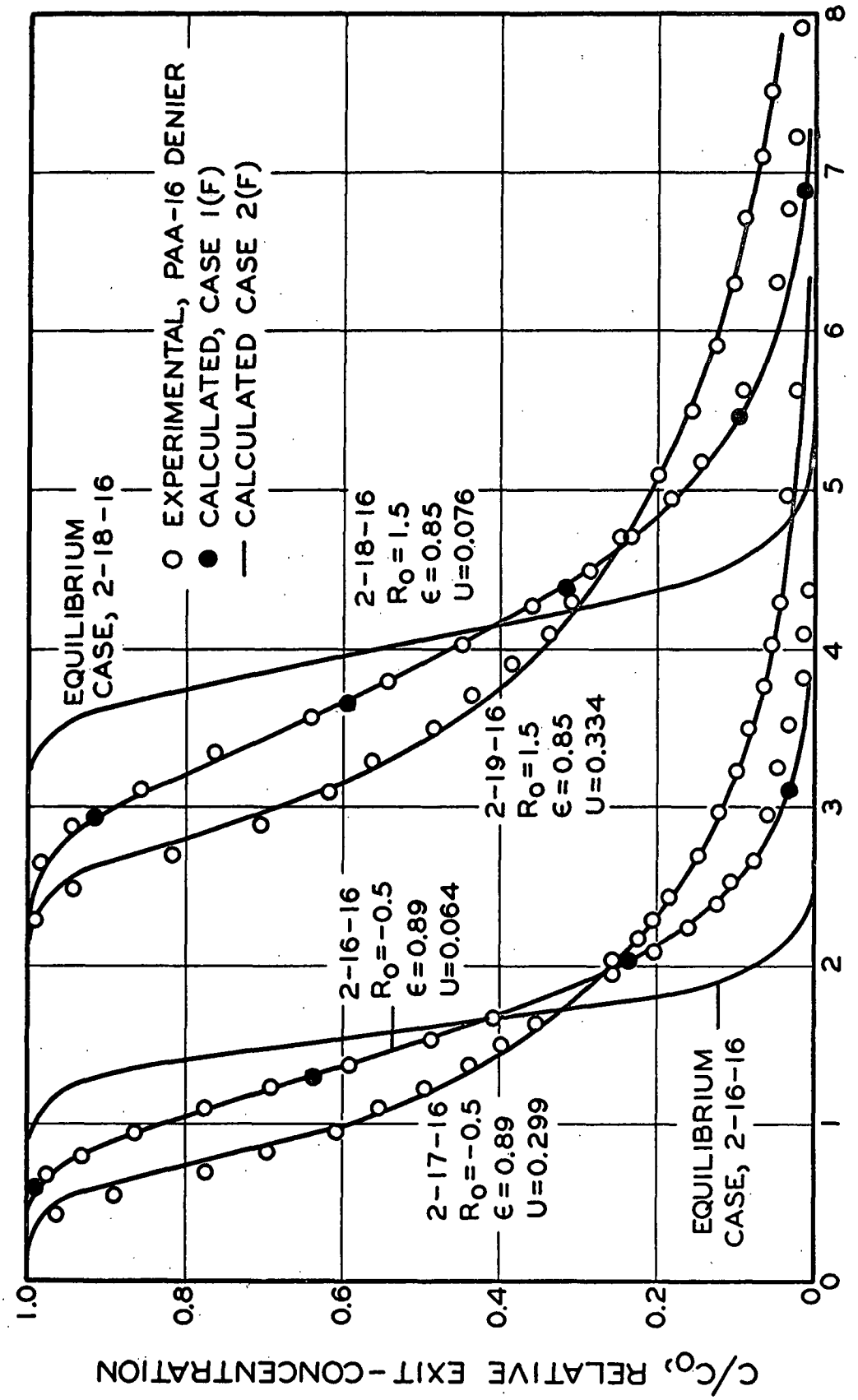

Figure 40. Breakthrough Curves for PAA-16 Denier System

ANALYSIS OF SHERMAN'S WASHING RUNS ON DIACETYL-1 AND 64-DENIER SYSTEMS

A number of washing runs that Sherman performed on the diacetyl-1 and 64-denier systems (1) were reanalyzed by this writer in terms of the Equilibrium case and Cases 1(F) and 2(F). Table XXI summarizes the run conditions and the results that were obtained. Figure 41 illustrates two breakthrough curves for the diacetyl-1 denier system. A third curve, calculated for Run 3-39-1 of this study, is shown for purposes of comparison. It is apparent that the results differed considerably for these two beds. This observation will be discussed later, as it reflects on the effects of bed structure on D_L/U.

Figures 42 and 43 illustrate the analyses of four washing runs that Sherman performed on the diacetyl-64 denier system. The apparent broadening of the breakthrough curves, as U was increased, indicated that solute transport was not effectively described by the assumption of an equilibrium condition. The analyses revealed that both intrafiber diffusion and liquid-phase mass transfer effects were important in this system.

WASHING RUNS ON BPP-1 DENIER SYSTEM

A limited number of washing runs were performed on the BPP-1 denier system. Here it was found difficult to bring the bed to an apparent equilibrium condition, despite saturation times of about 12 and 30 minutes in two attempted runs. In both cases the initial solute values (immediately after bed saturation) increased slowly at the inlet and exit, as the equipment was readied. A sorption run (3-47-1) was later performed after passing large quantities of wash water through the bed at intermittent intervals, over a period of several hours. Here the exit solute value (representing water) remained unchanged until the breakthrough of BPP was observed. Figure 44 illustrates the analysis of this run. The value of K used was evaluated from the area under the breakthrough curve.

TABLE XXI

SUMMARY OF RUN CONDITIONS AND WASHING PARAMETERS FOR ANALYSIS OF SHERMAN'S DATA

Run	Description	Denier	$\underline{Z}_e$, ($\underline{Z}_E$)	ϵ, (ϵ_E)	$\underline{U}$	$\underline{D}_L/\underline{U}$	$\underline{k}_L \times 10^4$	$\underline{D}_L/\underline{UZ}_E \times 10^3$	$\underline{K}$	$\underline{U}/\underline{Z}_E \times 10^2$	$\left(\frac{\underline{D}_F}{\underline{a}^2}\right)_A$	$\frac{\underline{ak}_L}{\underline{D}'_F}$ [a]
11-5	D,diacetyl	1	2.63 (3.05)	0.817 (0.835)	0.080	0.099	--	32.5	0.618	2.62	--	--
11-3	"	1	"	"	0.329	"	--	"	"	10.8	--	--
13-8	D-diacetyl	64	5.06 (5.39)	0.805 (0.814)	0.042	0.0512	2.47	9.5	0.618	0.780	0.009	0.45
13-2	"	64	"	"	0.154	"	7.14	"	"	2.86	0.018	1.3
13-5	"	64	"	"	0.636	"	65.9	"	"	11.8	0.065	12.0
13-6	"	64	"	"	1.316	"	330.0	"	"	24.4	0.085	60.0

[a] Based on $\underline{D}_F/\underline{a}^2 = 0.090$.

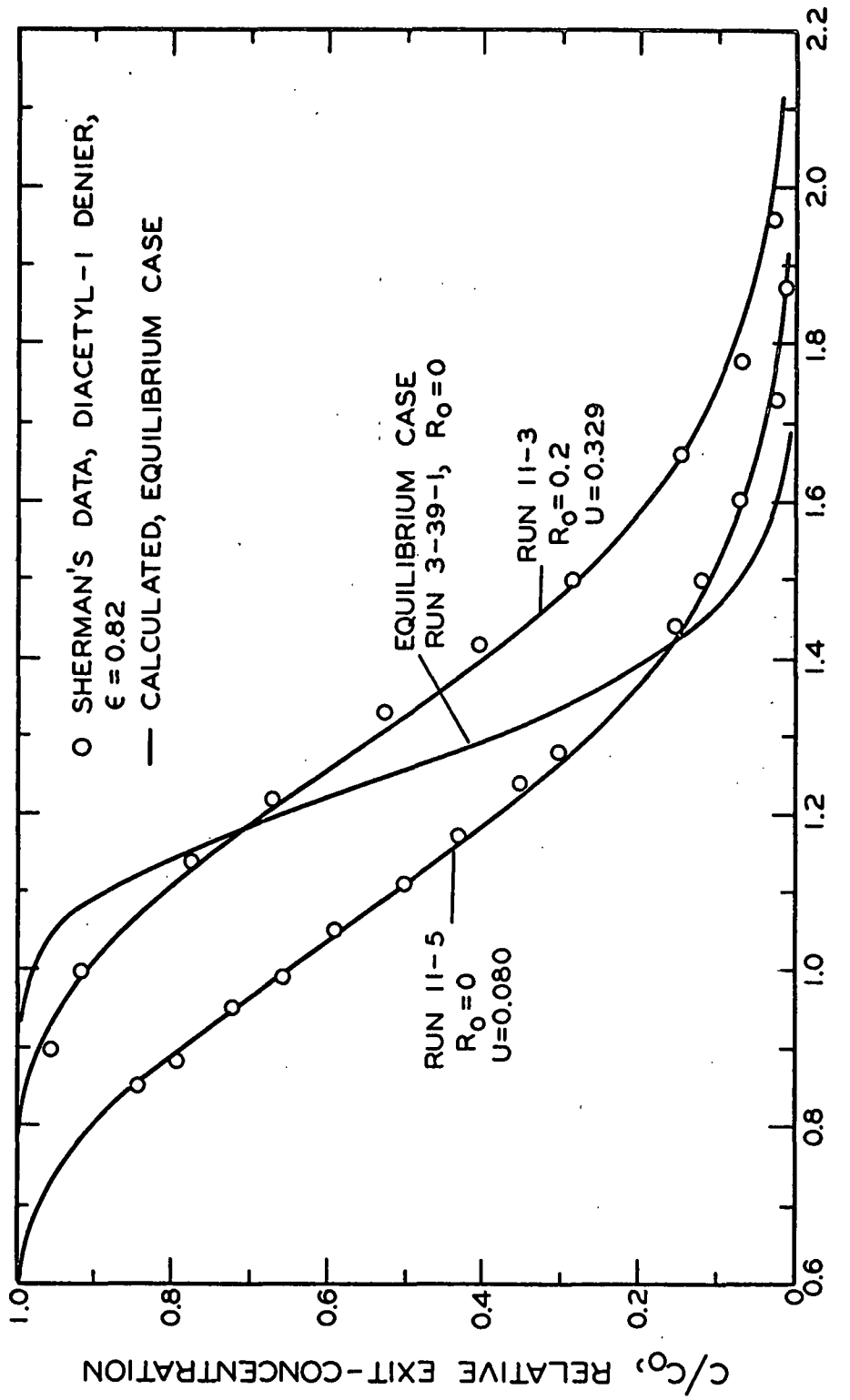

Figure 41. Analysis of Sherman's Data on the Diacetyl-1 Denier System

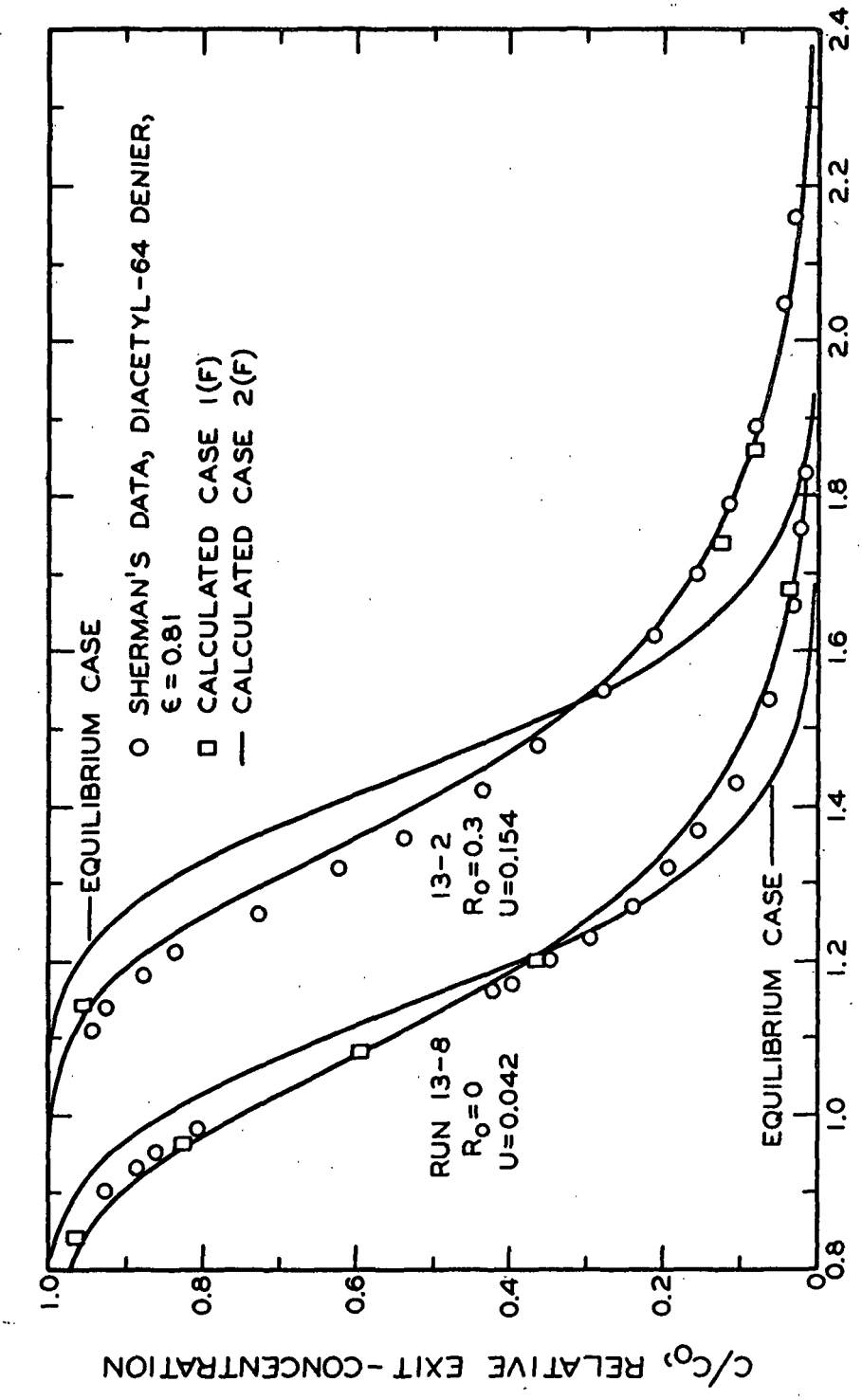

Figure 42. Analysis of Sherman's Data on the Diacetyl-64 Denier System

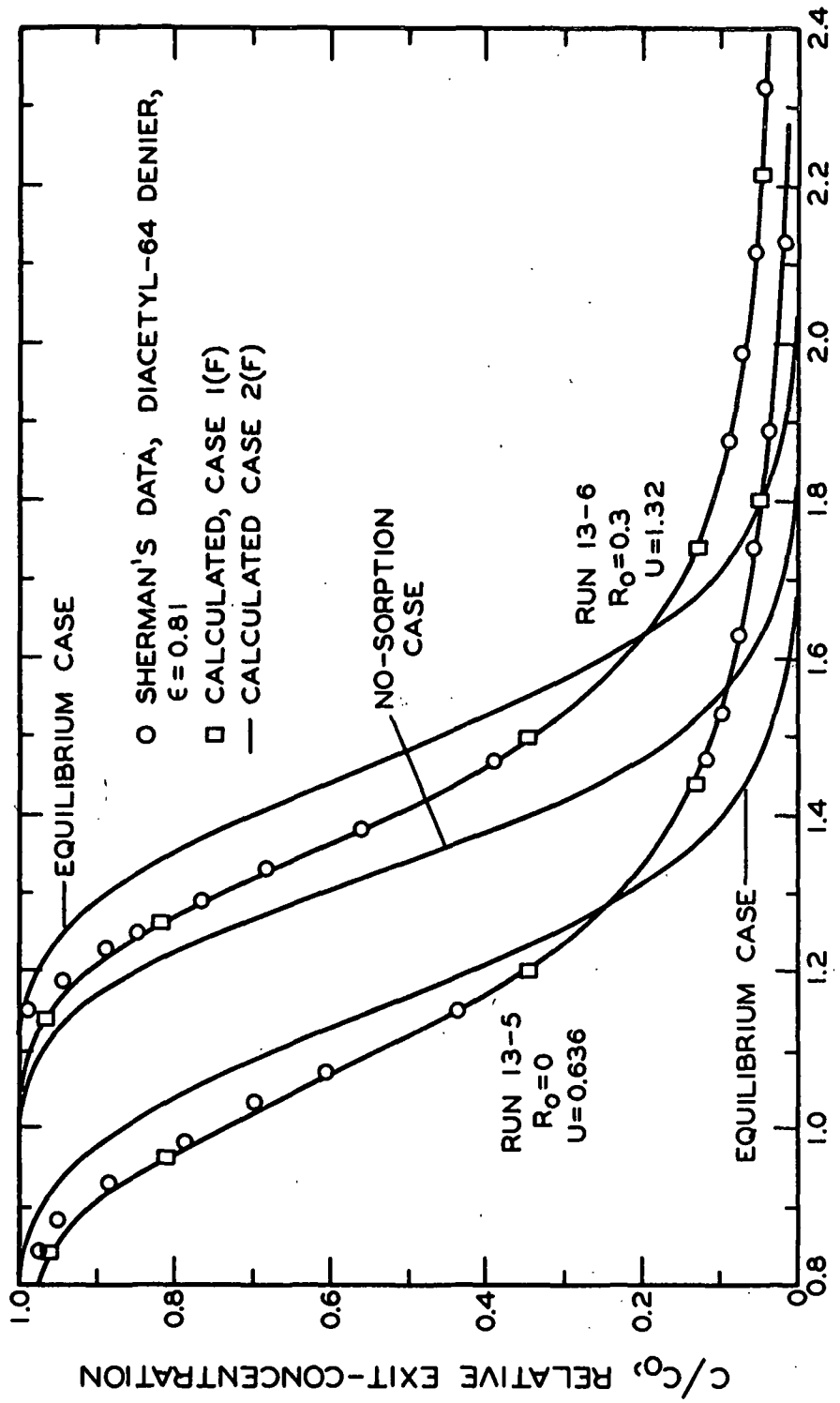

Figure 43. Analysis of Sherman's Data on the Diacetyl-64 Denier System

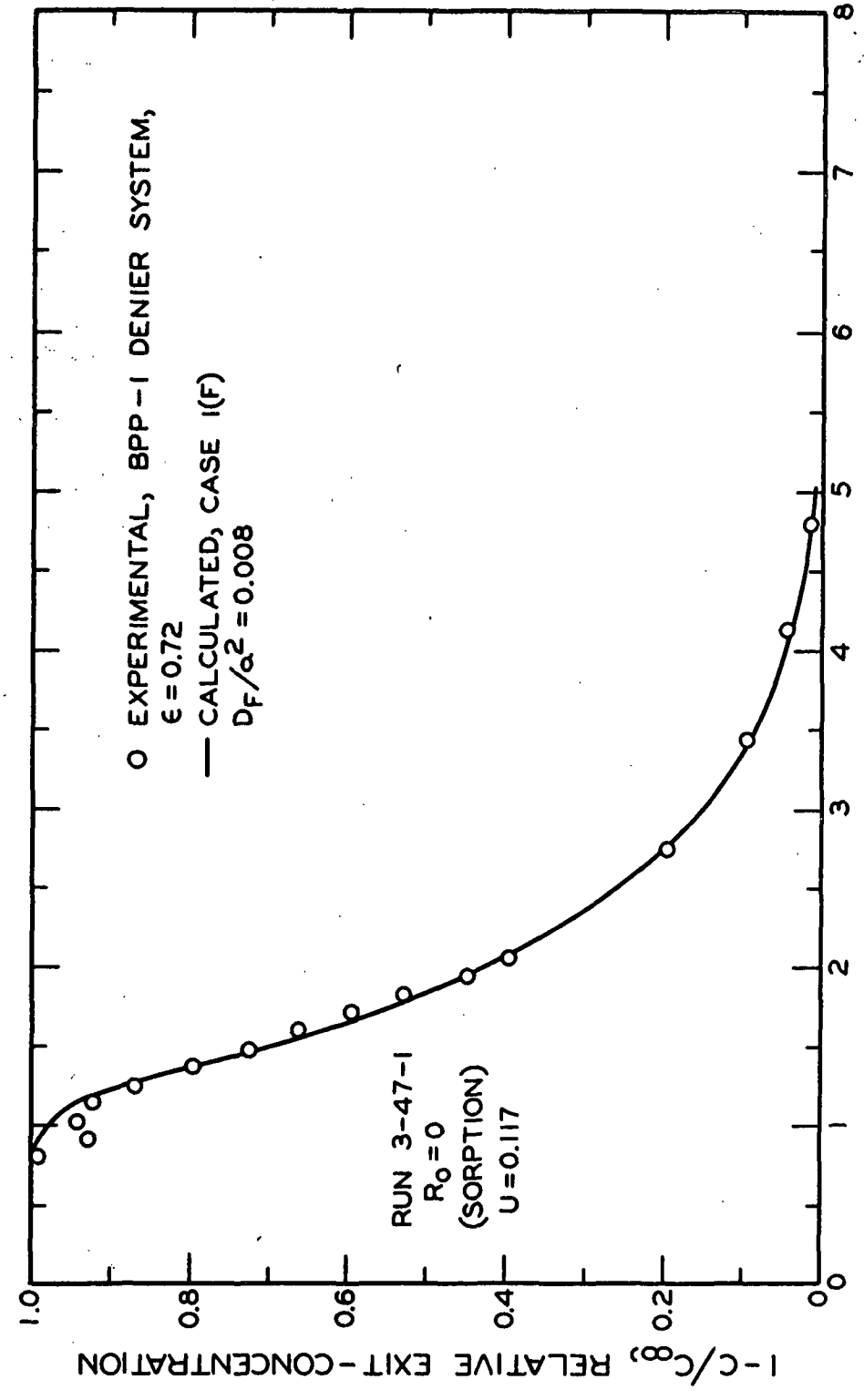

Figure 44. Breakthrough Curve for BPP-1 Denier System

RESULTS AND DISCUSSION

EXPERIMENTALLY DETERMINED LONGITUDINAL DISPERSION PROPERTIES

Table XXII summarizes the experimentally determined mixing parameters and the various geometrical parameters that characterize the fiber beds. The ℓ'/d values are the length-to-diameter ratios of the fibers. The a_c values represent the equivalent capillary radii, calculated as twice the hydraulic radius by $a_c = d\epsilon/2(1 - \epsilon)$. The indicated porosities represent the conditions under which the D_L/U values were determined, and not any other porosity levels where the same values may have been employed in the analysis. Although a limited amount of evidence indicated that D_L/U tended to increase slightly with U, the listed D_L/U values were considered to be effectively constant over the experimental velocity ranges.

The D_L/U values in parentheses represent Sherman's results in the dacron systems, and this author's analysis of Sherman's data in the viscose systems. His fiber lengths in the 3-denier dacron system were 1/4 inch; in the 1 and 64-denier viscose systems they were estimated to be 1/4 inch, but these should be considered close to the actual values.

In many of the succeeding discussions, the concept of a fluid element will be used. This concept is mathematically defined as a macroscopic quantity of fluid which is small enough to retain its identity during the course of an experimental observation. Although it is more correct to think of molecular distributions of solute molecules in solution, it is more convenient, when discussing dispersion effects in porous media, to consider the movement of fluid elements that contain solute at different concentrations.

TABLE XXII

LONGITUDINAL DISPERSION PROPERTIES AND BED CHARACTERISTICS

Denier	System	d, μ	ℓ'/d	Z_e, cm.	ϵ	a_c, μ	D_L/U, cm.	D_L/Ud
1	Diacetyl-viscose	15.91	121.0	4.67	0.7158	20.1	0.0309	19.4
1	Diacetyl-viscose	15.91	400.0	3.05	0.817	35.5	(0.0993)	62.4
4	Diacetyl-viscose	29.89	95.3	4.63	0.7460	43.9	0.0351	11.7
4	Diacetyl-viscose	29.89	95.3	6.06	0.8059	62.1	0.0388	13.0
4	Diacetyl-viscose	29.89	95.3	8.29	0.8598	91.8	0.0443	14.9
16	BPP-viscose	60.35	93.5	4.06	0.7636	97.6	0.080	13.3
64	Diacetyl-viscose	122.1	52.0	5.39	0.805	252.0	(0.0512)	4.20
3	Diacetyl-dacron	17.0	374.0	5.32	0.815	37.5	(0.0765)	45.0
3	Diacetyl-dacron	17.0	374.0	5.29	0.885	65.4	(0.132)	77.7
3	Diacetyl-dacron	17.0	374.0	5.29	0.916	92.8	(0.0470)[a]	27.7
3	Diacetyl-glass spheres	3020.0	1.0				(0.233)	0.772

[a] M_w was considerably smaller than unity in this series of runs.

FACTORS CAUSING LONGITUDINAL DISPERSION

The occurrence of longitudinal dispersion, during flow through porous media, can be roughly attributed to (a) differences in pore channel size, (b) differences in channel orientation, (c) radial velocity variations within channels, (d) channel shape variations, (e) interconnection of pore channels, and (f) molecular diffusion effects. The contributions of the first three factors can be simply illustrated if we first consider fully developed Poiseuille flow in a circular capillary, of radius a_c, that is inclined at an angle θ to the vertical Z axis, and is under a pressure gradient $\Delta p/\ell$ in the Z direction. The axial (Z) velocity of a fluid element, located at the radius r, is described by

$$u_z = (a_c^2 - r^2) \quad (\cos^2\theta)\, \Delta p/4\mu\ell \qquad (64).$$

Thus, the incremental axial distance traveled in the time increment τ is

$$\Delta Z = (a_c^2 - r^2) \quad (\cos^2\theta)\tau\, \Delta p/4\mu\ell \qquad (65)$$

From Equation (65) it can be readily seen that ΔZ depends on r, a_c, and θ. Thus, for a single capillary, or more generally a system of straight circular capillaries (under a uniform axial pressure gradient) characterized by known distributions of a_c and θ, the ΔZ displacements of discrete fluid elements can be characterized by a certain predictable distribution, if molecular diffusion effects are neglected in the system. If the capillaries are not circular, but have other regular shapes, the calculation of the distribution is complicated by the presence of nonparabolic velocity profiles.

Quite obviously, the description of longitudinal dispersion in a system of straight capillaries is an oversimplification of the phenomena that occur in a porous medium. In most real porous systems, very little is known about the

complex distributions of sizes, shapes, and orientations of pore channels, and how they are related to the over-all network structure. Even if an accurate description of a network structure were available for such a system, it would be virtually impossible to solve the Navier-Stokes equations, and account for molecular diffusion effects, in order to evaluate the dispersion properties of the medium.

The simplest case of fluid dispersion in a real system involves the displacement of one fluid by a second that is immiscible with, and has the same density and viscosity as the first. If the interfacial tension is much larger than μU, then the meniscus between the two fluids will extend across each channel and move with a velocity equal to the average speed through the channel (26). Thus, the dispersion of an initially sharp interface between these fluids is due only to the internal geometry of the porous medium, since radial intrachannel velocity variations, and radial and axial molecular diffusion, have no effect on the mixing of the two fluids.

In many real systems of practical interest, the dispersion of fluid elements is influenced by the simultaneous effects of radial velocity variations and molecular diffusion. This is obvious when we remember that the theoretical residence time of a fluid element is infinite at solid-fluid boundaries. Thus, molecular diffusion is responsible for the transport of molecules from the vicinity of a surface, to regions where fluid elements move at finite velocities. The relative contribution of molecular diffusion to longitudinal dispersion would be determined by the molecular diffusivity, the geometry of the pore channels, the characteristic intrachannel velocity profiles, and the average velocity.

STATISTICAL PROPERTIES OF LONGITUDINAL DISPERSION

The statistical properties of longitudinal dispersion have been treated theoretically by a number of workers (1, 26-30). As an example, Sherman (1) has demonstrated how the diffusionlike differential equation, for longitudinal dispersion, is derived from probability considerations involving the irregular movements of fluid elements. It is useful to summarize the highlights of Sherman's development as a basis for later discussions. He assumed that fluid elements undergo variable axial displacements, $\underline{U}\tau + \Delta$, in the time increment τ, according to a certain probability law that is determined by the geometry of the void spaces, and the average linear pore velocity $\underline{U}$. The time increment is taken to be small, compared to the observed time interval, but always large enough so that the axial displacement of each fluid element, relative to the average fluid displacement, $\underline{U}\tau$, is statistically independent of (a) the element's previous movements, and (b) the relative movements of other fluid elements. In addition to these restrictions, it was necessary to assume that the frequency function, $\Phi(\Delta)$, is symmetrical. Sherman obtained Equation (1) and identified the longitudinal dispersion coefficient as

$$D_L = \frac{1}{2\tau} \int_{-\infty}^{+\infty} \Delta^2 \, \Phi(\Delta) \, d\Delta \qquad (66).$$

The significance of Sherman's definition for the longitudinal dispersion coefficient becomes more meaningful if it is assumed that $\Phi(\Delta)$ is of Gaussian or normal form, described by

$$\Phi(\Delta) = (1/(\sqrt{2\pi}\,\sigma)) \exp(-\Delta^2/2\sigma^2) \qquad (67)$$

where σ^2 is the variance of $\Phi(\Delta)$. In this case it is easily shown that

$$D_L = \sigma^2/2\tau \qquad (68).$$

The direct proportionality between D_L and U has been predicted from several viewpoints (27-30). Sherman accomplished this by defining D_L/U, from Equation (66), and reasoning that the probability distribution $\Phi(\Delta)$ should be independent of U, in the laminar regime, if the average displacement, $\overline{\Delta Z} = U\tau$, is kept constant. His basic assumptions were that, when laminar flow is maintained, (a) the streamline flow patterns remain unchanged with flow rate changes, and (b) the local velocities of fluid elements, in various channels of different size and orientation, remain in the same proportion to each other, regardless of the average velocity. Thus, changes in U should have no effect on the relative displacements of fluid elements, defined by $\Phi(\Delta)$, when $\overline{\Delta Z}$ is always the same. If, as before, we assume that $\Phi(\Delta)$ obeys a normal distribution, it follows from Equation (68) that

$$D_L/U = \sigma^2/2\overline{\Delta Z} \qquad (69)$$

Up to this point, longitudinal dispersion has been defined in terms of a length $\overline{\Delta Z}$, which is considered to be sufficiently large so that fluid elements become statistically independent of their initial positions, and the relative positions of other initially neighboring fluid elements. In a bed of packed solids, $\overline{\Delta Z}$ would represent a distance of several particle diameters. Since we are concerned with measuring longitudinal dispersion in beds of length Z_e, where Z_e is always much larger than $\overline{\Delta Z}$, it is appropriate to define the effect of bed length on the total longitudinal dispersion that takes place. If Equation (66) is accepted as a valid definition of D_L, division by UZ_e yields

$$D_L/UZ_e = \frac{1}{2Z_e\,\overline{\Delta Z}} \int_{-\infty}^{+\infty} \Delta^2\, \Phi(\Delta)\, d\Delta \qquad (70).$$

Also, if $\Phi(\Delta)$ is normally distributed,

$$D_L/UZ_e = \sigma^2/2Z_e\overline{\Delta Z} \qquad (71).$$

Since the solution of the differential equation for longitudinal dispersion specifies that the parameter $\underline{D_L}/\underline{UZ_e}$ determines the exact shape of a dimensionless $\underline{C}/\underline{C_o}$ vs. $\underline{R} = \underline{Ut}/\underline{Z_e}$ breakthrough curve, the relations given for $\underline{D_L}/\underline{UZ}$ can be considered as statistical definitions of the total longitudinal dispersion effect in a given porous medium.

EFFECT OF BED STRUCTURE ON $\underline{D_L}/\underline{U}$ WHEN GEOMETRIC SIMILARITY IS MAINTAINED

In order to illustrate the effect of bed structure on $\underline{D_L}/\underline{U}$, let us first consider systems where the particle shape is spherical, and where it is relatively simple to maintain geometric similarity among beds of different particle size. Let us assume again that (a) molecular diffusion effects are unimportant, and (b) the streamline flow patterns in a bed remain the same at low $\underline{Re}$, regardless of $\underline{U}$. Under these conditions it can be reasoned that σ, the standard deviation of $\Phi(\Delta)$, should be directly proportional to the particle size, $\underline{d}$, in geometrically similar beds that have $\underline{n}$ particle layers. Thus, if we let $\sigma_{\underline{n}} = \underline{\bar{k}_n d}$, $\overline{\Delta Z} = \underline{nd}$, and make these substitutions in Equation (69),

$$\frac{D_L}{U} = \frac{\bar{k}_n^2\, d^2}{2\, n\, d} = \frac{\bar{k}_n^2\, d}{2\, n} \qquad (72).$$

Since we have already shown that $\underline{D_L}/\underline{U}$ is constant in a given bed of particles when $\underline{n}$ is sufficiently large [large enough so that $\Phi(\Delta)$ becomes asymptotically

normal], it follows that $\bar{k}_n^2/n$ should be constant in a given bed. Since both $\bar{k}_n$ and n are independent of d, we can conclude from Equation (72) that $\bar{k}_n^2/n$ is constant and D_L/U is directly proportional to d, when laminar flow is maintained in geometrically similar beds of sufficient thickness.

The same proportionality between D_L/U and d has been predicted by other authors (26-30), using slightly different lines of reasoning. The proportionality has been verified experimentally in beds of spherical particles by Ebach (31) and by Raimondi, et al. (32).

It is evident from Equation (72) that $\bar{k}_n^2/n$ depends only on the packing or geometrical arrangement of particles in a bed. This concept can be applied more generally to geometrically similar beds by simply choosing a characteristic scale factor which is proportional to the repeating distance between particle layers.

EFFECT OF FIBER BED STRUCTURE ON D_L/U

The application of statistical concepts to the variation of D_L/U with fiber bed structure is much more difficult than in granular systems. The major problem involves the definition and maintenance of geometric (or structural) similarity. In order to establish a useful basis, let us review briefly some pertinent facts concerning ideal fiber bed systems, i.e., beds which result when circular cylinders are randomly oriented in the horizontal plane.

The presence of elongated particles greatly complicates the system. The fiber diameter d, fiber length ℓ', and average bed porosity ϵ, are the most obvious geometrical parameters, but they have a number of interacting effects on bed structure. When a fiber bed is compacted, the fibers can slip, with respect to each other, and bend. In general, the amount of slippage and bending

that occurs can depend on $\underline{d}$, $\underline{\ell}'$, and ϵ, as well as the stiffness, frictional, and elastic properties of the individual fibers.

Jones (33) has investigated the effect of fiber structural properties on the compression response of nylon and glass fiber beds. The beds were carefully formed, and only the central portions were tested in order to avoid the edge effect. He observed that the compressibility constants, $\overline{M}$ and $\overline{N}$, varied significantly over relatively wide $\underline{\ell}'/\underline{d}$ ranges in his glass and nylon systems; $\underline{d}$ alone was found to be unimportant. In his 5.12 μ glass fiber system, the greatest percentage of nonrecoverable deformation, and consequently the greatest amount of nonreversible fiber repositioning, occurred in the $\underline{\ell}'/\underline{d}$ range 500-600. In the 46.2 μ nylon system, the maximum occurred in the $\underline{\ell}'/\underline{d}$ range 75-100. The observed difference between glass and nylon fibers was tentatively attributed to differences in elastic moduli and coefficients of friction. Jones concluded from his results that compression – recovery response is highly dependent on $\underline{\ell}'/\underline{d}$, as it affects the structure of the bed formed. Fiber diameter by itself was thought to be a relatively unimportant factor in bed compression because "Its effect on mat structure is apparently counterbalanced by its effect on fiber flexibility."

From the results cited above, the following hypotheses of fiber bed structure are suggested.

1. As a first approximation, it appears likely that the respective structures of 1, 4, 16, and 64-denier viscose fiber beds should be geometrically similar when ϵ and $\underline{\ell}'/\underline{d}$ are the same. Furthermore, the fiber diameter should be an appropriate scale factor for these systems.

2. It appears likely that the respective structures of viscose beds, at very large $\underline{\ell}'/\underline{d}$ ratios, should be structurally similar when ϵ is the same.

If geometric (or structural) similarity is maintained under the above conditions, and if molecular diffusion has a negligible effect on longitudinal dispersion in the present systems (the latter appears to be true since D_L/U was found to be essentially independent of U), the following results should be observed:

1. D_L/Ud should vary only with ℓ'/d when ϵ is constant.
2. D_L/Ud should approach an asymptotic value at very large ℓ'/d when ϵ is constant.

As a preliminary test of the experimental results, the independently determined values of D_L/Ud in Table XXII (at the respective porosity levels) were plotted against ℓ'/d in Fig. 45. For purposes of comparison, Sherman's results on the 17 μ dacron system were included (the value at $\epsilon = 0.916$ was discarded because of possible air inclusion in the bed). It is seen that (a) D_L/Ud was dependent on ℓ'/d to a much greater extent than ϵ, and (b) D_L/Ud tended to approach an asymptotic value at large ℓ'/d.

A further test of the experimental results was applied as follows. In the diacetyl-4 denier system, it was empirically determined that D_L/Ud was approximately proportional to ϵ over the investigated range. By assuming that similar relationships would also apply in the 1, 16, and 64-denier viscose systems, and the 17 μ dacron systems, the parameter $D_L/Ud\epsilon$ was plotted against ℓ'/d in Fig. 46; all the porosity levels that were employed are included in this figure.

The results in Fig. 45 and 46 appear to indicate that (a) geometric similarity was achieved in the 4 and 16-denier viscose systems, to a good approximation, when ϵ and ℓ'/d were maintained constant, and (b) the ℓ'/d ratio had a much stronger effect than ϵ on the geometrical properties that were responsible

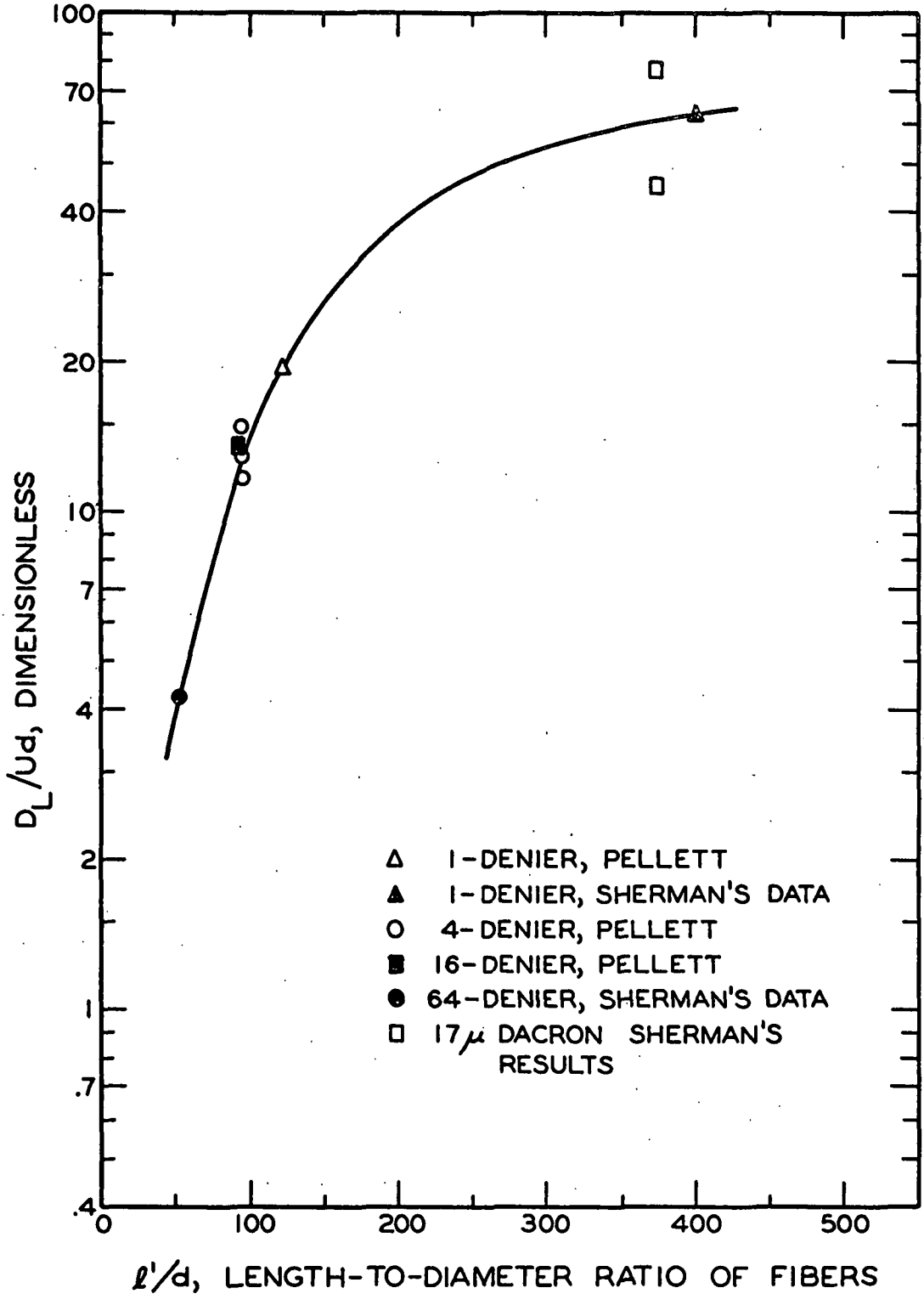

Figure 45. Effect of Fiber-Length-to-Diameter Ratio on Longitudinal Dispersion Properties

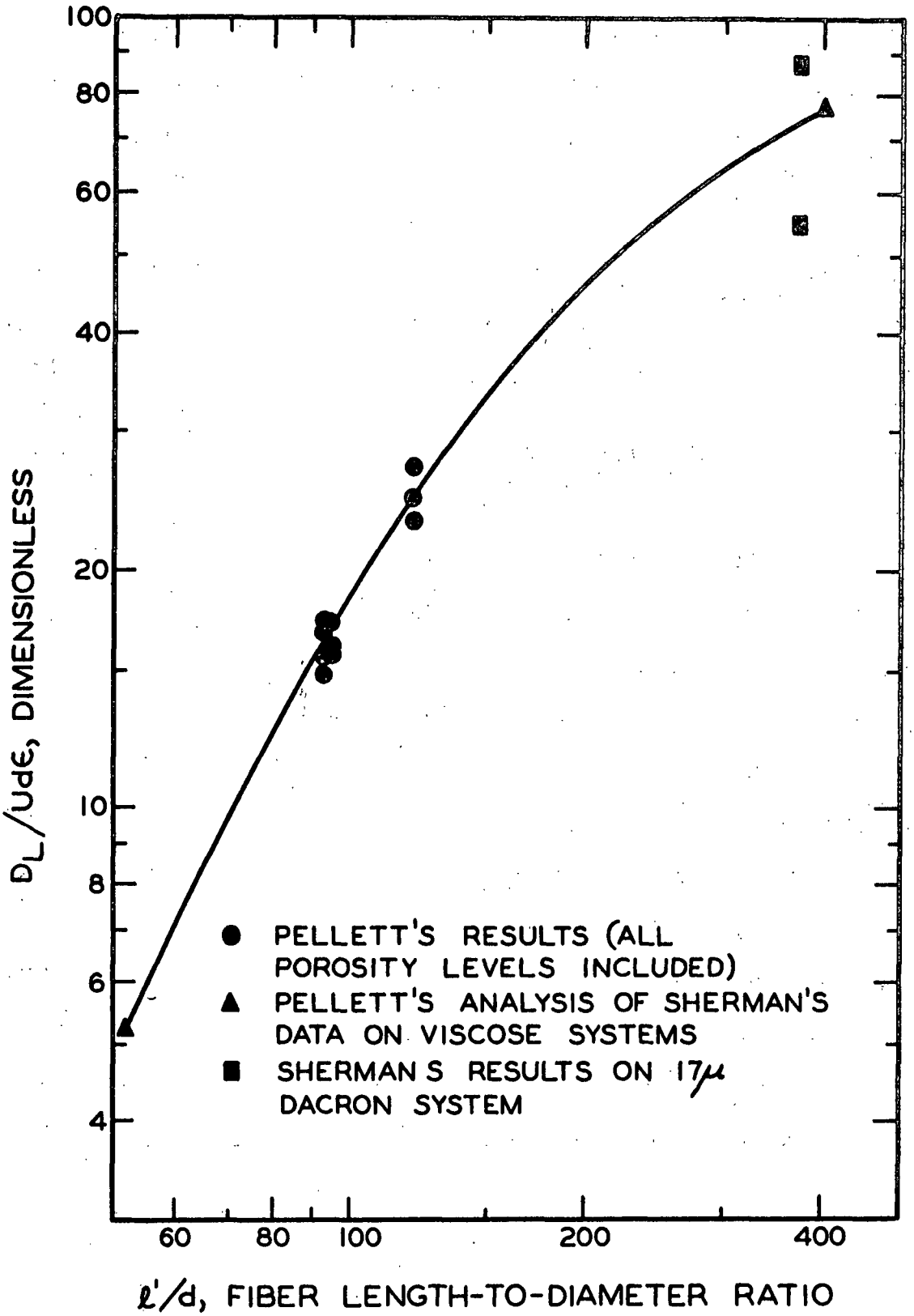

Figure 46. Effect of Fiber-Length-to-Diameter Ratio on Longitudinal Dispersion Properties of Fiber Beds

for longitudinal dispersion in these beds. The latter finding, concerning the effect of ℓ'/d on $D_L/Ud\epsilon$, was a somewhat unexpected result. In the future it may be possible to explain this result in terms of (a) direct observations of fiber beds, and/or (b) the application of a network model to flow through fiber beds.

It should be noted that the above results are limited in scope, and therefore the conclusions concerning geometric similarity and the effect of ℓ'/d should be viewed with caution until further experimental results are available.

OBSERVED RELATIONSHIPS OF APPARENT INTRAFIBER DIFFUSION PARAMETER

Figure 47 illustrates the relationships that were found to exist between the apparent intrafiber diffusion parameter, $(D_F/a^2)_A$, and U, at various porosity levels in the PAA-1, 4, and 16-denier systems. In the lower velocity regions of all three systems, it is seen that $(D_F/a^2)_A$ increased significantly with both U and ϵ. In the higher velocity regions of the PAA-1 and 4-denier systems, $(D_F/a^2)_A$ was considerably less sensitive to increases in U and ϵ. Here it appears that true asymptotic values, D_F/a^2 (at sufficiently large values of U), were not attained, but the approach was quite close. In the PAA-16 denier system, however, an effectively asymptotic value ($D_F/a^2 = 0.0050$) was obtained at $\epsilon = 0.76$. Here numerous washing experiments were performed at pore velocities up to 2.04 cm./sec. (four of them, at $U > 1$ cm./sec., are not shown in Fig. 47), where no indication of further increase in $(D_F/a^2)_A$ was found when D_L/U was assumed to be constant and independent of U; in the event that D_L/U actually increased with U, D_F/a^2 would likely remain about the same, since the long tails in these breakthrough curves were insensitive to moderate changes in D_L/U.

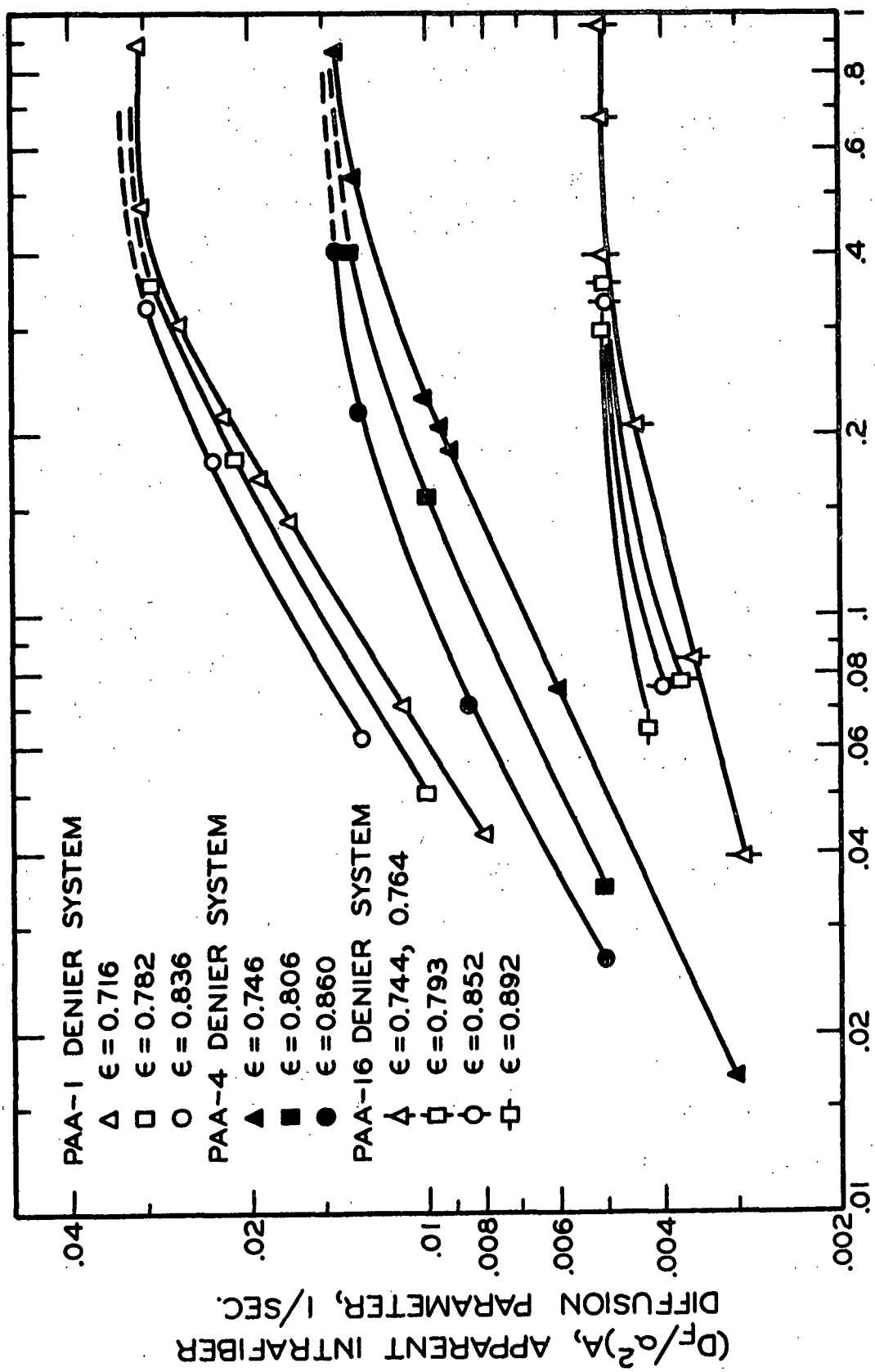

Figure 47. Results Obtained from Application of Case 1(F) to the PAA-Viscose Systems

The results shown for the PAA-4 denier system probably best represent the effect of ϵ on $(\underline{D_F}/\underline{a}^2)_A$, since $\underline{D_I}/\underline{U}$ was determined independently (using diacetyl) at each porosity level. It is possible that the asymptotic values, $\underline{D_F}/\underline{a}^2$, may have been found to increase to some extent with ϵ in this system, if the velocity ranges had been extended.

In both the 1 and 16-denier systems, $\underline{D_I}/\underline{U}$ was determined independently only at the lowest porosity level, and these values were employed in the analysis of data at the remaining higher porosity levels. If the possibility were true, that $\underline{D_I}/\underline{U}$ increased with ϵ in these systems (as it actually did in the 4-denier system), (a) the observed increases in $(\underline{D_F}/\underline{a}^2)_A$ with ϵ would have been proportionally greater than shown, and (b) the asymptotic values, $\underline{D_F}/\underline{a}^2$ (if they had been attained) would have been found to increase to some extent, with ϵ.

The possibility that $\underline{D_F}/\underline{a}^2$ increases with ϵ, bears importantly on our concept of mass transfer in a fiber bed. It would support the likely hypothesis that, as ϵ increases, the resultant decrease in the effect of fiber-fiber contacts in a bed should increase the effective rate of intrafiber diffusion that is ultimately achieved at high pore velocities. This possibility was reinforced by results in the PAA-16 denier system, where the numerous washing experiments at $\epsilon = 0.76$ yielded a value of $\underline{D_F}/\underline{a}^2$ that was about one half that obtained from the sorption rate experiments, on stirred fiber slurries.

Despite the facts that asymptotic values of $(\underline{D_F}/\underline{a}^2)_A$ were not exactly defined in the PAA-1 and 4-denier systems, and were possibly dependent on ϵ in all the systems, $\underline{D_F}/\underline{a}^2$ was assigned values of 0.030, 0.014, and 0.005, in the PAA-1, 4, and 16-denier systems, respectively. These values should be considered to be most reliable at the lowest porosity levels of each system, where (a) $\underline{D_I}/\underline{U}$

was determined independently in each case, (b) the data was more extensive, and (c) the effects of intrafiber diffusion, on the shape of the breakthrough curves, were greatest and therefore easiest to measure.

SUMMARY OF DIFFUSIONAL PROPERTIES OF SOLUTE-FIBER SYSTEMS

Table XXIII summarizes the evaluated diffusional properties and related characteristics of the various solute-fiber systems. The intrapore diffusion coefficient $\underline{D}_F'$, which applies to the diffusion of solute in hypothetical intrafiber pores, was calculated from the intrafiber diffusion coefficient $\underline{D}_F$ as $\underline{D}_F \underline{K}/\epsilon'$. It is important to note that the use of $\underline{D}_F'$ permits a more meaningful comparison of intrafiber diffusion phenomena in different solute systems, since the expression for mass flux in a fiber is based only on a solution concentration driving force, $(\partial \underline{P}/\partial \underline{r})$, and is independent of the degree of adsorption exhibited by the particular solute. This is in keeping with the likely assumption that true surface diffusion of adsorbed solute contributes negligibly to the rate of solute movement. Thus, the particular value of $\underline{K}$ for a system relates only to the solute capacity of a fiber (similar to heat capacity, in heat transfer systems), and is assumed to have no effect on the mechanism of solute transport.

The molecular diffusion coefficients of PAA and diacetyl were estimated to be roughly 5×10^{-6} and 8×10^{-6} sq.cm./sec., respectively, in aqueous solution at 26°C.

A number of observations can be made concerning the intrapore diffusion coefficients. These are summarized as follows:

1. The $\underline{D}_F'$ values were all considerably smaller than the respective molecular diffusion coefficients in aqueous solution.

TABLE XXIII

DIFFUSIONAL PROPERTIES AND RELATED CHARACTERISTICS OF SOLUTE-VISCOSE FIBER SYSTEMS

Denier	Dye	$\underline{d}$, μ	V, wet cc./g., o.d.	ϵ'	$\underline{K}$[a]	$\underline{D_F}/\underline{a}^2$, sec.$^{-1}$	$\underline{D_F}$, sq.cm./sec.	$\underline{D_F'}$,[b] sq.cm./sec.
1	PAA	15.91	1.925	0.690	8.15	0.030	1.90×10^{-8}	2.24×10^{-7}
1	BPP	15.91	1.925	0.690	3.025	0.008	5.06×10^{-9}	2.22×10^{-8}
4	PAA	29.89	1.694	0.638	10.32	0.014	3.13×10^{-8}	5.07×10^{-7}
4	Diacetyl	29.89	1.694	0.638	0.618	0.35	7.8×10^{-7}	7.8×10^{-7}
16	PAA	60.35	1.622	0.618	9.30	0.005	4.55×10^{-8}	6.85×10^{-7}
16	BPP	60.35	1.622	0.618	3.025	0.0005	4.55×10^{-9}	2.23×10^{-8}
64	Diacetyl	122.1	1.612	0.618	0.618	0.090	3.35×10^{-6}	3.35×10^{-6}

[a] $\underline{K}$ values used in analysis of washing runs.

[b] $\underline{D_F'} = \underline{D_F}\ \underline{K}/\epsilon'$, intrapore diffusion coefficient.

2. The $\underline{D'_F}$ values for PAA were relatively smaller than those for diacetyl.

3. The $\underline{D'_F}$ values for PAA increased as the fiber diameter was increased.

4. The independently determined values of $\underline{D'_F}$, from rate of sorption experiments on the PAA-4 and 16-denier systems, were about a factor of two larger than the corresponding $\underline{D'_F}$ values from the washing experiments.

Observations 1 and 2 have reasonably straightforward explanations that are based on the physical phenomena involved in the intrafiber diffusion process. The explanations for observations 3 and 4 are less certain because of complicating factors.

INTRAFIBER DIFFUSION

Let us begin the discussion of intrafiber diffusion by reviewing the mechanism of molecular diffusion in a liquid. In the absence of restricting physical boundaries in a system (such as the walls of a very narrow pore), solute molecules undergo random movements in solution, as they possess thermal motion and exchange momentum with neighboring solvent and solute molecules. In dilute solutions, most of the momentum exchange occurs when solute and solvent molecules collide, or interact; here the molecular diffusion process is effectively independent of concentration, and the diffusion obeys Fick's law (provided that the average molecular configuration remains the same with concentration changes).

Now the movements of solute molecules in a swollen cellulose fiber are physically restricted by the structure of the solid. Swollen regenerated cellulose partly consists of numerous impenetrable crystalline regions, wherein the cellulose molecules are highly ordered. The remainder of the structure consists of amorphous regions in which the cellulose molecules are less well ordered. In these regions the intermolecular distances are great enough to permit penetration

by water molecules which can hydrogen bond with available hydroxyl groups of the cellulose chains. Furthermore, the structure of the amorphous regions is sufficiently open that it may be deformed easily, or swollen, to allow additional water molecules to enter. It is within these swollen amorphous regions that solute molecules diffuse. It might be visualized that the solute molecules undergo numerous random motions in these regions, colliding frequently with partially mobile cellulose chain segments and irregularly defined surfaces of bordering crystalline regions. From these considerations of how the solute molecule effectively diffuses through a network of amorphous regions, it is obvious that the $\underline{D}_F'$ value for any solute in viscose should be lower than its respective molecular diffusion coefficient. The $\underline{D}_F'$ values for the diacetyl-4 and 64-denier systems probably best represent this effect in the absence of complicating adsorption phenomena.

EFFECT OF ADSORPTION

The diffusion of PAA in viscose would appear to be further retarded by adsorption effects. Undoubtedly, PAA molecules are adsorbed and desorbed numerous times during their diffusion through the relatively dense amorphous regions. A characteristic distribution of residence times would be associated with the adsorption-desorption cycle, describing the effective time a PAA molecule is likely to be adsorbed on a given site. Here, even a relatively short average residence time could have a highly significant effect on the average transport rate by diffusion. This may partly explain the fact that the $\underline{D}_F'$ values for the PAA systems were relatively smaller than those for diacetyl. The remainder of the difference in $\underline{D}_F'$ values may have been due to the larger physical size of the PAA molecule.

EFFECT OF CRYSTALLITE ORIENTATION

The marked increase in D'_F with fiber diameter may have been due to differences in the physical properties of the fibers. In relation to this problem, Preston and Kapadia (14) studied the effect of crystallite orientation on the rate of dyeing, and equilibrium dye uptake, in the Sky Blue FF (direct dye)-viscose system. Their viscose was prepared under well-controlled conditions, and was coagulated in an ammonium sulfate bath. The freshly coagulated cellulose ammonium xanthate was stretched under widely different spinning tensions before regeneration of the cellulose in a sulfuric acid bath. The resulting homologous series of viscose filaments had approximately circular cross sections that were relatively free from a marked skin-core structure (it appears that these were quite similar to the all-skin fibers used in this study). The crystallite orientation of the viscose filaments was characterized by (a) the ratio of x-ray intensities at the equators and poles, on the 101 and 002 rings, and (b) the double refraction (or birefringence) of the fibers. Since the x-ray orientation was shown to increase regularly with spinning tension, and since the double refraction was found to increase approximately linearly with spinning tension, the double refraction was used as a convenient quantitative measure of crystallite orientation.

The results of their dye sorption experiments indicated that the initial rate of sorption (measured by the uptake at 15 minutes and corrected for surface area differences) decreased approximately by a factor of five as the double refraction at 65% R.H. increased from about 0.015 to 0.040. At the same time, the equilibrium dye sorption decreased by a factor of 1.5, and the fiber dry strength increased by a factor of three. Thus, in every case (represented by four fiber diameters, with each drawn at several different spinning tensions)

the initial rate of dye sorption, which is theoretically proportional to $\underline{D}_F'^{1/2}$, was found to decrease with increasing orientation.

The results of Preston and Kapadia are in qualitative agreement with the result of this study that $\underline{D}_F'$ increased with fiber size, since the x-ray diffraction patterns, swollen specific volumes, and axial swelling measurements indicated that crystallite orientation decreased with increasing fiber size, in the present systems. The quantitative accuracy of the observed increase of $\underline{D}_F'$ with fiber diameter is less certain, however, because of the previously mentioned complications involving the possible functional dependence of $\underline{D}_F/\underline{a}^2$ on ϵ.

APPLICABILITY OF A DIFFUSION EQUATION WHEN FIBERS ARE IN CONTACT

The results up to this point indicate that, in cases where intrafiber diffusion effects were essentially controlling, the effective rate of intrafiber diffusion was dependent to some extent on factors related to bed structure. Qualitatively, we know that the number of fiber-fiber contacts, and the average surface area involved per intimate contact, should both decrease with increasing ϵ. Therefore, the effective surface area available for liquid-phase mass transfer should increase with ϵ. An attempt to account for this effect, quantitatively, is made at a later point in the text, when the problem of correlating the mass transfer coefficient is discussed.

In relating the effect of bed structure on intrafiber diffusion, an additional factor should be considered. It is obvious that the diffusion of solute from two crossed fibers, in intimate contact, is not properly described by the diffusion equation for circular cylinders of radii $\underline{a}$. As an alternative, however, the diffusion process may be quite well approximated if an effective fiber radius

is employed in the solution of the diffusion equation. This possibility is readily evident when simple boundary condition solutions (12) are compared for solids of different shape, such as the infinitely long slab, the sphere, and the infinitely long circular cylinder.

Comparisons of this type serve to emphasize that (a) a diffusion equation is likely to yield good agreement with experimental results, regardless of particle geometry and particle-particle contact (provided that Fick's law applies), and (b) the resulting intraparticle diffusion coefficient is not meaningful unless the exact geometry of discrete particles, or particle units, is known and accounted for.

Intrafiber diffusion in fiber beds is further complicated by the possible effects of bed compaction (or ϵ) on the deswelling of viscose in the regions of intimate fiber-fiber contact. In this case it is likely that the value of D_F/a^2 would be affected by local changes in both K and D'_F.

THE MASS TRANSFER PARAMETER

EXPERIMENTALLY OBSERVED RELATIONSHIPS

Figures 48 and 49 illustrate experimental relationships between the mass transfer parameter $L = ak_L/D'_F$ and U, at various porosity levels in the PAA-1, 4, and 16-denier systems; the latter system was not as well defined because of insufficient data at low velocities. It is seen that L increased rapidly with U, and increased moderately with ϵ. Again, the observed effect of ϵ in the 4-denier system is considered to be the most reliable, since D_L/U was determined independently at all three porosity levels. It is important to note that the results of the sorption runs, in the 1 and 4-denier systems, were in good agreement with the

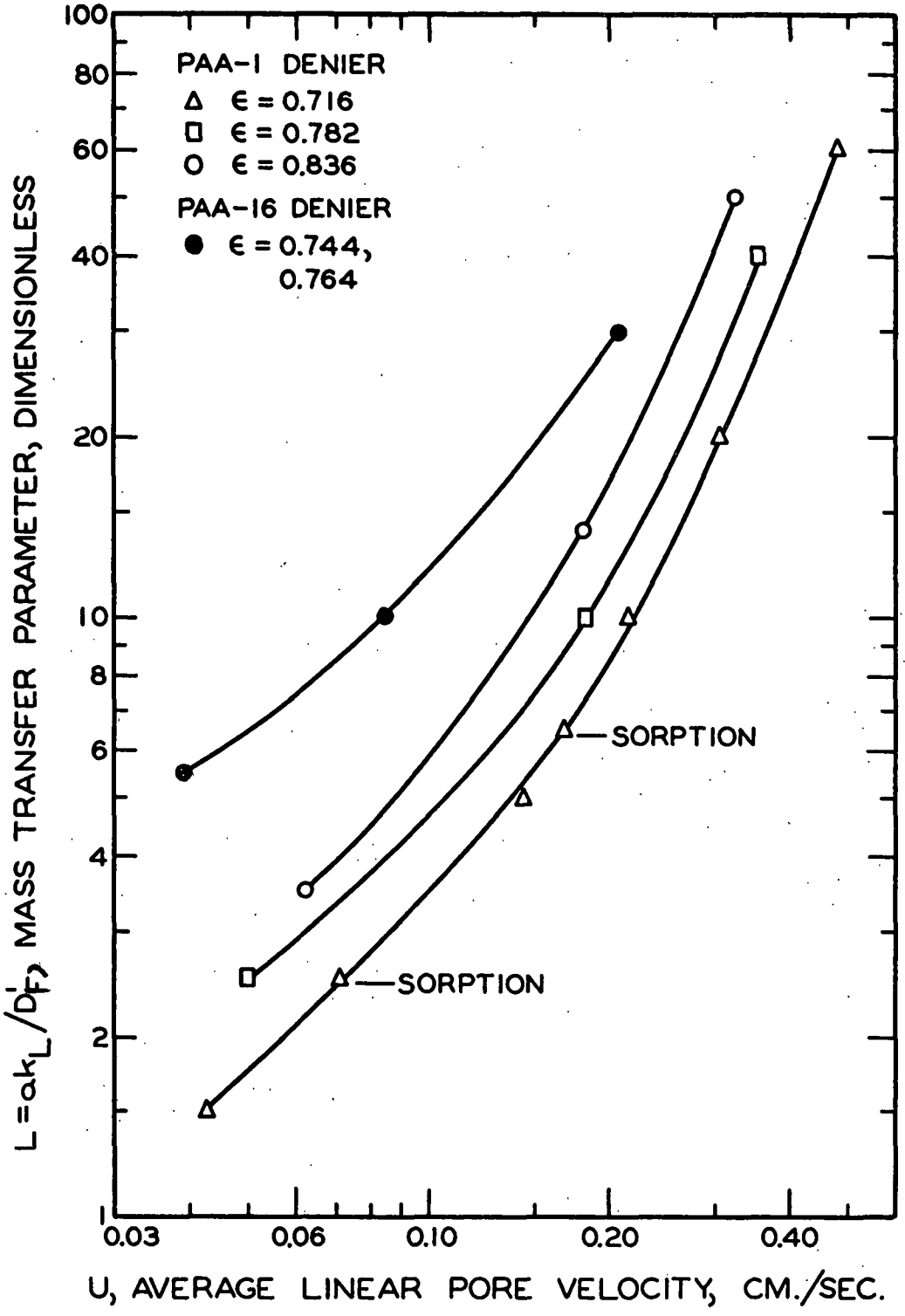

Figure 48. Mass Transfer Parameter Obtained From Application of Case 2(F) to the PAA-Viscose Systems

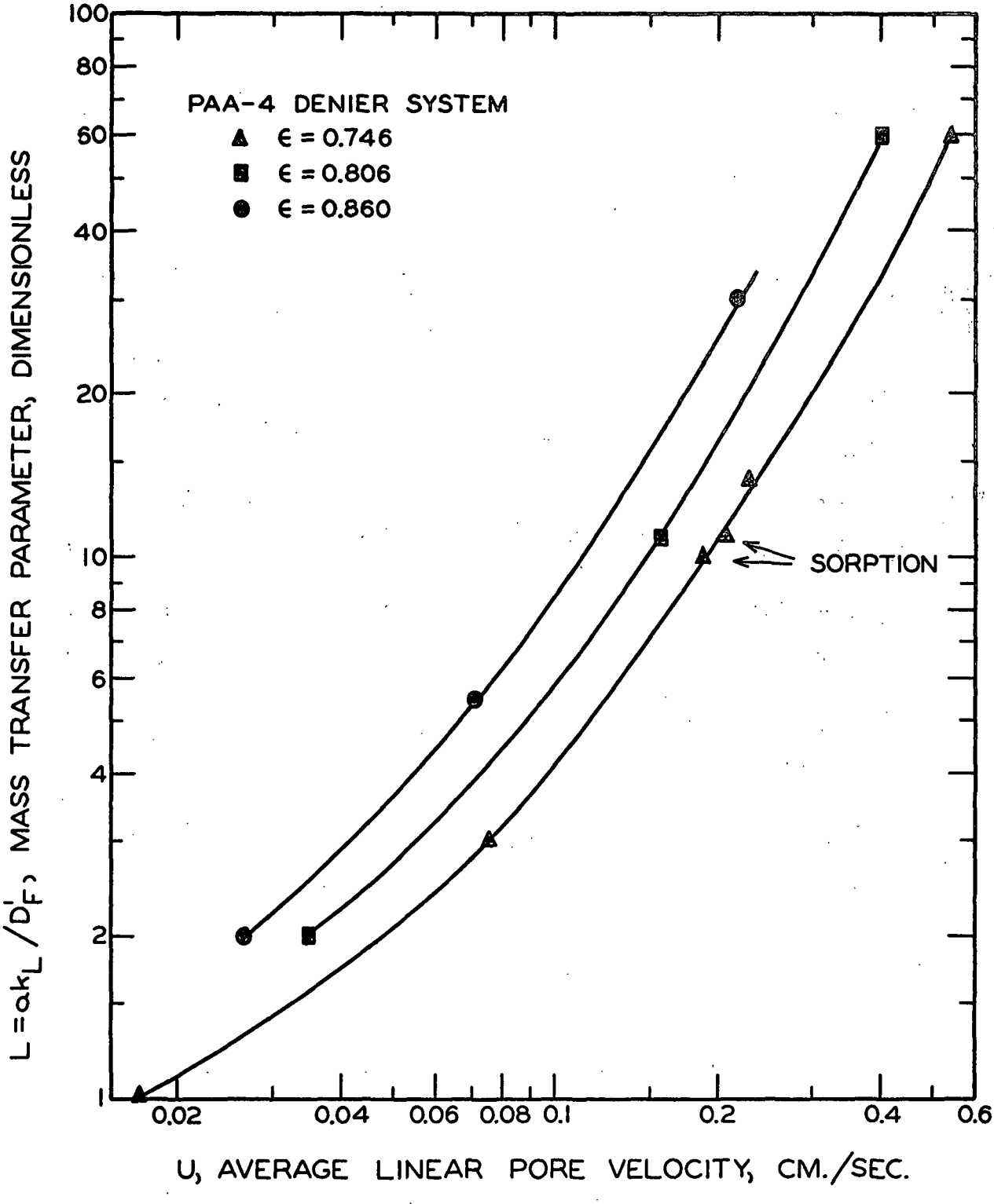

Figure 49. Mass Transfer Parameter Obtained From Application of Case 2(F) to the PAA-Viscose Systems

results of the desorption runs; this suggests that the mechanisms of mass transfer were essentially the same.

SIGNIFICANCE OF THE MASS TRANSFER PARAMETER

The significance of $\underline{L}$ is apparent when the mass flux relationship at the fiber surface is rewritten for Case 2(F) as

$$L = ak_L/D'_F = \frac{-(\partial P/\partial r)_{r=a}}{(P(a,t) - C(t))/a} \qquad (73).$$

This expression for $\underline{L}$ is seen to define the average ratio of the pore concentration gradient, just inside the fiber surface, to the assumed driving force in solution, divided by an arbitrary distance of one fiber radius. The fact that $\underline{L}$ was found to be greater than 1, in the PAA-1, 4, and 16-denier systems, indicates that intrafiber diffusion effects were always important in these systems. In velocity regions where $\underline{L} \geq 60$, it was assumed that intrafiber diffusion effects were entirely controlling. This was effectively demonstrated when the difference between predicted breakthrough curves, using $\underline{L} = 60$ and $\underline{L} = \infty$ [Case 1(F)], was found to be essentially negligible.

EFFECT OF BED POROSITY ON MASS TRANSFER PARAMETER

Both linear pore velocity and porosity have been shown to affect $\underline{L}$. In order to demonstrate an empirical rectification of the porosity effect, the relationship between $\underline{L}$ and $\underline{U}\epsilon^3$ is shown in Fig. 50 for all the mass transfer results in this study, including the analysis of Sherman's diacetyl-64 denier system. That the results of the PAA-16 denier and diacetyl-64 denier systems define different curves than the PAA-1 and 4-denier systems, indicates that (a) more variables are involved, and (b) the apparent correlation of results in the PAA-1 and 4-denier systems is possibly fortuitous.

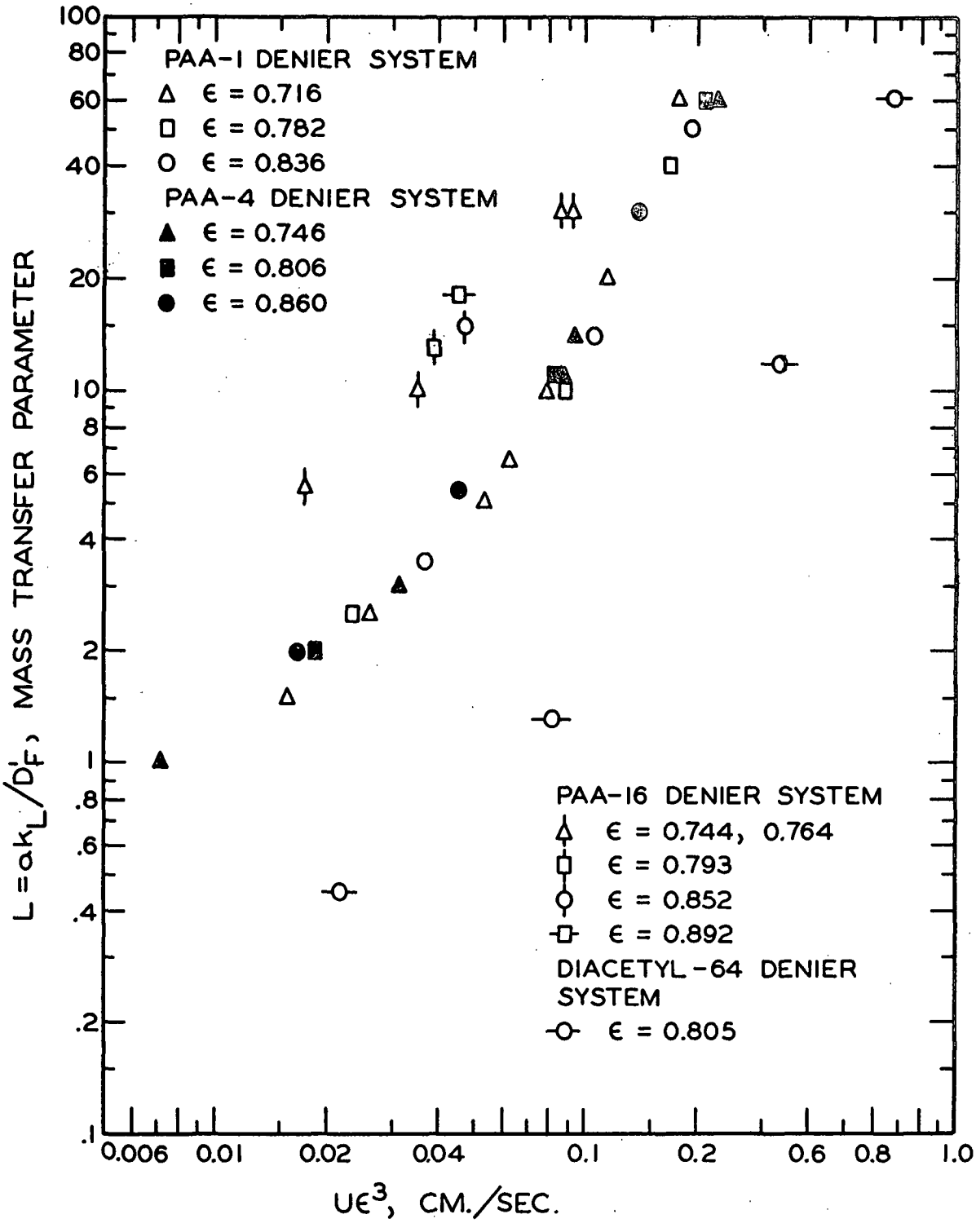

Figure 50. Initial Correlation of Liquid-Phase Mass Transfer Results

OBSERVED RELATION BETWEEN PARAMETERS OF CASES 1(F) AND 2(F)

It is useful to demonstrate a relationship between the results obtained for Case 1(F), involving $(\underline{D}_F/\underline{a}^2)_A$, and Case 2(F), involving $\underline{L}$ and $\underline{D}_F/\underline{a}^2$. As previously indicated, it was generally possible to choose parameters for Cases 1(F) and 2(F) which resulted in nearly identical breakthrough curves, even in the lowest velocity runs where intrachannel mass transfer effects were especially significant. This result was quite surprising in view of the mathematical differences between the two cases. Although the expressions for the two cases do not indicate a simple equivalence of parameters, an empirical relationship was found to exist between $\underline{L}$ and $(\underline{D}'_F)_A/\underline{D}'_F$. Figure 51 illustrates this relationship, where the respective results from the PAA-1, 4, and 16-denier systems, and the diacetyl-64 denier system, are compared.

It is evident from Fig. 51 that the porosity level, and the nature of the solute-fiber system involved, did not have an appreciably significant effect on the relationship between the two models. The fact that the two cases resulted in nearly identical breakthrough curves, indicates that neither case yields significantly better predictive results. From the standpoint of physical reality, however, the application of Case 2(F) is clearly more appropriate since it is based on the assumption that changes in pore velocity have no effect on the intrafiber diffusion coefficient.

MASS TRANSFER IN RELATED SYSTEMS

An important aspect of the mass transfer analysis is to explore the possibility of relating the mass transfer coefficient, $\underline{k}_L$, to the various parameters that characterize the solute-fiber systems. Although numerous experimental results have been reported in the literature on heat and mass transfer in packed

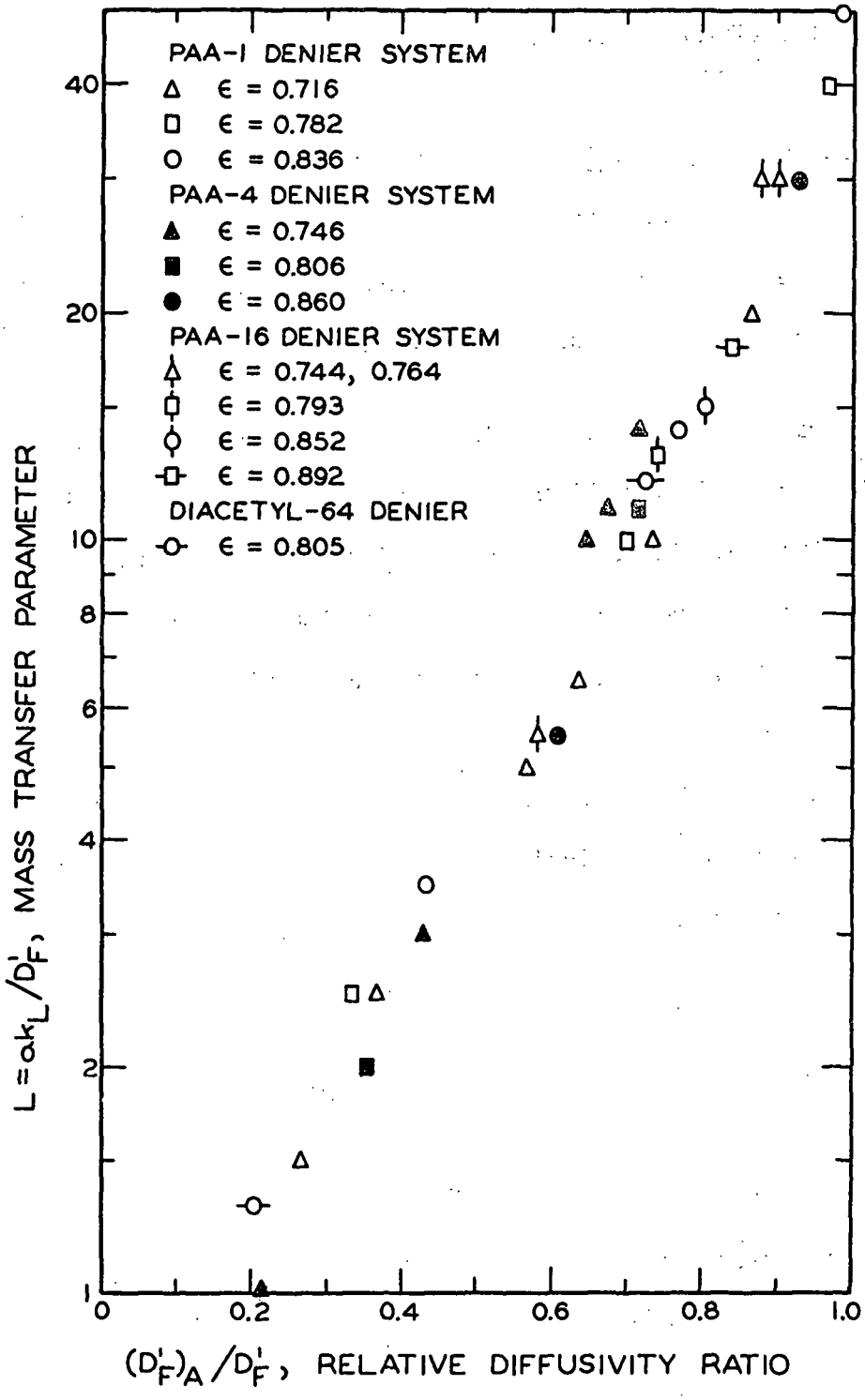

Figure 51. Comparison Between Results From Cases 1(F) and 2(F)

beds, it has been found that few, if any, can be applied to the analysis of the present systems without raising serious questions about their suitability.

THE "FREE SURFACE MODEL" FOR MASS TRANSFER IN MULTIPARTICLE SYSTEMS

Pfeffer and Happle (34) have made a recent breakthrough by applying the "free surface model" to describe heat or mass transfer in fluid flow through arrays of spherical particles, at low Reynolds numbers. As a matter of convenience, the following discussion will be confined to mass transfer.

The "free surface model" in this case was used to specify the fluid velocity components for a sphere falling in a concentric sphere of fluid that has a free surface at its outer boundary. Happle (35) previously obtained a relatively simple solution to the creeping motion equations that apply to this model. By specifying constant fluid properties, and constant solute concentrations at the inner sphere surface (C_1), and the outer free surface boundary (C_o), Pfeffer and Happle were able to find a suitable approximate solution to the partial differential equation for Fick's law diffusion, under the desired boundary conditions. The local coefficient of mass transfer, k, was defined at the surface of the inner sphere by

$$-D\left[\frac{\partial C}{\partial r}\right]_{r=a} = k(C_1 - C_o) \qquad (74).$$

The resulting expression for the local Sherwood number was integrated around the surface of the sphere to obtain an average Sherwood number as a function of the Peclet number and the porosity of the free surface model.

Pfeffer and Happle suggested that this model be applied to describe mass transfer in an idealized bed of particles by making two assumptions. The first

was to suppose that the spherical cell geometry of the model approximates a typical cell in a packed bed, even though the actual free surface boundaries would be distorted in shape. The second was to suppose that the slow flow from one cell to another is taken at the concentration of the outside boundary.

A few results of Pfeffer and Happle's calculations are shown in Fig. 52, where the average Sherwood number is plotted against the particle Peclet number (based on the average linear pore velocity) at various porosity levels.

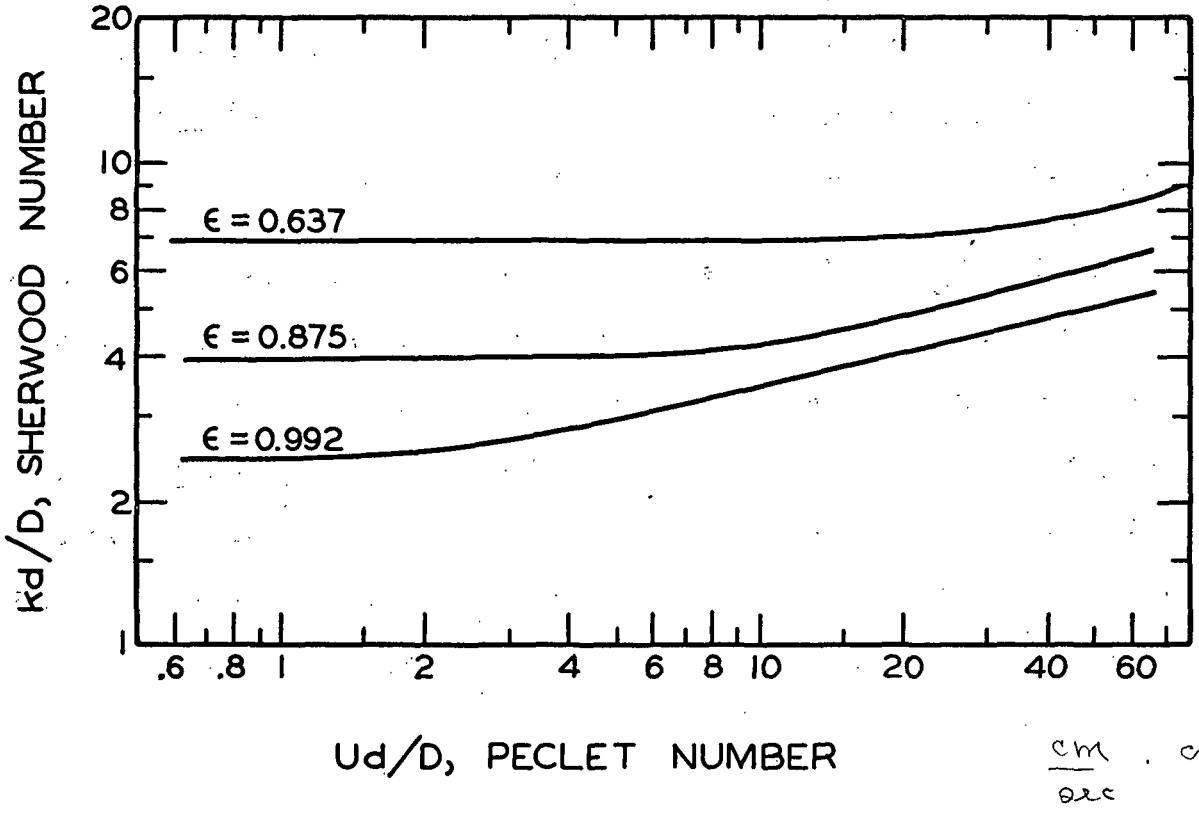

Figure 52. Mass Transfer in a Multiparticle Bed According to the "Free Surface Model" (34)

The most obvious result from their theory, is that the Sherwood number is completely described as a function of the Peclet number and porosity. Therefore, neither fluid density nor viscosity should enter into mass transfer correlations for multiparticle beds at low Peclet numbers, provided that the fluid properties are uniform. In this connection, Pfeffer and Happle demonstrated

that the commonly used modified "j" factor correlation (which is based on boundary layer theory)

$$j_\epsilon = \frac{k_L}{U}\left[\frac{\mu}{\rho D}\right]^{2/3} \text{ vs. } \frac{dU\rho}{\mu} \qquad (75)$$

is incorrectly applied as a general means of correlating mass transfer data at low Reynolds numbers, since j_ϵ was shown to be a function of the Schmidt number, Sc = $\mu/\rho D$, rather than being independent of it. Three additional observations from Pfeffer and Happle's results are that (a) Sh varies as $Pe^{1/3}$, in the limiting case, at large Pe, (b) Sh decreases with increasing ϵ, and (c) Sh approaches asymptotic values Sh_o, at low Pe, that are determined by ϵ.

The fact that $Sh_o \rightarrow 2$ (as $\epsilon \rightarrow 1$) is the lowest possible value of Sh for a bed of spherical particles, suggests the importance of specifying particle shape and particle orientation, since Brenner predicted that both of these factors determine Sh for a single particle at low Pe (36). Thus, the Sh vs. Pe predictions of Pfeffer and Happle apply only to beds of spheres, and the "free surface model" for mass transfer in a bed of long circular cylinders (arranged in parallel for simplicity) would probably yield significantly different results.

EFFECT OF PARTICLE-PARTICLE INTERACTION ON MASS TRANSFER

DEVELOPMENT AND DESTRUCTION OF CONCENTRATION GRADIENTS

It was predicted by the "free surface model" that Sh should decrease with ϵ. The effect of ϵ was accounted for in terms of the dimensions of a typical concentric sphere cell, and thus no attempt was made to account for the possible interactions between adjacent cells in a packed bed.

One possible mass transfer interaction in a fiber bed might be described by two opposing effects in which (a) concentration gradients that are developed during exposure to one "fiber layer," tend to decrease the effective rate of mass transfer upon exposure to succeeding "layers," and (b) the flow of fluid is divided upon passing each fiber with the net result that the existing concentration profiles tend to be destroyed, thus increasing mass transfer.

It is of interest to note that a series of experiments could be performed to examine the effect of concentration gradient development, on mass transfer, by measuring $\underline{k_L}$ in beds that contain different proportions of porous and nonporous fibers. The results of these experiments would be meaningful, however, only if (a) the fiber and bed geometry were the same (assuming that the effect of differences in fiber flexibility could be accounted for), and (b) suitable control experiments were performed, such as measuring $\underline{D_I}/\underline{U}$ independently.

FIBER-FIBER CONTACT EFFECTS

A second possible particle-particle interaction effect, on mass transfer, results from the presence of intimate contact areas between fibers. The effective surface area available for mass transfer would be lowered, in this case, necessitating the use of an appropriate correction factor. The effect can be simply illustrated if the average intimate contact area between two fibers is designated as $\underline{A'_c}$, the total number of fiber-fiber contacts in a bed as $\underline{C'_t}$, and the total surface area of the fibers (in the absence of contacts) as $\underline{A_t}$. The fractional surface area (based on $\underline{A_t}$) involved in intimate contact would thus be

$$\alpha = 2\, C'_t\, A'_c/A_t \qquad (76).$$

If the correct value of α were known in a system, the experimentally determined

$\underline{Sh}$ (based on $\underline{A}_t$) could be corrected for surface area in contact by evaluating $\underline{Sh}$ $(1 - \alpha)$, thus obtaining a value based on the effective surface area available for mass transfer.

In Appendix VII, a derivation is given for α under highly idealized conditions in a fiber bed; α is shown to be described in this simplified case by

$$\alpha = \frac{2}{\pi^{1/3}} \left[\frac{3(1 - \nu^2)}{4\bar{E}(V\bar{M})^{1/\bar{N}}} \right]^{2/3} (1 - \epsilon)^{(2 - \bar{N})/3\bar{N}} \qquad (77)$$

where $\bar{N}$ and $\bar{M}$ are the usual compressibility constants, $\underline{V}$ is the swollen specific volume, $\bar{E}$ is the appropriate elastic modulus, and ν is Poisson's ratio. Figure 53 illustrates the calculated variation of α with $(1 - \epsilon)$ for a 4-denier viscose bed, assuming Poisson's ratio to be 0.5, and letting $\bar{E}$ take on a wide range of values. For purposes of comparison, α was also calculated on the assumption that the contact area between two fibers is $\pi \underline{d}^2/4$, regardless of the normal force per contact.

It is seen in Fig. 53 that α depends to a considerable degree on the value taken for $\bar{E}$. Unfortunately, it is not easy to estimate a realistic value for $\bar{E}$ in the present viscose systems, since (a) the literature appears devoid of appropriate data, and (b) the statics of compressing an anisotropic fiber, in a direction perpendicular to the longitudinal axis, are complex, and require the knowledge of several other characteristic fiber properties. Nevertheless, a value for $\bar{E}$ was estimated as follows. Of four types of viscose, Meredith (37) gave the lowest value for the initial modulus in tension to be 486.0 g. wt./tex., at 65% R.H. (Courtaulds continuous filament viscose). In terms of the present 4-denier viscose, this is 3.08×10^7 g./sq. cm. Farrow (38) found that the ratio of the initial wet modulus, to that at 65% R.H., is about 0.03 for normal viscose.

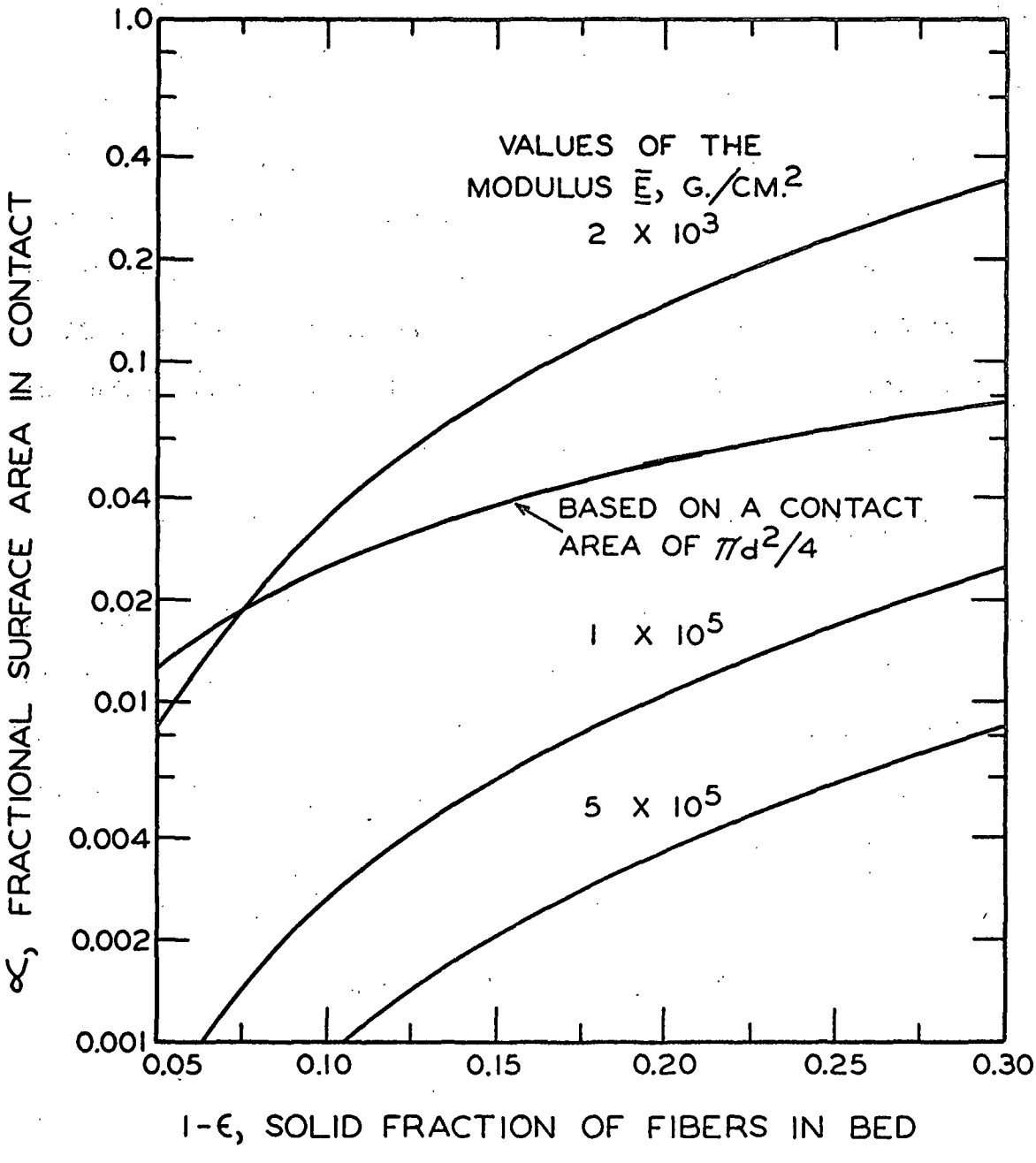

Figure 53. Fractional Surface Area Involved in Fiber-Fiber Contact

Thus, the initial wet modulus in tension is roughly 9×10^5 g./sq. cm. In view of the high degree of anisotropy that characterizes the 4-denier viscose, the initial wet modulus in compression, perpendicular to the fiber axis, could be at least 9 times smaller; thus, let us arbitrarily estimate that $\underline{\bar{E}} = 1 \times 10^5$ g./sq. cm.

It can be seen from Fig. 53 that when $\underline{\bar{E}} = 10^5$ g./sq. cm., the fractional surface area in contact is predicted to be 2.5% at $\epsilon = 0.70$, and only 1% at $\epsilon = 0.80$. In these cases the effect of contact area on Sh would be essentially negligible. In view of the numerous simplifying assumptions involved, it seems best to view this result as a rough estimate, however. The previously illustrated cross-section photomicrographs indicate quite clearly that surface irregularities can contribute considerably to contact area.

EFFECT OF RELATIVELY STAGNANT REGIONS

It seems likely that fiber surface areas near intimate fiber contacts would tend to be relatively ineffective for mass transfer, since conditions are favorable for fluid stagnation at these points. If it is assumed that the ineffective surface area, about an intimate contact, is proportional to the predicted contact area when a purposely low value for the modulus is used, the effect of the stagnant regions can be roughly accounted for by this means.

CORRELATION OF MASS TRANSFER RESULTS

The experimentally determined Sh are plotted in Fig. 54, as a function of $\underline{Pe}\ \epsilon^3$. It is apparent that the diacetyl-64 denier viscose results are considerably displaced from the results on the PAA-1, 4, and 16-denier systems. It is further evident that (a) the experimentally determined Sherwood number exhibited

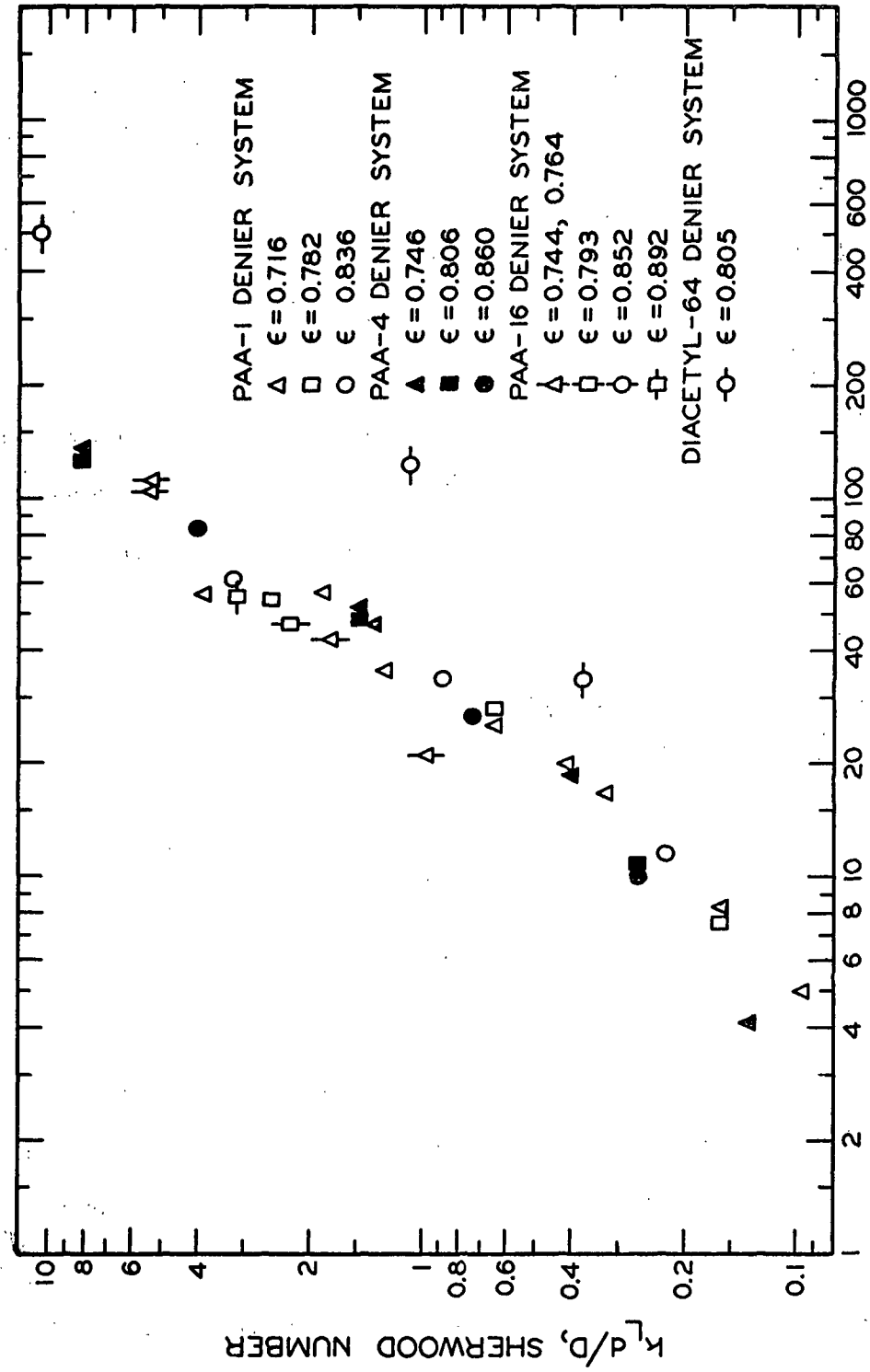

Figure 54. Correlation of Mass Transfer Results

a much stronger dependence on U than predicted by the "free surface model," and (b) the experimental relationship between Sh and Pe ϵ^3 was independent of ϵ, which is contrary to the results of the "free surface model."

The experimentally determined Sherwood numbers were plotted against a modified Reynolds number, $dU\rho\epsilon^3/\mu$, in Fig. 55 (despite the fact that Sh was predicted to be independent of density and viscosity, by the "free surface model") since this correlation is useful for comparing mass transfer data on multiparticle systems under dynamically similar conditions. It is noted that the range of $dU\rho/\mu$ in the PAA-viscose systems was about 0.006-0.2, which represents the regime of very low Reynolds numbers. The disagreement between results in the diacetyl system and the PAA systems is greater in this case than in the previous correlation, where a modified Peclet number was employed as the dependent variable.

If the observed mass transfer differences between the diacetyl-64 denier system and the PAA-viscose systems were due only to differences in fiber diameter and rates of molecular diffusion, we might expect from previous considerations that the respective experimental Sh vs. Pe relationships should coincide at a given porosity level. The fact that the diacetyl system was observed to be a significant exception, suggests that additional system parameters have an important effect on fiber-fluid mass transfer.

An analysis of the factors which determine k_L is difficult in the present systems. Some complexities become apparent when one remembers that k_L describes an average mass transfer rate that is experienced under unsteady-state conditions. At the present time our knowledge of the differences between quasi steady-state and unsteady-state mass transfer is insufficient to evaluate the importance of this factor. That k_L adequately described wide ranges of the breakthrough curves

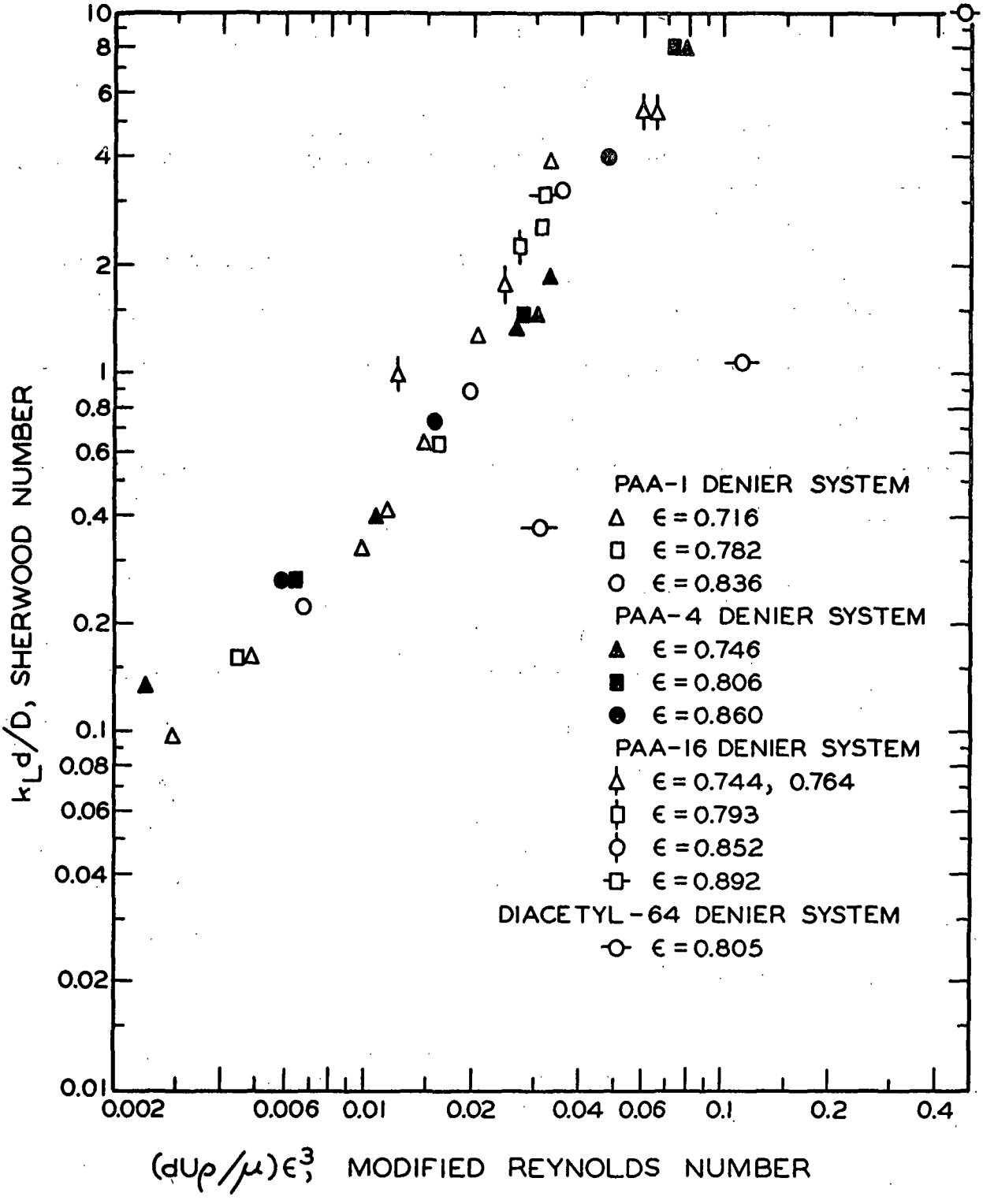

Figure 55. Correlation of Mass Transfer Results

was encouraging support for the simplified treatment of Case 2(F); on the other hand, this result may have been merely a consequence of the averaging process. An additional unknown is that fiber beds exhibit considerably wider pore size distributions than found in granular systems (39). Although it is suspected that this factor had an important effect on the properties of the k_L vs. U and ϵ relationships, no proof can be offered at this time.

It seems likely that a significant breakthrough in understanding may not be attained until (a) the effects of a pore size distribution can be accounted for, and (b) the fiber-fluid mass transfer process is treated in terms of unsteady-state molecular diffusion. In the absence of this development, it was not possible to extend the analysis of mass transfer results further without resorting to purely empirical means.

EMPIRICAL RELATIONSHIPS

A number of empirical relationships were tested in an attempt to achieve a more satisfactory correlation of the mass transfer results in the PAA-1, 4, and 16-denier systems, and the diacetyl-64 denier system. Unfortunately, it was not possible to evaluate the separate effects of D'_F, d, and K empirically, since both D'_F and K were found to vary with d. It was speculated, however, that the parameter D'_F/d might be useful in initial attempts at relating the results, since D'_F/d is one of the parameters which characterizes the mass transfer flux (in terms of surface area) from a fiber surface.

By assuming that the Sh vs. Pe relationship is basically correct, a modified correlation of

$$\frac{k_L d}{D} \quad \text{vs.} \quad \left[\frac{Ud}{D}\right] \left[\frac{d}{D'_F}\right] \epsilon^3 \tag{78}$$

was plotted, as shown in Fig. 56. It is noted here that a reasonably good correlation was obtained for all the data, but the respective systems defined curves of different slope. Also, the use of $\underline{d}/\underline{D'_F}$ makes the abscissa dimensional.

In Fig. 57, a correlation is shown of

$$k_L \ \underline{vs.} \ \left[\frac{dU\rho}{\mu}\right] \left[\frac{D}{D'_F}\right] \epsilon^3 \qquad (79).$$

In this case it is noted that the various systems are reasonably well correlated, but the relationships for each system are slightly displaced with respect to the independent variable. A similar correlation is shown in Fig. 58, where the porosity function $\underline{f}(\epsilon) = \epsilon/(1 - \epsilon)$ was employed, although it was previously shown to be inferior to $\underline{f}(\epsilon) = \epsilon^3$.

Finally, the modified $\underline{j}$ factor was correlated with a modified Reynolds number in Fig. 59. It was previously discussed, from Pfeffer and Happle's results, that it is incorrect to employ this correlation at low Reynolds numbers, since $\underline{j}_\epsilon$ was predicted to vary with $\underline{Sc}$. Since $\underline{Sc}$ was constant in the PAA-1, 4, and 16-denier systems, however, it is apparent that the $\underline{j}$ factor correlation is basically inadequate for correlating mass transfer data on the present systems.

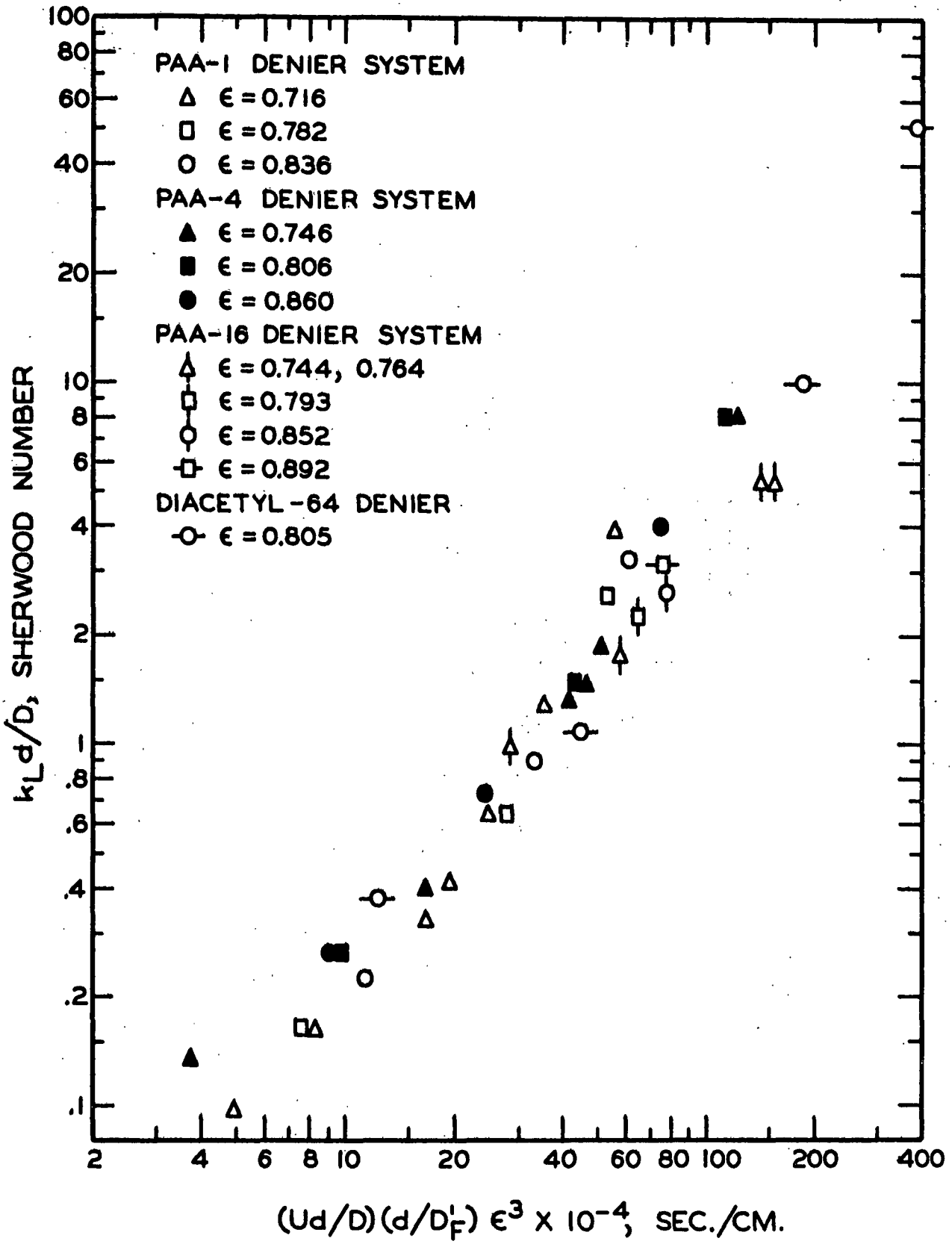

Figure 56. Correlation of Mass Transfer Results

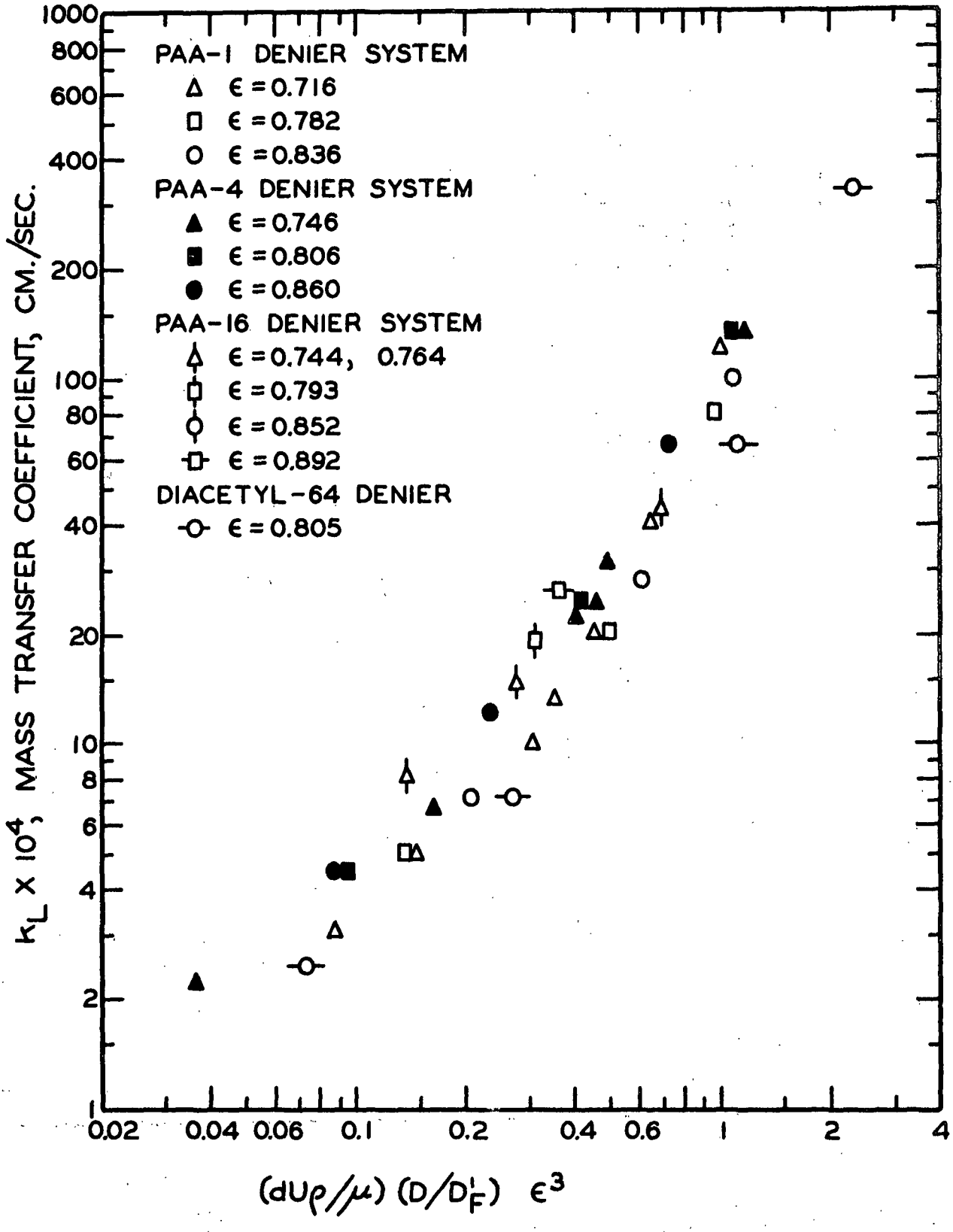

Figure 57. Correlation of Mass Transfer Results

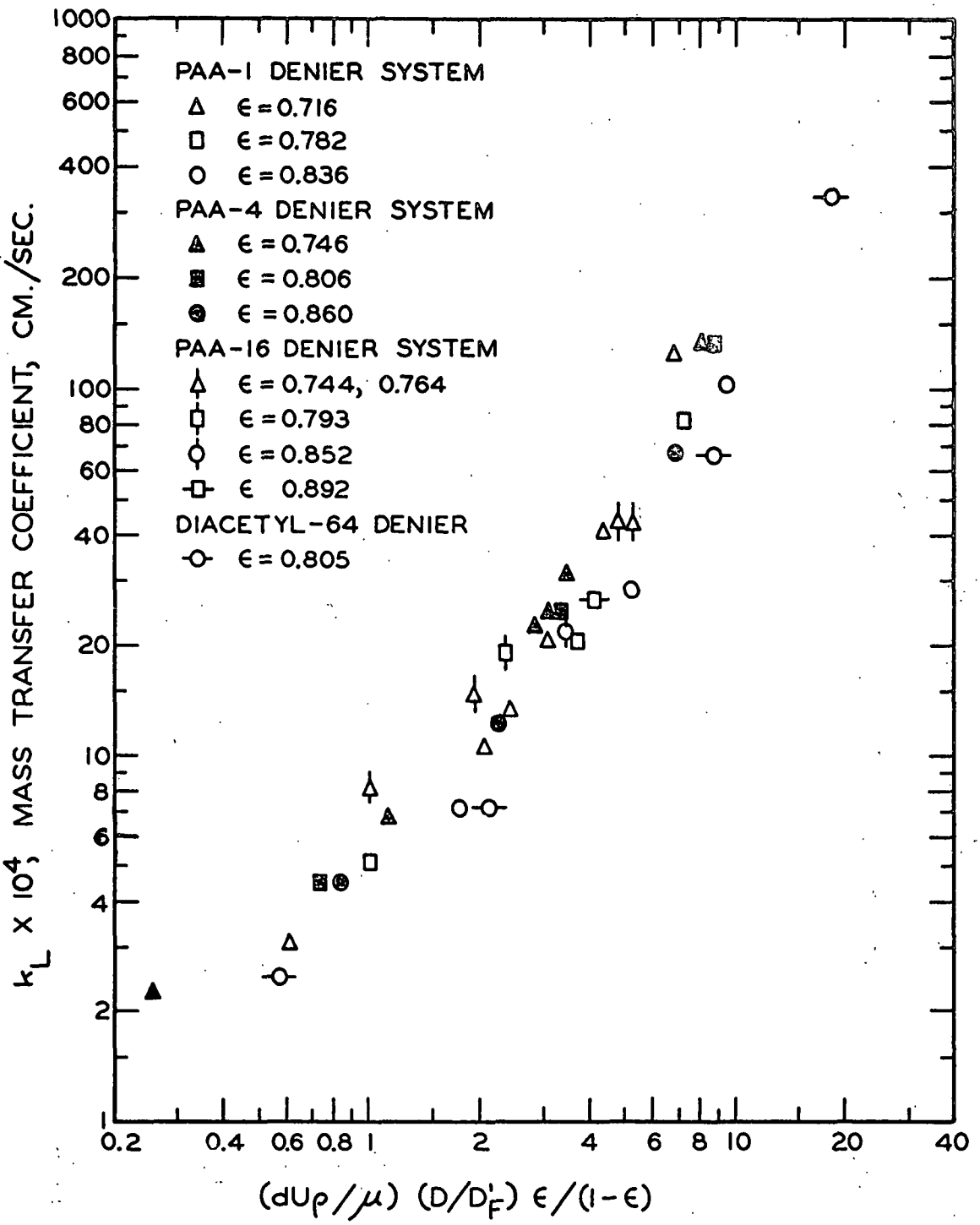

Figure 58. Correlation of Mass Transfer Results

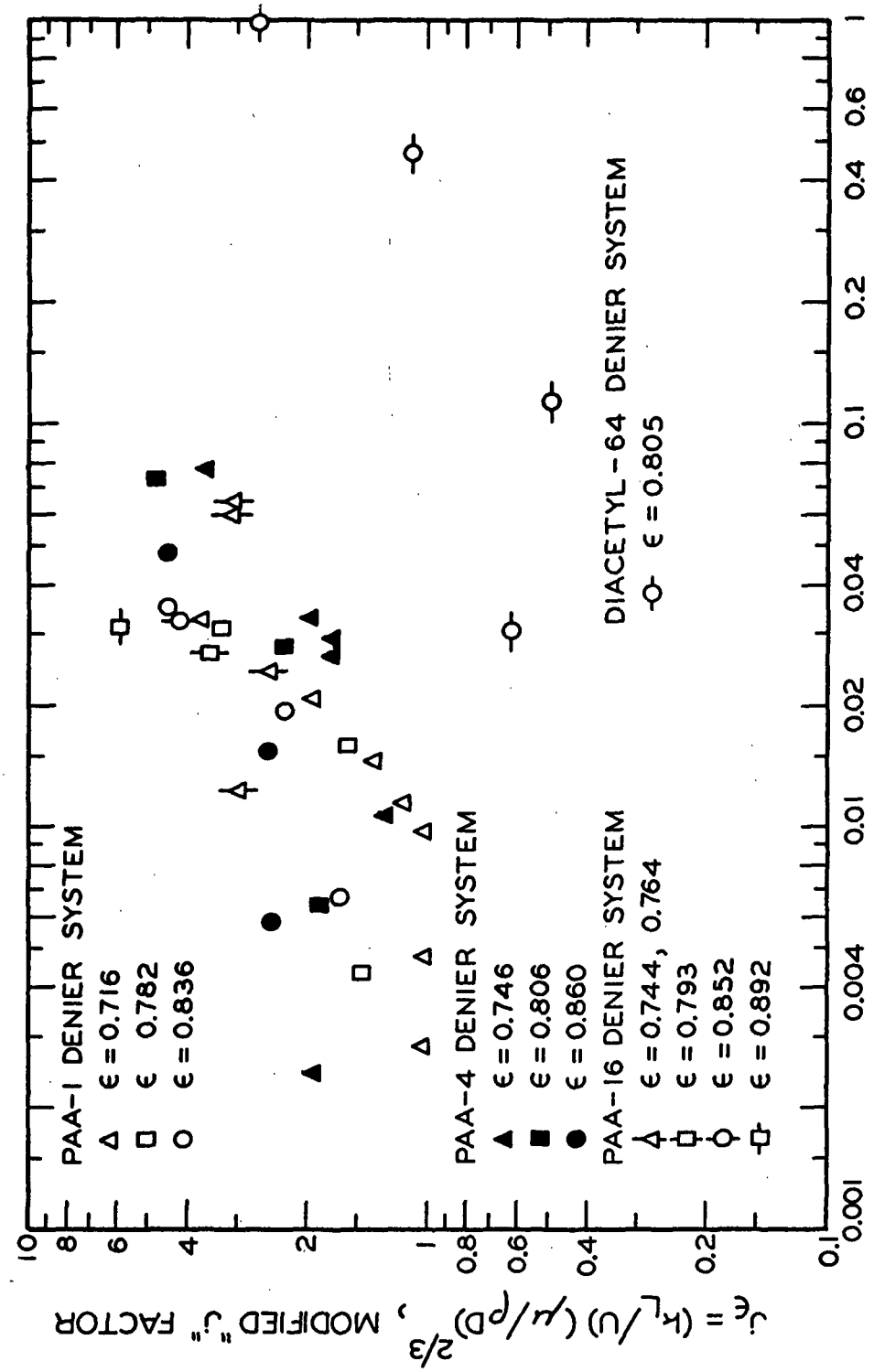

Figure 59. Correlation of Mass Transfer Results

SUMMARY AND CONCLUSIONS

Mathematical models of the desorption (and sorption) washing process were developed to describe the movement of an adsorbable solute in the intraparticle pores and interparticle channels of a bed of porous particles during fluid flow. These models account for three simultaneous rate phenomena, described as (a) longitudinal dispersion of fluid, according to the usual one-dimensional differential equation, (b) intraparticle Fick's-law diffusion of a solute which is linearly adsorbed by the solid phase, and (c) liquid-phase mass transfer from particle surfaces, assuming a driving force equal to the surface minus bulk concentration. Analytical solutions of the partial differential equations were obtained to permit calculation of exit-concentration breakthrough curves. The initial conditions correspond to bed saturation and sorption equilibrium at a uniform concentration; the inlet boundary condition for the wash fluid is a modified step-function, expressed as an exponentially damped polynomial with arbitrary coefficients. The most refined models, Cases 2(F) and 2(S), account for all three phenomena and apply to cylindrical and spherical particle geometries, respectively. Cases 1(F) and 1(S) account for longitudinal dispersion and intraparticle diffusion, but are based on the assumption that no mass transfer resistance exists at the particle surfaces. The Equilibrium and No-Sorption cases, which are essentially the same as those derived by Sherman (1), both account for longitudinal dispersion but represent infinitely rapid and infinitely slow intraparticle diffusion cases, respectively. Finally, a simple first-order chemical reaction case was derived that accounts for surface reactions and/or intraparticle reactions, when intraparticle diffusion is described by the Equilibrium case.

The experimental technique for a washing experiment first involved saturation of a mechanically compressed fiber bed with dye solution until sorption equilibrium was attained at concentration $\underline{C}_o$. A desorption displacement was then commenced by flowing water through the bed at a uniform rate. Both the inlet and exit solute concentrations, $\underline{C}$, were measured as a function of $\underline{R}$, the number of pore volumes of fluid displaced. Although the inlet concentration decreased very rapidly to zero as an approximate step-function, it was still necessary to account for this nonideality in the subsequent analysis. The immediate objective of the analysis was to fit the resulting $\underline{C}/\underline{C}_o$ vs. $\underline{R}$ exit-concentration breakthrough curves with predicted curves from the appropriate mathematical models. By performing a number of trial and error calculations it was eventually possible to evaluate the desired washing parameters which resulted in "best fits" of the breakthrough curves.

It was shown that sorption washing experiments, where a bed is initially saturated with water and subsequently "washed" with dye solution, could also be described and analyzed by a simple modification of the cases for desorption washing.

The experimental fiber systems consisted of 1, 4, 16, and 64-denier all-skin viscose, which had approximately circular cross sections. The solutes consisted of (a) diacetyl, which was not appreciably adsorbed on viscose and is nonionic, (b) p-phenylazoaniline (PAA), which was linearly adsorbed, having a partition coefficient of about 9, and is nonionic, and (c) Benzopurpurine 4B (BPP), an ionic direct dye of relatively high molecular weight. The pertinent experimental ranges included the porosity range $0.7 < \epsilon < 0.9$; the Reynolds number range $0.006 < \underline{dU}\rho/\mu < 1.8$; and the Peclet number range $10 < \underline{Ud}/\underline{D} < 2000$. The Schmidt number, $\mu/\rho\underline{D}$, was about 1700 in the PAA systems, and 1100 in the diacetyl systems.

The longitudinal dispersion properties of the various fiber beds were determined independently by applying the Equilibrium case to the diacetyl-1 and 4 denier systems, and the No-Sorption case to the BPP-16 denier system. It was generally possible to find a value for the longitudinal dispersion coefficient, D_L, that resulted in a satisfactory fit of a given breakthrough curve over the entire exit-concentration history. Thus, the longitudinal dispersion of fluid was adequately described by the usual one-dimensional diffusionlike differential equation. Any radial dispersion and/or wall effects that occurred were absorbed by the treatment and included as part of the longitudinal dispersion effect.

This writer's results on the viscose fiber systems, and Sherman's results on the dacron (nonporous) and viscose systems, indicated that D_L was directly proportional to the linear pore velocity U. The constancy of D_L/U with U has been predicted theoretically for miscible displacements where streamline flow prevails, and where radial and axial (intrachannel) molecular diffusion effects are negligible. Thus, the results suggest that molecular diffusion effects were relatively unimportant in the present systems.

Results from the 4- and 16-denier systems indicated that D_L/U was approximately proportional to d, when ϵ and the fiber-length-to-diameter ratio, ℓ'/d, was the same; it was also demonstrated that D_L/U was roughly proportional to ϵ in the 4-denier system. By tentatively assuming that the above results applied throughout, $D_L/Ud\epsilon$ was plotted against ℓ'/d. That $D_L/Ud\epsilon$ increased from 5 to 75, over the ℓ'/d range 50-400, indicated that ℓ'/d had a strong effect on the bed structural properties which determined the extent of longitudinal dispersion. The constancy of D_L/Ud, when ϵ and ℓ'/d were constant, suggested that viscose beds of different fiber diameter are geometrically similar under these conditions; further experimental evidence is necessary to confirm this, however.

Intrafiber diffusion Case 1(F), which was derived on the assumption that no mass transfer resistance exists in the fluid, was applied to the PAA-1, 4, and 16-denier systems, and the diacetyl-64 denier system. It was found that (a) satisfactory fits of the breakthrough curves were generally obtained, (b) the resulting apparent intrafiber diffusion coefficients, $(\underline{D}_F)_A$, increased with $\underline{U}$ to approximately asymptotic values, $\underline{D}_F$, in each given system, and (c) breakthrough curves from two different 16-denier beds were reproducible within 2% or better. It was apparent that, in velocity regions where $(\underline{D}_F)_A < \underline{D}_F$, the fiber boundary condition for Case 1(F) was physically unsatisfactory, and thus a finite mass transfer resistance existed in the fluid adjacent to the fiber surfaces; this region was characterized by the fact that both intrafiber diffusion and intrachannel mass transfer were important. In the higher velocity regions, where $(\underline{D}_F)_A \cong \underline{D}_F$, intrafiber diffusion was the rate-controlling step.

Although significant nonuniform porosity distributions resulted from relatively high fluid pressure drops in some washing runs, it was demonstrated that (a) the porosity distributions were nearly linear, and (b) the breakthrough curves from these runs, and the subsequent analyses, were not significantly affected by the porosity distributions when the average bed porosity was used as a calculation parameter. Although this result was only calculated, and was not experimentally demonstrated, it was considered good evidence that nonuniform porosity distributions did not contribute significantly to the interparameter relationships that were observed.

Intrafiber diffusion was affected by average porosity changes in the region where both intrafiber diffusion and liquid-phase mass transfer were controlling. A significant increase in $(\underline{D}_F)_A$ with ϵ evidenced the importance of particle-particle interaction effects which are normally unaccounted for in mass transfer considerations.

It also appeared possible that particle-particle interactions (such as physical contact) influenced the effective rate of intrafiber diffusion that was ultimately achieved at high flow rates. Some independent evidence for this behavior was obtained from a number of sorption rate experiments on well-stirred fiber slurries. The resulting value for $\underline{D}_F$, in the PAA-16 denier system, was found to be approximately twice the value obtained from washing experiments at $\epsilon = 0.76$. Although one would expect to find $\underline{D}_F$ increasing with ϵ, in the washing experiments, this point was difficult to confirm. The best direct evidence for this behavior was found in the PAA-4 denier system, where $\underline{D}_L$ was determined independently at all three porosity levels. Here $\underline{D}_F$ appeared to increase slightly with ϵ (by extrapolation) over the range $0.75 < \epsilon < 0.86$, although the experimental evidence was somewhat incomplete. A similar trend was found in the PAA-1 denier system, over the porosity range $0.72 < \epsilon < 0.84$, but here the result was less certain since $\underline{D}_L/\underline{U}$ was determined independently only at the lowest porosity level. In the PAA-16 denier system, where $\underline{D}_L$ was again determined at only the lowest porosity level, $\underline{D}_F$ appeared to be essentially constant over the porosity range $0.74 < \epsilon < 0.89$; a subsequent reconsideration of this result, however, indicated that $\underline{D}_L$ may have increased with ϵ, in which case a revised analysis would yield a $\underline{D}_F$ that increased with ϵ.

The approximately asymptotic intrafiber diffusion coefficients, $\underline{D}_F$, that best represented each solute-fiber system at all the experimental porosity levels, were assumed to characterize the real diffusion behavior of these systems in the presence of whatever fiber-fiber contact effects that might exist. These values were used in Case 2(F) to reanalyze all the breakthrough curves that were previously characterized by the condition $(\underline{D}_F)_A < \underline{D}_F$. Here it was found that (a) equally satisfactory fits of the breakthrough curves were obtained, in comparison

to those from Case 1(F), (b) the resulting mass transfer coefficients, $\underline{k_L}$, increased rapidly with $\underline{U}$ to large values at relatively high velocities, and (c) $\underline{k_L}$ increased with ϵ. The effect of porosity was rectified empirically in the respective PAA-1, 4, and 16-denier systems when $\underline{k_L}$ was plotted against $\underline{U}\epsilon^3$.

A number of sorption washing runs were performed on the PAA-1, 4, and 16-denier systems, and analyzed in essentially the same manner as the previous desorption runs. The respective washing parameters, $\underline{D_L}$, $(\underline{D_F})_A$, $\underline{D_F}$, and $\underline{k_L}$ that applied, were found to be described by the same interparameter relationships that characterized the desorption washing runs. This was considered good evidence that (a) the intrafiber diffusion process obeyed Fick's law to a good approximation, and (b) the mechanisms responsible for longitudinal dispersion and liquid-phase mass transfer were not concentration dependent.

The generally observed fact that Cases 1(F) and 2(F) resulted in equally adequate and nearly identical fits of the breakthrough curves, indicated that neither model had a predictive advantage over the other. From the standpoint of physical reality, however, Case 2(F) was clearly more appropriate since only one value of $\underline{D_F}$ was required to characterize each solute-fiber system, regardless of $\underline{U}$.

An empirical relationship was found to exist between $(\underline{D_F})_A$ of Case 1(F) and $\underline{k_L}$ of Case 2(F). This relationship applied over the range, $0.2 < (\underline{D_F})_A/\underline{D_F} < 1$, and it appeared to be essentially independent of porosity and the nature of the solute-fiber systems involved.

Although the intrafiber diffusion coefficient, $\underline{D_F}$, was used to characterize washing behavior, the differential equations for intrafiber diffusion and fiber-fluid mass transfer were actually based on an intrapore diffusion coefficient,

$\underline{D}'_{\underline{F}}$. The equivalence between the two was shown to be $\underline{D}'_{\underline{F}} = \underline{D}_{\underline{F}}\underline{K}/\epsilon'$, where $\underline{K}$ is the partition coefficient of the solute-fiber system and ϵ' is the internal porosity of the swollen fiber. If the very likely assumption is made that true surface diffusion, of adsorbed solute, contributes negligibly to the rate of solute movement, then the use of $\underline{D}'_{\underline{F}}$ permits a more meaningful comparison of intrafiber diffusion phenomena with (a) molecular diffusion, and (b) intrafiber diffusion in different solute-fiber systems, since the instantaneous rate of solute movement is always based on a solution concentration driving force, and is independent of the degree of solute adsorption.

A number of conclusions were evident from the intrapore diffusion coefficients which were obtained from the washing experiments. That the $\underline{D}'_{\underline{F}}$ values were considerably smaller than the respective molecular diffusion coefficients of PAA and diacetyl, was in accordance with the concept of diffusion in a swollen solid. That the $\underline{D}'_{\underline{F}}$ values for PAA were relatively smaller than those for diacetyl, was expected from the larger size of the PAA molecule, and also its greater affinity for viscose. That (a) the $\underline{D}'_{\underline{F}}$ values of the PAA-1, 4, and 16-denier systems were observed to increase with fiber diameter, and (b) the respective crystallite orientations of the fibers decreased with increasing fiber diameter, were shown to be in qualitative agreement with previously published results on direct dye-viscose systems.

Considerable caution should be exercised in applying intraparticle diffusion cases to multiparticle beds when the particle size and shape varies. For example, it was indirectly demonstrated that Cases 1(F) and 2(F) would probably yield good agreement with experimental breakthrough curves from beds of spheres or slabs, when Fick's law is obeyed. Similar considerations apply to beds having a particle size distribution. Thus, the resulting intraparticle diffusion coefficient is

not strictly meaningful unless the exact geometry of discrete particles, or particle units, is known and accounted for by the appropriate diffusion equation.

The experimental observations that $\underline{k}_{\underline{L}}$ varied approximately as $\underline{U}^{1.2}$ and ϵ^{3}, in all the systems that were analyzed according to Case 2(F), suggest that unsteady-state mass transfer in the present systems is a complex phenomenon involving a number of interaction effects.

SUGGESTIONS FOR FUTURE RESEARCH

1. Study the effect of radial dispersion in synthetic fiber beds. Information on this property would be important to our understanding of the flow structure in fiber beds. Harleman and Rumer (40) have recently discussed the theoretical and experimental aspects of radial dispersion; experimental results were given for both longitudinal and radial dispersion in a bed of spheres.

2. Extend the present work to beds of classified pulp fibers, using diacetyl to determine the longitudinal dispersion properties, and PAA to determine the intrafiber diffusion and liquid-phase mass transfer properties. It seems likely that the longitudinal dispersion effect would be especially strong in pulp fiber beds, due to the inherently wide pore size distribution. An important aspect of this study would be to test the effective applicability of intrafiber diffusion cases, 1(F) and 2(F). It is likely that changes in fiber geometry, with bed compaction, would result in significant changes in the effective intrafiber diffusion coefficient with bed porosity.

3. Apply the intrasphere diffusion cases, 1(S) and 2(S), to a suitable system such as an adsorption column or an ion exchange column. A number of aqueous ion-resin systems are well described by Fick's law diffusion (41). One important feature in this work would be to examine the velocity dependence of the mass transfer coefficient. Previous studies in ion-exchange systems (a) have evaluated liquid-phase mass transfer coefficients that are based on unrealistic driving forces (e.g., the difference between the average intraparticle solute concentration and the bulk solution concentration), and/or (b) have neglected longitudinal dispersion. Both of the above simplifications tend to falsify the velocity dependence of the liquid-phase mass transfer coefficient,

in certain velocity regions, and thus the interpretations of many published results are subject to question.

4. Extend the present investigation of longitudinal dispersion in synthetic fiber beds, and examine, in greater detail, the effects of fiber length, fiber diameter, and bed porosity. The use of nonporous fibers would considerably simplify the analysis by eliminating the effects of solute exchange from the fibers. Comparisons of results from miscible displacements with those from immiscible displacements (using liquids with a relatively large interfacial tension) may help to define the relative importance of (a) purely geometrical effects, and (b) the combined effects of molecular diffusion and radial velocity variations in flow channels. An objective in this study would be to achieve a more complete characterization of fiber bed structure.

5. Extend the present work to achieve a detailed description of intrafiber diffusion and liquid-phase mass transfer in the PAA-64 denier system. The longitudinal dispersion properties could be evaluated independently by using a very slowly diffusing dye such as Benzopurpurine 4B. The high degree of circularity and relatively large size of the 64-denier fibers would provide a very well-defined system; an independent determination of the intrafiber diffusion coefficient, in a well-stirred fiber slurry, would be relatively easy in this case. An important objective in this study would be to examine the effects of bed porosity on intrafiber diffusion and liquid-phase mass transfer. In doing so it might be possible to explain the unresolved discrepancy (concerning the possible variation of $\underline{D}_F/\underline{a}^2$ with ϵ) that was observed in the PAA-16 denier system of this work. Direct measurements of the variation of fiber deswelling with compaction might be necessary to support the results obtained.

NOMENCLATURE

A = local intrafiber solute concentration, mg./cc. fiber (cc. fiber refers to volume enclosed by external surface of fiber)

$\hat{A}$ = cathetometer reading of slit upper edge (inlet), cm.

A_c = cross section area of bed, 43.54 sq. cm.

A'_c = intimate contact area between fibers, sq. cm.

A_n = a factor which characterizes a specific intraparticle diffusion case when defined, dimensionless

A_t = total external surface area of fibers in a bed, sq. cm.

$\overline{AA}$ = a characteristic bed dimension, cm.

a = $d/2$, radius of a circular cylinder or sphere, cm.

a_c = radius of a circular capillary, defined for circular capillary permeability model as $d\epsilon/2(1 - \epsilon)$

a_e = effective radius of a particle

B = $1 + K(1 - \epsilon)/\epsilon$

$\hat{B}$ = cathetometer reading of slit lower edge, cm.

$\overline{BB}$ = a characteristic bed dimension

b = coefficient of the imaginary number i

C = $C(Z,t)$, average solute concentration in fluid, mg./cc. solution

$\bar{C}$ = transformed variable with respect to time; resulting from C

$\hat{C}$ = cathetometer reading of screen upper edge, cm.

C' = mat consistency, g., o.d. fiber/cc.

C_D = concentration of dye solution added, mg./cc.

C_I = a designated constant

C_n = solution concentration at stage n, mg./cc. solution

C_t = solution concentration at time t, mg./cc. solution

C'_t = total number of fiber-fiber contacts in a bed

C_o = initial (uniform) solution concentration, mg./cc. solution

C_∞ = equilibrium solution concentration (after large elapsed times), mg./cc. solution

C/C_o = relative solute concentration, dimensionless

$\overline{CS}$ = chart speed, mm./sec.

c = a characteristic real number

c_z = a local solute concentration at Z, mg./cc. solution

D = molecular diffusion coefficient, sq. cm./sec.

D = intraparticle diffusion coefficient, used as equivalent of D_F and D_S in Appendix I

$\overline{D}$ = dark current value (light blocked off) from which solute, solution, and water values are based

$\hat{D}$ = cathetometer reading of screen lower edge (top of fiber bed), cm.

D' = DK/ϵ', intrapore diffusion coefficient, used as equivalent of D'_F and D'_S in Appendix I

D_F = intrafiber diffusion coefficient, sq. cm./sec.

D'_F = intrapore diffusion coefficient, $D_F K/\epsilon'$, sq. cm./sec.

$(D_F)_A$ = apparent intrafiber diffusion coefficient, sq. cm./sec.

D_F/a^2 = intrafiber diffusion parameter, 1/sec.

$(D_F/a^2)_A$ = apparent intrafiber diffusion parameter, 1/sec.

D_L = longitudinal dispersion coefficient, sq. cm./sec.

D_L/U = mixing parameter, cm.

D_S = intrasphere diffusion coefficient, sq. cm./sec.

d = fiber diameter, cm.

d = coefficient of the imaginary number i

E = area under C/C_o vs. R exit breakthrough curve, dimensionless

$\overline{E}$ = elastic modulus, g. wt./sq. cm.

$\hat{E}$ = cathetometer reading of screen upper edge (bottom of fiber bed), cm.

F = D_F/a^2, intrafiber diffusion parameter, 1/sec.

$\hat{F}$ = cathetometer reading of screen lower edge, cm.

$\underline{F}$ = normal load at a contact, g. wt.

$\underline{f}$ = an integer representing last term in input polynomial

$\underline{f}(\ )$ = a function of the term in brackets

$\underline{\hat{G}}$ = cathetometer reading of slit upper edge (exit), cm.

$\underline{G}(\underline{p})$ = a characteristic function representing a Laplace transform

$\underline{g}$ = $\underline{U}^2/4\underline{D}_{\underline{L}}$

$\underline{\hat{H}}$ = cathetometer reading of slit lower edge, cm.

$\underline{H}(\underline{p})$ = a characteristic function representing a Laplace transform

$\underline{h}$ = $4\underline{D}_{\underline{F}}\underline{K}(1 - \epsilon)/\underline{a}^2\epsilon$

$\underline{h}'$ = $6\underline{D}\underline{K}(1 - \epsilon)/\underline{a}^2\epsilon$

$\underline{I}$ = area under a $\underline{C}/\underline{C}_o$ vs. $\underline{R}$ input curve, dimensionless

$\underline{i}$ = $\sqrt{-1}$, imaginary number

$J_o(\ )$ = zero order Bessel function of term in brackets

$J_1(\ )$ = first order Bessel function of term in brackets

$\underline{j}_\epsilon$ = $(\underline{k}_{\underline{L}}/\underline{U})\ (\mu/\rho\underline{D})^{2/3}$, modified "$\underline{j}$" factor, dimensionless

$\underline{K}$ = partition coefficient, (mg. dye/cc, fiber)/(mg. dye/cc. solution)

$\underline{K}'$ = $\underline{K}(1 - \epsilon)/\epsilon$

$\underline{K}''$ = partition coefficient, (mg. dye/g. fiber, o.d.)/(mg. dye/cc. solution)

$\underline{K}_{\underline{I}}$ = partition coefficient determined from adsorption isotherm, same units as $\underline{K}$

$\underline{K}_{\underline{S}}$ = partition coefficient determined from sorption rate experiment, same units as $\underline{K}$

$\underline{K}_{\underline{W}}$ = partition coefficient determined from washing experiment, same units as $\underline{K}$

~~$\underline{k}$ = local mass transfer, coefficient, cm./sec.~~

$\underline{k}$ = Kozeny factor, dimensionless

$\underline{k}^*$ = reaction rate constant for first-order reaction, (mg./cc.-fiber sec.)/(mg./cc. solution)

$K'' = K(1 - \epsilon)/\epsilon$

k_L = mass transfer coefficient, cm./sec.

k_b = Beer's law constant

k_n = $k'_n(Z/U)^n$, an input constant, dimensionless

$\bar{k}_n$ = a proportionality factor which is a function of n

k'_n = an input constant

k_o = an input constant, dimensionless

L = ak_L/D'_F, mass transfer parameter, dimensionless

L' = total length of timing trace, mm.

ℓ = length of a circular capillary

ℓ' = fiber length

$\mathcal{L}$ = symbol used to denote a Laplace transform

M = a dimensionless expression in the washing equation which characterizes a specific case when defined

$\bar{M}$ = an empirical constant describing the compressibility of a fiber bed

M_n = the n'th moment of a residence time distribution, with respect to the origin

M_w = estimate of the solute ratio; calculated as the difference in areas under the C/C_o vs. R exit and input curves

M_o = solute ratio, or ratio of solute in a fiber bed system to that contained in the interfiber voids; calculated as $1 + (1 - \epsilon_E)K_I/\epsilon_E$

N = a dimensionless expression in the washing equation which characterizes a specific case when defined

$\bar{N}$ = an empirical constant describing the compressibility of a fiber bed

n = an integer

$\bar{n}$ = mean number of random walk steps

$\tilde{n}$ = $\sqrt{\bar{n}}$

P = local intrapore solute concentration, mg./cc. solution

ΔP = over-all fluid pressure drop, dyne/sq. cm.

P_s = static compacting pressure, dyne/sq. cm.

Pe = Ud/D, modified Peclet number, dimensionless

p = a real number which appears in a Laplace transform

Δp = incremental fluid pressure drop, dyne/sq. cm.

Q = average intrafiber solute concentration, mg./cc. fiber

Q_F = Q_t/Q_∞, fractional sorption of solute at time t, dimensionless

Q_n = equilibrium dye concentration in fibers at a solution concentration C_n, mg./cc. fiber

Q_t = intrafiber solute content at time t, mg./cc. fiber

Q_w = volume of fluid displaced from a bed, cc.

Q_o = initial dye concentration in fibers at equilibrium, mg./cc. fiber

Q_∞ = intrafiber solute concentration at equilibrium (after large elapsed times), mg./cc. fiber

q = $(Z^2/D_L)^{1/2}$

q' = flow rate of fluid, cc./sec.

q_n = dye sorbed by fibers in going from stage n-1 to stage n, mg.

Δq_n = dye sorbed by fibers in going from stage zero to stage n, mg.

q_t = dye sorbed by fibers during the elapsed time t, mg.

q_o = dye sorbed by fibers initially, mg.

q_∞ = dye sorbed by fibers at equilibrium, mg.

R = gas constant

R = Ut/Z_e, pore volumes of fluid displaced; based on a bed of porosity ϵ, and length Z_e; dimensionless

R_F = total pore volumes of fluid displaced in a washing run

R_o = an assigned constant designating horizontal shift in R, dimensionless

R_1 = $R - R_o$

R_2 = $R_1 \bar{\epsilon}_1/\bar{\epsilon}_2$

R_2' = $(R_2 + R_o)(\bar{\epsilon}_2/2\epsilon)$

r = a characteristic radial distance, cm.

$\underline{r}$ = $(\underline{c}^2 + \underline{d}^2)^{1/2}$, length of radius vector

$\underline{S}$ = $\underline{D_L}/\underline{UZ_e}$, dispersion parameter, dimensionless

$\overline{\underline{S}}$ = solute value, representing light transmission when a bed is saturated with solute at $\underline{C_o}$ or $\underline{C_\infty}$

$\underline{S'}$ = local adsorbed solute concentration, mg./cc. fiber

$\underline{S_v}$ = $4/\underline{d}$, specific surface of a long circular cylinder, 1/cm.

$\underline{Sc}$ = $\mu/\rho\underline{D}$, Schmidt number, dimensionless

$\underline{Sh}$ = $\underline{k_L d}/\underline{D}$, Sherwood number based on characteristic diameter, dimensionless

$\underline{Sh_o}$ = $\underline{k_L d}/\underline{D}$ at zero fluid velocity (stagnant medium), dimensionless

$\underline{s}$ = a real number

$\underline{T}$ = temperature, °C.

$\underline{t}$ = time, sec.

$\underline{t_F}$ = total duration of a washing run, sec.

$\underline{U}$ = average linear pore velocity based on ϵ, cm./sec.

$\underline{U_s}$ = superficial velocity based on $\underline{A_c}$, cm./sec.

$\underline{u_z}$ = a local velocity in axial direction, cm./sec.

$\underline{V}$ = water-swollen specific volume of fibers, cc. fiber/g., o.d.

$\underline{V_B}$ = void volume of fiber bed only, cc.

$\underline{V_D}$ = volume of dye solution added, cc.

$\underline{V_S}$ = volume of solution, initially, cc.

$\underline{V'_S}$ = volume of solution after sample is taken at time $\underline{t}$, cc.

$\underline{V_T}$ = total void volume of fiber bed system included between the inlet and exit light paths, cc.

$\underline{V_{VSP}}$ = void volume of valve, screens and piston, cc.

$\underline{V_p}$ = pycnometric specific volume, or volume of fiber denied to water per gram of ovendry fiber, cc./g., o.d.

$\underline{V_s}$ = solution volume in a finite dyebath, cc.

$\underline{V_\phi}$ = effective volume of cellulose phase, cc./g., o.d.

$\overline{W}$ = water value, representing light transmission when a bed is saturated with water at zero solute concentration

W_F = fiber mass, g., o.d.

W_t = mass of fiber plus solution after sample has been taken at time t, g.

W_o = mass of fiber plus water initially, g.

X_n = R^n

Y = $(C(O,R)/C_o)\exp(\gamma R)$

$(Y)_n$ = solution value, n 5-mm. increments from time zero, representing light transmission at inlet (I) or exit (E)

Z = axial distance from top of bed, cm.

$\overline{\Delta Z}$ = $U\tau$, average displacement of fluid elements in the time increment, cm.

Z_e = axial distance representing length of bed, cm.

Z_E = effective axial distance between inlet and exit light paths, cm.

Greek Letters

α = fraction of fiber surface area (external) involved in fiber-fiber contact

α_n = n'th root of a designated equation

β_n = n'th root of a designated equation

γ' = a constant in exponential of input expression

γ = $\gamma'(Z_e/U)$, a constant in exponential of input expression

Δ = an incremental distance, in the Z direction, traveled by a fluid element undergoing convection

$\Delta\mu^o$ = affinity of a dye for a substrate, defined as the change in standard chemical potential

ϵ = average bed porosity, or void fraction, cc. voids/cc. bed

ϵ' = porosity of a swollen fiber, cc. voids/cc. fiber

ϵ_1 = porosity at top of bed

ϵ_2 = porosity at bottom of bed

$\bar{\epsilon}_1$ = average porosity of top half of a bed

$\bar{\epsilon}_2$ = average porosity of bottom half of a bed

$\epsilon_{\underline{E}}$ = effective porosity of a bed system, total cc. voids/total cc. bed system

η = dimensionless variable of integration

θ = angle, radians

λ = variable of integration representing time, sec.

λ' = ratio of fluid volume to effective fiber volume in a well-stirred dyebath of finite size, dimensionless

μ = viscosity, poise

υ = Poisson's ratio

π = 3.14159 . . ., Pi

ρ = density of water, g./cc.

σ^2 = variance of $\Phi(\Delta)$

$\sigma_{\underline{n}}$ = standard deviation of $\Phi(\Delta)$ after flow through $\underline{n}$ particle layers

τ = time interval, sec.

$\Phi(\Delta)$ = frequency function of Δ

ϕ = angular co-ordinate

$\phi(\underline{t})$ = solution concentration expressed as an arbitrary function of time, mg./cc. solution

ψ = $(\underline{M}^2 + \underline{N}^2)^{1/2}$, dimensionless

ω = dimensionless variable of integration

ACKNOWLEDGMENTS

The author expresses his acknowledgment to Dr. William R. Sherman, whose Ph.D. thesis provided the basic development and logical approach underlying this work, and whose inspiration and guidance in numerous conversations was greatly appreciated.

The author extends further acknowledgment to his advisory committee: Dr. W. L. Ingmanson, Chairman, and Drs. H. D. Wilder, and R. W. Nelson, whose guidance and objective criticisms were especially helpful. Special appreciation is extended to Dr. Nelson, with whom the author had many enlightening discussions concerning the mathematical details.

Aid from the following people is also gratefully acknowledged: Mr. John Hankey and Mrs. Marguerite Davis for obtaining the photomicrographs; Dr. Carl Jentzen for his assistance in obtaining the x-ray diffraction patterns; Mr. L. Dearth and Mr. W. Shillcox for assistance with the optical system; Mr. John Bachhuber for his guidance and assistance with the computations; Dr. John Happle for supplying a recent revised copy of the paper presented by Pfeffer and Happle (34).

The author is especially grateful to Mrs. Lea Pellett, who typed the manuscript, and who exerted the continuous patience and understanding that made this work possible.

Finally, the author wishes to thank all those responsible for making The Institute of Paper Chemistry scholarship fund available, and those whose efforts maintain the fine research environment in which he was privileged to carry out his investigation.

LITERATURE CITED

1. Sherman, William R. The movement of a soluble material during the washing of a bed of packed solids. Doctor's Dissertation. Appleton, Wis., The Institute of Paper Chemistry, 1962. 113 p.

2. Kasten, P. R., Lapidus, L., and Amundson, N. R., J. Phys. Chem. 56:683-8 (1952).

3. Rosen, J. B., J. Chem. Phys. 20:387-94(1952).

4. Rosen, J. B., Ind. Eng. Chem. 46, no. 8:1590-4(1954).

5. Turner, G. A., Chem. Eng. Sci. 7:156-65(1958).

6. Turner, G. A., Chem. Eng. Sci. 10:14-21(1959).

7. Aris, R., Chem. Eng. Sci. 10:80-7(1959).

8. Aris, R., Proc. Roy. Soc. A245:268(1958).

9. Butt, J. B., A.I.Ch.E. Journal 8, no. 4:553-6(1962).

10. Glaser, M. B., and Litt, M., A.I.Ch.E. Journal 9, no. 1:103-5(1963).

11. Wilson, A. H., Phil. Mag. 39:48(1948).

12. Crank, J. The mathematics of diffusion. London, Oxford Univ. Press, 1957. 347 p.

13. Preston, J. M., J. Soc. Chem. Ind. 50:199T(1931).

14. Preston, J. M., and Kapadia, A. H., J. Soc. Dyers Colorists 63:434-8(1947).

15. Hermans, P. H., Textile Res. J. 18, no. 1:9-17(1948).

16. Jentzen, C. A. The effect of stress applied during drying on some of the properties of individual pulp fibers. Doctor's Dissertation, Appleton, Wis., The Institute of Paper Chemistry, 1964. 129 p.

17. Aspland, J. R., and Bird, C. L., J. Soc. Dyers Colorists 77:9-12(1961).

18. Hodgman, C. D. Handbook of chemistry and physics. 39th ed. p. 764. Cleveland, Ohio, The Chemical Rubber Pub. Co., 1958.

19. Marshall, W. J., and Peters, R. H., J. Soc. Dyers Colorists 63:446(1947).

20. Bird, C. L., and Firth, J. M., J. Textile Inst. 51:T1342(1960).

21. Ingmanson, W. L., and Andrews, B. D., Tappi 46, no. 3:150-5(1963).

22. Ingmanson, W. L., Andrews, B. D., and Johnson, R. C., Tappi 42, no. 10:840-9 (1959).

23. Ingmanson, W. L. Personal communication, April, 1963.

24. Ingmanson, W. L., Tappi 35, no. 10:439-48(1952).

25. Standing, A. H., Warwicker, J. O., and Willis, H. F., J. Textile Inst. 38:T335-49(1947).

26. Saffman, P. G., J. Fluid Mech. 6:321-49(1959).

27. Scheidegger, A. E. The physics of flow through porous media. 2nd ed. Toronto, Canada, Toronto University Press. 1957.

28. McHenry, K. W., and Wilhelm, R. H., J. Am. Inst. Chem. Engrs. 3:83(1957).

29. Baron, T., Chem. Eng. Progr. 48:118(1952).

30. Klinkenberg, A., and Sjenitzer, F., Chem. Eng. Sci. 5:258-70(1958).

31. Ebach, E. A. The mixing of liquids flowing through beds of packed solids. Doctoral Dissertation. Ann Arbor, Mich., University of Michigan, 1957. [Or Ebach, E. A., and White, R. R., A.I.Ch.E. Journal 4:161(1958).]

32. Raimondi, P., Gardner, G. H. F., and Petrick, C. B. Effect of pore structure and molecular diffusion on the mixing of miscible liquids flowing in porous media. Preprint 43, Fifty-second Annual Meeting, A.I.Ch.E., Dec., 6-9, 1959.

33. Jones, R. L. An investigation of the effect of fiber structural properties on the compression response of fibrous beds. Doctor's Dissertation, Appleton, Wis., The Institute of Paper Chemistry, 1962. 150 p.

34. Pfeffer, R., and Happle, J., A.I.Ch.E. Journal (1964) (to be published).

35. Happle, J., A.I.Ch.E. Journal 4:197(1958).

36. Brenner, H., Chem. Eng. Sci. 18:109-22(1963).

37. Meredith, R., J. Textile Inst. 36:T107(1945).

38. Farrow, B., J. Textile Inst. 47:T58(1956).

39. Parker, J. D. An investigation of the permeability to water of partially saturated beds of glass fibers. Doctor's Dissertation. Appleton, Wis., The Institute of Paper Chemistry, 1958. 203 p.

40. Harleman, D. R , and Rumer, R. R., J. Fluid Mech. 16:385-94(1963).

41. Hering, B., and Bliss, H., A.I.Ch.E. Journal 9, no. 4:495-503(1963).

42. Carslaw, H. S., and Jaeger, J. C. The conduction of heat in solids. 2nd ed. London, Oxford Univ. Press, 1959. 510 p.

43. Finch, R. B., Textile Res. J. 21, no. 6:383-92(1951).

44. Onogi, S., and Sasaguri, K., Tappi 44, no. 12:874-80(1961).

APPENDIX I

DERIVATION OF WASHING EQUATIONS

The derivation of Case 1(F), where it is assumed that no mass transfer resistance exists adjacent to the fiber surfaces, is carried through in detail. Then Cases 2(F), 2(S), 1(S), the Equilibrium and No-Sorption cases, and finally a first-order reaction case are derived. Throughout the latter derivations, reference is made to the development for Case 1(F) where convenient. It is assumed that the reader is familiar with the basic assumptions that are discussed in the theoretical development section.

DEVELOPMENT OF INTRAFIBER DIFFUSION CASE 1(F)

The basic differential equation for intrafiber diffusion in an infinite circular cylinder is

$$D\left[\frac{\partial^2 P}{\partial r^2} + \frac{1}{r}\frac{\partial P}{\partial r}\right] = \frac{\partial P}{\partial t} \qquad (11)$$

where

$\underline{D}$ = intrafiber diffusion coefficient, sq. cm./sec. (note that the subscript $\underline{F}$ is not used here)

$\underline{P}$ = intrapore solute concentration, mg./cc. solution

$\underline{r}$ = radial distance, cm.

$\underline{a}$ = fiber radius, cm.

$\underline{t}$ = time, sec.

The following two solutions of Equation (11) have been derived by Carslaw and Jaeger (42). For the initial and boundary conditions

$$P = P_o \qquad 0 \leq r \leq a \qquad t = 0 \qquad (80)$$

$$P = 0 \qquad r = a \qquad t > 0 \qquad (81)$$

$$P = \frac{2P_o}{a} \sum_{n=1}^{\infty} \frac{J_o(r\alpha_n)}{\alpha_n J_1(a\alpha_n)} \exp(-\alpha_n^2 Dt) \qquad (82).$$

For the initial and boundary conditions

$$P = 0 \qquad 0 \leq r \leq a \qquad t = 0 \qquad (83)$$

$$P = \phi(t) \qquad r = a \qquad t > 0 \qquad (84)$$

$$P = \frac{2D}{a} \sum_{n=1}^{\infty} \frac{\alpha_n J_o(r\alpha_n)}{J_1(a\alpha_n)} \exp(-\alpha_n^2 Dt) \int_0^t \exp(\alpha_n^2 D\lambda)\, \phi(\lambda)\, d\lambda \qquad (85),$$

where

$\phi(t)$ = surface concentration as a function of time

$J_o(\ )$ = Bessel function of zero order

$J_1(\ )$ = Bessel function of first order

α_n's = positive roots of $J_o(a\alpha_n) = 0$

According to the superposition principle, the following solution can be obtained for the initial condition (80) plus (83) and the boundary condition (81) plus (84).

$$P = P_o \qquad 0 \leq r \leq a \qquad t = 0 \qquad (86)$$

$$P = \phi(t) \qquad r = a \qquad t > 0 \qquad (87)$$

$$P = \frac{2P_o}{a} \sum_{n=1}^{\infty} \frac{J_o(r\alpha_n)}{\alpha_n J_1(a\alpha_n)} \exp(-\alpha_n^2 Dt)$$

$$+ \frac{2D}{a} \sum_{n=1}^{\infty} \frac{\alpha_n J_o(r\alpha_n)}{J_1(a\alpha_n)} \exp(-\alpha_n^2 Dt) \int_0^t \exp(\alpha_n^2 D\lambda)\, \phi(\lambda)\, d\lambda \qquad (88).$$

It can be shown readily, from Equation (88), that $\underline{P} = \underline{P}_o$ when $\phi(\lambda) = \underline{P}_o$ at $\underline{r} = \underline{a}$.

The total quantity of solute, $\underline{Q}$ (mg./cc. solid), which is contained by a cylinder at any time, is obtained by the following integration.

$$Q = (2\pi K/\pi a^2) \int_0^a P(r,t)\, r\, dr \qquad (89)$$

where $\underline{K}$ is the partition coefficient of the solute-fiber system.

$$Q = \frac{4KP_o}{a^3} \sum_{n=1}^{\infty} \exp(-\alpha_n^2 Dt) \int_0^a \frac{J_o(r\alpha_n)}{\alpha_n J_1(a\alpha_n)}\, r\, dr$$

$$+ \frac{4KD}{a^3} \sum_{n=1}^{\infty} \exp(-\alpha_n^2 Dt) \int_0^t \exp(\alpha_n^2 D\lambda)\, \phi(\lambda)\, d\lambda \int_0^a \frac{\alpha_n J_o(r\alpha_n)}{J_1(a\alpha_n)}\, r\, dr \qquad (90)$$

Since

$$\int_0^a J_o(r\alpha_n)\, r\, dr = aJ_1(a\alpha_n)/\alpha_n \qquad (91)$$

when $\underline{n} > -1$ (see Carslaw and Jaeger), it follows that

$$Q = \frac{4KP_o}{a^2} \sum_{n=1}^{\infty} \frac{1}{\alpha_n^2} \exp(-\alpha_n^2 Dt)$$

$$+ \frac{4KD}{a^2} \sum_{n=1}^{\infty} \exp(-\alpha_n^2 Dt) \int_0^t \exp(\alpha_n^2 D\lambda)\, \phi(\lambda)\, d\lambda \qquad (92).$$

In order to obtain the rate of solute removal from the cylinder, the expression for $\underline{Q}$ is differentiated with respect to time.

$$\frac{\partial Q}{\partial t} = \frac{-4KP_oD}{a^2} \sum_{n=1}^{\infty} \exp(-\alpha_n^2 Dt)$$

$$- \frac{4KD^2}{a^2} \sum_{n=1}^{\infty} \alpha_n^2 \exp(-\alpha_n^2 Dt) \int_0^t \exp(\alpha_n^2 D\lambda)\, \phi(\lambda)\, d\lambda$$

$$+ \frac{4KD}{a^2} \sum_{n=1}^{\infty} \exp(-\alpha_n^2 Dt) \frac{\partial}{\partial t} \int_0^t \exp(\alpha_n^2 D\lambda)\, \phi(\lambda)\, d\lambda \qquad (93)$$

As a check on the validity of Equation (93), it can be shown that $\partial\underline{Q}/\partial\underline{t} = 0$ when $\phi(\lambda) = \underline{P}_o$. Since

$$\frac{\partial}{\partial t} \int_0^t \exp(\alpha_n^2 D\lambda)\, \phi(\lambda)\, d\lambda = \exp(\alpha_n^2 Dt)\, \phi(t) \qquad (94),$$

Equation (93) becomes

$$\frac{\partial Q}{\partial t} = \frac{-4KP_oD}{a^2} \sum_{n=1}^{\infty} \exp(-\alpha_n^2 Dt)$$

$$+ \frac{4KD}{a^2} \sum_{n=1}^{\infty} \left[\phi(t) - D\alpha_n^2 \int_0^t \exp(-\alpha_n^2 D(t - \lambda)\, \phi(\lambda)\, d\lambda \right] \qquad (95).$$

It can be shown that Equation (95) converges; for convenience sake, however, the second term in Equation (95) will be split into two terms, as follows (note that the ~~last~~ second term does not converge).

$$\frac{\partial Q}{\partial t} = \frac{-4KP_o D}{a^2} \sum_{n=1}^{\infty} \exp(-\alpha_n^2 Dt) + \frac{4KD}{a^2} \sum_{n=1}^{\infty} (1)^n \, \phi(t)$$

$$- \frac{4KD^2}{a^2} \sum_{n=1}^{\infty} \alpha_n^2 \exp(-\alpha_n^2 Dt) \int_0^t \exp(\alpha_n^2 D\lambda) \, \phi(\lambda) \, d\lambda \qquad (96).$$

APPLICATION OF LAPLACE TRANSFORMATION

The Laplace transformation is performed on Equation (96) as follows:

$$\left(\overline{\frac{\partial Q}{\partial t}}\right) = \frac{-4KP_o D}{a^2} \int_0^{\infty} \sum_{n=1}^{\infty} \exp(-pt - \alpha_n^2 Dt) \, dt$$

$$- \frac{4KD^2}{a^2} \int_0^{\infty} \sum_{n=1}^{\infty} \alpha_n^2 \exp(-pt - \alpha_n^2 Dt) \int_0^t \exp(\alpha_n^2 D\lambda) \, \phi(\lambda) \, d\lambda \, dt$$

$$+ \frac{4KD}{a^2} \int_0^{\infty} \sum_{n=1}^{\infty} (1)^n \exp(-pt) \, \phi(t) \, dt \qquad (97).$$

The Laplace transform is simplified in the following series of steps:

$$\left(\overline{\frac{\partial Q}{\partial t}}\right) = \left[\frac{-4KP_o D}{a^2} \sum_{n=1}^{\infty} \frac{-1}{p + \alpha_n^2 D} \exp(-pt - \alpha_n^2 Dt) \right]_0^{\infty}$$

$$- \frac{4KD^2}{a^2} \sum_{n=1}^{\infty} \alpha_n^2 \mathcal{L}_1 + \frac{4KD}{a^2} \sum_{n=1}^{\infty} (1)^n \, \overline{\phi(t)} \qquad (98).$$

The first term can be simplified to

$$(-4KP_o D/a^2) \sum_{n=1}^{\infty} 1/(p + \alpha_n^2 D) \qquad (99).$$

To evaluate

$$\mathcal{L}_1 = \int_0^{\infty} \exp(-pt - \alpha_n^2 Dt) \int_0^t \exp(\alpha_n^2 D\lambda)\, \phi(\lambda)\, d\lambda \; dt \qquad (100),$$

Using integration by parts, let

$$u = \int_0^t \exp(\alpha_n^2 D\lambda) \; \phi(\lambda) \; d\lambda; \quad dv = \exp(-pt - \alpha_n^2 Dt)\, dt \qquad (101, 102)$$

$$du = \exp(\alpha_n^2 Dt) \; \phi(t)\, dt; \quad v = \frac{-1}{p + \alpha_n^2 D} \exp(-pt - \alpha_n^2 Dt) \qquad (103, 104).$$

Thus,

$$\mathcal{L}_1 = \left[\frac{-1}{p + \alpha_n^2 D} \exp(-pt - \alpha_n^2 Dt) \int_0^t \exp(\alpha_n^2 D\lambda)\, \phi(\lambda)\, d\lambda \right]_0^{\infty}$$

$$+ \int_0^{\infty} \frac{1}{p + \alpha_n^2 D} \exp(-pt) \; \phi(t)\, dt \qquad (105).$$

By inspection, the first term equals zero if Real ($\underline{p}$) > 0; thus

$$\mathcal{L}_1 = \frac{1}{p + \alpha_n^2 D} \qquad \overline{\phi(t)} \qquad (106).$$

Equation (98) now becomes

$$\left(\overline{\frac{\partial Q}{\partial t}}\right) = \frac{-4KP_o D}{a^2} \sum_{n=1}^{\infty} \frac{1}{p + \alpha_n^2 D}$$

$$- \frac{4KD}{a^2} \left[\sum_{n=1}^{\infty} \frac{\alpha_n^2 D}{p + \alpha_n^2 D} - \sum_{n=1}^{\infty} (1)^n \right] \overline{\phi(t)} \qquad (107).$$

By recombining the summations in the second term of Equation (107) to obtain a convergent series, the final form of the Laplace transform becomes

$$\left(\overline{\frac{\partial Q}{\partial t}}\right) = \frac{-4KP_o D}{a^2} \sum_{n=1}^{\infty} \frac{1}{p + \alpha_n^2 D} + \frac{4KD}{a^2} \sum_{n=1}^{\infty} \frac{p}{p + \alpha_n^2 D} \overline{\phi(t)} \qquad (108).$$

It is convenient to recognize at this point that $\underline{P}_o = \underline{C}_o$, where $\underline{C}_o$ is the initially uniform solution concentration. It should also be recognized that $\phi(\underline{t}) = \underline{C}$, where $\underline{C}$ is the average concentration of solute in solution, outside the fibers, at a given $\underline{Z}$ level, and is defined as

$$C = (1/A_c \epsilon) \int_{S'} c \, dA_c \qquad (109)$$

where $\underline{A}_c$ is the bed cross section, and $\underline{c}$ represents the local concentration variable at $\underline{Z}$. The Laplace transform of $\phi(\underline{t})$ will hereafter be taken as $\overline{\phi(\underline{t})} = \overline{\underline{C}}$.

SOLUTION OF THE DIFFERENTIAL EQUATION FOR LONGITUDINAL DISPERSION

Now that the Laplace transform of $\partial \underline{Q}/\partial \underline{t}$ has been obtained, the one-dimensional diffusionlike differential equation for longitudinal dispersion must be solved. Thus,

$$D_L \frac{\partial^2 C}{\partial Z^2} - U \frac{\partial C}{\partial Z} = \frac{\partial C}{\partial t} + \frac{(1 - \epsilon)}{\epsilon} \frac{\partial Q}{\partial t} \qquad (2),$$

where

D_L = longitudinal dispersion coefficient, sq. cm./sec.

C = average solute concentration in solution, mg./cc. solution

Z = axial distance from top of bed, cm.

U = average linear pore velocity in Z direction, cm./sec.

t = time, sec.

ϵ = porosity of bed, cc. voids/cc. bed

Q = intraparticle solute content, mg./cc. solid

The initial condition is

$$C = C_o = P_o \qquad Z \geq 0 \qquad t = 0 \qquad (3)$$

The inlet boundary condition used by Sherman (1) for $Z = 0$, $t > 0$, is

$$C(0,t) = C_o(k_o + k_1't + k_2't^2 + k_3't^3 + \ldots) \exp(-\gamma' t) \qquad (4)$$

where k_o, k_1', k_2', k_3', ..., and γ' are experimentally determined constants.

The Laplace transform of Equation (2) is

$$D_L \frac{\partial^2 \bar{C}}{\partial Z^2} - U \frac{\partial \bar{C}}{\partial Z} = p\bar{C} - C_o + \frac{(1 - \epsilon)}{\epsilon} \left(\overline{\frac{\partial Q}{\partial t}}\right) \qquad (110)$$

Substitution of Equation (108) for $(\overline{\partial Q/\partial t})$, and subsequent rearrangement yields

$$D_L \frac{\partial^2 \bar{C}}{\partial Z^2} - U \frac{\partial \bar{C}}{\partial Z} - \left[p + \frac{4DK(1 - \epsilon)}{a^2 \epsilon} \sum_{n=1}^{\infty} \frac{p}{p + \alpha_n^2 D} \right] \bar{C}$$

$$= - \left[1 + \frac{4DK(1 - \epsilon)}{a^2 \epsilon} \sum_{n=1}^{\infty} \frac{1}{p + \alpha_n^2 D} \right] C_o \qquad (111).$$

Let the following notation be used to represent Equation (111):

$$D_L \frac{\partial^2 \bar{C}}{\partial Z^2} - U \frac{\partial \bar{C}}{\partial Z} - G(p)\bar{C} = - H(p)C_o \tag{112}$$

where, if we define

$$h = 4DK(1 - \epsilon)/a^2\epsilon \tag{113},$$

$$H(p) = 1 + h \sum_{n=1}^{\infty} \frac{1}{p + \alpha_n^2 D} \tag{114},$$

$$G(p) = p + h \sum_{n=1}^{\infty} \frac{p}{p + \alpha_n^2 D} \tag{115}.$$

Note that $\underline{H}(\underline{p})/\underline{G}(\underline{p}) = 1/\underline{p}$.

An inspection of Equation (112) indicates that it is a linear, nonhomogeneous, second-order differential equation. The solution to this equation has the general form

$$\bar{C} = \frac{H(p)C_o}{G(p)} + K_m \exp(mZ) + K_v \exp(vZ) \tag{116}$$

where

$$m = \frac{U}{2D_L} - \left[\left(\frac{U}{2D_L}\right)^2 + \frac{G(p)}{D_L}\right]^{1/2} \tag{117}$$

$$v = \frac{U}{2D_L} + \left[\left(\frac{U}{2D_L}\right)^2 + \frac{G(p)}{D_L}\right]^{1/2} \tag{118}$$

Since $\underline{\bar{C}}$ must be bounded as $\underline{Z} \rightarrow \infty$, and since $\underline{v}$ is always positive, it follows that $\underline{K_v}$ must equal zero and

$$\bar{C} = C_o/p + K_m \exp(mZ) \tag{119}$$

The Laplace transform of the inlet boundary condition (4) at $\underline{Z} = 0$, $\underline{t} > 0$, in terms of $\underline{C}_o = \underline{C}(0,0) = \underline{C}(\underline{Z},0)$, is

$$\overline{C}(0,p) = C_o \left[\frac{k_o}{\gamma'+p} + \frac{k_1'}{(\gamma'+p)^2} + \frac{2k_2'}{(\gamma'+p)^3} + \frac{6k_3'}{(\gamma'+p)^4} + \ldots \right] \qquad (120)$$

which can be represented by $\underline{f}_2(\underline{p})$. As $\underline{Z} \rightarrow 0$ in Equation (119), substitution of Equation (120) yields

$$K_m = -C_o/p + f_2(p) \qquad (121).$$

The Laplace transform of the desired solution is obtained by substituting the expression for $\underline{K}_m$ in Equation (119) as follows:

$$\overline{C} = C_o/p - (C_o/p) \exp(mZ) + f_2(p) \exp(mZ) \qquad (122)$$

Since $\underline{m}$ is negative, it can be seen that $\overline{\underline{C}} = \underline{C}_o/\underline{p}$ and $\underline{C} = \underline{C}_o$ as $\underline{Z} \rightarrow \infty$ in Equation (122). This result is in accordance with the boundary conditions of the problem.

EVALUATION OF INVERSE TRANSFORMS

The following is an evaluation of the inverse transform of $\exp(\underline{mZ})$. Unfortunately there is no published form which corresponds to this function. Therefore, it is necessary to resort to the definition of the inverse transform and evaluate the required integral. When the expression for $\underline{G}(\underline{p})$, from Equation (115), is substituted in Equation (117), it can be shown that $\exp(\underline{mZ})$ is expressed as follows:

$$\exp(mZ) = \exp(UZ/2D_L) \exp\left[-q \left(g + p + h \sum_{n=1}^{\infty} \frac{p}{p + \alpha_n^2 D} \right)^{1/2} \right] \qquad (123)$$

where

$$q = (Z^2/D_L)^{1/2} \; ; \qquad g = U^2/4D_L \tag{124, 125}$$

Since $\exp(\underline{UZ}/2\underline{D_L})$ is independent of $\underline{p}$, let Equation (123) be represented by

$$f_3(p) = \exp(UZ/2D_L)\, f_4(p) \tag{126}$$

where

$$f_4(p) = \exp\left[-q\left(g + p + h\sum_{n=1}^{\infty}\frac{p}{p + \alpha_n^2 D}\right)^{1/2}\right] \tag{127}$$

By definition, the inverse transform of $\underline{f}(\underline{p})$ is

$$F(t) = \frac{1}{2\pi i}\int_{s-i\infty}^{s+i\infty}\exp(tp)\, f(p)\, dp \tag{128}$$

where $\underline{p}$ is no longer a real number, but takes the form of a complex number such as $\underline{s} + \underline{ib}$, where $\underline{s}$ is a real constant, large enough so that all the singularities of $\underline{f}(\underline{p})$ lie to the left of the line $\text{Real}(\underline{p}) = \underline{s}$. After the necessary substitutions are made, the following expression is obtained for the inverse transform of $\underline{f_4}(\underline{p})$:

$$F_4(t) = \frac{1}{2\pi}\exp(ts)\int_{-\infty}^{+\infty}\exp(tbi)\exp(-q(\overline{SR}))\; db \tag{129}$$

where

$$(\overline{SR})^2 = g + (s + bi)\left[1 + h\sum_{n=1}^{\infty}\frac{1}{s + \alpha_n^2 D + bi}\right] \tag{130}$$

The term $(\overline{\underline{SR}})^2$ is simplified as follows:

$$(\overline{SR})^2 = g + (s + bi)\left[1 + h\sum_{n=1}^{\infty}\frac{s + \alpha_n^2 D - bi}{(s + \alpha_n^2 D)^2 + b^2}\right] \qquad (131)$$

$$(\overline{SR})^2 = g + s + sh\sum_{n=1}^{\infty}\frac{s + \alpha_n^2 D}{(s + \alpha_n^2 D)^2 + b^2} + bh\sum_{n=1}^{\infty}\frac{b}{(s + \alpha_n^2 D)^2 + b^2}$$

$$+ bi - sh\sum_{n=1}^{\infty}\frac{bi}{(s + \alpha_n^2 D)^2 + b^2} + bh\sum_{n=1}^{\infty}\frac{(s + \alpha_n^2 D)i}{(s + \alpha_n^2 D)^2 + b^2} \qquad (132).$$

By combining the real and imaginary terms separately, the following is obtained:

$$(\overline{SR})^2 = g + s + h\sum_{n=1}^{\infty}\frac{s^2 + b^2 + s\alpha_n^2 D}{(s + \alpha_n^2 D)^2 + b^2} + \left[b + h\sum_{n=1}^{\infty}\frac{b\alpha_n^2 D}{(s + \alpha_n^2 D)^2 + b^2}\right] i \qquad (133).$$

If $\underline{c}$ and $\underline{di}$ are used to symbolize the real and imaginary parts, respectively,

$$(\overline{SR}) = (c + di)^{1/2} \qquad (134)$$

Thus, in terms of the above nomenclature simplification

$$F_4(t) = (1/2\pi)\exp(ts)\int_{-\infty}^{+\infty}\exp(tbi)\exp(-q(c + di)^{1/2})\,db \qquad (135).$$

From Euler's relation

$$c + di = \overline{r}^2\exp(i\theta) = \overline{r}^2(\cos\theta + i\sin\theta) \qquad (136)$$

where

$$\overline{r}^2 = (c^2 + d^2)^{1/2}\ ; \qquad \theta = \tan^{-1}(d/c) \qquad (137, 138)$$

Thus, Equation (135) becomes

$$F_4(t) = \frac{\exp(ts)}{2\pi} \int_{-\infty}^{+\infty} \exp(tbi) \exp(-q\bar{r}(\cos \theta/2 + i \sin \theta/2)) \, db \qquad (139)$$

which can be rewritten as

$$F_4(t) = \frac{\exp(ts)}{2\pi} \int_{-\infty}^{+\infty} \exp(-q\bar{r} \cos \theta/2) \exp((tb - q\bar{r} \sin \theta/2)i) \, db \qquad (140).$$

By using Euler's relationship a second time it is possible to form a real and an imaginary integral from Equation (140) as follows:

$$F_4(t) = \frac{\exp(ts)}{2\pi} \int_{-\infty}^{+\infty} \exp(-q\bar{r} \cos \theta/2) \cos(tb - q\bar{r} \sin \theta/2) \, db$$

$$+ \frac{\exp(ts)}{2\pi} \int_{-\infty}^{+\infty} \exp(-q\bar{r} \cos \theta/2) \sin(tb - q\bar{r} \sin \theta/2) \, idb \qquad (141).$$

The remaining task is to show that the imaginary (second) integral of Equation (141) is equal to zero. The following facts and arguments are presented to demonstrate this.

1. Since $\underline{c}(\underline{b}) = \underline{c}(-\underline{b})$ and $\underline{d}(\underline{b}) = -\underline{d}(-\underline{b})$, it follows that $\theta(\underline{b}) = -\theta(-\underline{b})$.

2. Since $\underline{q\bar{r}} = \underline{q}(\underline{c}^2 + \underline{d}^2)^{1/4}$ is unchanged when $(-\underline{b})$ is substituted for $(+\underline{b})$, and since $\sin(\theta/2) = -\sin(-\theta/2)$, it follows that the value of $\sin(\underline{tb} - \underline{q\bar{r}} \sin\theta/2)$ merely reverses sign when the sign of $(\underline{b})$ is reversed.

3. Since $\cos(\theta/2) = \cos(-\theta/2)$, it follows that $\exp(-\underline{q\bar{r}} \cos\theta/2)$ is unchanged when $(-\underline{b})$ is substituted for $(\underline{b})$.

From points 2 and 3 it follows that the value of the imaginary integrand in Equation (141) merely reverses sign when the sign of ($\underline{b}$) is reversed. Because of the reversal of sign about $\underline{b} = 0$, the value of the integral from $\underline{b} = -\infty$ to $\underline{b} = 0$ must be equal to the negative of the value from $\underline{b} = 0$ to $\underline{b} = +\infty$; therefore, the value of the imaginary integral is zero over the limits $\underline{b} = -\infty$ to $\underline{b} = +\infty$.

If it is now remembered that $\cos(-\underline{x}) = \cos(\underline{x})$, it is concluded that the value of the real integral in Equation (141) is equal to twice the value obtained by integrating from $\underline{b} = 0$ to $\underline{b} = +\infty$. Thus, Equation (141) becomes

$$F_4(t) = \frac{\exp(ts)}{\pi} \int_0^{+\infty} \exp(-q\bar{r} \cos \theta/2) \cos(tb - q\bar{r} \sin \theta/2)\, db \qquad (142).$$

Since θ always lies in the first quadrant here, the cosine and sine functions of $\theta/2$ can be expressed in terms of half-angle relationships as

$$\cos \theta/2 = (1/2 + c/2\bar{r}^{-2})^{1/2} \qquad (143)$$

$$\sin \theta/2 = (1/2 - c/2\bar{r}^{-2})^{1/2} \qquad (144).$$

Thus, Equation (142) becomes

$$F_4(t) = \frac{\exp(ts)}{\pi} \int_0^{+\infty} \exp(-q(\bar{r}^{-2}/2 + c/2)^{1/2}$$

$$\cos(tb - q(\bar{r}^{-2}/2 - c/2)^{1/2})\, db \qquad (145).$$

It is now appropriate to summarize the inverse Laplace transforms that are needed for the final solution:

$$f_1(p) = \frac{H(p)}{G(p)} \quad C_o = \frac{C_o}{p} \quad ; \qquad F_1(t) = C_o \qquad (146, 147).$$

For

$$f_2(p) = C_o\left[\frac{k_o}{\gamma'+p} + \frac{k_1'}{(\gamma'+p)^2} + \frac{2k_2'}{(\gamma'+p)^3} + \frac{6k_3'}{(\gamma'+p)^4} + \ldots\right] \tag{120}$$

$$F_2(t) = C_o(k_o + k_1't + k_2't^2 + k_3't^3 + \ldots)\exp(-\gamma't) \tag{4}.$$

For $\underline{f_3}(\underline{p}) = \exp(\underline{mZ})$,

$$f_3(p) = \exp(UZ/2D_L)\exp\left[-q\left(g + p + h\sum_{n=1}^{\infty}\frac{p}{p + \alpha_n^2 D}\right)^{1/2}\right] \tag{123}.$$

Since the singularities of $\underline{f_3}(\underline{p})$ are at $\underline{p} = -\underline{\alpha_n^2 D}$, where $\underline{b} = 0$, all of the singularities lie to the left of $\underline{s} = 0$. Thus, it is permissible to let $\underline{s} = 0$ in the terms $\exp(\underline{ts})$, $\underline{c}$, and $\underline{d}$ (or $\underline{\bar{r}}$) of Equation (145). In accordance with this simplification

$$F_3(t) = \frac{\exp(UZ/2D_L)}{\pi}\int_0^{+\infty}\exp(-q(\bar{r}^2/2 + c/2)^{1/2})$$

$$\cos(tb - q(\bar{r}^2/2 - c/2)^{1/2})\,db \tag{148}$$

where $\underline{c}$, $\underline{d}$, and $\underline{\bar{r}}$ are now defined as

$$\bar{r}^2 = (c^2 + d^2)^{1/2} \tag{137}$$

$$c = g + h\sum_{n=1}^{\infty}\frac{b^2}{b^2 + \alpha_n^4 D^2} \tag{149}$$

$$d = b + h\sum_{n=1}^{\infty}\frac{b\alpha_n^2 D}{b^2 + \alpha_n^4 D^2} \tag{150}.$$

The above inverse transforms are now combined as follows:

$$f_5(p) = (C_o/p) \exp(mZ) = f_1(p)\, f_3(p) \tag{151}$$

$$F_5(t) = \int_0^t F_1(t - \tau)\; F_3(\tau)\, d\tau \tag{152}$$

$$f_6(p) = f_2(p)\, f_3(p) \tag{153}$$

$$F_6(t) = \int_0^t F_2(t - \tau)\; F_3(\tau)\, d\tau \tag{154}.$$

The final solution for $\underline{C}(\underline{Z},\underline{t})$ is apparent after Equation (122) is rewritten as follows:

$$\overline{C} = f_1(p) - f_5(p) + f_6(p) \tag{155}.$$

Thus

$$C = F_1(t) - F_5(t) + F_6(t) \tag{156}$$

which can be rewritten as

$$C = C_o - \int_0^t (C_o - F_2(t - \tau))\, F_3(\tau)\, d\tau \tag{157}.$$

THE FINAL SOLUTION IN DIMENSIONAL VARIABLES

After performing the required substitutions, rewriting $\underline{F}_2(\underline{t} - \tau)$ as a finite sum, and rearranging, one obtains

$$\frac{C}{C_o} = 1 - \frac{1}{\pi} \int_0^{\tau=t} \left[1 - \left(k_o + \sum_{n=1}^{f} k_n'(t - \tau)^n \right) \exp(-\gamma'(t - \tau)) \right]$$

$$\int_0^{b=\infty} \exp\left[UZ/2D_L - q(\bar{r}^2/2 + c/2)^{1/2}\right]$$

$$\cos\left[\tau b - q(\bar{r}^2/2 - c/2)^{1/2}\right] db \; d\tau \qquad (158)$$

where for Case 1(F)

$$\bar{r}^2 = (c^2 + d^2)^{1/2}, \qquad q = (Z^2/D_L)^{1/2} \qquad (137, 124)$$

$$c = g + h \sum_{n=1}^{\infty} \frac{b^2}{b^2 + \alpha_n^4 D^2}, \qquad g = U^2/4D_L \qquad (149, 125)$$

$$d = b + h \sum_{n=1}^{\infty} \frac{b\alpha_n^2 D}{b^2 + \alpha_n^4 D^2}, \qquad h = 4DK(1 - \epsilon)/a^2\epsilon \qquad (150, 113).$$

α_n's are the positive nonzero roots of

$$J_o(a\alpha_n) = 0 \qquad (159).$$

THE FINAL SOLUTION IN DIMENSIONLESS VARIABLES

Equation (158) can be rewritten in terms of dimensionless variables as

$$\frac{C}{C_o} = 1 - \frac{1}{\pi} \int_0^{\omega=R} \left[1 - \left(k_o + \sum_{n=1}^{f} k_n(R - \omega)^n \right) \exp(-\gamma(R - \omega)) \right]$$

$$\int_0^{\eta=\infty} \exp\left[\frac{1}{2S} - \left(\frac{\psi}{2S}(1 + M/\psi)\right)^{1/2}\right]$$

$$\cos\left[\omega\eta - \left(\frac{\psi}{2S}(1 - M/\psi)\right)^{1/2}\right] d\eta \; d\omega \qquad (160)$$

where the bed length is now given by $\underline{Z}_e$,

$$\underline{R} = \underline{Ut}/\underline{Z}_e \quad , \quad \underline{S} = \underline{D}_L/\underline{UZ}_e \quad , \quad \psi = (\underline{M}^2 + \underline{N}^2)^{1/2} \quad ,$$

$\omega(= \underline{U\tau}/\underline{Z}_e)$ and $\eta\ (= \underline{Z}_e\underline{b}/\underline{U})$ are dimensionless variables of integration, and the input constants are given by $\underline{k}_n = \underline{k}'_n(\underline{Z}_e/\underline{U})^n$ and $\gamma = \gamma'(\underline{Z}_e/\underline{U})$. The variables $\underline{M}$ and $\underline{N}$ are given for Case 1(F) as

$$M = \frac{1}{4S} + \frac{4DK(1 - \epsilon)}{a^2\epsilon} \sum_{n=1}^{\infty} \frac{\eta^2\, U/Z_e}{(\eta U/Z_e)^2 + (D^2/a^4)\beta_n^4} \tag{161}$$

$$N = \eta + \frac{4D^2K(1 - \epsilon)}{a^4\epsilon} \sum_{n=1}^{\infty} \frac{\eta\beta_n^2}{(\eta U/Z_e)^2 + (D^2/a^4)\beta_n^4} \tag{162}$$

and the β_n's are positive roots of $J_o(\beta_n) = 0$.

DEVELOPMENT OF INTRAFIBER DIFFUSION CASE 2(F)

Case 2(F) will now be considered, where a finite mass transfer resistance exists in the fluid adjacent to the fiber surfaces. The boundary condition which characterizes this simplified treatment of mass transfer is

$$-D' \frac{\partial P}{\partial r} = k_L(P - C(Z,t)) \qquad r = a \qquad t > 0 \qquad (14)$$

where $\underline{D}' = \underline{DK}/\epsilon'$ is the intrapore diffusion coefficient, cm.^{2}/sec., and $\underline{k}_L$ is the mass transfer coefficient, cm./sec.

The basic differential equation for intrafiber diffusion in an infinite circular cylinder is again Equation (11). A useful solution to Equation (11) for the "radiation" boundary condition is given by Carslaw and Jaeger (42) as follows:

$$P = 0 \qquad 0 \leq r \leq a \qquad t = 0 \qquad (83)$$

$$\frac{\partial P}{\partial r} = \frac{-k_L}{D'}(P - 1) \qquad r = a \qquad t > 0 \qquad (163)$$

$$P = 1 - 2L \sum_{n=1}^{\infty} \frac{J_o(r\alpha_n)}{L_n J_o(a\alpha_n)} \exp(-\alpha_n^2 Dt) \qquad (164)$$

where the α_n's are positive roots of

$$a\alpha_n J_1)a\alpha_n) = LJ_o(a\alpha_n) \qquad (165)$$

$$L = ak_L/D' \quad \text{and} \quad L_n = a^2\alpha_n^2 + L^2 \qquad (166, 167).$$

According to Duhamel's theorem (see Carslaw and Jaeger), the solution to the initial and boundary conditions

$$P = 0 \qquad 0 \leq r \leq a \qquad t = 0 \qquad (83)$$

$$\frac{\partial P}{\partial r} = \frac{-k_L}{D'} (P - \phi(t)) \qquad r = a \qquad t > 0 \qquad (168)$$

is obtained as follows:

$$P = \int_0^t \phi(\lambda) \frac{\partial}{\partial t} (P_1(r, t - \lambda)) \, d\lambda \qquad (169)$$

where $\phi(t)$ again represents $C(Z,t)$, the average solution concentration, and $P_1(r,t)$ is given by Equation (164). Thus, by substitution

$$P = \int_0^t \phi(\lambda) \frac{\partial}{\partial t} \left[1 - 2L \sum_{n=1}^{\infty} \frac{J_o(r\alpha_n)}{L_n J_o(a\alpha_n)} \exp(-\alpha_n^2 D(t - \lambda)) \right] d\lambda \qquad (170).$$

Differentiating,

$$P = 2LD \sum_{n=1}^{\infty} \frac{\alpha_n^2 J_o(r\alpha_n)}{L_n J_o(a\alpha_n)} \exp(-\alpha_n^2 Dt) \int_0^t \exp(\alpha_n^2 D\lambda) \, \phi(\lambda) \, d\lambda \qquad (171).$$

It is now necessary to change the co-ordinates of $\underline{P}$ by $\underline{P}_o$ units, substituting $(\underline{P} - \underline{P}_o)$ for $\underline{P}$, and $\phi(\lambda) - \underline{P}_o$ for $\phi(\lambda)$. The differential equation for intra-fiber diffusion becomes in this case

$$D\left[\frac{\partial^2(P-P_o)}{\partial r^2} + \frac{1}{r}\frac{\partial(P-P_o)}{\partial r}\right] = \frac{\partial(P-P_o)}{\partial t} \tag{172}$$

for the initial and boundary conditions

$$P-P_o = 0 \qquad 0 \leq r \leq a \qquad t = 0 \tag{173}$$

$$\frac{\partial(P-P_o)}{\partial r} = \frac{-k_L}{D'}\left[(P-P_o) - (\phi(t) - P_o)\right], \quad r = a, \quad t > 0 \tag{174}.$$

The solution to these equations now follows directly from Equation (171),

$$P-P_o = 2LD \sum_{n=1}^{\infty} \frac{\alpha_n^2 J_o(r\alpha_n)}{L_n J_o(a\alpha_n)} \exp(-\alpha_n^2 Dt) \; I_1 \tag{175}$$

where

$$I_1 = \int_0^t \exp(\alpha_n^2 D\lambda)\,(\phi(\lambda) - P_o)\; d\lambda \tag{176}$$

is evaluated as

$$I_1 = \int_0^t \exp(\alpha_n^2 D\lambda)\,\phi(\lambda)\, d\lambda \; - (P_o/\alpha_n^2 D)(\exp(\alpha_n^2 Dt) - 1) \tag{177}.$$

The desired solution can now be rewritten as

$$P = P_o \qquad 0 \leq r \leq a \qquad t = 0 \tag{80}$$

$$\frac{\partial P}{\partial r} = \frac{-k_L}{D'} (P - \phi(t)) \qquad r = a \qquad t > 0 \qquad (168)$$

$$P = P_o + 2LD \sum_{n=1}^{\infty} \frac{\alpha_n^2 J_o(r\alpha_n)}{L_n J_o(a\alpha_n)} \exp(-\alpha_n^2 Dt)$$

$$\left[\int_0^t \exp(\alpha_n^2 D\lambda)\, \phi(\lambda)\, d\lambda - (P_o/\alpha_n^2 D)\, (\exp(\alpha_n^2 Dt) - 1) \right] \qquad (178).$$

Expanding Equation (178),

$$P = P_o - 2P_o L \sum_{n=1}^{\infty} \frac{J_o(r\alpha_n)}{L_n J_o(a\alpha_n)} + 2P_o L \sum_{n=1}^{\infty} \frac{J_o(r\alpha_n)}{L_n J_o(a\alpha_n)} \exp(-\alpha_n^2 Dt)$$

$$+ 2LD \sum_{n=1}^{\infty} \frac{\alpha_n^2 J_o(r\alpha_n)}{L_n J_o(a\alpha_n)} \exp(-\alpha_n^2 Dt) \int_0^t \exp(\alpha_n^2 D\lambda)\, \phi(\lambda)\, d\lambda \qquad (179).$$

Since

$$Q = (2K/a^2) \int_0^a P(r,t)\, r\, dr \qquad (89)$$

and from Equation (91)

$$\int_0^a J_o(r\alpha_n)\, r\, dr = aJ_1(a\alpha_n)/\alpha_n \qquad (91)$$

it follows that

$$Q = KP_o \bar{\eta} + 4KP_oL \sum_{n=1}^{\infty} \frac{J_1(a\alpha_n)}{a\alpha_n L_n J_o(a\alpha_n)}$$

$$+ 4KP_oL \sum_{n=1}^{\infty} \frac{J_1(a\alpha_n)}{a\alpha_n L_n J_o(a\alpha_n)} \exp(-\alpha_n^2 Dt)$$

$$+ 4KLD \sum_{n=1}^{\infty} \frac{\alpha_n J_1(a\alpha_n)}{aL_n J_o(a\alpha_n)} \exp(-\alpha_n^2 Dt) \int_0^t \exp(\alpha_n^2 D\lambda)\ \phi(\lambda)\ d\lambda \qquad (180).$$

By differentiating with respect to t and recognizing that $a\alpha_n J_1(a\alpha_n) = LJ_o(a\alpha_n)$, we have

$$\frac{\partial Q}{\partial t} = \frac{-4KP_oL^2D}{a^2} \sum_{n=1}^{\infty} \frac{1}{L_n} \exp(-\alpha_n^2 Dt) + \frac{4KL^2D}{a^2} \sum_{n=1}^{\infty} \frac{1}{L_n}\ \phi(t)$$

$$- \frac{4KL^2D^2}{a^2} \sum_{n=1}^{\infty} \frac{\alpha_n^2}{L_n} \exp(-\alpha_n^2 Dt) \int_0^t \exp(\alpha_n^2 D\lambda)\ \phi(\lambda)\ d\lambda \qquad (181).$$

At this point the similarity between Equation (181) and Equation (96) is quite evident. The Laplace transform of Equation (181) is therefore obtained as follows:

$$\overline{(\partial Q/\partial t)} = \int_0^{\infty} \exp(-pt)\ (\partial Q/\partial t)\ dt \qquad (182)$$

$$\left(\overline{\frac{\partial Q}{\partial t}}\right) = \left[\frac{-4KP_oL^2D}{a^2} \sum_{n=1}^{\infty} \frac{-1}{L_n\ (p + \alpha_n^2 D)} \exp(-pt - \alpha_n^2 Dt)\right]_0^{\infty}$$

$$+ \frac{4KL^2D}{a^2} \sum_{n=1}^{\infty} \frac{1}{L_n}\ \overline{\phi(t)} - \frac{4KL^2D^2}{a^2} \sum_{n=1}^{\infty} \frac{\alpha_n^2}{L_n}\ \mathcal{L}_1 \qquad (183)$$

where

$$\mathcal{L}_1 = \int_0^\infty \exp(-pt - \alpha_n^2 Dt) \int_0^t \exp(\alpha_n^2 D\lambda)\, \phi(\lambda)\, d\lambda\, dt \qquad (100).$$

The first term in Equation (183) can be simplified to

$$\frac{-4KP_o L^2 D}{a^2} \sum_{n=1}^{\infty} \frac{1}{L_n(p + \alpha_n^2 D)} \qquad (184).$$

The expression for $\mathcal{L}_1$ was previously given by Equation (106) as

$$\mathcal{L}_1 = \overline{\phi(t)}/(p + \alpha_n^2 D) \qquad (106).$$

Making the appropriate substitutions in Equation (183)

$$\left(\overline{\frac{\partial Q}{\partial t}}\right) = \frac{-4KP_o L^2 D}{a^2} \sum_{n=1}^{\infty} \frac{1}{L_n(p + \alpha_n^2 D)} + \frac{4KL^2 D}{a^2} \sum_{n=1}^{\infty} \frac{1}{L_n}\, \overline{\phi(t)}$$

$$- \frac{4KL^2 D^2}{a^2} \sum_{n=1}^{\infty} \frac{\alpha_n^2}{L_n(p + \alpha_n^2 D)}\, \overline{\phi(t)} \qquad (185).$$

Combination of the second and third terms yields

$$\left(\overline{\frac{\partial Q}{\partial t}}\right) = \frac{-4KP_o L^2 D}{a^2} \sum_{n=1}^{\infty} \frac{1}{L_n(p + \alpha_n^2 D)} + \frac{4KL^2 D}{a^2} \sum_{n=1}^{\infty} \frac{p}{L_n(p + \alpha_n^2 D)}\, \overline{\phi(t)} \qquad (186).$$

It can now be seen that Equation (186) differs from Equation (108) by a factor of L^2/L_n.

Thus, the same development described by Equations (110) through (112) applies. The equation to be solved in this case is

$$D_L \frac{\partial^2 \bar{C}}{\partial Z^2} - U \frac{\partial \bar{C}}{\partial Z} - G_2(p)\bar{C} = -H_2(p)C_o \tag{187}$$

where $\underline{h}$ is the same as before, $\underline{L_n} = \underline{a}^2\underline{\alpha_n}^2 + \underline{L}^2$,

$$H_2(p) = 1 + h \sum_{n=1}^{\infty} \frac{L^2}{L_n(p + \alpha_n^2 D)} \tag{188}$$

$$G_2(p) = p + h \sum_{n=1}^{\infty} \frac{L^2 p}{L_n(p + \alpha_n^2 D)} \tag{189}$$

and the $\underline{\alpha_n}$'s are defined by

$$a\alpha_n J_1(a\alpha_n) = LJ_o(a\alpha_n) \tag{165}.$$

If the factor $\underline{L}^2/\underline{L_n}$ is rewritten as

$$\frac{L^2}{L_n} = \frac{1}{(a\alpha_n/L)^2 + 1} \tag{190}$$

it can be seen that $\underline{L}^2/\underline{L_n} \rightarrow 1$ as $\underline{L}$ (or $\underline{k_L}$) approaches infinity. Thus, in this limiting case it is found that $\underline{H_2(p)} = \underline{H(p)}$ and $\underline{G_2(p)} = \underline{G(p)}$. Likewise, the $\underline{\alpha_n}$'s defined by Equations (165) and (159) become identical. Therefore, Case 2(F) approaches Case 1(F) as a limit as $\underline{L} \rightarrow \infty$.

Because of the fact that $\underline{H_2(p)}$ and $\underline{G_2(p)}$ differ from $\underline{H(p)}$ and $\underline{G(p)}$ by only a factor of $\underline{L}^2/\underline{L_n}$ in the respective coefficients, it follows that the development from Equations (116) to (157) applies when this factor is accounted for. Thus, the final solution is given by Equation (158) as before, where $\underline{c}$ and $\underline{d}$ are now defined for Case 2(F) as

$$c = g + h \sum_{n=1}^{\infty} \frac{L^2 b^2}{L_n (b^2 + \alpha_n^4 D^2)} \tag{191}$$

$$d = b + h \sum_{n=1}^{\infty} \frac{L^2 b \alpha_n^2 D}{L_n (b^2 + \alpha_n^4 D^2)} \tag{192}.$$

In terms of dimensionless variables, the solution for Case 2(F) is Equation (160), where the dimensionless parameters $\underline{M}$ and $\underline{N}$ are defined for Case 2(F) as follows:

$$M = \frac{1}{4S} + \frac{4DK(1 - \epsilon)}{a^2 \epsilon} \sum_{n=1}^{\infty} \frac{L^2 \eta^2 \quad U/Z_e}{L_n [(\eta U/Z_e)^2 + (D^2/a^4)\, \beta_n^4]} \tag{193}$$

$$N = \eta + \frac{4D^2 K(1 - \epsilon)}{a^4 \epsilon} \sum_{n=1}^{\infty} \frac{L^2 \eta \quad \beta_n^2}{L_n [(\eta U/Z_e)^2 + (D^2/a^4)\, \beta_n^4]} \tag{194}.$$

Here $\underline{L_n} = \beta_n^2 + \underline{L}^2$, $\underline{L} = \underline{ak_L}/\underline{D}'$, and the β_n's are positive roots of the transcendental equation

$$\beta_n J_1(\beta_n) = L J_o(\beta_n) \tag{195}.$$

DEVELOPMENT OF INTRASPHERE DIFFUSION CASES 1(S) AND 2(S)

The equations for Cases 2(S) and 1(S) will now be derived. The basic differential equation for Fick's law diffusion in a sphere is

$$D \left[\frac{\partial^2 P}{\partial r^2} + \frac{2}{r} \frac{\partial P}{\partial r} \right] = \frac{\partial P}{\partial t} \tag{15}.$$

Carslaw and Jaeger (42) give the following solution to Equation (15) for the

initial and boundary conditions

$$P = P_o \qquad 0 \leq r \leq a \qquad t = 0 \qquad (80)$$

$$-D'(\partial P/\partial r) = k_L(P - 0) \qquad r = a \qquad t > 0 \qquad (196)$$

$$P = \frac{2P_o L}{ar} \sum_{n=1}^{\infty} \frac{(a\alpha_n)^2 + (L - 1)^2}{\alpha_n^2((a\alpha_n)^2 + L^2 - L)} \exp(-\alpha_n^2 Dt) \sin(a\alpha_n)\sin(r\alpha_n) \qquad (197)$$

where the nomenclature is the same as before except that the α_n's are the real roots of the transcendental equation

$$a\alpha_n \cot(a\alpha_n) + L - 1 = 0 \qquad (198).$$

Let the following nomenclature simplification apply:

$$L_n = \frac{(a\alpha_n)^2 + (L - 1)^2}{(a\alpha_n)^2 + L^2 - L} \qquad (199).$$

When $(-P + P_o)$ is substituted for (P) in Equations (80), (196), and (197), and P_o is set equal to unity, we have

$$P = 0 \qquad 0 \leq r \leq a \qquad t = 0 \qquad (83)$$

$$-D'(\partial P/\partial r) = k_L(P - 1) \qquad r = a \qquad t > 0 \qquad (200)$$

$$P = 1 - (2L/ar) \sum_{n=1}^{\infty} (L_n/\alpha_n^2) \exp(-\alpha_n^2 Dt) \sin(a\alpha_n) \sin(r\alpha_n) \qquad (201).$$

Applying Duhamel's theorem (see Carslaw and Jaeger), the following solution is obtained:

$$P = 0 \qquad 0 \leq r \leq a \qquad t = 0 \qquad (83)$$

$$-D'(\partial P/\partial r) = k_L(P - \phi(t)) \qquad r = a \qquad t > 0 \qquad (202)$$

$$P = \int_0^t \phi(\lambda) \frac{\partial}{\partial t} \left[1 - \frac{2L}{ar} \sum_{n=1}^{\infty} \frac{L_n}{\alpha_n^2} \sin(a\alpha_n) \sin(r\alpha_n) \right.$$

$$\left. \exp(-\alpha_n^2 D(t - \lambda)) \right] d\lambda \qquad (203).$$

Differentiating,

$$P = \frac{2LD}{ar} \sum_{n=1}^{\infty} L_n \sin(a\alpha_n) \sin(r\alpha_n) \exp(-\alpha_n^2 Dt) \int_0^t \exp(\alpha_n^2 D\lambda) \phi(\lambda) \, d\lambda \qquad (204).$$

If we substitute $(\underline{P} - \underline{P}_o)$ for $\underline{P}$ and $(\phi(\lambda) - \underline{P}_o)$ for $\phi(\lambda)$ in Equation (204), the following solution is obtained:

$$P = P_o \qquad 0 \leq r \leq a \qquad t = 0 \qquad (80)$$

$$-D'(\partial P/\partial r) = k_L(P - \phi(t)), \qquad r = a, \qquad t > 0 \qquad (202)$$

$$P = P_o + \frac{2LD}{ar} \sum_{n=1}^{\infty} L_n \sin(a\alpha_n) \sin(r\alpha_n) \exp(-\alpha_n^2 Dt)$$

$$\int_0^t \exp(\alpha_n^2 D\lambda) \quad (\phi(\lambda) - P_o) \quad d\lambda \qquad (205).$$

Since the total solute content of a sphere can be evaluated as

$$Q = (3K/a^3) \int_0^a P(r,t) \, r^2 \, dr \qquad (206)$$

it follows that

$$Q = KP_o + \frac{6KLD}{a^2} \sum_{n=1}^{\infty} L_n \sin(a\alpha_n) \exp(-\alpha_n^2 Dt) \quad I_1 \quad I_2 \qquad (207)$$

where

$$I_1 = \int_0^t \exp(\alpha_n^2 D\lambda) \quad (\phi(\lambda) - P_o) \quad d\lambda \tag{176}$$

is evaluated as

$$I_1 = \int_0^t \exp(\alpha_n^2 D\lambda) \quad \phi(\lambda) \quad d\lambda \; - \; (P_o/\alpha_n^2 D) \; (\exp(\alpha_n^2 Dt) - 1) \tag{177}$$

and where

$$I_2 = (1/a^2) \int_0^a \sin(r\alpha_n) \; r \; dr \tag{208}$$

is evaluated by letting

$$u = r \quad , \qquad dv = \sin(r\alpha_n) \; dr \tag{209, 210}$$

$$du = dr \quad , \qquad v = (-1/\alpha_n) \cos(r\alpha_n) \tag{211, 212}$$

Thus,

$$I_2 = [(-r/a^2\alpha_n) \cos(r\alpha_n)]_0^a \; + \; (1/a^2\alpha_n) \int_0^a \cos(r\alpha_n) \; dr \tag{213}$$

$$I_2 = (-1/a\alpha_n) \cos(a\alpha_n) + (1/a^2\alpha_n^2) \sin(a\alpha_n) \tag{214}.$$

Substituting for I_1 and I_2 in Equation (207)

$$Q = KP_o + (6KLD/a^2) \sum_{n=1}^{\infty} L_n \; T_n \exp(-\alpha_n^2 Dt) \int_0^t \exp(\alpha_n^2 D\lambda) \; \phi(\lambda) \; d\lambda$$

$$-6KP_oL \sum_{n=1}^{\infty} (L_n/a^2\alpha_n^2) \quad T_n \; (1 - \exp(-\alpha_n^2 Dt)) \tag{215}$$

where the trigonometric term $\underline{T_n}$ is given as follows

$$T_n = (\sin^2(a\alpha_n)/a^2\alpha_n^2) - (\sin(a\alpha_n)\cos(a\alpha_n)/a\alpha_n) \tag{216}$$

It is appropriate to define a new term, $\underline{E_n} = \underline{L}(\underline{L_n}\underline{T_n})$, and simplify it as follows. By substitution

$$E_n = L\left[\frac{(a\alpha_n)^2 + (L-1)^2}{(a\alpha_n)^2 + L^2 - L}\right]\left[\frac{\sin^2(a\alpha_n)}{(a\alpha_n)^2} - \frac{\sin(a\alpha_n)\cos(a\alpha_n)}{a\alpha_n}\right] \tag{217}$$

Recalling that

$$-a\alpha_n \cot(a\alpha_n) = -a\alpha_n\,(\cos(a\alpha_n)/\sin(a\alpha_n)) = L - 1 \tag{218}$$

it can be shown that

$$E_n = L^2/(a^2\alpha_n^2 + L^2 - L) \tag{219}$$

Thus, $\underline{Q}$ is now given as

$$Q = KP_o + (6KD/a^2)\sum_{n=1}^{\infty} E_n \exp(-\alpha_n^2 Dt)\int_0^t \exp(\alpha_n^2 D\lambda)\,\phi(\lambda)\,d\lambda$$

$$-6KP_o\sum_{n=1}^{\infty}(E_n/a^2\alpha_n^2)\,(1 - \exp(-\alpha_n^2 Dt)) \tag{220}$$

Taking the derivative of $\underline{Q}$ with respect to $\underline{t}$

$$\frac{\partial Q}{\partial t} = -(6KD^2/a^2)\sum_{n=1}^{\infty}\alpha_n^2 E_n \exp(-\alpha_n^2 Dt)\int_0^t \exp(\alpha_n^2 D\lambda)\,\phi(\lambda)\;\,d\lambda$$

$$+ (6KD/a^2)\sum_{n=1}^{\infty} E_n\,\phi(t) - (6KP_oD/a^2)\sum_{n=1}^{\infty} E_n \exp(-\alpha_n^2 Dt) \tag{221}$$

The Laplace transform of $\partial Q/\partial t$ is evaluated as follows:

$$\left(\overline{\frac{\partial Q}{\partial t}}\right) = -(6KD^2/a^2) \sum_{n=1}^{\infty} \alpha_n^2 E_n \mathcal{L}_1 + (6KD/a^2) \sum_{n=1}^{\infty} E_n \overline{\phi(t)}$$

$$-(6KP_oD/a^2) \sum_{n=1}^{\infty} E_n \int_0^{\infty} \exp(-pt - \alpha_n^2 Dt) \quad dt \qquad (222)$$

where

$$\mathcal{L}_1' = \int_0^{\infty} \exp(-pt - \alpha_n^2 Dt) \int_0^t \exp(\alpha_n^2 D\lambda) \quad \phi(\lambda) \quad d\lambda \quad dt \qquad (100).$$

In this case $\mathcal{L}_1$ was previously given by Equation (106) as

$$\mathcal{L}_1 = \overline{\phi(t)}/(p + \alpha_n^2 D) \qquad (106).$$

The last term in Equation (222) is

$$-(6KP_oD/a^2) \sum_{n=1}^{\infty} E_n/(p + \alpha_n^2 D) \qquad (223).$$

Substituting for $\mathcal{L}_1$ and rearranging

$$\left(\overline{\frac{\partial Q}{\partial t}}\right) = \frac{-6KP_oD}{a^2} \sum_{n=1}^{\infty} \frac{E_n}{p + \alpha_n^2 D} + \frac{6KD}{a^2} \sum_{n=1}^{\infty} \frac{E_n p}{p + \alpha_n^2 D} \quad \overline{\phi(t)} \qquad (224).$$

It can now be seen that the terms in Equation (224) differ from those in Equation (108) by a factor of $6E_n/4$.

Thus, the same development described by Equations (110) through (112) applies. The differential equation to be solved in this case is

$$D_L \frac{\partial^2 \overline{C}}{\partial Z^2} - U \frac{\partial \overline{C}}{\partial Z} - G_3(p)\overline{C} = -H_3(p)C_o \qquad (225)$$

where

$$H_3(p) = 1 + h' \sum_{n=1}^{\infty} \frac{E_n}{p + \alpha_n^2 D} \tag{226}$$

$$G_3(p) = p + h' \sum_{n=1}^{\infty} \frac{E_n p}{p + \alpha_n^2 D} \tag{227}$$

$$h' = 6DK(1 - \epsilon)/a^2\epsilon \tag{228}$$

$$E_n = L^2/(a^2\alpha_n^2 + L^2 - L) \tag{219}$$

and the α_n's are defined by Equation (198).

Because of the fact that $H_3(p)$ and $G_3(p)$ differ from $H(p)$ and $G(p)$ by only a factor of $6E_n/4$ in the respective infinite sums, it follows that the development from Equations (116) to (157) applies when this factor is accounted for. Thus, the final solution is given by Equation (158) as before, where c and d are now defined for Case 2(S) as

$$c = g + h' \sum_{n=1}^{\infty} \frac{E_n b^2}{b^2 + \alpha_n^4 D^2} \tag{229}$$

$$d = b + h' \sum_{n=1}^{\infty} \frac{E_n b \alpha_n^2 D}{b^2 + \alpha_n^4 D^2} \tag{230}.$$

In terms of dimensionless variables, the solution for Case 2(S) is Equation (160), where the dimensionless parameters M and N are defined for Case 2(S) as follows:

$$M = \frac{1}{4S} + \frac{6DK(1 - \epsilon)}{a^2\epsilon} \sum_{n=1}^{\infty} \frac{E_n \eta^2 \, U/Z_e}{(\eta U/Z_e)^2 + (D^2/a^4)\, \beta_n^4} \tag{231}$$

$$N = \eta + \frac{6D^2K(1 - \epsilon)}{a^4\epsilon} \sum_{n=1}^{\infty} \frac{E_n \eta \, \beta_n^2}{(\eta U/Z_e)^2 + (D^2/a^4)\, \beta_n^4} \tag{232}.$$

Here,

$$E_n = L^2/(\beta_n^2 + L^2 - L) \tag{233}$$

and the β_n's are defined as

$$\beta_n \cot(\beta_n) + L - 1 = 0 \tag{234}.$$

In view of the previously demonstrated equivalence between Cases 2(F) and 1(F) as $L \rightarrow \infty$, it is possible to obtain expressions for Case 1(S) as follows. Equation (233) can be rewritten as

$$E_n = \frac{1}{\beta_n^2/L^2 + 1 - 1/L} \tag{235}.$$

Therefore, as $L \rightarrow \infty$, $E_n \rightarrow 1$, and the β_n's are defined for Case 1(S) as

$$\beta_n \cot(\beta_n) = - \infty \tag{24}.$$

Thus, Case 1(S) is obtained from Case 2(S) by letting $E_n = 1$ and employing the roots defined above.

NO-SORPTION AND EQUILIBRIUM CASES

The simplest cases that will be considered here are the No-Sorption and Equilibrium cases. Sherman (1) has already derived analytical expressions for these cases; however, for a number of reasons, it is desirable to express these solutions in the integral form that has applied to the preceding developments.

The differential equation for longitudinal dispersion is again Equation (2). If $\underline{Q}$ always equals $\underline{KC}$, then

$$\partial Q/\partial t = K\, \partial C/\partial t \qquad (5).$$

Thus, the differential equation can be rewritten as

$$D_L \frac{\partial^2 C}{\partial Z^2} - U \frac{\partial C}{\partial Z} = B \frac{\partial C}{\partial t} \qquad (236)$$

where

$$B = 1 + K(1 - \epsilon)/\epsilon \qquad (237).$$

The Laplace transform of Equation (236) is

$$D_L \frac{\partial^2 \bar{C}}{\partial Z^2} - U \frac{\partial \bar{C}}{\partial Z} - G_4(p)\bar{C} = -H_4(p)C_o \qquad (238)$$

where $\underline{H_4(p)} = \underline{B}$ and $\underline{G_4(p)} = \underline{pB}$.

The solution of Equation (238) follows in the same manner as given before by Equations (116) through (122). In this case the expression for $\exp(\underline{mZ})$ can be written as

$$\exp(mZ) = f_3(p) = \exp(UZ/2D_L)\, f_4(p) \qquad (239)$$

$$f_4(p) = \exp(-q(g + pB)^{1/2}) \qquad (240).$$

The inverse transform of $\underline{f_4(p)}$ is expressed as

$$F_4(t) = \frac{\exp(ts)}{2\pi} \int_{-\infty}^{+\infty} \exp(tbi)\, \exp(-q(g + sB + bBi)^{1/2})db \qquad (241).$$

By inspection, it follows that Equation (241) is the same as Equation (135) when $\underline{c} + \underline{di}$ is defined as follows:

$$c + di = g + sB + bBi \tag{242}$$

Since $\underline{c}$ is indifferent to changes in the sign of $\underline{b}$, and since the sign of $\underline{d}$ is the sign of $\underline{b}$, the same development given by Equations (136) through (145) applies. Since the singularity of $\underline{f_3}(\underline{p})$ exists at $\underline{p} = -\underline{g}/\underline{B}$, it follows that $\underline{s}$ can be given a value of zero as before and $\underline{F_3}(\underline{t})$ is therefore defined by Equation (148) when the appropriate values of $\underline{c}$ and $\underline{d}$ are used.

Thus, the final solution for the Equilibrium case is given by Equation (158) when

$$c = g \tag{243}$$

$$d = b(1 + K(1 - \epsilon)/\epsilon) \tag{244}.$$

In terms of dimensionless variables the solution for the Equilibrium case is given by Equation (160) when

$$M = 1/4S \tag{245}$$

$$N = \eta(1 + K(1 - \epsilon)/\epsilon) \tag{246}.$$

The solution for the No-Sorption case is also given by Equation (160), since for this case $\underline{K} = 0$, $\underline{M} = 1/4\underline{S}$ and $\underline{N} = \eta$.

FIRST-ORDER REACTION CASE

A simple case of first-order reaction can be treated if the assumption is made that

$$\partial Q/\partial t = -k''\tilde{C} \tag{247}$$

where $\underline{k}$ is a reaction rate constant. The transformed differential equation for

Note that $\underline{k}$ must be negative.

longitudinal dispersion can therefore be written as

$$D_L \frac{\partial^2 \bar{C}}{\partial Z^2} - U \frac{\partial \bar{C}}{\partial Z} - G_5(p)\bar{C} = -H_5(p)C_o \tag{248}$$

where

$$H_5(p) = 1 \tag{249}$$

$$G_5(p) = p - k(1 - \epsilon)/\epsilon = p - k'' \tag{250}.$$

The solution of Equation (248) follows in the same manner as given before by Equations (116) through (122). In this case the expression for $\exp(\underline{mZ})$ can be written as

$$\exp(mZ) = f_3(p) = \exp(UZ/2D_L)\, f_4(p) \tag{239}$$

$$f_4(p) = \exp(-q(g + p - k'')^{1/2}) \tag{251}.$$

The inverse transform of $\underline{f}_4(\underline{p})$ is then expressed as

$$F_4(t) = \frac{\exp(ts)}{2\pi} \int_{-\infty}^{+\infty} \exp(tbi)\, \exp(-q(g - k'' + s + bi)^{1/2})db \tag{252}.$$

By inspection, it follows that Equation (252) is the same as Equation (135) when $\underline{c} + \underline{di}$ is defined as follows:

$$c + di = g - k'' + s + bi \tag{253}.$$

Since $\underline{c}$ is indifferent to changes in the sign of $\underline{b}$, and since the sign of $\underline{d}$ is the sign of $\underline{b}$, the same development given by Equations (136) through (145) applies.

Since the singularities of $\underline{f}_3(\underline{p})$ exist at $\underline{p} \leq (\underline{k}'' - \underline{g})$, it is necessary to specify that $\underline{s} > (\underline{k}'' - \underline{g})$ in $\underline{F}_3(\underline{t})$. Therefore, since $\underline{g}$ is always positive, $\underline{s}$ will

arbitrarily be taken as $\underline{s} = \underline{k}''$. Thus, $\underline{F_3}(\underline{t})$ becomes

$$F_3(t) = \frac{\exp(UZ/2D_L)}{\pi} \int_0^\infty \exp(k''t - q(\bar{r}^2/2 + c/2)^{1/2})$$

$$\cos(tb - q(\bar{r}^2/2 - c/2)^{1/2}\, db \qquad (254)$$

where $\underline{c}$, $\underline{d}$, and $\underline{\bar{r}}$ are now defined as

$$\bar{r}^2 = (c^2 + d^2)^{1/2} \qquad (137)$$

$$c = g \qquad (255)$$

$$d = b \qquad (256).$$

The final solution for the first-order reaction case follows from the previous developments and is given by Equation (158) when the inner integral is expressed as

$$\int_0^{b=\infty} \exp\,[UZ/2D_L + k''\tau - q(\bar{r}^2/2 + c/2)^{1/2}]$$

$$\cos\,[\tau b - q(\bar{r}^2/2 - c/2)^{1/2}]\; db \qquad (257).$$

In terms of dimensionless variables, the final solution is given by Equation (160) when the inner integral is expressed as

$$\int_0^{\eta=\infty} \exp\left[\frac{1}{2S} + \frac{k''Z_e\omega}{U} - \left(\frac{\psi}{2S}\,(1 + M/\psi)\right)^{1/2}\right]$$

$$\cos\left[\omega\eta - \left(\frac{\psi}{2S}\,(1 - M/\psi)\right)^{1/2}\right]\; d\eta \qquad (258)$$

where

$$\psi = (M^2 + N^2)^{1/2} \qquad (18)$$

$$M = 1/4S \quad , \qquad N = \eta \qquad (259, 260)$$

$$K'' = K(1 - \epsilon)/\epsilon$$

APPENDIX II

COMPUTER PROGRAMS

Numerous Fortran programs were required for the numerical calculations in this work. Representative results from every program were checked by independent means (generally by slide rule calculation from original formulas). With the exception of a few that follow, these programs are not listed and discussed because of space limitations.

Two of the above-mentioned programs (listed as P-1 and P-2 at the end of this appendix) represented successive halves of the calculation sequence needed to evaluate C/C_o vs. R for the first four cases; P-1 can be easily modified to calculate Cases 1(S) and 2(S). These programs (especially P-1) were "streamlined" a number of times in order to reduce running time, but a single breakthrough curve calculation for Case 1(F) or 2(F) still required from one to two hours (depending mostly on the value of S) on a conventional IBM 1620 computer.

DESCRIPTION OF PROGRAMS P-1 AND P-2

The purpose of Program P-1 was to calculate values of the inner integral of Equation (160), namely

$$I_1 = \int_0^\infty \exp\left[\frac{1}{2S} - \left(\frac{\psi}{2S}(1 + M/\psi)\right)^{1/2}\right] \cos\left[\omega\eta - \left(\frac{\psi}{2S}(1 - M/\psi)\right)^{1/2}\right] d\eta \qquad (261).$$

The input data and results of this program were punched out in the correct order to serve as the input data for Program P-2, which was used to calculate

$$\frac{C}{C_o} = 1 - \frac{1}{\pi}\int_0^R \left[1 - \left(k_o + \sum_{n=1}^{f} k_n (R-\omega)^n\right) \exp(-\gamma\,(R-\omega))\right] I_1 \; d\omega \qquad (262)$$

at several equally spaced values of $\underline{R}$, and also

$$M_o = \int_0^{R_F} (C/C_o)\, dR \qquad (263)$$

at one or three values of $\underline{R_F}$.

The cases that were calculated by P-1 were (a) the No-Sorption case when CALC = 1, (b) the Equilibrium case when CALC = 2, (c) Case 1(F), when CALC = 3, $\underline{L} > 999$, and the first 124 values of $\beta_{\underline{n}}$ were loaded, (d) Case 2(F) when CALC = 3, $\underline{L} < 999$, and the first 124 values of $\beta_{\underline{n}}$ were loaded.

PROGRAM FOR ROOTS OF $J_o(\beta_{\underline{n}}) = 0$

This program calculated 124 positive roots of the above equation from the following asymptotic series

$$\beta_n = \frac{1}{4}\pi a \left[1 + \frac{2}{\pi^2 a^2} - \frac{62}{3\pi^4 a^4} + \frac{15116}{15\pi^6 a^6} - \frac{12554474}{105\,\pi^8 a^8} + \frac{8368654292}{315\,\pi^{10} a^{10}}\right] \qquad (264)$$

where $\underline{a} = 4\underline{n} - 1$ and $\underline{n}$ is a positive integer designating the root number.

A comparison of the calculated roots with those published by Carslaw and Jaeger (42) established that (a) the program was correct, and (b) sufficient accuracy was being obtained, since agreement to the fourth decimal was achieved

on the second to sixth roots. The first root was slightly inaccurate due to lack of convergence, and was corrected to 2.4048 for subsequent use.

PROGRAMS FOR ROOTS OF $\beta_n J_1(\beta_n) = \underline{L} J_o(\beta_n)$

Two programs were used to calculate 124 roots of the above equation. The first program was used to calculate the zero and first-order Bessel functions $J_o(\beta)$ and $J_1(\beta)$ as a function of β at 0.35 intervals. The following expressions were used, since they apply when β is large and positive.

$$J_o(\beta) = (2/\pi\beta)^{1/2} [P_o(\beta)\cos(\beta-\pi/4) - Q_o(\beta)\sin(\beta-\pi/4)] \quad (265)$$

$$J_1(\beta) = (2/\pi\beta)^{1/2} [P_1(\beta)\cos(\beta-3\pi/4) - Q_1(\beta)\sin(\beta-3\pi/4)] \quad (266)$$

where $\underline{P}_o(\beta)$, $\underline{Q}_o(\beta)$, $\underline{P}_1(\beta)$, and $\underline{Q}_1(\beta)$ are asymptotic series given in the British Mathematics Association Tables (BMT). The following results were obtained and compared with those published in the BMT.

	$J_o(\beta)$		$J_1(\beta)$	
β	Calculated	BMT	Calculated	BMT
2.00	0.22486	0.22389	0.58117	0.57672
5.15	-0.127392	-0.127389	-0.340590	-0.340584
9.35	-0.167448	-0.167448	0.191234	0.191234

The second program was used to calculate 124 roots of

$$\beta_n J_1(\beta_n) = L J_o(\beta_n) \quad (23)$$

from the output of the first program. The effect of the increment size on the accuracy of the roots is illustrated as follows, for $\underline{L} = 10$.

β_n, (42)	β_n, $\Delta\beta = 0.35$	β_n, $\Delta\beta = 0.15$
2.1795	2.1864	2.1811
5.0332	5.0342	5.0335
7.9569	7.9571	7.9569
10.9363	10.9361	10.9363
13.9580	13.9585	13.9579
17.0099	17.0091	17.0099

It can be seen that an increment size of 0.35 for the input Bessel functions yielded nearly three decimal accuracy in the roots, which was more than adequate for the problem. Because of the inherent inaccuracy at small values of β, the first two roots from subsequent calculations were replaced by published values from Carslaw and Jaeger, for use as input to Program P-1. To illustrate the effect of L, the following values of the sixth root were calculated, using $\Delta\beta = 0.35$.

L	β_6, (42)	β_6, Calc.
0.1	16.4767	16.4763
0.4	16.4949	16.4943
1.0	16.5312	16.5302
5.0	16.7630	16.7632
30.0	17.5348	17.5356
60.0	17.7807	17.7814

NUMERICAL CHECKS ON PROGRAMS P-1 AND P-2

In order to establish that Programs P-1 and P-2 were calculating correctly, it was necessary to make a number of numerical checks. While the testing was in progress, it was especially important to consider the critical balance between

accuracy and running time. It was finally decided that Programs P-1 and P-2 would be set to yield three-place accuracy in the final result. The following is a step by step summary of the tests which were made on P-1 and P-2.

THE INFINITE SUMS M AND N IN PROGRAM P-1

The calculation of M and N for the intrafiber diffusion cases was first checked at $\eta = 0.4$ by effectively limiting each sum to two terms, using S = 0.04, K = 0.3, $\epsilon = 0.7$, $U/Z_e = 0.2$, $D_F/a^2 = 0.01$, CALC = 3, $\beta_1 = 2.4048$, $\beta_2 = 5.520$, and β_3 through β_{124} equal to 10000. For Case 1(F), letting L = 1000,

$$M = 6.25 + 0.515(0.0329 + 0.00324) = 6.2686 \text{ (slide rule)}$$

$$SM = 6.26854 \text{ (computer)}$$

$$N = 0.4 + 0.515(0.0236 + 0.0122) = 0.4184 \text{ (slide rule)}$$

$$SN = 0.41852 \text{ (computer)}$$

For Case 2(F), letting L = 4,

$$M = 6.25 + 0.515(0.0242 + 0.001115) = 6.2630$$

$$SM = 6.26297$$

$$N = 0.4 + 0.515(0.01738 + 0.0042) = 0.4111$$

$$SN = 0.41114$$

A number of tests were performed on the infinite sums that were required for the computation of M and N in Cases 1(F) and 2(F). It can be seen from the derived expressions that M converges quite rapidly in comparison to N. The respective n'th terms in the sums for M and N are denoted in terms of program variables as $(SSM)_n$ and $(SSN)_n$. After several convergence tests were performed, by terminating the summations at various points, Program P-1 was finally set to stop computing $(SSM)_n$ when $(SSM)_n < 0.0001\ (SSM)_1$, and $(SSN)_n$ when $n = 124$, where β_{124} is roughly 390. Although the truncation error in N was sometimes significant

at large values of η, the final value of the integral $\underline{I}_1$ was found to be quite insensitive to this error since the exponential term decreased rapidly as η increased. In other words, the integrand was very small whenever the truncation error in $\underline{N}$ became significant. Normally, the exponential in the integrand of $\underline{I}_1$ converged to the preset value of 0.00008 when η was in the vicinity of 30; at this point the integration $\underline{I}_1$ was terminated.

THE INTEGRATION $\underline{I}_1$ IN PROGRAM P-1

The integrand of $\underline{I}_1$ was checked at $\eta = 10$, $\omega = 0.85$ by letting $\underline{S} = 0.025$, $\underline{K} = 0.3$, $\epsilon = 0.7$, and $\underline{CALC} = 1$. In this case the hand-calculated value of the integrand was 0.114; the computer value was $\underline{ZY(I)} = 0.1145$.

In order to demonstrate that the integration $\underline{I}_1$ was being performed properly, the following procedure was used. A new program was compiled in which only the source statements related to the integrand were changed. Thus, in place of $\underline{I}_1$, the exact integral

$$I_1' = \int_0^\infty \exp(-ax)\cos((\omega + a)x)\,dx = a/(a^2 + (\omega + a)^2) \qquad (267)$$

was evaluated numerically. The results of this integration were then compared to the analytical results as follows (Table XXIV), letting $\underline{S} = 1$, and $\underline{a} = 1/4\underline{S} = 0.25$.

In a number of subsequent tests on P-1 it was established that an increment size of $\Delta\eta = 0.4$ was sufficiently small to yield nearly four-place accuracy in $\underline{I}_1$ also.

TABLE XXIV

CHECK ON NUMERICAL INTEGRATION IN PROGRAM P-1

Calculation	Values of $\underline{I}_1'$			
	$\omega = 0$	$\omega = 0.05$	$\omega = 0.10$	$\omega = 0.75$
(slide rule)	2.000	1.639	1.351	0.2352
$\Delta\eta = 0.17$	2.00016	1.63915	1.35136	0.23529
$\Delta\eta = 0.2$	2.00020	1.63914	1.35132	0.23523
$\Delta\eta = 0.4$	2.00011	1.63917	1.35139	---
$\Delta\eta = 1.0$	1.99998	1.63930	1.35142	0.23546[a]

[a] In this case the numerical integration was carried out over about 5 cycles, with approximately 6 increments per cycle in the exponentially damped cosine function.

THE INTEGRATION $\underline{I}_2$ IN PROGRAM P-2

The accuracy of the integration $\underline{I}_2$, yielding $\underline{C}/\underline{C}_o$ vs. $\underline{R}$, was checked by letting $\underline{I}_1 = 1$ at all values of ω, and $\underline{k}_o = \underline{k}_2 = \underline{k}_3 = \ldots = 0$, so that the actual integration which was performed in this case was

$$I_2' = 1 - (1/\pi) \int_0^R [1 - k_1(R - \omega) \exp(-\gamma (R - \omega))] \, d\omega \qquad (268).$$

It can be shown that $\underline{I}_2'$ is an exact integral given by

$$I_2' = 1 - (1/\pi) [R + Rk_1 \exp(-\gamma R)/\gamma + k_1 \exp(-\gamma R)/\gamma^2 - k_1/\gamma^2] \qquad (269).$$

The numerical integration of Equation (268) was checked at $\underline{R} = 1.44$ by using the values $\underline{k}_1 = 10$ and $\gamma = 3$. The hand-calculated value was found to be 0.8705. The computer values for $\underline{C}/\underline{C}_o$ were found to be 0.8702869 when $\Delta\omega$ was 0.03, and also 0.06.

CONVERGENCE CHECKS ON OVER-ALL CALCULATIONS

A number of convergence tests were performed on the over-all calculation sequence, involving the sequential use of Programs P-1 and P-2. When the appropriate input constants for a step-function were used, it was observed in one test that changing the $\Delta\omega$ increment from 0.02 to 0.03 had no effect on the first seven decimal places of $\underline{C}/\underline{C}_o$. When typical sets of input constants were used, however, it became apparent that the inclusion of higher order terms, in the exponentially damped polynomial, had a tendency to disrupt the convergence of $\underline{I}_2$.

To demonstrate that adequate convergence was effectively obtained during the subsequent analyses of breakthrough curves, a number of representative calculations were compared; some important results of these checks are given in Table XXV.

In view of the above results, increment sizes of $\Delta\eta = 0.3$ and $\Delta\omega = 0.06$ were considered sufficient for achieving approximately three-place accuracy in $\underline{C}/\underline{C}_o$, over the pore volume range $0 \leq \underline{R} \leq 6.84$. These increment sizes were therefore used in all calculations that applied to the PAA systems, where $\underline{K}$ was relatively large. For the No-Sorption cases, and Equilibrium cases in the diacetyl systems, where $\underline{K}$ was small, $\Delta\omega = 0.02$ was used to obtain closer spaced values of $\underline{C}/\underline{C}_o$ over the range $0 \leq \underline{R} \leq 2.28$.

CONSISTENCY CHECKS ON PROGRAMS P-1 AND P-2

A check was made against Sherman's calculation for Run 9-8 (glass beads) with the following results. He used a $\Delta\omega$ increment size of 0.01, and 0.02 was used by this writer.

TABLE XXV

CONVERGENCE CHECKS ON USE OF PROGRAMS P-1 AND P-2

Run No.	$\Delta\eta$	$\Delta\omega$	S	D_F/a^2	L	C/C_o, R=1.80
3-27-1	0.3	0.02	0.00357	0.013	∞	0.94575
3-27-1	0.3	0.06	0.00357	0.013	∞	0.94621
3-27-1	0.25	0.06	0.00357	0.013	∞	0.94605
3-27-1	0.3	0.02	0.00357	0.013	998.0	0.94584
3-27-1	0.3	0.02	0.00357	0.030	3.5	0.94968
3-27-1	0.3	0.06	0.00357	0.030	3.5	0.94998
3-28-1	0.3	0.02	0.00357	0.0295	∞	0.85613
3-28-1	0.3	0.06	0.00357	0.0295	∞	0.85621
3-28-1	0.3	0.02	0.00357	0.03	50.0	0.84863
3-28-1	0.3	0.06	0.00357	0.03	50.0	0.84870
3-35-1	0.3	0.02	0.006	0.03	∞	0.96427
3-35-1	0.3	0.06	0.006	0.03	∞	0.96439
1-9-16	0.3	0.02	0.0185	0.005	∞	0.39705
1-9-16	0.3	0.06	0.0185	0.005	∞	0.39705
1-9-16	0.25	0.06	0.0185	0.005	∞	0.39755
1-9-16	0.3	0.06	0.0185	0.005	998.0	0.39700
2-18-16	0.3	0.02	0.00959	0.004	∞	0.76500
2-18-16	0.3	0.06	0.00959	0.004	∞	0.76502

Description	C/C_o, R=0.60	C/C_o, R=1.2	M_o, R_F=2.28
P-1 & P-2	0.97854	0.27233	1.0583
Sherman	0.97832	0.27247	1.058

It is important to note here that Sherman's calculation was based on an equation having a different form than the writer's equation, the essential difference being that Sherman expressed I_1 in terms of exponential and error functions, thus eliminating the numerical integration in this case.

A check was made on the accuracy and internal consistency of the four separate cases that were calculated with P-1 and P-2. This was accomplished by comparing the results of certain limiting calculations for the intrafiber diffusion cases against the Equilibrium and No-Sorption cases. The first seven rows of results in Table XXVI were obtained from the parameters, S = 0.025, K = 0.3, ϵ = 0.7, k_o - k_4 = 0 (step-function), and U/Z_e = 0.2. The last two rows represent a typical calculation from the analysis of the diacetyl-64 denier system. The increment sizes were $\Delta\eta$ = 0.4 and $\Delta\omega$ = 0.02 in all cases. For the results given in the first four rows, $M_o = 1 + K(1 - \epsilon)/\epsilon = 1.1287$. It was concluded from these results that the respective solutions for all four cases, and the corresponding computer programs, were mutually consistent.

NOTES ON USE OF PROGRAM P-1

SW 1 on, $\Delta\omega$ = 0.02

SW 1 off, $\Delta\omega$ = 0.06

SW 2 on, $\Delta\eta$ = 0.3

SW 4 on, $\Delta\eta$ = 0.25

SW 2 and 4 off, $\Delta\eta$ = 0.4

TABLE XXVI

NUMERICAL COMPARISONS OF LIMITING CASES

Case	D_F/a^2	L	C/C$_o$ at R=0.72	at R=1.08	at R=1.44	M_o, R_F=2.28
Equil.	∞	∞	0.973156	0.534777	0.113215	1.12870
1(F)	1000.0	∞	0.973040	0.534113	0.112903	1.12828
1(F)	100.0	∞	0.972951	0.534097	0.112985	1.12828
1(F)	10.0	∞	0.972076	0.533911	0.113824	1.12827
No-Sorp.	0.0	0.0	0.915353	0.323833	0.039221	0.999996
1(F)	0.0001	∞	0.916327	0.329302	0.044222	1.00700
1(F)	0.001	∞	0.918715	0.342743	0.055863	1.02347
1(F)	0.085	∞	0.997833	0.578549	0.136145	1.19636
2(F)	0.085	998.0	0.997830	0.578550	0.136218	1.19643

INPUT DATA NOMENCLATURE

NO = number of separate calculations to be performed

SP = S ; EQILP = K ; EPSP = ϵ_E ;

AKP = k_o ; BP = k_1 ; CP = k_2 ;

DP = k_3 ; EP = k_4 ; GAMP = γ ;

UOZP = U/Z_E ; DFASP = D_F/a^2 ; ALP = $L = ak_L/D'_F$;

CALCP = 1, No-Sorption case

CALCP = 2, Equilibrium case

CALCP = 3, Case 1(F) when L > 999 and Case 2(F) when L < 999

BETA(II) = appropriate set of roots (124 required)

NOTES ON USE OF PROGRAM P-2

Program for $\Delta\omega = 0.06$ is shown; modification required for 0.02.

Punched output from P-1 is used as input for P-2.

OUTPUT NOMENCLATURE

RR = R ; COC = C/C_o ; (at $6\Delta\omega$ intervals)

ACOC = area under breakthrough curve at various R values

PROGRAM P-1

```
50      READ,NO
        DIMENSION SP(10),EQILP(10),EPSP(10),AKP(10),BP(10)
        DIMENSION CP(10),DP(10),EP(10),GAMP(10),UOZP(10)
        DIMENSION DFASP(10),ALP(10),CALCP(10),ZY(7)
        DIMENSION BETA(1250),Z(155),Y(155),BE(10)
        L=1
        LL=125
        II=1
72      READ,SP(L),EQILP(L),EPSP(L),AKP(L),BP(L),CP(L),DP(L)
        READ,EP(L),GAMP(L),UOZP(L),DFASP(L),ALP(L),CALCP(L)
        IF(CALCP(L)-2.) 74,74,73
73      READ,BETA(II)
        BE(L)=BETA(II)
        BETA(II)=BETA(II)*BETA(II)
        II=II+1
2       READ,BETA(II)
        BETA(II)=BETA(II)*BETA(II)
        II=II+1
        IF(II-LL) 2,74,74
74      II=LL
        LL=LL+124
        L=L+1
        PRINT,L
        IF(L-NO) 72,72,75
75      L=1
        LL=1
76      BB=.0001
        S=SP(L)
        EQUIL=EQILP(L)
        EPS=EPSP(L)
        AK=AKP(L)
        B=BP(L)
        C=CP(L)
        D=DP(L)
        E=EP(L)
        GAM=GAMP(L)
        UOZ=UOZP(L)
        DFOAS=DFASP(L)
        AL=ALP(L)
        CALC=CALCP(L)
        PTS=.5/S
        PSI=EQUIL*((1.-EPS)/EPS)
        ROS=.25/S
        CALCC=CALC-2.
        IF(SENSE SWITCH 4) 70,71
70      DELN=.25
        GO TO 67
71      IF(SENSE SWITCH 2) 65,66
65      DELN=.3
        GO TO 67
66      DELN=.4
```

```
67      UUOZ=UOZ*UOZ
        DOASS=DFOAS*DFOAS
        ALL=AL*AL
        ALLL=AL-999.
        IF(ALLL) 52,51,51
51      H=4.*PSI
        GO TO 53
52      H=4.*ALL*PSI
53      U=DELN/140.
        IF(CALCC) 31,30,31
30      ALAM=1.+PSI
        GO TO 32
31      ALAM=1.
32      I=1
        V=0.
        W=0.
        EATA=0.
        JJ=1
3       IF(CALCC) 10,10,4
4       II=LL
        SSSM=0.
        SSSN=0.
        SSM=1.
        EATAS=EATA*EATA
        ETUOZ=EATAS*UUOZ
        SSMM=EATAS*UOZ*DFOAS
5       BETT=BETA(II)
        BETTD=BETT*DOASS
        BOT=ETUOZ+BETTD*BETT
        IF(ALLL) 54,55,55
54      BOT=BOT*(BETT+ALL)
55      BOTT=1./BOT
        SSN=BETTD*EATA*BOTT
        IF(SSM-BB) 8,6,6
6       SSM=SSMM*BOTT
        IF(II-LL) 68,68,69
68      BB=.0001*SSM
69      SSSM=SSSM+SSM
8       SSSN=SSSN+SSN
        II=II+1
        IF(II-LL-124) 5,9,9
9       SM=SSSM*H + ROS
        SN=SSSN*H + EATA
        IF(CALCC) 10,10,34
34      IF(EATA) 11,11,13
10      IF(EATA) 11,11,12
11      SM=ROS
        SN=0.
        P=SM
        GO TO 14
12      SM=ROS
        SN=EATA*ALAM
13      P=SQRT(SM*SM+SN*SN)
14      ZOAP=P/S
```

```
      COTH=(.5*SM)/P
      Z(JJ)=EXP(PTS-SQRT((.5+COTH)*ZOAP))
      Y(JJ)=SQRT((.5-COTH)*ZOAP)
43    ZY(I)=Z(JJ)*COS(W*EATA-Y(JJ))
      I=I+1
      EATA=EATA+DELN
      JJ=JJ+1
      IF(W) 36,36,35
35    IF(I-8) 43,15,15
36    IF(I-8) 3,15,15
15    I=1
      VVV=41.*(ZY(I)+ZY(I+6))+216.*(ZY(I+1)+ZY(I+5))
      VV=VVV+27.*(ZY(I+2)+ZY(I+4))+272.*ZY(I+3)
      V=V+VV
      ZY(I)=ZY(I+6)
      I=2
      IF(W) 38,38,37
37    IF(Z(JJ-1)-.00008) 16,43,43
38    IF(Z(JJ-1)-.00008) 16,3,3
16    IF(W) 39,39,40
39    II=LL
40    BETA(II)=V*U
      IF(SENSE SWITCH 3) 63,64
63    PRINT,BETA(II)
64    II=II+1
      I=1
      JJ=1
      V=0.
      EATA=0.
      IF(SENSE SWITCH 1) 98,99
98    W=W+.02
      IF(2.28-W) 17,43,43
99    W=W+.06
      IF(6.84-W) 17,43,43
17    L=L+1
      PRINT,L
      LL=LL+124
      IF(L-NO) 76,76,77
77    L=1
      LL=1
      LLL=115
78    PUNCH,SP(L),EQILP(L),EPSP(L),AKP(L),BP(L),CP(L),DP(L)
      PUNCH,EP(L),GAMP(L),UOZP(L),DFASP(L),ALP(L),CALCP(L)
      IF(CALCP(L)-2.) 81,81,82
81    PUNCH,DELN
      GO TO 83
82    PUNCH,DELN,BE(L)
83    DO 79 II=LL,LLL
79    PUNCH,BETA(II)
      L=L+1
      LL=LL+124
      LLL=LLL+124
      IF(L-NO) 78,78,80
80    GO TO 50
      STOP
      END
```

PROGRAM P-2 FOR $\Delta\omega$ = 0.06

```
50    READ,S,EQUIL,EPS,AK,B,C,D,E,GAM,UOZ,DFOAS,AL,CALC
      PRINT,S,EQUIL,EPS,AK,B,C,D,E,GAM,UOZ,DFOAS,AL,CALC
      DIMENSION X(9),V(125),COC(20)
      IF(CALC-2.) 63,63,64
63    READ,DELN
      BETAI=0.
      GO TO 65
64    READ,DELN,BETAI
65    PRINT,DELN,BETAI
      RR=.36
      RF=6.84
      DELR=.36
      DELW=.06
      PI=3.1415926
      PII=1./PI
      UU=DELW/140.
      ZZ=0.
      AREA=0.
      W=0.
      L=1
      K=1
39    READ,V(K)
      K=K+1
      IF(116-K) 17,17,39
17    K=1
      J=1
18    R=RR-W
      RS=R*R
      GAMR=GAM*R
      IF(GAMR-40.) 60,61,61
61    XX=PII
      GO TO 62
60    XXX=AK+B*R+C*RS+D*R*RS+E*RS*RS
      XX=PII*(1.-(XXX*(EXP(-GAMR))))
62    X(J)=V(K)*XX
      J=J+1
      W=W+DELW
      K=K+1
      IF(J-8) 18,19,19
19    J=1
      ZZZ=41.*(X(J)+X(J+6))+216.*(X(J+1)+X(J+5))+27.*(X(J+2)+X(J+4))
      ZZZ=ZZZ+272.*X(J+3)
      ZZ=ZZ+ZZZ
27    X(J)=X(J+6)
      J=2
      IF(RR-W) 20,18,18
20    COC(L)=1.-ZZ*UU
      PRINT,RR,COC(L)
      L=L+1
22    RR=RR+DELR
```

```
      J=1
      K=1
      ZZ=0.
      W=0.
      IF(RF-RR) 23,18,18
23    L=1
24    AREA=AREA+41.*COC(L)+216.*COC(L+1)+27.*COC(L+2)+272.*COC(L+3)
      AREA=AREA+27.*COC(L+4)+216.*COC(L+5)+41.*COC(L+6)
      ACOC=.36+(DELR/140.)*AREA
      PRINT,ACOC
      L=L+6
      IF(L-16) 24,25,25
25    IF(SENSE SWITCH 1) 50,51
51    STOP
      END
```

APPENDIX III

ADSORPTION ISOTHERM DETERMINATION

EXPERIMENTAL TECHNIQUE

The adsorption isotherm of PAA, on 1, 4, and 16-denier viscose, was determined in aqueous media by using the following technique. About 10-12 g. of cut viscose fibers, having a length-to-diameter ratio greater than 100, were placed in a 500-ml. flask. The fibers were washed first with 95% ethanol, and then several times with distilled water. The wash fluid was removed each time by suction, using a glass tube having a 200-mesh brass screen filter tip to prevent any loss of fiber from the flask. About 350 ml. of distilled water (at approximately 26.5°C.) were then added, the flask was weighed, and the slurry was stirred intermittently at a low rate for about 5 min. to assure equilibrium. A 15-ml. sample of solution was taken, and then an aliquot of PAA solution was added, followed by intermittent stirring. (The dye solution was prepared by dissolving 24-28 mg. of PAA in about 5 ml. of 95% ethanol, and then adding the ethanol concentrate to 2 liters of water.) After 5 min. or more (which was shown to be adequate for attainment of equilibrium) the slurry temperature was taken and a 15-ml. sample was obtained. A second aliquot of PAA was added, and another sample was taken as before. This process was generally repeated until a total of five aliquots was added. When a given series was completed, the flask was weighed to check the mass balance.

The solution samples were analyzed spectrophotometrically at 372 mμ. During the experimental work, samples were also spot checked at 600 mμ for the presence of light-absorbing impurities such as finely divided viscose particles. (PAA solution does not absorb light at this wavelength.) The absorbance (log of

1/transmission) of these impurities was generally found to be 0.005 or less, which was 1 to 3% of the total absorbance at 372 mμ.

At the conclusion of each series of determinations, the fiber charge was thoroughly washed with water and the above procedure was repeated, using a different initial quantity of water and aliquot size. This provided a check on the results, and better defined the adsorption isotherm. After a sufficient number of data points were obtained, the fiber mass was determined, after drying at 105°C. for at least 12 hours.

ANALYSIS OF ADSORPTION DATA

The stepwise performance of the adsorption isotherm determination can be represented by the following flow diagram (all items are expressed in terms of mg. of dye);

$$q_o + V_S C_o \xrightarrow[15C_o]{V_D C_D} q_1 + (V_S + V_D - 15)C_1 \xrightarrow[15C_1]{V_D C_D} q_2 + (V_S + 2V_D - 30)C_2$$

$$\xrightarrow[15C_2]{V_D C_D} q_3 + (V_S + 3V_D - 45)C_3 \quad \text{etc.}$$

Here,

$\underline{V_S}$ = $(\underline{W_o} - \underline{W_F})/\rho - \underline{W_F}\underline{V}\epsilon'$, volume of solution initially, cc.

$\underline{q}$'s = dye sorbed by fibers in each stage, mg.

$\underline{C}$'s = dye concentrations calculated from Beer's law, using $\underline{C} = 0.00939\ \underline{A}$ (mg./cc.), where $\underline{A}$ is the absorbance at 372 mμ

$\underline{V_D}$ = volume of dye solution added, cc.

$\underline{W}_o$ = mass of fiber plus water initially, g.

$\underline{W}_F$ = fiber mass, g., o.d.

ρ = solution density, g./cc.

$\underline{V}$ = swollen specific volume of fibers, wet cc./g., o.d.

ϵ' = porosity of fibers, dimensionless

From the representation it can be seen that the total amount of dye sorbed by the fibers, $\Delta q_{\underline{n}}$ (mg. dye), in going from stage zero to stage $\underline{n}$, is expressed as

$$\Delta q_n = nV_D C_D + V_S C_o - [V_S + n(V_D - 15)]C_n$$

$$- 15(C_{n-1} + C_{n-2} + \ldots C_o) \qquad (270)$$

Letting $\underline{Q}_o$ represent the initial dye concentration in the fibers, the concentration of dye in the fibers, $\underline{Q}_{\underline{n}}$, that is in equilibrium with the solution at concentration $\underline{C}_{\underline{n}}$, (mg. dye/cc. solution), is therefore

$$Q_n = Q_o + \Delta q_n / W_F V \quad \text{(mg. dye/cc. fiber)} \qquad (271)$$

The relationship between $\underline{Q}_{\underline{n}}$ and $\underline{C}_{\underline{n}}$ describes an adsorption isotherm. If the isotherm is linear, with a positive intercept at $\underline{Q}_{\underline{I}}$, the partition coefficient $\underline{K}_{\underline{I}}$ is conveniently defined as the slope of the isotherm, or is calculated from individual data points by using the expression

$$K_I = (Q_n - Q_o - Q_I)/(C_n - C_o) \qquad (272)$$

In order to establish adsorption isotherms and calculate partition coefficients, for the PAA-viscose systems, it was first assumed that for small values of $\underline{C}_o$

$$Q_o = C_o (Q_1 - Q_o)/(C_1 - C_o) \qquad (273)$$

Using $\underline{Q_o}$, $\underline{Q_n}$ was then calculated as a function of $\underline{C_n}$ from the experimental data, the isotherms were plotted, and both $\underline{Q_I}$ and $\underline{K_I}$ were evaluated from the linear plots.

APPENDIX IV

SORPTION RATE DETERMINATION IN A WELL-STIRRED FINITE DYEBATH

A method was developed for measuring the rate of sorption, of PAA, by viscose fibers in a well-stirred dilute slurry. The objective here was to obtain data corresponding to a known diffusion case; i.e., unsteady state sorption in a well-mixed dyebath of finite size.

EXPERIMENTAL TECHNIQUE

A schematic of the sorption rate apparatus is pictured in Fig. 60. About 10-12 g. of cut viscose fibers, having a length-to-diameter ratio greater than 100, were placed in the three mouth flask, washed with distilled water, 95% ethanol, and then washed several times with distilled water. Distilled water was added to the fibers until the contents of the flask reached a predetermined weight (300-400 g.). The slurry was stirred intermittently for 5 min. and a 15-ml. sample was taken. In each experiment (of a given series) it was important to maintain the same ratio of fluid volume to fiber volume, during the sorption process, since the relative rate of uptake depends on this parameter (as previously discussed). A predetermined volume of PAA solution was then poured into the funnel, the stirrer was set at a high rate and a partial vacuum was drawn on the pipet. The pinchclamp holding the dye solution was released and a stopwatch was started. The dye solution was observed to flow into and mix uniformly with the fiber slurry in less than a second. After the desired passage of time, the stopcock at [A] was opened and the watch was stopped at the instant the 15-ml. sample was drawn into the dry, evacuated, sampling system. Generally, the sampling was complete in less than a half second. The temperature and total mass of the slurry were recorded at this point. The slurry was then

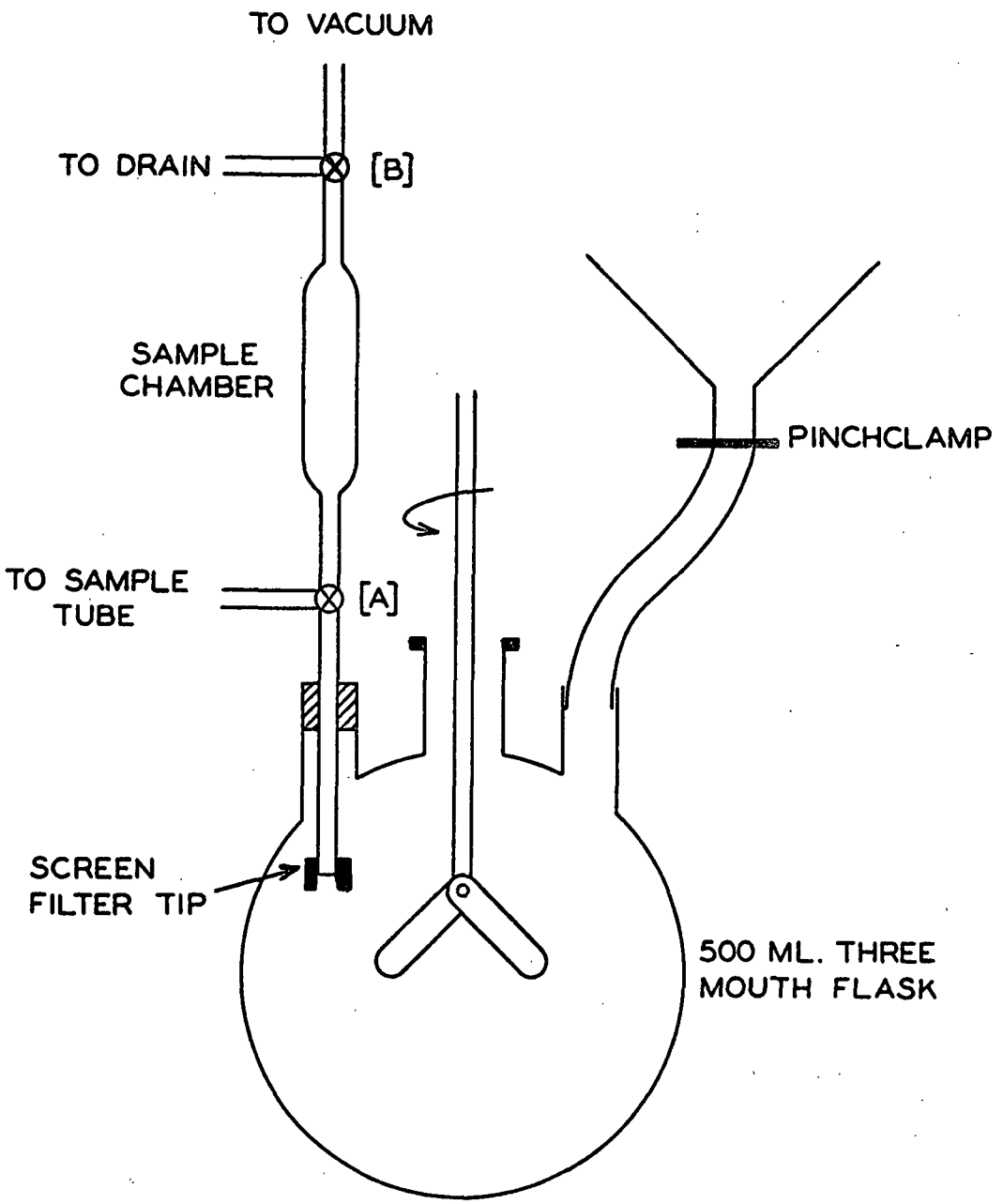

Figure 60. Sorption Rate Apparatus

stirred intermittently for 5 min. to achieve equilibrium, and a final 15-ml. sample was taken to represent the equilibrium condition. Care was taken to assure that the temperature was maintained relatively constant over the duration of each experiment. All three samples were analyzed spectrophotometrically at 372 mμ.

At the conclusion of each sorption rate experiment, the fibers were washed several times with distilled water in preparation for subsequent experiments. The fiber mass was determined after the fractional sorption vs. time relationship was believed to be sufficiently well defined.

REDUCTION OF SORPTION RATE DATA

The stepwise performance of the sorption rate experiments can be represented by the following flow diagram (all items are expressed in terms of mg. of dye),

$$q_o + (V_S' - V_D + 30)C_o \xrightarrow{V_D C_D,\ 15C_o} q_t + V_S' C_t \xrightarrow{15C_t} q_\infty + (V_S' - 15)C_\infty \xrightarrow{15C_\infty}$$

where the same nomenclature that previously described the adsorption data in Appendix III applies, with the addition that

$\underline{V_S'}$ = $(\underline{W_t} - \underline{W_F})/\rho - \underline{W_F}\underline{V}\epsilon'$, volume of solution after sample has been taken at time $\underline{t}$, cc.

$\underline{W_t}$ = mass of fiber plus solution after sample has been taken at time $\underline{t}$, g.

From the flow diagram it can be seen that

$$q_t - q_o = V_D C_D + (V_S' - V_D + 15)C_o - (V_S' + 15)C_t \qquad (274)$$

and

$$q_\infty - q_o = V_D C_D + (V_S' - V_D + 15)C_o - V_S' C_\infty - 15C_t \qquad (275).$$

Thus, the fractional sorption of dye, based on the sorption at equilibrium, was calculated from

$$Q_F = (q_t - q_o)/(q_\infty - q_o) \qquad (276)$$

As a check on the experimental data, the partition coefficient, K_S, associated with each sorption rate experiment, was calculated from essentially the same expression as used before in the analysis of adsorption data.

$$K_S = (((q_\infty - q_o)/W_F V) - Q_I)/(C_\infty - C_o) = (\Delta Q - Q_I)/\Delta C \qquad (277).$$

The rate of PAA sorption for 4- and 16-denier viscose is given in Tables XXVII and XXVIII.

TABLE XXVII

RATE OF PAA SORPTION ON FOUR-DENIER VISCOSE ($\lambda' = 2.33$)[a]

t, sec.	Q_F	$\Delta Q/\Delta C$	C_o, mg./l.	C_∞, mg./l.
8.1	0.895	10.69	0.31	2.33
8.3	0.832	10.77	0.39	2.40
9.3	0.960	10.08	0.30	2.36
9.3	0.956	10.55	0.48	2.48
10.1	0.920	10.26	0.28	2.32
10.2	0.854	10.66	0.06	2.13
11.0	0.880	10.66	0.44	2.43
11.1	1.037	10.21	0.51	2.17
11.5	1.046	9.92	0.51	2.54
12.1	0.955	10.06	0.29	2.34
13.4	1.037	9.66	0.22	1.95
		10.32	0.34	2.31

[a] λ' = (solution volume)/(K)(fiber volume).

TABLE XXVIII

RATE OF PAA SORPTION ON 16-DENIER VISCOSE

t, sec.	Q_F	$\Delta Q/\Delta C$	C_o, mg./l.	C_∞, mg./l.
Series 1 ($\lambda' = 2.435$)				
7.3	0.629	10.96	0.26	2.09
8.3	0.642	10.74	0.23	2.08
9.6	0.673	10.70	0.39	2.22
10.5	0.732	10.67	0.57	2.56
12.0	0.738	10.65	0.38	2.40
12.2	0.767	10.60	0.24	2.10
14.4	0.770	11.06	0.40	2.40
14.6	0.791	10.49	0.26	2.12
16.2	0.822	10.59	0.32	2.17
18.0	0.870	10.67	0.26	2.31
18.4	0.879	10.70	0.43	2.45
20.4	0.870	11.56	0.23	2.04
22.4	0.886	11.04	0.40	2.40
		10.80	0.34	2.26
Series 2 ($\lambda' = 2.71$)				
13.2	0.815	10.55	0.04	3.48
17.0	0.860	10.60	0.04	3.47
19.0	0.887	10.91	0.04	3.45
23.2	0.909	10.46	0.04	3.48
		10.64	0.04	3.47

APPENDIX V

MATERIAL BALANCE DETERMINATIONS IN THE PAA-16 DENIER SYSTEMS

It was considered impractical to extend the numerical evaluation of the washing equation to large values of R, thus establishing a theoretical relationship between K_w, C/C_o, and R. This would have provided a direct means of estimating the desired water values. Also, the washing equation did not appear to have a simple asymptotic form, which would have accomplished the same purpose.

An alternative approach was to establish two limiting cases that would confirm the reliability of asymptotic water values that were estimated from the experimental data. The first of these defined the highest possible rate of desorption (or sorption) of PAA from a fiber bed, describing the hypothetical condition at an infinite flow rate. More specifically this case corresponded to the diffusion of PAA from 16-denier fibers (initially at uniform concentration) into a well-stirred bath of infinite extent at zero concentration. The fractional desorption was calculated as a function of time from Equation (35). The value assigned to the intrafiber diffusion parameter, $D_F/a^2 = 0.0050$, was considered appropriate for these calculations (to be demonstrated later). The results of the calculations are shown in Table XXIX. The apparent values of K_w were calculated on the basis that $K_w = 9.45$ at 100% desorption.

A second case was used to define a lower limiting rate of desorption from Bed 1-16. This was accomplished by determining apparent values of K_w, as a function of elapsed time, that were achieved over the finite pore volume range $0 \leq R \leq 6.84$. The numerical integrations were performed on exit concentration curves that were calculated from the washing equation (approximately the same results would have been obtained from the experimental data).

TABLE XXIX

DIFFUSION OF PAA FROM 16-DENIER FIBERS INTO A WELL-STIRRED INFINITE DYEBATH AT ZERO CONCENTRATION

t, sec.	Q_F [a]	K_w [b]
12	0.489	4.62
24	0.651	6.15
36	0.755	7.13
48	0.827	7.82
60	0.878	8.29
72	0.914	8.63
108	0.970	9.15
132	0.985	9.30
156	0.992	9.36
180	0.996	9.41

[a] $Q_F = Q_t/Q_\infty$, fractional desorption assuming $D_F/a^2 = 0.005$.

[b] $K_w = 9.45\ Q_F$

The results of the calculations are shown in Table XXX, where the apparent values of K_w were normalized, as before, to 9.45 for 100% effective desorption of solute. These results should effectively represent a lower limiting rate of solute removal, on an equal time basis, since all the prematurely terminated washing runs were concluded at R values much greater than 6.84.

Figure 61 illustrates the K_w vs. t envelope that was defined by the respective limiting cases. The experimentally determined values of K_w (based on the entire experimental range of R) for the 15 prematurely terminated washing runs

TABLE XXX

PAA DESORBED FROM 16-DENIER BED DURING INITIAL STAGE OF WASHING

Run	Variables Defined at $\underline{R}_1 = 6.84$		
	$\underline{Q}_1$ [a]	$\underline{K}_w$ [b]	$\underline{t}$, sec. [c]
1- 6-16	2.135	7.48	74.4
1-10-16	1.864	6.53	44.6
1- 2-16	1.613	5.65	31.1
1- 5-16	1.472	5.16	23.9
1- 9-16	1.372	4.81	20.03
1- 3-16	1.268	4.44	16.47
1- 7-16	1.203	4.22	14.5

[a] $$\underline{Q}_1 = \int_0^{\underline{R}_1=6.84} [(\underline{C}/\underline{C}_o)_{\underline{E}} - (\underline{C}/\underline{C}_o)_{\underline{I}}]\, \underline{dR} - 1.$$

[b] $\underline{K}_w = 9.45\, \underline{Q}_1/2.70.$

[c] $\underline{t} = 6.84\, \underline{Z}_{\underline{E}}/\underline{U}.$

in the PAA-16 denier system, are also shown. It is seen that seven runs were very close to completion. The other eight runs (at the highest pore velocities) were bracketed by the envelope of the two limiting cases. Since roughly a 4% change in $\underline{K}_w$ was found to result from a 1% change in the water value here, it was felt that the water values had been defined at an acceptable level of accuracy. Further justification was made by the fact that $\underline{C}/\underline{C}_o$ was always above 0.1 in these runs, over the applied range of the washing equation ($0 \leq \underline{R} \leq 6.84$). Thus, the regions of low relative concentrations, which were more sensitive to the water values, were of no concern in the later analyses of breakthrough curves.

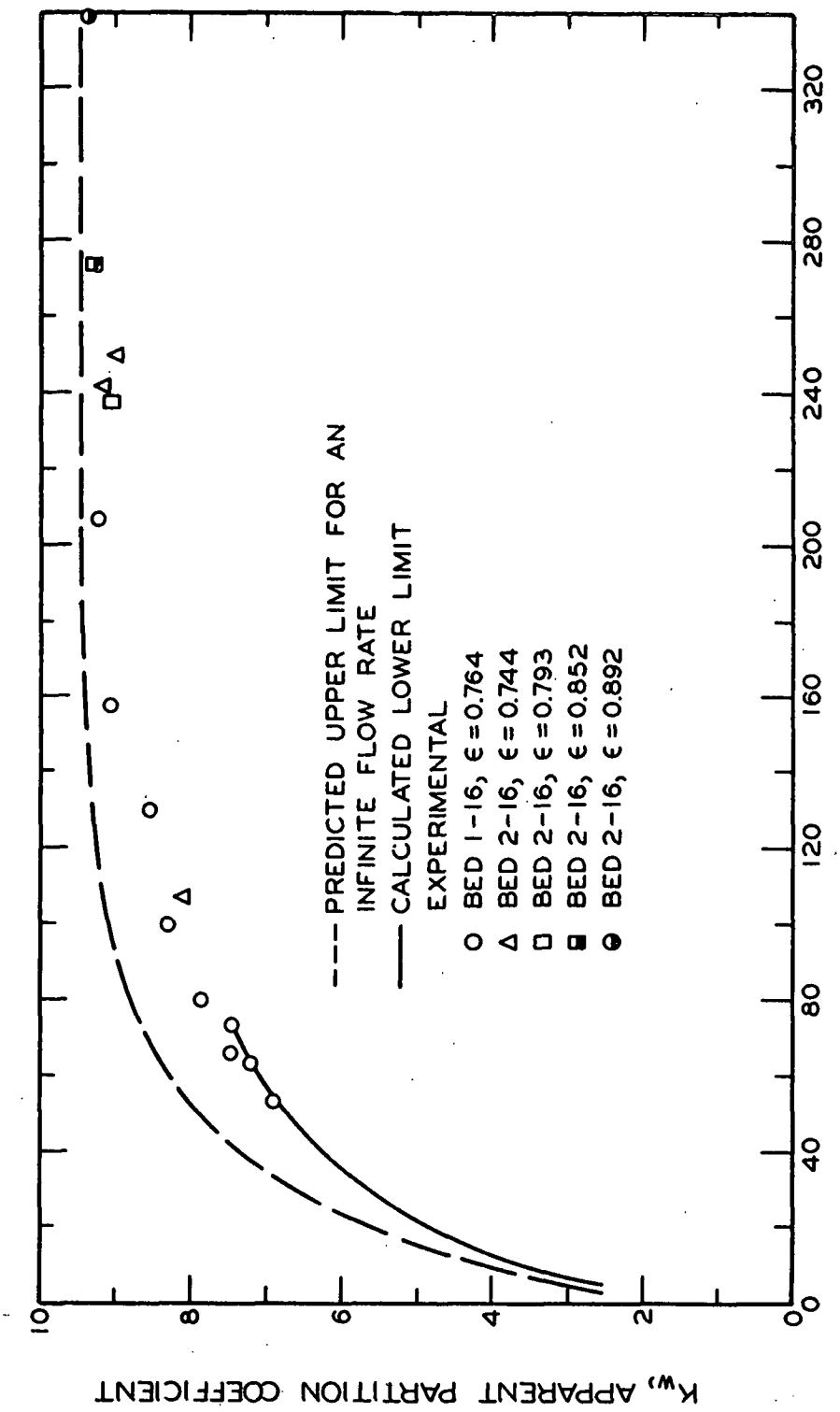

Figure 61. Effectiveness of Washing in the PAA-16 Denier System

Tables XXXI and XXXII summarize the experimental conditions and material balance data that characterize the washing runs in the 16-denier viscose system. The R_F, t_F, and $(C/C_o)_F$ values indicate the prevailing conditions at the termination of each experiment. The K_W values represent the effective removal of solute at R_F, as plotted in Fig. 61.

TABLE XXXI

WASHING RUN CONDITIONS AND MATERIAL BALANCE DATA

Run	Description	Z_e, (Z_E), cm.	ϵ, (ϵ_E)	U, cm./sec.	I	M_w	R_F	t_F, sec.	$(C/C_o)_F$	K_w
1- 8-16	D,PAA	4.06 (4.315)	0.7636 (0.7753)	0.0391	0.043	3.77	9	995	0.000	9.55
1- 4-16	"	"	"	0.206	0.072	3.74	23	482	0.002	9.45
1- 6-16	"	"	"	0.397	0.067	3.68	19	207	0.005	9.24
1-10-16	"	"	"	0.662	0.044	3.47	20	130	0.007	8.52
1- 2-16	"	"	"	0.950	0.086 0.043	3.37 3.41	22	100	0.008	8.17 8.31
1- 5-16	"	"	"	1.237	0.088 0.043	3.13 3.17	19	66	0.007	7.35 7.48
1- 9-16	"	"	"	1.473	0.094 0.043	3.11 3.16	25	73	0.010	7.27 7.45
1- 3-16	"	"	"	1.793	0.100 0.043	3.03 3.09	26	63	0.010	7.00 7.20
1- 7-16	"	"	"	2.039	0.114 0.043	2.94 3.01	25	53	0.010	6.69 6.93
1-11-16	S,PAA	"	"	0.654	0.094	3.63	24	158	0.004	9.06
1-12-16	"	"	"	0.917	0.112 0.043	3.21 3.28	17	80	0.013	7.62 7.86

TABLE XXXII

WASHING RUN CONDITIONS AND MATERIAL BALANCE DATA

Run	Description	Z_e, (Z_E), cm.	ϵ, (ϵ_E)	U, cm./sec.	I	M_w	R_F	t_F, sec.	$(C/C_o)_F$	K_w
2-16-16	D,PAA	10.87 (11.25)	0.8920 (0.8949)	0.0642	0.026	2.12	7	1230	0.003	9.53
2-17-16	"	"	"	0.299	0.033	2.10	9	339	0.005	9.35
2-18-16	"	7.90 (8.34)	0.8515 (0.8576)	0.0760	0.071	2.57	8	880	0.000	9.45
2-19-16	"	"	"	0.334	0.060	2.54	11	274	0.010	9.27
2-20-16	"	5.68 (6.235)	0.7934 (0.8067)	0.0778	0.053	3.23	13	1040	0.000	9.30
2-21-16	"	"	"	0.341	0.074	3.16	13	238	0.018	9.02
2-23-16	"	4.59 (5.105)	0.7443 (0.7639)	0.0846	0.059	3.92	17	1025	0.002	9.44
2-22-16	"	"	"	0.209	0.166	3.87	15	366	0.014	9.27
2-24-16	"	"	"	0.358	0.063	3.82	17	242	0.013	9.11
2-26-16	"	"	"	0.955	0.077	3.50	20	107	0.010	8.08
2-25-16	S,PAA	"	"	0.307	0.089	3.78	15	250	0.017	8.98

APPENDIX VI

CALCULATION OF NONUNIFORM POROSITY DISTRIBUTION

When a fluid flows through a compressible fiber bed, which initially has been compacted to a fixed length and uniform porosity, the bed assumes a nonuniform porosity distribution that satisfies a balance between the local compacting forces and the cumulative fluid drag forces. This distribution is a function of (a) the compressibility of the bed, as determined by the properties of the fibers, (b) the average porosity, and (c) the over-all fluid pressure drop across the bed. To give a rough indication of the relative importance of this effect, Table XXXIII shows how the ratio of fluid pressure drop to static compacting pressure varied with linear pore velocity, for the 1, 4, and 16-denier viscose beds. It is evident that the ratio generally became larger and more significant as the fiber diameter decreased and the average porosity increased.

TABLE XXXIII

FLUID PRESSURE DROP VERSUS STATIC COMPACTING PRESSURE

Bed	ϵ	$\Delta P/UP_s$, sec./cm.[a]
3 - 1	0.7158	2.12
4 - 4	0.7460	0.31
4 - 4	0.8059	0.59
4 - 4	0.8598	1.46
1 - 16	0.7636	0.081
2 - 16	0.7443	0.087

[a] ΔP = experimentally determined fluid pressure drop.
P_s = calculated static compacting pressure.

To represent a test case, the following bed parameters and run conditions were chosen (these correspond to washing run 3-35-1 with the minor exception that the average bed porosity was taken as 0.7242 instead of 0.7158).

$\underline{q}'$ = 15.13 cc./sec., flow rate

$\underline{W_F}/\underline{A_c}$ = 0.689 g., o.d./sq. cm., basis weight

$\underline{Z}$ = 4.67 cm., bed length

ϵ = 0.7242, average bed porosity

$\underline{U}$ = 0.480 cm./sec., average linear pore velocity

$\underline{U_s}$ = 0.3475 cm./sec., superficial velocity

$\underline{P_s}$ = 86 cm. water, static compacting pressure

$\Delta\underline{P}$ = 91 cm. water, over-all fluid pressure drop, extrapolated from experimental data

$\Delta\underline{P}$ = 111 cm. water, over-all fluid pressure drop, calculated from Equation (40) using average bed properties

$\Delta\underline{P}$ = 100 cm. water, nominal fluid pressure drop (assumed)

A number of calculations were first performed to describe a 1-denier bed which had no mechanical compacting pressure at the top surface. The objective here was to characterize the over-all pressure drop, and porosity, as functions of distance from the top surface (at a constant flow rate). It was reasoned that, at some unknown distance from the top surface $\underline{Z_1}$, the portion of the bed included between $\underline{Z_1}$ and $\underline{Z_2} = \underline{Z_1} + 4.67$ cm. would correspond in every detail to the properties of the desired test bed that was under mechanical compaction.

The analysis of this case was based on an application of the Kozeny-Carman equation, for viscous flow, to a differential layer of mat (22).

$$\frac{d(\Delta p)}{dZ} = \mu S_v^2 U_s \frac{\bar{k}(1 - \epsilon)^2}{\epsilon^3} \qquad (278)$$

On substituting the empirical correlation for the Kozeny factor (41), the frictional pressure gradient becomes

$$\frac{d(\Delta p)}{dZ} = 3.5\ \mu S_v^2\ U_s(1 - \epsilon)^{3/2}\ [1 + 57(1 - \epsilon)^3] \qquad (279).$$

Substituting the usual compressibility relationship for the solid fraction

$$1 - \epsilon = V\bar{M}(\Delta p)^{\bar{N}} \qquad (280)$$

one obtains

$$\frac{d(\Delta p)}{dZ} = 3.5\ \mu S_v^2\ U_s\left[V\bar{M}(\Delta p)^{\bar{N}}\right]^{3/2}\ \left[1 + 57\left(V\bar{M}(\Delta p)^{\bar{N}}\right)^3\right] \qquad (281).$$

Thus, in order to calculate Z as a function of ΔP, the following improper integration is required.

$$Z = \frac{1}{3.5\ \mu S_v^2\ Us}\int_0^{\Delta P} \frac{d(\Delta p)}{\left[V\bar{M}(\Delta p)^{\bar{N}}\right]^{3/2}\left[1 + 57\left(V\bar{M}(\Delta p)^{\bar{N}}\right)^3\right]} \qquad (282)$$

Although the integral is defined for small values of $\bar{N}$, it is noted that the integrand tends toward infinity as Δp approaches zero. In order to avoid this complication, it was assumed that the contribution of

$$1 + 57\left[V\bar{M}(\Delta p)^{\bar{N}}\right]^3 = 1 + 57\ (1 - \epsilon)^3 \qquad (283)$$

was unity over the porosity range of 1.00-0.93. The integral over this region was represented by

$$Z = \frac{\Delta P}{3.5\ \mu S_v^2\ U_s(1 - 3N/2)\left[V\bar{M}(\Delta P)^{\bar{N}}\right]^{3/2}} \qquad (284)$$

Beyond this point, the integrand was found to be sufficiently well defined to evaluate the integral numerically by using the Newton-Cotes seven-point integration formula for evenly spaced values of $\Delta \underline{p}$. Values of $\underline{Z}$ agreeing to four figures were obtained when the integration interval was changed from 0.2 to 0.1 cm. water. The resulting pressure drop and porosity distributions are shown in Fig. 62 as functions of distance through the bed. It is apparent that the porosity distribution is nearly linear in this case.

From Fig. 62, the fluid pressure drop $\Delta \underline{P} = \Delta \underline{P}_2 - \Delta \underline{P}_1$, corresponding to the preselected distance increment of $\underline{Z}_2 - \underline{Z}_1 = 4.67$ cm. (equal to the length of the test bed), was obtained as a function of $\underline{Z}_1$. These results are shown in Table XXXIV. From a plot of $\Delta \underline{P}$ vs. $\underline{Z}_1$, the desired value of $\underline{Z}_1$, corresponding to the previously calculated over-all pressure drop, $\Delta \underline{P} = 111$, was interpolated. (A solution for a nominal pressure drop of 100 cm. water was also determined.) The calculated end conditions for the 1-denier test bed are summarized in Table XXXV. For comparison purposes, some results that were obtained by initially assuming a linear porosity distribution are also shown; here, trial and error calculations were performed to determine an over-all porosity change that would yield a compacting pressure difference equal to the over-all fluid pressure drop. It is seen that the agreement between the two methods was excellent when the calculated over-all pressure drop was used. The agreement was not as good at the assumed nominal pressure drop of 100 cm. water.

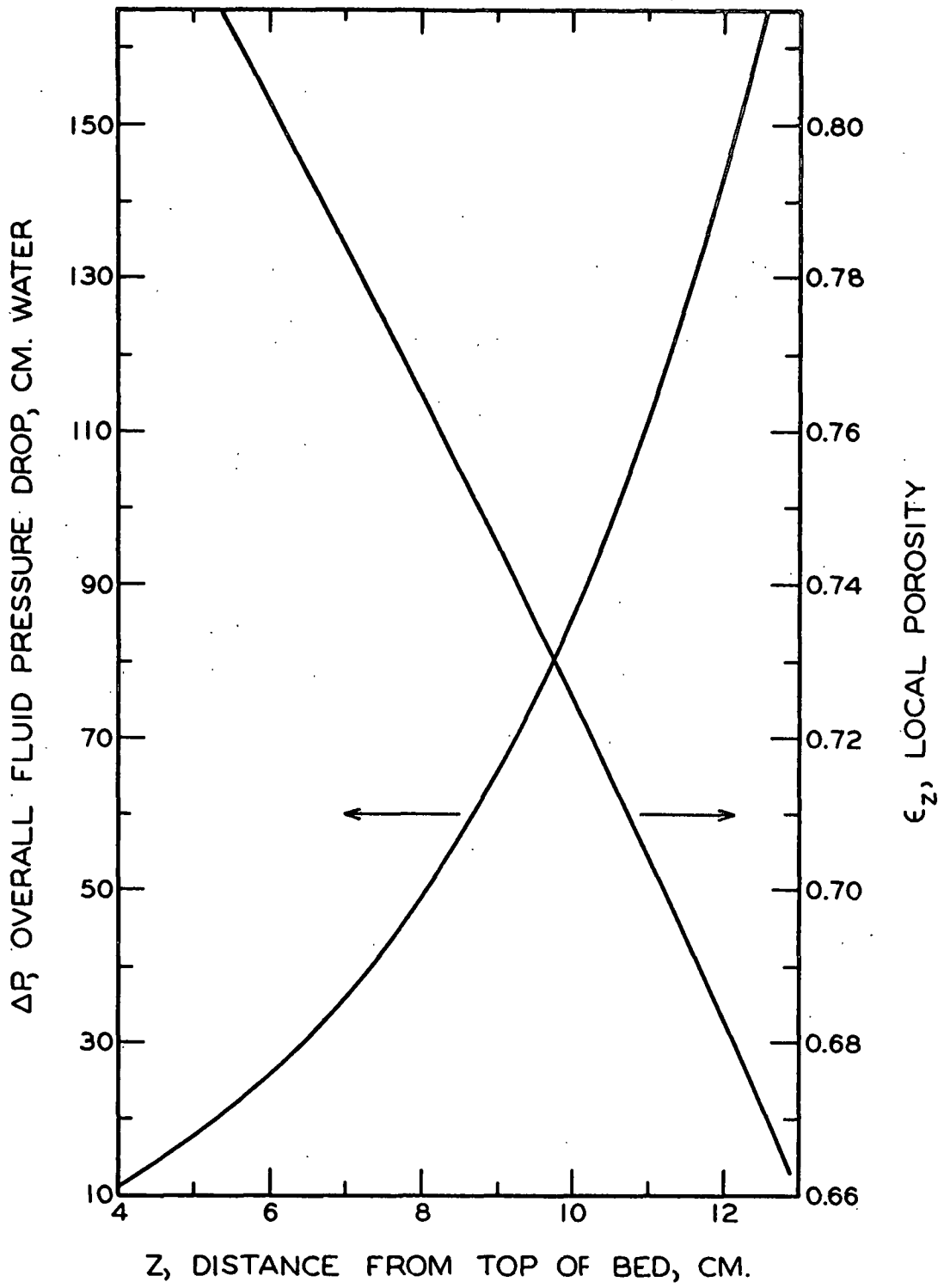

Figure 62. Pressure Drop and Porosity Distribution

TABLE XXXIV

INCREMENTAL PRESSURE DROP DISTRIBUTION

Z_1, cm.	Z_2, cm.	ΔP_1, cm. water	ΔP_2, cm. water	ΔP, cm. water
4.00	8.67	11.2	59.0	47.8
4.50	9.17	14.0	67.9	53.9
5.00	9.67	17.7	78.0	60.3
5.50	10.17	21.4	89.2	67.8
6.00	10.67	25.9	101.5	75.6
6.50	11.17	30.8	116.0	85.2
7.00	11.67	35.8	131.5	95.7
7.50	12.17	41.7	149.5	107.8
8.00	12.67	48.8	170.5	121.7
8.50	13.17	56.4	192.7	136.3

TABLE XXXV

CALCULATED END CONDITIONS FOR ONE-DENIER TEST BED UNDER MECHANICAL COMPACTION

Z_1, cm.	Z_2, cm.	ΔP_1	ΔP_2	ΔP, cm. water	ϵ_1	ϵ_2
7.63[a]	12.30[a]	43.5[a]	154.5[a]	111.0[a]	0.772[a]	0.675[a]
[ΔZ =	4.67][b]	43.1[b]	154.2[b]	111.1[b]	0.7726[b]	0.6759[b]
7.20[a]	11.87[a]	38.0[a]	138.0[a]	100.0[a]	0.780[a]	0.685[a]
[ΔZ =	4.67][b]	46.3[b]	146.4[b]	100.1[b]	0.7680[b]	0.6805[b]

[a]From numerical integration of Equation (282).

[b]From assumption of linear porosity variation with distance through the bed.

APPENDIX VII

ESTIMATION OF FIBER-FIBER CONTACT AREA

The contact area between two identical, homogeneous, and Hookean circular cylinders (fibers), crossing at right angles, is obtained from equations derived by Finch (43) as

$$A_c' = \pi \left[\frac{3\bar{F}d\ (1 - \nu^2)}{4\bar{E}} \right]^{2/3} \qquad (285)$$

where $\bar{F}$ is the normal load, d is the fiber diameter, ν is Poissons ratio, and $\bar{E}$ is the elastic modulus. Thus, in a fiber bed, the fractional surface area in contact (based on the total surface area) should be $\alpha = 2A_c'C_t'/A_t$, where C_t' is the total number of fiber contacts, and A_t is the total surface area of the fibers, initially. If it is assumed that the average fiber diameter, d, does not change appreciably upon compaction of the fibers in a bed then $A_t = 4W_F V/d$, where W_F is the total fiber mass, and V is the swollen specific volume of the fibers (cc./g.). By substitution,

$$\alpha = \frac{\pi d C_t'}{2W_F V} \left[\frac{3\bar{F}d\ (1 - \nu^2)}{4\bar{E}} \right]^{2/3} \qquad (286).$$

Now if a fiber bed of length Z_e, and cross-section area A_c, is assumed to consist of Z_e/d layers, the total load per contact is expressed in terms of the compacting pressure P_s as $\bar{F} = P_s A_c Z_e / C_t' d$. By substitution we now have

$$\alpha = \frac{\pi d}{2W_F V} C_t'^{1/3} (AZ)^{2/3} \left[\frac{3\ (1 - \nu^2) P_s}{4 \quad \bar{E}} \right]^{2/3} \qquad (287).$$

The remaining problem is to find a suitable expression for $\underline{C}_t'$, the total number of fiber-fiber contacts in a bed. Onogi and Sasaguri (44) have derived a relatively simple expression for $\underline{C}_t'$, if it is assumed that all the fibers lie in the horizontal plane. Obviously, this assumption is not correct for a real fiber bed, such as the viscose beds in this study, but it is not easy to improve it. In terms of the present nomenclature, it can be shown that Onogi and Sasaguri's expression for $\underline{C}_t'$, in this case, is

$$2\pi C_t' = 64 W_F^2 V^2 / \pi^4 d^3 A_c Z_e \qquad (288).$$

By substituting $(\underline{C}_t')^{1/3}$ in Equation (287), and setting $(1 - \epsilon) = \underline{W}_F \underline{V} / \underline{A}_c \underline{Z}_e$, it is found that

$$\alpha = \frac{2}{\pi^{1/3} (1 - \epsilon)^{1/3}} \left[\frac{3 (1 - \nu^2) P_s}{4 \quad \bar{E}} \right]^{2/3} \qquad (289).$$

If the usual simplified expression for the compacting pressure on a fiber bed, undergoing first compression, is used as

$$P_s = [(1 - \epsilon)/V\bar{M}]^{1/\bar{N}} \qquad (290)$$

where $\bar{M}$ and $\bar{N}$ are empirical constants, the following expression for α, the fractional surface area involved in intimate fiber-fiber contact, is shown to be

$$\alpha = \frac{2}{\pi^{1/3}} \left[\frac{3(1 - \nu^2)}{4\bar{E}(V\bar{M})^{1/\bar{N}}} \right]^{2/3} (1 - \epsilon)^{(2-\bar{N})/3\bar{N}} \qquad (291).$$